WASM: Minerals, Energy and Chemical Engineering

Carbo-catalysis in Liquid Phase Selective Oxidation Reactions

Jiaquan Li
0000-0001-7924-0573

This thesis is presented for the Degree of
Doctor of Philosophy
of
Curtin University

August 2021

Declaration

To the best of my knowledge and belief this thesis contains no material previously published by any other person except where due acknowledgment has been made.

This thesis contains no material which has been accepted for the award of any other degree or diploma in any university.

Signature: Jiaquan Li ……...

Date: 26/08/2021 ……..

To my beloved family

Abstract

Selective oxidation reactions are fundamentally important to the chemical industry. Value-added products and intermediates for fine chemical synthesis can be obtained *via* liquid phase selective oxidation of primary chemicals such as hydrocarbons and alcohols. Current reaction methods usually rely on precious or hazardous metal-based catalysts, employing either inert oxygen gas or explosive peroxides as oxidant. Attention is still required for the development of facile and environmentally benign routes for selective oxidation processes. Carbon-based materials can perform as green and recyclable catalysts in various oxidation reactions. Peroxymonosulfate (PMS), as a stable oxidant, can be activated by a broad variety of catalysts under mild conditions and subsequently oxidize organics. Recent applications of the activated PMS mainly focused on the degradation of aqueous contaminants, whereas its potential in selective oxidation reactions was rarely explored. This study focuses on tuning the activation process of PMS with carbo-catalysts to provide an alternative approach for liquid phase selective oxidation of hydrocarbons and alcohols into their corresponding aldehydes and ketones.

In the first part, the feasibility of adopting PMS for selective oxidation of benzyl alcohol (BzOH) was tested, using modified carbon nanotubes (CNTs) as the catalyst. Thermal annealed o-CNTs were equipped with electrophilic oxygen species and nucleophilic carbonyl groups, which could induce the generation of radicals from PMS *via* the electron transfer between PMS and CNTs. The catalytic roles of the active sites were identified by both designed experiments and theoretical calculations. The optimized reaction system could afford the selective oxidation of BzOH into benzaldehyde (BzH) with over 80% selectivity *via* the radical pathway.

In the second part, nitrogen-doped graphene oxide (NGO) was prepared from graphite

to enable the selective oxidation with higher efficiency. The NGO catalyst contained abundant dual active sites of pyridinic N and ketonic C=O to oxidize BzOH through joint contributions of radical and non-radical routes. The non-radical pathway was enabled by the mediated electron transfer *via* the surface coordinated complex and was more selective in yielding BzH compared with the highly oxidative radicals. Over 96% BzOH conversion and 82% BzH yield were achieved within 3 hours at 50 ºC. The oxidation behaviour of BzOH and BzH was investigated to enrich the scientific understandings towards the oxidation pathways in the reaction system.

The third part of this thesis describes a metal-free method for the synthesis of N-doped graphene-like carbon (NG) catalyst without producing hazardous wastes. The addition of nitrate salts facilitated the formation of thin-layered graphene sheets and the generation of electrophilic oxygen species which were active sites to produce radicals from PMS. Non-radical oxidation process was also observed during the reaction. The NG activated PMS was efficient in the highly selective conversion of aromatic alcohols including BzOH and 1-phenylethanol into BzH and acetophenone, respectively.

In the last part, single cobalt atoms were doped on carbon materials including graphene and g-C_3N_4 substrates to derive robust single atom catalysts (SAC) for PMS activation. The atomically dispersed Co atoms were chemically coordinated with N atoms on carbon materials and exhibited excellent catalytic activity and high stability in the selective oxidation of BzOH and ethylbenzene. The corresponding yield of BzH and acetophenone over the Co SACs could reach 84.7% and 93.2%, respectively, superior to the Co nanoparticles and precious metal catalysts.

In summary, this thesis paves an alternative way for liquid phase selective oxidations of alcohols and hydrocarbons by carbo-catalysts activated PMS under mild conditions without additives. In-depth understanding of the catalysis and oxidation processes was unveiled for the future application of this system in organic synthesis.

Acknowledgements

I would like to express my most sincere thanks to my supervisor, Prof. Shaomin Liu, for his support throughout my PhD study. He not only offered me the chance to work on my project, but also provided his best resources to help me overcome any difficulties encountered during my research. He is modest and enthusiastic. His passion towards scientific research and inspiring ideas set a good role model for me to learn from. His precious guidance and encouragement have greatly influenced me on my attitude to science and will continuously benefit my future life.

Equally, I would like to show my deepest gratitude to Prof. Shaobin Wang and Prof. Hongqi Sun for their professional supports and suggestions on my choice of research topic, experiment design and mechanism proposal. I have learned a great deal from their enormous knowledge and every discussion with them was a precious opportunity to exploit my research to a deeper extent and to correct the deficiencies. I am also deeply grateful to Prof. Sanping Jiang and Prof. Zongping Shao, to generously support me with my work and to open up new frontier in my research.

I am also thankful to my friends and colleagues, Dr Fuping Li, Dr Xiaoguang Duan, Dr Xiaojie Li, Dr Huayang Zhang and Kai Wang for being supportive with my lab work, teaching me how to use the electric devices and helping me with the catalyst characterizations. I am really proud to have such talented friends and colleagues in Curtin, who are always ready to offer me their generous help. My research wouldn't be completed smoothly without your support.

My gratitude also goes to the lab technicians in Curtin, Dr Roshanak Doroushi, Dr Dipok Sarker, Mr Xiao Hua, Ms Jennifer Wang, Ms Angelina Rossiter for their technical support on my lab work. I appreciate the support from Curtin John de Laeter

Centre to let me perform the characterization works of XPS, XRD, SEM and TEM.

I would like to thank Curtin International Postgraduate Research Scholarship to financially support my PhD research.

And last, but not the least, I want to show my deepest love to my family, my parents, my grandparents, and my elder sister in China. Thank you for all the love you put on me, believing in me and the unconditionally supporting me chasing my dreams. Your care and love help me crash through the walls blocking my way to go further. I love you forever.

List of Publications

Publications by the author:

1. **Jiaquan Li**, Mengting Li, Hongqi Sun, Zhimin Ao, Shaobin Wang, and Shaomin Liu. "Understanding of the Oxidation Behaviour of Benzyl Alcohol by Peroxymonosulfate *via* Carbon Nanotubes Activation." ***ACS Catalysis*** 2020, 10 (6), 3516-3525.

2. **Jiaquan Li**, Shiyong Zhao, Lianji Zhang, San Ping Jiang, Shi-Ze Yang, Shaobin Wang, Hongqi Sun, Bernt Johannessen, and Shaomin Liu. "Cobalt Single Atoms Embedded in Nitrogen-Doped Graphene for Selective Oxidation of Benzyl Alcohol by Activated Peroxymonosulfate." ***Small*** 2021, 17 (16), 2004579.

3. **Jiaquan Li**, Shiyong Zhao, Shi-Ze Yang, Shaobin Wang, Hongqi Sun, San Ping Jiang, Bernt Johannessen, and Shaomin Liu. "Atomically dispersed cobalt on graphitic carbon nitride as a robust catalyst for selective oxidation of ethylbenzene by peroxymonosulfate." ***Journal of Materials Chemistry A*** 2021, 9 (5), 3029-3035.

4. **Jiaquan Li**, Fuping Li, Qi Yang, Shaobin Wang, Hongqi Sun, Qingning Yang, Junwang Tang, and Shaomin Liu. "Tailoring collaborative N-O functionalities of graphene oxide for enhanced selective oxidation of benzyl alcohol" ***Carbon*** 2021, 182, 715-724.

5. **Jiaquan Li**, Hongqi Sun, Shaobin Wang, Yu Dong, and Shaomin Liu. "Selective oxidation of alcohols by graphene-like carbon with electrophilic oxygen and integrated pyridinic nitrogen active sites". ***Nanoscale*** 2021, 13, 12979-12990.

Table of Contents

Chapter 1 Introduction

1.1 Background

Selective oxidations contain a wide variety of reactions and constitute around 30% of the total synthetic chemical industry.[1] The oxidation products such as alcohols, ketones, aldehydes, organic acids and epoxides serve as crucial chemicals or intermediates in almost all chemical industry branches, including synthesis of polymers, pharmaceuticals, etc. The fundamental importance of selective oxidation to the current industry and its intimate relation to the human society have triggered vast research interest since 1960s. After decades of scientific and industrial development, various research strategies have been proposed for selective oxidation reactions, especially the conversion of alcohols and hydrocarbons into the corresponding ketones, aldehydes and organic acids.[2-3] A key challenge for the current selective oxidation process is to establish green and environmental-benign route with high reaction efficiency and the minimized non-selective by-products such as CO_2.

Traditional selective oxidation reactions employ stoichiometric oxidants such as dichromate and permanganate, which are still used in some fine chemical synthesis. However, these oxidants are expensive and produce toxic and hazardous wastes. Another oxidant, the oxidizing acid HNO_3, suffers from similar issues releasing the undesired NO_x during the selective oxidation reactions.[4] Liquid peroxides have also been widely applied for the selective oxidations and epoxidation reactions.[5-7] Hydrogen peroxide and *tert*-butylhydroperoxide (TBHP) are active oxidants with weak O–O bonds ready to be activated, but they are unstable and explosive, resulting in the inconvenience for both transportation and storage and causing safety issues. The direct use of oxygen gas or air as terminal oxidant receives the most research efforts nowadays because this process not only reduces the cost but also avoids the

environmental concerns. However, O_2 is the least active oxidant compared with others because of its triplet ground state structure, especially when reacting with hydrocarbons. Therefore, the oxidation is performed with excess energy input to activate the inert O_2 molecules. Measures such as high reaction temperature, photo-catalysis, electro-catalysis and extra additives/co-catalysts are usually taken into account for this purpose.

For the catalytic activation of the oxidants, pursuing novel catalysis processes to satisfy the increasing demand of high reaction efficiency, robust catalytic performance, facile separation and environmentally benign reagents is always at the core of the research on liquid phase selective oxidation. In this context, the selective oxidations can be divided into homogeneous and heterogeneous catalysis processes. Homogeneous catalytic reactions normally hold high reactivity because the reactants and catalysts are in the same phase, but the catalyst separation and recycling are the intractable problems. Heterogeneous catalysts include noble-metal or transition-metal based catalysts and metal-free catalysts.[3, 8-9] Metal-based catalysis inevitably suffer from issues like high cost, environmental toxicity, metal-leaching and deactivation during the reaction. In contrast, carbon-based materials are extensively studied over the past years, not only because they perform as multi-functional supports for the embedded metal complexes, but also exhibit inherent catalytic activity owing to their high specific surface area, unique electronic properties and tunable surface chemistry.[10-11] Carbo-catalysts are sustainable substitutes towards metal catalysts, but the sophisticated understanding of their intrinsic catalytic behaviour still exists as the major challenge due to the complicated surface functionalities and morphology.

Peroxymonosulfate (PMS, HSO_5^-) is a soluble solid oxidant.[12] Compared with the aforementioned oxidants, PMS is cheap, stable and environmentally benign, and has been applied as a promising oxidant for the degradation of the organic pollutants in water *via* advanced oxidation processes (AOPs). A wide variety of carbon catalysts have been reported to effectively activate PMS to mineralize the target organics,

including carbon nanotubes, graphene, nanodiamonds, porous carbon, etc.[13] Various oxidative oxygen species such as $SO_4^{\bullet-}$, $^{\bullet}OH$, $SO_5^{\bullet-}$, $O_2^{\bullet-}$ and $^1O_2$, can be generated through the catalytic activated PMS to non-selectively oxidize the organic chemicals. Non-radical based process enabled by the surface adsorbed complex and mediated electron transfer also exists in PMS activation, which makes the oxidation by PMS more selective.[14] The activation of PMS is conducted without the need of high reaction temperature or any homogeneous additives and can be adapted to wide range of reaction pH. However, the catalytic activated PMS is rarely applied to the selective oxidation reactions for organic synthesis. The oxidation behaviour of many substrates including alcohols and hydrocarbons towards heterogeneous catalysts-activated PMS is still unknown. This provides opportunities to expand the application of carbo-catalysis activated PMS to selective oxidation reactions through the engineering of reaction method and catalyst design.

1.2 Research Objectives

This thesis aims to enable the selective oxidation of substrates such as alcohols and hydrocarbons to yield the industrial demanding products by carbo-catalysts activated PMS oxidant. This research dedicates to both the development of highly efficient carbo-catalysis and the insight into the mechanism of the catalysis and oxidation behaviour. The specific objectives of this thesis include:

- To investigate the feasibility of liquid phase selective oxidation with catalytic activated PMS using benzyl alcohol and carbon nanotube as the benchmark alcohol reactant and carbo-catalyst;
- To optimise the reaction method for selective oxidation by studying the effects of solvent, temperature, reaction time, catalyst loading and reactant concentration on the product yield and selectivity;
- To develop novel carbo-catalysts with advanced activity in PMS activation;

- To reveal the reaction mechanism of the catalytic activation of PMS and the subsequent selective oxidation;
- To unveil the effect of different heteroatoms on the catalytic performance of the carbo-catalysts;
- To identify the effect of different reaction pathways (radical and non-radical routes) towards the reaction efficiency and selectivity;
- To exhibit the reaction behaviour of different reactants (alcohols and hydrocarbons) towards the carbo-catalyst/PMS system.

1.3 Thesis Outline

This thesis contains seven chapters according to the specific objectives as listed above. Each chapter is outlined below:

Chapter 1: Introduction

This chapter outlines the current development of selective oxidation from the viewpoints of oxidants and catalysts, listing the advantages and shortcomings of the present reaction systems and the potential of applying catalytic activated PMS in selective oxidation. The objectives and thesis outlines are also presented.

Chapter 2: Literature review

This chapter introduces the typical liquid phase selective oxidation reactions with common research interest from the up-to-date literatures. The development of the reaction methodology of selective oxidation including oxidants and catalysts is provided. The catalytic activation of PMS is also summarised in this chapter.

Chapter 3: Understanding of oxidation behaviour of benzyl alcohol by peroxymonosulfate via carbon nanotubes activation

This chapter reports the pilot study of activated PMS oxidant in the selective oxidation of benzyl alcohol (BzOH) into benzaldehyde (BzH) with carbon nanotube (CNT) catalysts. The modified CNT and the optimized reaction conditions can induce the generation of proper concentrations of radicals from PMS and endow the selective oxidation of benzyl alcohol. The active sites for PMS activation are identified with experimental observations and DFT calculations.

Chapter 4: Tailoring collaborative N-O functionalities of graphene oxide for enhanced selective oxidation of benzyl alcohol

This chapter presents the N-doped graphene oxides (NGO) activating PMS for highly efficient oxidation of BzOH to BzH. The catalytic roles of pyridinic N and carbonyl functionalities as dual active sites are identified. The oxidation behaviour of BzOH and BzH in the oxidation reactions is also studied to gain in-depth understanding of the reaction process.

Chapter 5: Selective oxidation of alcohols by graphene-like carbon with electrophilic oxygen and integrated pyridinic nitrogen active sites

This chapter provides a metal-free synthesis method of N-doped graphene-like carbon and its catalytic activity in selective oxidation of different alcohols with activated PMS. The active sites and reaction mechanism are determined by designed experiments.

Chapter 6: Cobalt single atom catalysts on carbon supports for highly efficient selective oxidations with activated peroxymonosulfate

Part 1: Cobalt single atoms embedded in nitrogen-doped graphene for selective oxidation of benzyl alcohol by activated peroxymonosulfate

This part presents the synthesis of single atom catalyst with atomically embedded Co atoms on graphene support used as excellent catalyst for selective oxidation of BzOH with PMS. The atomically dispersed Co atoms are well characterized by sophisticated techniques. The chemically bonded Co atoms on graphene are robust active sites to activate PMS *via* both radical and non-radical sites.

Part 2: Atomically dispersed cobalt on graphitic carbon nitride as robust catalyst for selective oxidation of ethylbenzene by peroxymonosulfate

This part reports the successful synthesis of Co based single atom catalyst on carbon nitride. The Co atoms are coordinated with N atoms to form highly stable configurations to produce radicals from PMS which can induce the highly efficient oxidation of ethylbenzene into acetophenone.

Chapter 7: Conclusions and recommendations

This chapter summarises the major findings in this thesis and recommendations for further research related to this area.

References

1. Guo, Z.; Liu, B.; Zhang, Q.; Deng, W.; Wang, Y.; Yang, Y., Recent advances in heterogeneous selective oxidation catalysis for sustainable chemistry. *Chem. Soc. Rev.* **2014,** *43* (10), 3480-3524.

2. Davis, S. E.; Ide, M. S.; Davis, R. J., Selective oxidation of alcohols and aldehydes over supported metal nanoparticles. *Green Chem.* **2013,** *15* (1), 17-45.

3. Sheng, S. D.; Guodong, W.; Shuchang, W.; Feng, P.; Robert, S., Carbocatalysis in Liquid-Phase Reactions. *Angew. Chem. Int. Ed.* **2017,** *56* (4), 936-964.

4. Christof, A.; Christophe, G.; Ive, H., Aerobic Alcohol Oxidations Mediated by Nitric Acid. *Angew. Chem. Int. Ed.* **2011,** *50* (51), 12355-12360.

5. Borah, P.; Ma, X.; Nguyen, K. T.; Zhao, Y., A Vanadyl Complex Grafted to Periodic Mesoporous Organosilica: A Green Catalyst for Selective Hydroxylation of Benzene to Phenol. *Angew. Chem. Int. Ed.* **2012,** *51* (31), 7756-7761.

6. Xie, R.; Fan, G.; Yang, L.; Li, F., Hierarchical flower-like Co–Cu mixed metal oxide microspheres as highly efficient catalysts for selective oxidation of ethylbenzene. *Chem. Eng. J.* **2016,** *288*, 169-178.

7. Grigoropoulou, G.; Clark, J. H.; Elings, J. A., Recent developments on the epoxidation of alkenes using hydrogen peroxide as an oxidant. *Green Chem.* **2003,** *5* (1), 1-7.

8. Kesavan, L.; Tiruvalam, R.; Rahim, M. H. A.; bin Saiman, M. I.; Enache, D. I.; Jenkins, R. L.; Dimitratos, N.; Lopez-Sanchez, J. A.; Taylor, S. H.; Knight, D. W.; Kiely, C. J.; Hutchings, G. J., Solvent-Free Oxidation of Primary Carbon-Hydrogen Bonds in Toluene Using Au-Pd Alloy Nanoparticles. *Science* **2011,** *331* (6014), 195.

9. Parmeggiani, C.; Matassini, C.; Cardona, F., A step forward towards sustainable aerobic alcohol oxidation: new and revised catalysts based on transition metals on solid supports. *Green Chem.* **2017,** *19* (9), 2030-2050.

10. Bianco, A.; Chen, Y.; Frackowiak, E.; Holzinger, M.; Koratkar, N.; Meunier, V.; Mikhailovsky, S.; Strano, M.; Tascon, J. M. D.; Terrones, M., Carbon science perspective in 2020: Current research and future challenges. *Carbon* **2020,** *161*, 373-391.

11. Su, D. S.; Perathoner, S.; Centi, G., Nanocarbons for the Development of Advanced Catalysts. *Chem. Rev.* **2013,** *113* (8), 5782-5816.

12. Hussain, H.; Green, I. R.; Ahmed, I., Journey Describing Applications of Oxone in Synthetic Chemistry. *Chem. Rev.* **2013,** *113* (5), 3329-3371.

13. Duan, X.; Sun, H.; Wang, S., Metal-Free Carbocatalysis in Advanced Oxidation Reactions. *Acc. Chem. Res.* **2018,** *51* (3), 678-687.

14. Duan, X.; Sun, H.; Shao, Z.; Wang, S., Nonradical reactions in environmental remediation processes: Uncertainty and challenges. *Appl. Catal. B-Environ.* **2018,** *224*, 973-982.

Chapter 2 Literature Review

2.1 Introduction

Selective oxidation is one of the most important processes in chemical industry, producing millions of tons of intermediates for the manufacture of fine chemicals and diverse commodities. Selective oxidation, or artificial partial oxidation, is the second largest industrial reactions following polymerization.[1] Due to the increasing demand of the widely used products of selective oxidation, immense research has been devoted to this area since the latter part of last century. A crucial objective for selective oxidation study is to pursue greener and more sustainable reaction processes. The basis is on the engineering of the oxidation system with mild conditions, facile operation, cost-effective and clean oxidants, and catalysts that are highly efficient, environmentally benign, and easily recyclable. Beyond that, the selectivity of the oxidation system is also a major concern, aiming to avoid over-oxidizing the product into the undesired CO_2, to satisfy the requirement of green chemistry. Liquid phase selective oxidation includes various industrial relevant processes, such as the selective oxidation of alcohols, aromatic hydrocarbons, epoxidation of olefins, etc.[2] The use of stoichiometric noxious oxidants such as sodium bromate, dichromate, lead tetraacetate and permanganate still exists in the industrial synthesis of fine chemicals,[3] which inevitably produces a great amount of non-recyclable wastes and by-products. Metal-based catalysts can afford high activity and high selectivity towards the target products. Nevertheless, homogeneous catalysts cause separation and recycling problems, and heterogeneous catalysts suffer from metal leaching, deactivation or high cost of the noble metals.

Carbo-catalysts, dominantly composed of the earth-abundant element C, are among the most promising non-metallic catalysts which undergo fast development in the

recent decades. Nanocarbon materials are increasingly used in various catalytic reactions owing to the nanoscale features with tailored functional properties.[4] In liquid phase selective oxidations, the process-tailored carbo-catalysts cast very dynamic and active performances. The modification of nanocarbon catalysts with heteroatoms-doping and structure engineering enables their successful application in activating most of the oxidants, such as oxygen gas, hydrogen peroxide and *tert*-butyl hydroperoxide, which are the most frequently used oxidants in recent research of liquid phase selective oxidations. Besides, carbo-catalysts are extensively employed in the activation of peroxymonosulfate (PMS) to deliver highly oxidizing reaction system for the degradation of organic contaminants in wastewater, based on the proposed radical or non-radical oxidation mechanism. Though PMS has already been reported to endow the liquid phase selective oxidation reactions, however, PMS reacts with homogeneous additive chemicals such as ketones or halides to form the actual oxidizing species like dioxirane or hypohalous acid. The direct use of heterogeneously catalyzed PMS in selective oxidation can simplify the reaction process and get rid of the homogeneous additives, but this practice has scarcely been performed.

This chapter contains the basic knowledge of selective oxidation reactions, dominantly focusing on the C-H bond activation in hydrocarbons and selective oxidation of alcohols (section 2.2). These two reactions are investigated as benchmark reactions in the next chapters for the pilot study of catalytic activated PMS in liquid phase selective oxidations. The oxidants and catalysts for liquid phase selective oxidations are summarised (section 2.3). In addition, the catalytic activation of PMS is reviewed (section 2.4). In the end, the potential of applying carbo-catalysis activated PMS in selective oxidation reactions is outlined.

2.2 Liquid phase selective oxidation

The liquid phase selective oxidations cover a broad range of reactions with diverse

oxidation substrates.[5] This section introduces two major kinds of reactions, namely the selective oxidation of alcohols into aldehydes/ketones and the C-H bond activation in hydrocarbons.

2.2.1 Selective oxidation of alcohols

Selective conversion of alcohols to produce aldehydes or ketones is a fundamental liquid phase selective oxidation reaction.[6] The products are highly valued precursors in the manufacture of pharmaceuticals, dyes, perfumes and plastic additives. The partial oxidation of primary alcohols will generate aldehydes and the selective oxidation of secondary alcohols can produce ketones. In this part, several classes of alcohols of both academic and industrial interest are selected as illustrative examples to provide a brief concept of the current development of the selective oxidation of alcohols.

2.2.1.1 Benzyl alcohol

Benzyl alcohol (BzOH) is a reactive aromatic alcohol and its oxidation into benzaldehyde (BzH) has been extensively investigated as a model reaction of liquid phase selective oxidation. The oxidation process of BzOH is depicted in Figure 2-1(1). BzOH oxidation has frequently been used to probe the efficiency of catalysts because the reaction produces very limited by-products as the structure of BzH is free from enolization. Therefore, in most of the reactions only BzH and benzoic acid are detected as organic products. Both O_2 and liquid peroxides are adopted to accomplish the selective oxidation of BzOH. Interestingly, the BzH selectivity is high in most of the reported studies by O_2 with very little benzoic acid formed, even though BzH is highly oxidisable and readily suffers from autoxidation at ambient temperature.[7] Sankar *et al*. explained this paradox with designed experiments and electron paramagnetic resonance (EPR) techniques, showing that the presence of BzOH even at very low concentration, could effectively prevent the oxidation of BzH.[7] This is because the α–

H in BzOH is very active towards radicals while the BzH oxidation is a radical based chain reaction, thus the unreacted BzOH performs as an inhibitor to intercept the autooxidation of BzH. A broad variety of reaction systems have been developed for the highly efficiency oxidation of BzOH, and the highest reported BzH yield reached 99%.[8]

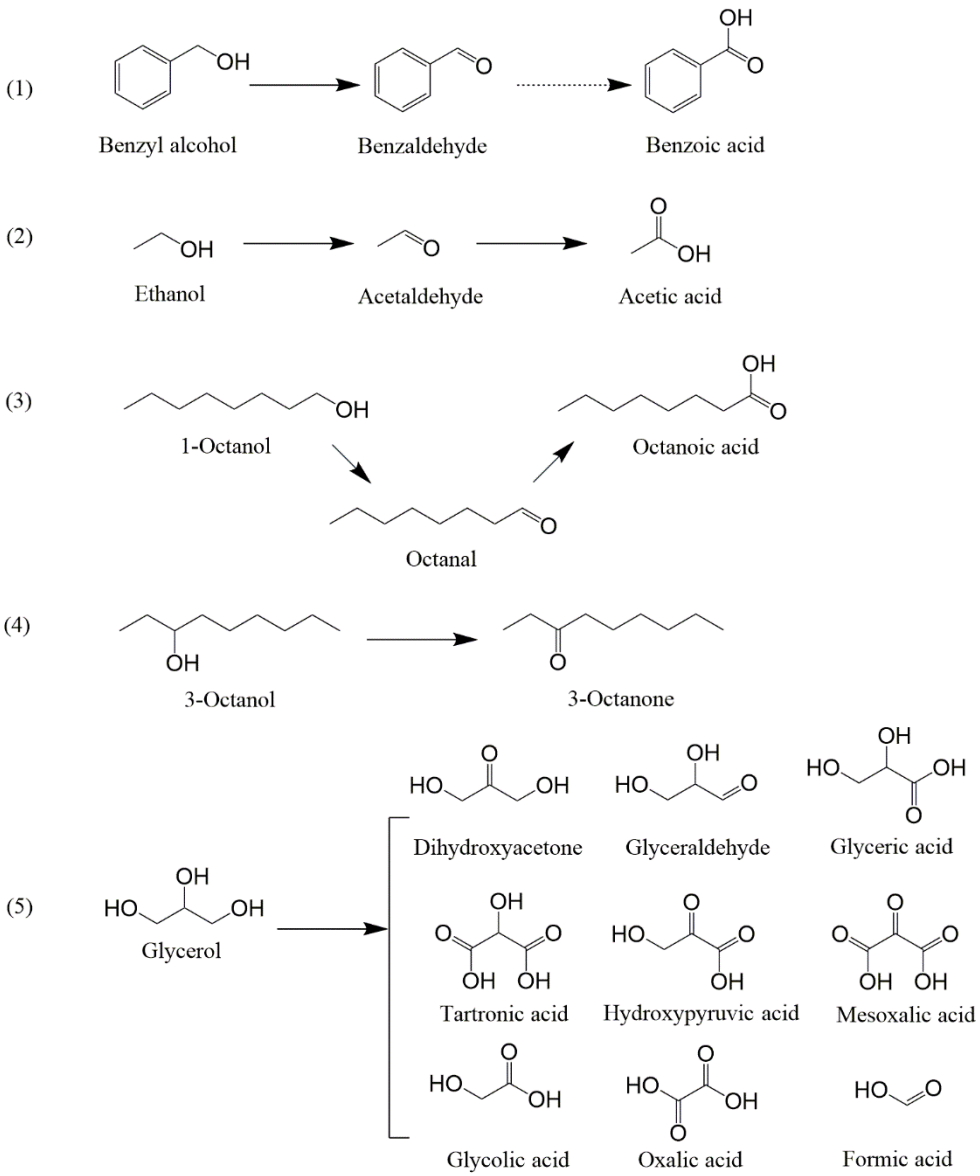

Figure 2-1 Scheme of selective oxidation of typical alcohols.

2.2.1.2 Ethanol & Octanol

Ethanol and octanol are two of the most explored aliphatic alcohols. Ethanol is an abundant liquid fuel produced from biomass. The oxidation of ethanol, as displayed in Figure 2-1(2), could yield acetic acid which are building blocks for the manufacture of synthetic fabrics and fibers, and the synthesis of vinyl acetate. In addition to acetic acid as the dominant products, a series of by-products are also detected during the oxidation of ethanol, including acetaldehyde, ethyl acetate and CO_2. The existence of acetaldehyde confirms that the acetaldehyde is the intermediate during the formation of acetic acid. A 95% acetic acid yield could be obtained over Au/TiO_2 catalysts with O_2 as reported by Jorgensen *et al*.[9] Studies indicate that the composition of products is tunable by adjusting the reaction conditions, for instance, increasing the ethanol concentration will facilitate the generation of ethyl acetate.

The selective oxidation of octanol includes primary 1-octanol and secondary 3-octanol (Figure 2-1(3) and (4)). The oxidation of 1-octanol can lead to the formation of octanal and octanoic acid while the oxidation of 3-octanol produces 3-octanone. Compared with ethanol, octanol is less active to be oxidized and the conversion of octanol is usually low. Therefore, this reaction can be used to evaluate the advanced catalytic performance of catalysts, such as precious metal-based catalysts.[10] The addition of base, e.g., NaOH, is speculated to enable the H extraction and thus can improve the reaction rate, whereas the reaction cannot occur at low temperature without base additives.[10-11] For the oxidation of 1-octanol, the added base can also alter the product composition, leading to higher selectivity towards octanoic acid.[10]

2.2.1.3 Glycerol

Glycerol is the major by-product during the production of biodiesel and is produced in large scale. However the use of raw glycerol from biodiesel is limited and the selective oxidation of glycerol into its higher valued derivatives is highly favoured in the biodiesel economics. Glycerol contains three hydroxyl groups, resulting in a series of products according to different oxidation level as presented in Figure 2-1(5).[12] Due to

this, glycerol is used as a model chemical with poly alcohols in one molecule for the study of the complex oxidation processes. There are two primary alcohol groups and one secondary alcohol group in one glycerol molecule, hence the oxidation of glycerol can derive aldehydes, ketones and acids (glyceraldehyde, dihydroxyacetone and glyceric acid). Furthermore, the cleavage of C-C bond may also occur in the oxidation, leading to the formation of glycolic acid, oxalic acid and formic acid. The oxidation extent of glycerol heavily relies on the catalysts and reaction conditions, especially the pH value of the oxidation environment greatly influences the selectivity of products.

2.2.2 Selective oxidation of C-H bonds

Activation of C-H bonds in hydrocarbons to produce alcohols or ketones is of great importance in petroleum industry, especially for the industrial production of synthetic resin, fiber and rubber. Owing to the high activation energy of the inert C-H bond, the oxidation of hydrocarbon is usually performed at harsh conditions, and the over-oxidation is easy to happen to produce CO_2. Therefore, hydrocarbon oxidation *via* selective functionalization is among the most challenging tasks in chemical industry. For catalytic oxidation of hydrocarbons, it has been widely accepted that the oxidation occurs *via* radical chain reactions, and the key step is the activation of oxidants by catalysts. In this section, three hydrocarbons are taken as examples for the description of the C-H bond activation.

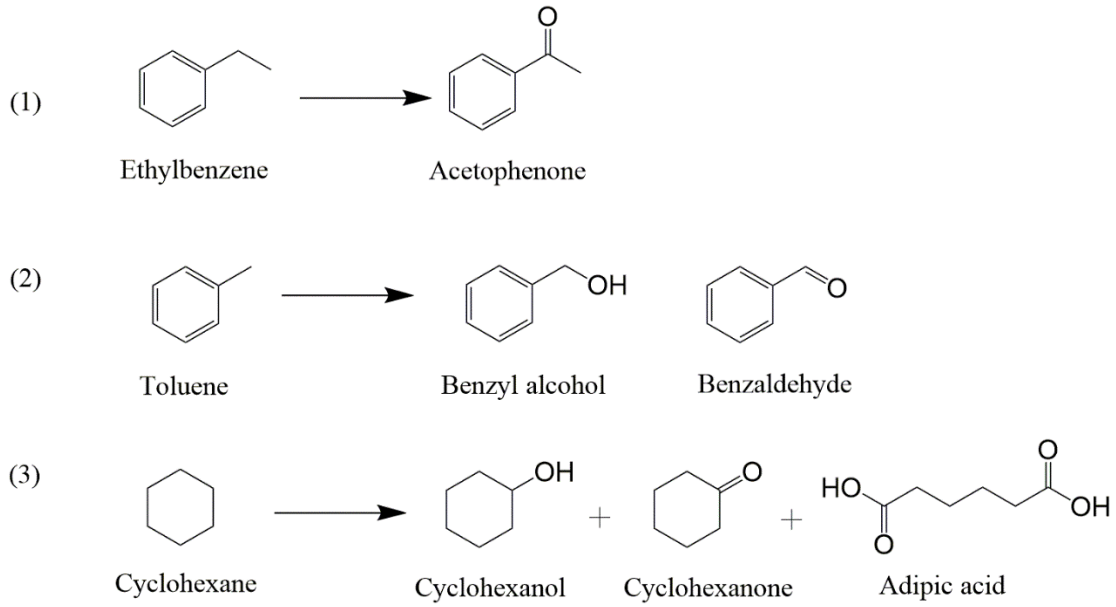

Figure 2-2 Scheme of selective oxidation of typical hydrocarbons.

2.2.2.1 Ethylbenzene

Ethylbenzene is a relatively active aromatic hydrocarbon compared with the other stubborn hydrocarbons. The α-C–H bond in ethylbenzene is easier to be activated than the β-C–H bond. Therefore, the activation of ethylbenzene molecules usually happens at the benzylic α-C–H bond, forming benzylic radicals by the activated oxidizing species and making acetophenone the dominant product in ethylbenzene oxidation reactions (Figure 2-2(1)). Homogeneous catalysis and heterogeneous catalysis by metal-catalyst and carbon-based catalysts have been reported for ethylbenzene oxidation. For O_2 based oxidation, high temperature and pressure are normally required to gain a moderate reaction rate.[13] Environmentally benign liquid peroxides are also frequently reported for the oxidation of ethylbenzene and presented higher efficiency than O_2 operated at milder conditions.[14]

2.2.2.2 Toluene

Toluene is another alkyl-substituted arene and is the most important aromatic hydrocarbon. The selective oxidation of toluene can produce benzyl alcohol or benzaldehyde as seen in Figure 2-2(2). Industrial oxidation of toluene relies on the use of heavy metal catalysts and the reaction is performed at temperatures higher than 200 ºC. The reported toluene oxidation with strong oxidants such as H_2O_2 is also conducted at high temperature (e.g., 150 ºC).[15] Furthermore, the extent of toluene oxidation is hard to control, easily leading to the over-oxidation product of benzoic acid rather than the desired benzyl alcohol and benzaldehyde.[16] Therefore, in order to attain high selectivity towards benzyl alcohol or benzaldehyde, the toluene conversion is kept at a low level. The highly efficient, selective, and environmentally benign process of toluene oxidation is still demanded.

2.2.2.3 Cyclohexane

Cyclohexane is a typical cycloalkane. The yielded products after selective oxidation include cyclohexanol, cyclohexanone and adipic acid, which are important materials for the fabrication of nylon polymers (Figure 2-2(3)). The aerobic oxidation of cyclohexane is often carried out at temperatures higher than 100 ºC *via* a radical chain autooxidation mechanism.[17] Homogeneous and heterogeneous transition metal-based catalysts are frequently adopted for liquid phase partial oxidation of cyclohexane. Like the other hydrocarbons, the major challenge for the selective oxidation of cyclohexane is the controllable synthesis of alcohol and ketone products instead of the further oxidation product of acid.[18]

2.3 Methodology of selective oxidation

The engineering of selective oxidation process towards higher reaction efficiency with mild condition, greener oxidants, and sustainable catalysts is never outdated in both industrial and academic perspectives. The evolution of oxidants and catalysts is at the

core of the development of liquid phase selective oxidations. With the increasing worldwide concern on environment protection, environmentally benign oxidants coupled with heterogeneous catalysts are highly valued by the researchers to replace the traditional homogeneous oxidation processes that heavily depend on toxic and expensive oxidants and catalysts. The oxidants include liquids (e.g., H_2O_2, TBHP), soluble solids (peroxymonosulfate, peroxydisulfate) and gases (e.g., O_2, O_3). The catalysts cover a broad variety of functional materials, from the soluble precious/transition metal complex with ligands, supported metal particles, to the metal-free carbo-catalysts. Basically, thermal heating is required as the only external energy input in liquid phase selective oxidations to accelerate the reaction activity. Sometimes additives or co-catalysts such as HNO_3 is introduced to obtain higher reaction efficiency.

In addition, photo-catalysis is also extensively studied for liquid phase selective oxidations, but it is beyond the scope of this chapter. This chapter focuses on the review of selective oxidations with thermal heating as the only extra energy.

2.3.1 Oxidants in selective oxidation

2.3.1.1 Conventional stoichiometric oxidants

Stoichiometric high-valent metal oxidants are usually used in liquid phase selective oxidation reactions. For instance, dichromate ($Cr_2O_7^{2-}$) and permanganate can be used for the selective oxidation of alcohols to aldehydes and ketones in both laboratory and industry scale.[19-20] These oxidants are highly active as oxygen donor for alcohols, even without catalysts. It's reported that 80% of BzH yield could be obtained from the selective oxidation of BzOH by $K_2Cr_2O_7$ at room temperature without solvent.[21] However a large amount of oxidant is needed by this means because of the high molecular mass of these oxidant, as well as producing hazardous wastes, especially the Cr containing wastes which are detrimental to the environment. Beyond that,

ruthenium- and osmium-based complexes could also serve as stoichiometric oxidants for the selective oxidation of different chemicals including aromatic hydrocarbons and alcohols.[22]

2.3.1.2 Liquid peroxides

Hydrogen peroxide and *tert*-butylhydroperoxide (TBHP) are also popular oxidants for liquid phase selective oxidation reactions, especially for the activation of stubborn hydrocarbons. Liquid peroxides could be easily activated to generate highly oxidizing radicals or other reactive oxidation species through the cleavage of peroxide bonds. In addition, the general temperatures for the oxidation with H_2O_2 and TBHP are relatively lower compared with that by O_2. For example, the oxidation of benzene into phenol was dominantly carried out with H_2O_2 to break the inertness of benzene. Borah *et al.* reported the activated H_2O_2 by vanadyl complex catalyst to oxidize benzene at 50 ºC.[23] H_2O_2 could form peroxo radicals on the vanadium active centres which served as the oxidizing species for the transformation of benzene into phenol as shown in Figure 2-3. In the view of green chemical process, H_2O_2 is the second-best oxidant following oxygen gas, producing only H_2O after the oxidation.

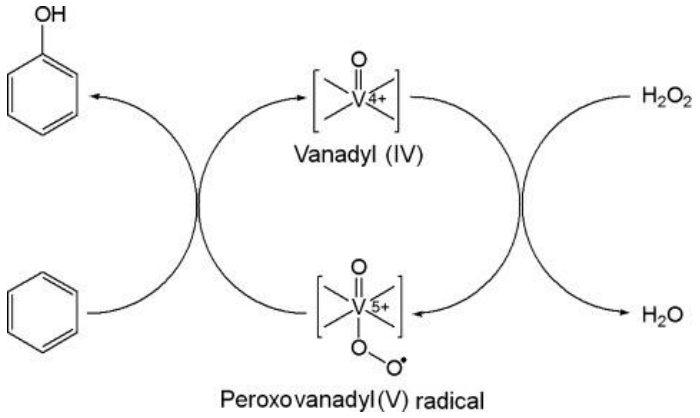

Figure 2-3 Proposed mechanism of benzene oxidation by activated H_2O_2 with vanadyl complex catalyst. Reprinted from ref.[23] with permission.

TBHP has been widely applied in the oxidation of both alcohols and hydrocarbons. TBHP has a weaker O-O bond than H_2O_2, thus it is easier to be activated to produce reactive oxidizing species.[3] However, the utilization of TBHP brings along the *tert*-butylalcohol as by-product. Xie *et al.* proposed the reaction mechanism of TBHP activated by dual metal-based catalyst (Co–Cu) to oxidize ethylbenzene *via* a radical based process.[14] The electron transfer between TBHP and metal led to the cleavage of the peroxide O-O bond and the generation of hydroxyl radicals and *tert*-butyl oxygen radicals which are responsible for the conversion of ethylbenzene into acetophenone, benzaldehyde and 1-phenylethanol. The major concern of using the liquid phase peroxides is the instability, which causes issues on transportation, storage and operation safety.

2.3.1.3 Oxygen

Directly using dioxygen for selective oxidation is among the most attractive research topics nowadays and is also a challenging task. Oxygen gas and air are absolutely clean and cost-effective oxidants free from environmental or healthy issues. Dioxygen molecule is paramagnetic with two unpaired electrons. The ground state O_2 is quite inactive, requiring thermal-catalytic activation to generate more reactive oxygen species. High reaction temperatures and noble metals are usually applied for its activation. This could be accomplished by introducing electrons to the oxygen molecules, forming superoxo radical ($O_2^{\bullet-}$) or peroxide species (O_2^{2-}) which has longer O-O bond and lower dissociation energy. Most of the selective oxidation reactions with oxygen are believed to involve radicals and endowed by radical chain reactions. Taking cyclohexane as an example, its oxidation by dioxygen is widely accepted to follow a radical chain autoxidation mechanism as depicted in Equations (2-1) and (2-2).[24-28] The CyOO· radicals abstract a H atom from cyclohexane (CyH) to form CyOOH. The remaining Cy· reacts with O_2 to form another CyOO· for the next reaction to continue the chain reaction. Numerous research efforts are dedicated to the design of catalysts in the perspectives of catalytic efficiency, cost, stability,

recyclability, etc.

$$CyOO\cdot + CyH \rightarrow CyOOH + Cy\cdot \qquad (2\text{-}1)$$

$$Cy\cdot + O_2 \rightarrow CyOO\cdot \qquad (2\text{-}2)$$

2.3.2 Catalytic activation of oxidants

2.3.2.1 Homogeneous catalysts

Homogeneous catalyzed oxidation reactions still occupy a considerable part in the chemical industry. Homogeneous catalysis can afford high reaction rate and selectivity, as well as high atomic efficiency because the catalyst and oxidation substrates are in the same phase and the catalysts are homogeneously dispersed in the solvent. The homogeneous catalysts are dominantly metal salts, metal complex with ligands and organometallic complexes. The use of metal salts usually requires basic or acidic environment, and the metal ions tends to aggregate. The metal complexes coordinated with ligands present much higher stability and the catalytic activity is less affected by the solvent.

A series of metals including both precious metals and transition metals are employed to form homogeneous catalysts, such as Pd,[29] Ru,[30] Cu,[31-32] Co[33] and Ni.[34] These catalysts are highly active in catalyzing the selective oxidation of alcohols and hydrocarbons by dioxygen and liquid peroxides. For example, Gao *et al.* reported that copper complex coordinated with zwitterionic calix[4]arene ligand could activate both O_2 and H_2O_2 for the selective oxidation of benzyl alcohol.[31] Co(III) complex with 2-pyridinecarboxamide ligands was able to deliver 70.4% ethylbenzene conversion and produce acetophenone with 90.2% selectivity by O_2.[33] Apart from the metal-based complex, metal-free organic catalysts have also been reported for the homogeneous

oxidation reactions. Yang *et al.* used 1,4-diamino-2,3-dichloro-anthraquinone (DACAQ), *N*-hydroxyphthalimide (NHPI) and HY as organic catalyst for the oxidation of ethylbenzene by O_2.[35]

The major drawbacks of homogeneous catalysis are the product separation and reusability/recyclability of catalyst. In addition, co-catalysts/additives such as NHPI and TEMPO are frequently required and the reactions are carried out under either acidic or basic solutions, restraining the further application. Therefore, heterogeneous catalysis has been the focus of research on liquid phase selective oxidation nowadays to develop economically and environmentally favourable processes.

2.3.2.2 Heterogeneous metal based catalysts

Numerous heterogeneous metal-based catalysts have been developed for liquid phase selective oxidation reactions.[6, 36] They can be classified into novel metal catalysts, transition metal catalysts and metal composites according to the types of the metal active sites. Most of the metal-catalysts are deposited on supporting materials, such as TiO_2, Al_2O_3, SiO_2 and carbon-based materials. The most frequently reported metals for liquid phase selective oxidation contain noble-metals Pd, Pt, Au and Ru, and transition metals Cu, Mn, Co, V and Cr.

Precious metals exhibit excellent catalytic activities towards many selective oxidation reactions, especially the selective oxidation of alcohols. The mechanism of primary alcohol oxidation over noble metals with O_2 oxidant is widely accepted to follow the steps illustrated in Figure 2-4.[1] Taking Pd catalyst as an example, the Pd atom is firstly inserted into the O-H bond of the target alcohol, forming a Pd-O-CH_2-R complex. Then the Pd centre abstract the H atom from alcohol by β-hydride elimination, generating aldehyde product. The dioxygen molecule reacts with the two H atoms to form H_2O and finalise the reaction cycle. Hutchings and co-workers have reported the successful application of noble metals supported on TiO_2 or carbon in selective oxidation of

primary alcohols,[37] toluene,[38] alkenes[39] and glycerol.[12, 40] Pd, Pt, Au and their alloys have been studied. They synthesized Au particles covered by Pd shells and found that the Au core could improve the selectivity of the Pd active sites due to the electronic effect.[37] This core-shell structure of Pd and Au metals have been further studied by Wang and co-workers with more detailed work.[41] Pt was also widely used in alcohol oxidations and exhibited higher catalytic activity than Pd in the selective oxidation of cyclic alcohols, but the aldehyde selectivity is relatively low, and the Pt(0) was easy to be oxidized into Pt(II) which might cause deactivation of the Pt active sites.[42] Au possesses lower catalytic activity than Pd, and base additives like K_2CO_3 are frequently used to attain a higher reactivity.[43] Supported Ru catalysts showed high efficiency in the oxidation of a wide range of alcohols by O_2, because of the multi-valence nature of Ru.[44] Yamaguchi *et al.* reported the highly selective oxidation of benzyl alcohol with over 99% benzaldehyde yield by Al_2O_3 supported Ru catalyst in 1 h under 1 atm O_2.[8]

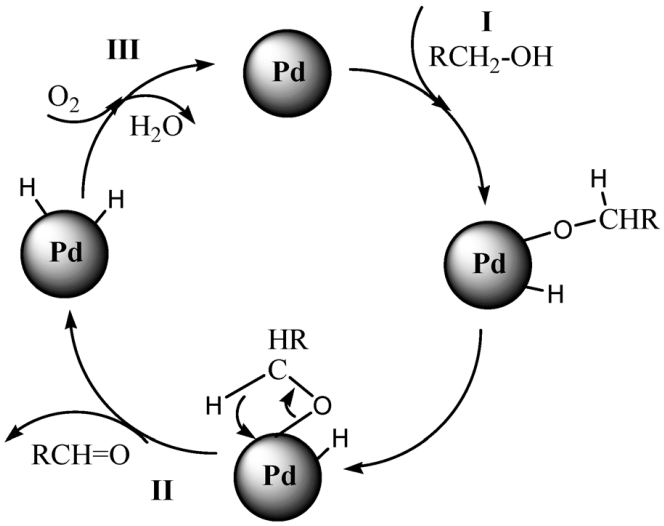

Figure 2-4 Reaction mechanism of selective oxidation of primary alcohol into aldehyde with Pd catalyst and dioxygen. Reprinted from ref.[1] with permission.

Transition metal-based catalysts normally present lower catalytic activity than noble metals, but they are cost-effective and earth-abundant, thus the development of highly active transition metal catalysts attracted vast research interest. For the oxidation of

alcohols and hydrocarbons over transition metal catalysts with O_2, a widely accepted mechanism is the Mars–van Krevelen model based on the variable valence of transition metal oxides.[45] As shown in Equations (2-3) and (2-4), the metal at high oxidation state is firstly reduced by the alcohol/hydrocarbon reactant. As a result, the lattice oxygen on metal is removed and the oxidation substrate is oxidized into the corresponding product. Secondly, the adsorbed H atoms are oxidized by O_2, regenerating the metal oxide active sites. Makwana *et al.* found that the benzyl alcohol oxidation was accomplished *via* the transformation between Mn^{2+} and Mn^{4+}, well fitting the Mars–van Krevelen mechanism.[46] For alcohol oxidation, it is reported that the crucial site for the dissociation of O-H bond is the oxygen vacancy on the transition-metal oxides located at either the edge site of a metal atom or between two metal atoms. Supported cobalt catalysts have been applied in the selective oxidation ethylbenzene to acetophenone by O_2. Ma *et al.* reported the Co(II)O stabilized on SBA-15 support to obtain 70% ethylbenzene conversion and 83.7% acetophenone selectivity at 150 ºC and 1 MPa O_2 without use of solvent.[47] Apart from the supported metal particle, attention was also paid on engineering the morphology of transition metal oxides. Feng *et al.* synthesized α-MnO_2 nanorods with high specific surface area (198 m^2/g) for selective oxidation of benzyl alcohol with 95% conversion and 99% benzaldehyde selectivity.[48] Other supported metal catalysts including Cu,[49] Cr,[50-51] Mn,[52] Fe[53] and V[54] also have been reported for heterogeneous selective oxidations with O_2 or H_2O_2 as oxidant.

$$M\text{-}O + Substrate\text{-}H_2 \rightarrow M + Substrate\text{-}O + 2H_{adsorbed} \qquad (2\text{-}3)$$

$$M + 2H_{adsorbed} + O_2 \rightarrow M\text{-}O + H_2O \qquad (2\text{-}4)$$

Though metal-based heterogeneous catalysts present advanced catalytic activity, there are still some inevitable drawbacks. Firstly, the high cost of noble metals and the toxicity of Co and Cr cause economic and environmental concerns. The metal active sites could suffer from aggregation or metal leaching during the reaction, which would

significantly reduce the amount of exposed reaction centres. In this sense, metal-free catalysts, especially functional carbon materials are promising substitute for metal-based catalysts.

2.3.2.3 Carbo-catalysts

Carbon is among the most earth-abundant elements and can form a broad variety of structures. A series of popular carbon materials such as active carbon, graphene, carbon nitride and carbon nanotubes (CNTs) are extensively used as supports to anchor metal particles or single metal atoms. Compared with the metal based supporting materials like TiO_2 and Al_2O_3, carbon materials possess higher specific surface area and better adaptability towards acidic or basic environments. In addition, carbon materials have shown inherent catalytic activity in many fundamental chemical reactions due to the tunable surface chemistry and specific electronic/thermal properties. In early 20th century, charcoal was found to have catalytic activity in aerobic selective oxidation reactions.[2] However, the disordered carbon structure has rather low catalytic activity. The recent decades have witnessed the rapid development of carbo-catalysis and a great deal of highly ordered nanoscale carbon materials with tailored functionalities have been reported.[4]

Among the ordered carbon materials, carbon nanotubes and graphene derived catalysts are the most frequently investigated ones. Both of them are composed of sp^2 hybridized carbon forming a honeycomb-like lattice structure. Graphene oxide (GO) can be produced by exfoliating graphite *via* the Hummers' method or modified Hummers' methods.[55] This process involves a large amount of corrosive oxidants, such as potassium permanganate, sodium nitrate and concentrated sulfuric acid. The derived GO is rich in defects and a wide range of oxygen functional groups. CNTs can be regarded as rolled tubes of graphene layers. CNTs are dominantly produced by chemical vapor deposition (CVD) method or pyrolization of biomass in the presence of metal catalysts. However, metal residuals could be confined inside the tubes even

after the acid purification, which may affect the determination of the origin of the catalytic activity. The modification of carbon materials mainly focused on heteroatom doping (oxygen, nitrogen, boron, sulfur, phosphorus) or engineering of morphology (creating defects, tube opening, etc.). The catalytic activity is usually attributed to the doped heteroatom active sites, defect sites and conjugated π-electrons. Besides, nanodiamond (ND) composed of sp^3 hybridized carbon can also be used in oxidation reactions. After high temperature annealing, the sp^3 hybridized ND can be transformed into a sp^2/sp^3 configuration and exhibits enhanced catalytic activity. In this part, the catalytic behaviour of metal-free carbon materials in liquid phase selective oxidation of alcohols and hydrocarbons will be introduced.

(1) Selective oxidation of alcohols

BzOH is the most frequently employed alcohol substrate catalyzed by carbon materials for the selective production of BzH. Kuang *et al.* reported the highly efficient BzOH oxidation system employing both O_2 and HNO_3 as oxidants catalyzed with nanoshell carbon (NSC).[56] The NSC catalyst was prepared *via* pyrolization of mixed iron phthalocyanine and phenol resin. The selective oxidation was endowed with a non-radical process as illustrate in Figure 2-5. BzOH was oxidized by the adsorbed HNO_3 on the surface of the NSC catalyst, resulting in the formation of NO_2 and benzaldehyde. HNO_3 was subsequently regenerated from the oxidation of NO_2 by O_2. This reaction system could afford 96% BzOH conversion and 92% BzH selectivity at 90 ºC in 1,4-dioxane solvent. Based on this work, Peng and co-workers conducted similar oxidation reactions with CNT catalysts.[57] They proposed that the HNO_2 from decomposed HNO_3 was the actual oxidant for BzOH oxidation. Afterwards, Kuang *et al.* further developed a radical based BzOH oxidation using activated carbon catalyst, O_2, HNO_3 and nitroxide radicals (TEMPO) without solvent.[58] The alcohol was directly oxidized by nitroxide radicals. This system exhibited excellent efficiency in the oxidation of a variety of benzylic alcohols, delivering nearly 100% conversion and aldehyde selectivity. In these cases, the ultimate oxidant was O_2 and HNO_3 and TEMPO

performed as promoters for the oxidation of alcohols.

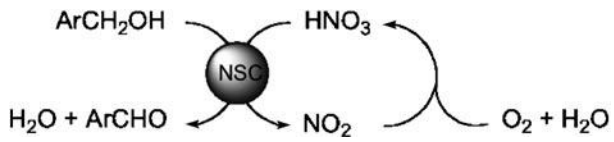

Figure 2-5 BzOH oxidation by O_2 and HNO_3 with NSC catalyst. Reprinted from ref.[56] with permission.

Bielawski and co-workers presented very interesting results on BzOH oxidation over GO. They were the first to report the BzOH oxidation with GO in the year of 2010, claiming that the GO produced from Hummers' method served as catalyst for the selective oxidation of BzOH into BzH with 92% yield, but the reaction was conducted with high catalysts loading (200 wt%) and high temperature (100 ºC) for 24 h.[59] They also carried out DFT calculations to unveil the reaction mechanism.[60] The oxidation of alcohol started with the transformation of H atom on alcohol to GO catalyst, leading to the formation of aldehyde. The GO catalyst could be re-oxidized by O_2 after the reaction. However, in 2018, Pumera *et al.* reported their finding and reclassified GO as a reagent rather than a catalyst in BzOH oxidation.[61] The GO was reduced after the reaction with a significant loss of oxygen groups, indicating that GO acted as the oxidant in the reaction. This highlighted the importance of correctly defining the catalytic role of carbo-catalysts to gain sophisticated understanding of the oxidation systems. Besides, another kind of graphene with homogeneously covered COOH groups, namely graphene acid, has also been reported for BzOH oxidation with HNO_3 or HNO_3/O_2.[62]

Luo *et al.* reported the BzOH oxidation by CNTs in the presence of high pressured O_2 (1.5 MPa).[63] They found that the carboxylic COOH groups were detrimental to the catalytic performance. The doped N atoms enhanced the reaction efficiency and the highest BzOH conversion of 44.7% with 94.1% selectivity to BzH were obtained. They proposed a radical-based mechanism presuming that the activation of O_2

molecules occurred on the surface of CNTs forming peroxide radicals for the oxidation of BzOH. Wang and co-workers demonstrated a nitrogen-doped graphene catalyst (NG) prepared by nitridation of GO with NH_3 gas at high temperature.[64] The NG catalyst could catalyze BzOH oxidation with 1 atm O_2, affording 12.8% conversion and 100% selectivity. The N species, particularly graphitic sp^2 N atoms were considered as the major active sites for the activation of O_2 molecules. The theoretical work conducted by Jeyaraj *et al.* also confirmed the pivotal role of graphitic N in activating O_2.[65] Watanabe *et al.* reported the oxidation of different alcohols including BzOH, cinnamyl alcohol and 5-(hydroxymethyl)-2-furaldehyde over graphitic N-doped active carbon (AC).[66] The catalyst was prepared by treating AC with hydrogen peroxide, followed by high temperature nitridation in NH_3 stream. The active sites were discovered by the correlation between the reaction activity and the N species on catalysts prepared at different conditions. X-ray photoelectron spectroscopy was employed to determine the composition of N species. They provided a possible reaction mechanism as shown in Figure 2-6. The activation of dioxygen molecules occurred on the adjacent carbon of the positively charged graphitic N and subsequently formed peroxide radicals to attack the BzOH molecules. After the generation of BzH, the N active sites were recovered for the next reaction cycle.

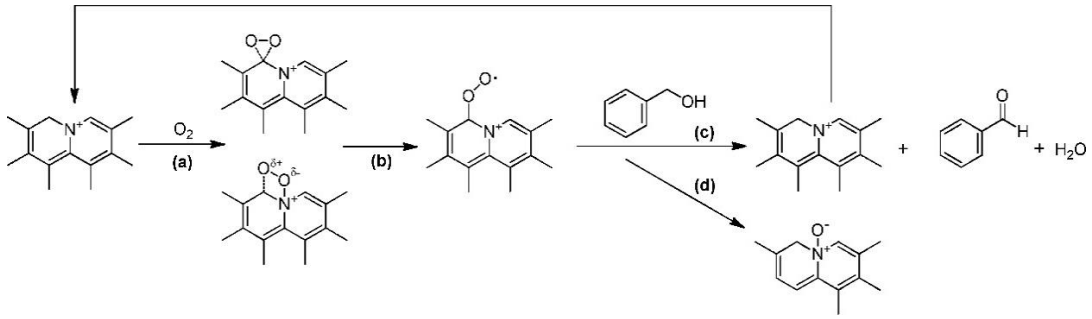

Figure 2-6 Proposed mechanism of BzOH oxidation by O_2 on N-doped active carbon catalyst. Reprinted from ref.[66] with permission.

Apart from the above carbo-catalysts endowed alcohol oxidation with O_2, some other carbon-based metal-free alcohol oxidation systems have been reported as well. Lin *et*

al. reported the N-doped annealed nanodiamond as effective catalyst for the selective oxidation of BzOH with activated TBHP.[67] The pyridinic N was regarded as active site to capture the H atom from BzOH with the assistant of radicals generated from TBHP. Patel *et al.* proposed a new mechanism of alcohol oxidation catalyzed by P-doped porous carbon with O_2.[68] The catalyst was synthesized by pyrolization of phytic acid and possessed high SSA (1200 m^2/g) due to the porous structure. The BzOH was coordinated with the P species as active sites to accomplish the selective oxidation reaction.

(2) Selective oxidation of hydrocarbons

Carbo-catalysts are extensively studied in C-H bond activation of hydrocarbons, such as the selective oxidation of cyclohexane and ethylbenzene. Compared with the alcoholic O-H groups, C-H bonds in hydrocarbons are more stable. Liquid peroxides such as TBHP are frequently used besides O_2. Bielawski and co-workers reported the application of GO as stoichiometric oxidant for the oxidation of aromatic hydrocarbons with 200 wt% to 800 wt% GO loading, similar to their reported work in alcohol oxidation.[69] CNTs without heteroatoms doping (containing only C and O elements) were found able to deliver 38.2% conversion of ethylbenzene with 60.9% selectivity of acetophenone by O_2.[13] A possible mechanism was raised, presuming that the delocalized π electrons of the catalysts could activate dioxygen, which subsequently attacked the ethylbenzene molecules to form radical intermediate and finally derived acetophenone. Li *et al.* reported aerobic toluene oxidation over mesoporous carbon nitride (g-C_3N_4) free from solvent.[15] They found the nanopores on g-C_3N_4 played the key role in selectively yielding benzaldehyde with over 99% selectivity. The nanocomposites consisted of graphene/g-C_3N_4 were reported as catalyst for the selective oxidation of a series of hydrocarbons with O_2 and the synergistic effect of graphene and g-C_3N_4 was identified.[70]

Some C-H oxidation reactions on carbo-catalysts shared similar active sites or reaction

mechanisms with the selective oxidation of alcohols, as in many cases the reaction process started with the activation of oxidants on the surface of carbon. N-doped graphene has been reported to oxidize aromatic hydrocarbons with high product yield by activated TBHP oxidant, and the N atoms induced charge redistribution of the adjacent C was responsible for the oxidation reaction.[71] A DFT study demonstrated that the OOH radical formed with the activated dioxygen impelled the oxidation.[72] Yu *et al.* reported the application of NCNT for the selective oxidation of cyclohexane with 1.5 MPa O_2 to obtain 45.3% conversion in 8 h.[27] The peroxide radicals were found crucial in the autooxidation chain reaction of cyclohexane, supported by another study using *in-situ* FTIR to probe the radicals.[73] Besides, the other carbon structures with N-doping have also been investigated, including ordered mesoporous carbon,[74-75] carbon nanofibers,[76] graphene-like carbon[77] and porous carbon beads[78] for the efficient selective oxidation of ethylbenzene with TBHP oxidant. The carbo-catalysts were prepared with pyrolysis method of carbon and nitrogen precursors. The morphological properties, such as the pore structures, high surface area and interconnection between the fibers have great impacts on the catalytic performances. Over 99% ethylbenzene conversion and acetophenone selectivity could be obtained with N-doped carbon nanofibers at 80 ºC.[76] Basically, the activated TBHP presented higher oxidation efficiency than dioxygen.

Besides oxygen and nitrogen, the roles of other heteroatoms including phosphorous, boron, fluorine and sulfur on carbo-catalysts have been tested as well. Wang *et al.* found that the B and F doped C_3N_4 showed much higher activity in the selective oxidation of cyclohexane to cyclohexanone by H_2O_2 than graphitic C_3N_4 with excellent stability.[79] They also reported another work demonstrating the superior catalytic activity of B-doped C_3N_4 against C_3N_4 in the selective oxidation of toluene and ethylbenzene in the presence of H_2O_2.[80] However, the B dopant in different compositions or substrates may lead to variable results. Cao *et al.* probed the individual effect of doped N, P, B atoms on CNTs on the catalytic performance in selective oxidation of cyclohexane with O_2.[81] The doped CNT catalysts were prepared by *in-*

situ CVD methods. It was found that the n-type heteroatom doping of N and P on CNTs was beneficial for the oxidation of cyclohexane, whereas the existence of the electron-deficient B was detrimental to the catalytic activity. Lu and co-workers synthesized N and S co-doped carbon nanospheres for the selective oxidation of ethylbenzene by TBHP.[82] The catalytic performance of co-doped catalyst surpassed the non-doping or N-doping only catalyst in ethylbenzene conversion.

Overall, carbon-based materials have been extensively investigated as sustainable catalysts, but there are still improvements to be made for their further application. For instance, the average catalytic efficiency of carbo-catalysts is still not comparable to metal-catalysts. Facile preparation of carbon materials is desired to avoid high cost and reduce the production of hazardous wastes. Sophisticated understanding of the relation between the chemistry/morphology of carbo-catalysts and their catalytic performances is required due to the complicated compositional and structural properties of carbon materials.

2.3.3 PMS in selective oxidation

Peroxymonosulfate (PMS, HSO_5^-), also called Caro's acid, was firstly discovered by Heinrich Caro. Its potassium salt combined with another two salts forms a stabilized oxidant named as Oxone ($2KHSO_5 \cdot KHSO_4 \cdot K_2SO_4$) and acts as a solid oxidant.[83] Compared with the other oxidants mentioned in section 2.3.1, oxone is environmentally benign, soluble, cheap and easy to handle. The oxidizing anion in oxone, PMS, has been applied in liquid phase selective oxidations, such as the C-H bond activation in hydrocarbons, the epoxidation of olefins, the oxidation of alcohols, etc. the chemical properties of PMS has been deeply explored for its potential use in synthetic organic chemistry. However, the reactions were carried out in homogeneous environments without catalysts. Instead, additives were introduced which could react with PMS to form the actual reactive oxidizing species for the selective oxidation. Ketones or halides were frequently employed as promoters to generate highly selective

oxidants for the target reactions. PMS can react with ketones and the produced dioxiranes are active for the oxidation of various hydrocarbons (Figure 2-7).[84-88] The reaction of PMS with halide salts such as NaBr could derive hypohalous acids (HBrO) which are more reactive than PMS to selectively convert alcohols into aldehydes.[89]

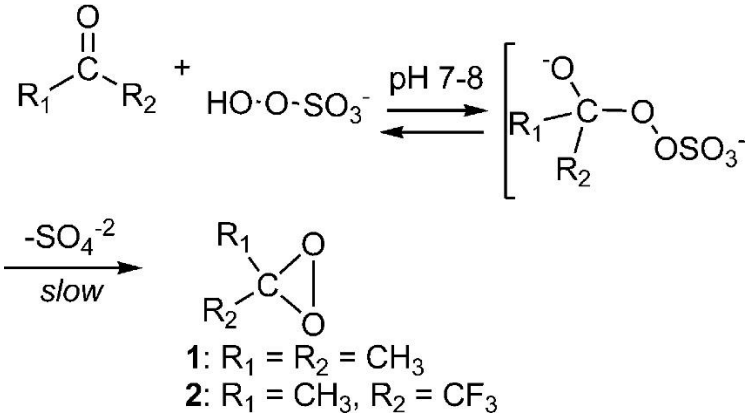

Figure 2-7 Reaction between ketone and PMS to generate dioxiranes. Reprinted from ref.[85] with permission.

Mello *et al.* reported the synthesis of methyl(trifluoromethyl)dioxirane from oxone as oxidant for the liquid phase selective oxidation of several hydrocarbons including cyclohexane and ethylbenzene.[90] The reactions were conducted at low temperature (-22 to 0 ºC) and were highly selective in yielding carbonyl compounds from hydrocarbons. A cyclohexanone selectivity of 99% and acetophenone selectivity of 95% were obtained in this reaction system. This reaction system has also been tested in the oxidation of aliphatic and aromatic alcohols.[91] For the oxidation of 1-phenylethanol, cyclohexanol and 3-octanol, over 98% selectivity towards their corresponding ketones was observed, whereas substantial amount of BzH and benzoic acid were produced in the oxidation of BzOH. The mechanism insight into the oxidation behaviour of dioxiranes was explored in the subsequent study, indicating that radical intermediates were involved in the long-time selective oxidations.[92-94]

Apart from the ketone additives, several organic iodine reagents have been reported to

react with PMS to produce oxidizing reactants. Thottumkara *et al.* reported that the *o*-iodoxybenzoic acid (IBX) generated from the reaction between PMS and 2-iodobenzoic acid could oxidize primary and secondary alcohols.[95] However, this reaction was prone to oxidize the primary alcohols into acids instead of aldehydes. Schulze *et al.* found that the addition of tetra-*n*-butylammonium sulfate (Bu_4NHSO_4) could tailor the reaction extent to selectively form aldehydes.[96] Another iodine agent, 2-iodoxybenzenesulfonic acid (IBS), prepared with PMS oxidized 2-iodobenzenesulfonic acid, also exhibited high ability for the selective oxidation of alcohols.[97-98]

Koo *et al.* reported that the addition of NaBr to PMS enabled the selective oxidation of BzOH with 87% BzH yield.[89] The reaction processes are depicted in Equations (2-5) and (2-6). PMS was activated by Br^- to form HOBr which directly reacted with BzOH to selectively generate BzH. The reaction was performed at room temperature in aqueous acetonitrile solvent. Without adding NaBr, the oxidation wouldn't occur, indicating that the inactivated PMS was not able to oxidize alcohols. Wissinger and co-workers employed NaCl as the promoter for alcohol oxidation with PMS.[99] NaCl played a similar role to NaBr by generating HOCl to oxidize borneol into camphor. $AlCl_3$ catalyzed PMS at room temperature has been adopted to the selective oxidation of a wide range of aliphatic and aromatic alcohols with high reactivity.[100] Nevertheless, the primary alcohols were completely oxidized into the corresponding acids rather than aldehydes.

$$HSO_5^- + Br^- \rightarrow HOBr + SO_4^{2-} \qquad (2\text{-}5)$$

$$PhCH_2OH + HOBr \rightarrow PhCH_2OBr \rightarrow PhCHO \qquad (2\text{-}6)$$

PMS could act as highly efficient oxidant for liquid phase selective oxidation reactions conducted at benign conditions, but it is currently applied in homogeneous systems reacting with soluble additives to generate the actual oxidizing species. The controlling

of the selectivity is still challenging to solely yield aldehydes instead of the further oxidized acid products in alcohol oxidation.[101] To the best of our knowledge, heterogeneous catalyst-activated PMS in organic synthesis still remains unexplored, which offers the potential to develop an alternative method for facile and sustainable selective oxidation reactions.

2.4 Catalytic activation of PMS

The catalytic activated PMS by both metal-based catalysts and metal-free carbo-catalysts has been extensively investigated in the recent years, focusing on the promising application of activated PMS in the degradation of aqueous contaminants.[102] With an asymmetry structure, PMS ($H\text{-}O\text{-}O\text{-}SO_3^-$) is prone to decompose by electron transfer and generate a variety of radicals including sulfate radicals and hydroxyl radicals, of which the $SO_4^{\bullet-}$ radicals possess a higher redox potential (2.5-3.1 V) and live longer than the $^{\bullet}OH$ radicals (2.7 V), thus $SO_4^{\bullet-}$ are reported more effective in the mineralization of organic pollutants.[103] Physical photolysis treatments of UV irradiation can facilitate the decomposition of PMS to generate radicals.[104-105] The catalytic activation of PMS is carried out under room temperatures or slightly heated environment. PMS could be catalyzed by homogeneous transition metals such as Co, Mn, Fe and Ni cations.[106-109] PMS activation is accomplished by the electron transfer between PMS and metals *via* the redox cycle. The transformation of $M^{n+}/M^{(n+1)+}$ enabled the cleavage of the O-O or O-H bond to generate $SO_4^{\bullet-}$ and $SO_5^{\bullet-}$ radicals. The basic routes of PMS decomposition *via* the electron transfer are elucidated in Equations (2-7) to (2-11).[103]

$$HSO_5^- + e^- \rightarrow {}^{\bullet}OH + SO_4^{2-} \qquad (2\text{-}7)$$

$$HSO_5^- + e^- \rightarrow OH^- + SO_4^{\bullet-} \qquad (2\text{-}8)$$

$$HSO_5^- - e^- \rightarrow H^+ + SO_5^{\bullet-} \qquad (2\text{-}9)$$

$$2SO_5^{\bullet-} \rightarrow {}^1O_2 + 2SO_4^{\bullet-} \quad (2\text{-}10)$$

$$OH^- + SO_4^{\bullet-} \leftrightarrow {}^{\bullet}OH + SO_4^{2-} \quad (2\text{-}11)$$

2.4.1 Heterogeneous metal catalysts

Both noble metals and transition metals present high ability for PMS activation. Lee and co-workers tested a wide range of different metal nanoparticles loaded on alumina and found that the noble metals such as Pt, Pd, Au, Ru and Rh outperformed the transition metals in the oxidation of trichlorophenol (TCP).[110-111] Pd turned out to be the most efficient metal for PMS activation while Ag exhibited the least activity among the noble metals. However, due to the high cost of noble metals, transition metals with satisfying capabilities of activating PMS have been studied more extensively. It was found that cobalt was superior to the other transition metals. The preparation of highly active heterogeneous Co catalysts received great research interest.[112-113] Fe, Cu and Mn are also widely tested metals.[114-116] The forms of the metal catalysts varies from zero valent metal,[117-118] metal oxides,[119-121] to supported metal oxides[122] and metal composites.[123-125] Anipsitakis *et al.* reported the PMS activation over cobalt oxide towards the oxidative degradation of 2,4-dichlorophenol (2,4-DCP).[126] The activation process of PMS on Co_3O_4 particles is depicted in Figure 2-8. The redox reaction between Co^{2+} and Co^{3+} induced the generation of radicals to attack the organic contaminants. Nevertheless, the metal leaching cannot be neglected for PMS involved oxidation reactions as the PMS solution is acidic. This issue is especially serious for the toxic Co cations. To reduce the metal-leaching, tremendous efforts were adopted to enhancing the coordination of Co species and the stabilized supporting substrates, such as molecular sieves, metal oxides, and carbon.[127-129] Some metal oxide supports could synergistically work with the metal active sites to activate PMS.[130] Carbon materials offered high SSA and abundant functionalities for the metal to attach on, and the delocalized π electrons of sp^2 carbon would facilitate the electron transfer.[131-132]

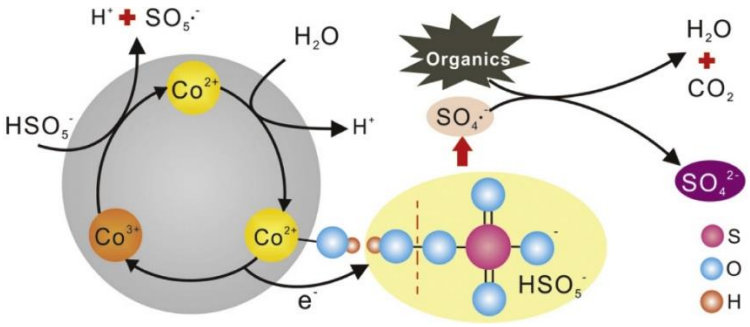

Figure 2-8 PMS activation over Co_3O_4 particle. Reprinted from ref.[133] with permission.

In addition to the insertion of metal particles on supports, some metal-containing carbon materials were in-situ synthesized *via* the pyrolysis of biomass. Special carbon morphologies such as CNTs were created by the metal salt catalysts and the metal residuals were confined with the carbon catalysts. The catalytic activity of the as prepared catalysts was originated from both the carbon structure and the metal residuals. Kang *et al.* reported that the Ni-containing bamboo-like CNTs and Mn-containing carbon nanosprings could destroy the organic pollutants and microplastics owing to the synergistic effects of the nanocarbon structure and the encapsulated metals.[134-135]

Beyond that, to stabilize the metal active sites and increase the atomic efficiency, single atom catalysts (SACs) are emerging to deliver exceptional high efficiency. Carbon materials are frequently selected as supports for the atomically dispersed metal atoms. The single metal atoms are chemically bonded with the substrate, basically coordinated with N atoms. The atomic utilization efficiency and stability of SACs are superior to the nanoparticles. Transition-metal based SACs (Cu, Fe, Co, etc.) have been reported to activate PMS for water treatment.[136-138]

2.4.2 Metal-free carbo-catalysts

Many carbon-based materials showed high activities in the heterogeneous activation

of PMS, which was particularly suitable for their application in water treatment to avoid the secondary pollution of the metal-leaching from the metal-based catalysts.[139-140] A broad range of carbo-catalysts have been tested for PMS activation showing diverse activities. Firstly, the plain carbon materials without complicated modification were studied. Sun *et al.* revealed the active role of reduced GO (rGO) to induce the generation of sulfate radicals from PMS to degrade several organic contaminants.[141] Subsequent experimental and DFT studies indicated that the surface carbonyl C=O groups were responsible for the breaking of peroxide O-O bond to produce $SO_4^{\bullet-}$.[142-143] The graphene edge and vacancies were more active than the inner plane. Besides the reactive radicals, non-radical based oxidation process could also occur during the PMS activation. Duan *et al.* discovered that the different composition of radical/non-radical oxidation pathways relied on the carbon structures.[144] CNTs and mesoporous carbon catalyzed oxidation was a radical process, while the defective graphene could induce a non-radical dominated oxidation pathway. High temperature annealed nanodiamonds have onion-like graphitic shells, offering a sp^2/sp^3 core-shell configuration. The pure nanodiamond could barely activate PMS due to the inert sp^3 hybridized carbon, while the graphene shell covered nanodiamond could endow both radical and non-radical oxidations with PMS.[145-146] The activity of radical/non-radical oxidation depended on the sp^2/sp^3 ratio of nanodiamond.

Nitrogen is the most frequently adopted heteroatom that could be facilely incorporated into the carbon frameworks and the N species played a crucial role in the catalytic activity of carbo-catalyst. It was reported that the N-doping on graphene could significantly enhance its ability to activate PMS.[147] Among the N species, graphitic N appeared to play a dominant role in the catalytic activation of PMS because it induced the charge redistribution of the adjacent C atoms.[148] The positively charged carbon around graphitic N on CNTs could adsorb the O-O bond in PMS to facilitate the direct oxidation through the electron transfer without the generation of radicals (non-radical oxidation). The radical and non-radical pathways over N-doped CNTs are elucidated in Figure 2-9. The pivotal role of N species in inducing non-radical activation of PMS

has also been confirmed by the other studies of N-doped graphene.[149-151] The capability of a non-radical oxidation by PMS also relies on charge density of the organic substrate which determines its adsorption behaviour on carbon catalysts. On the other side, the generated $SO_4^{\bullet-}$, $SO_5^{\bullet-}$ and $^{\bullet}OH$ radicals are highly oxidative to destroy the organics in the solvent. The non-radical oxidation process could be more selective than the radicals because its oxidative potential could be tuned by the catalyst modification to form a suitable adsorbed complex.

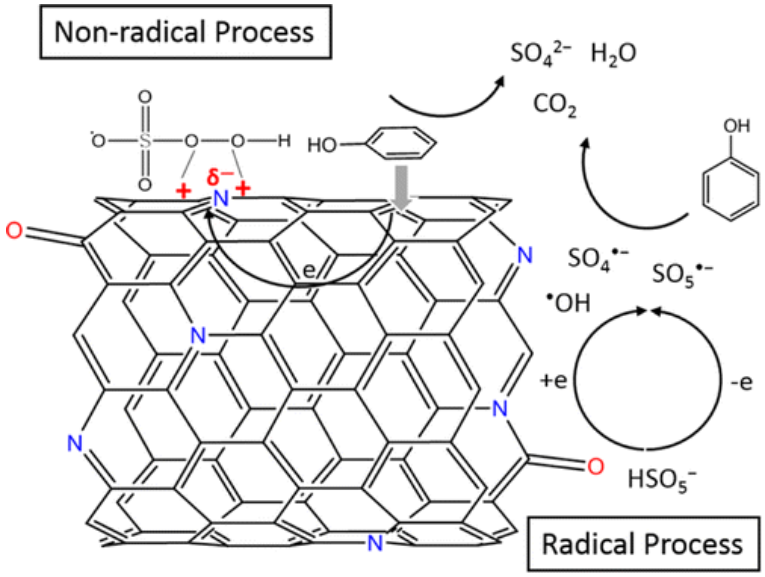

Figure 2-9 Radical and non-radical PMS activation over NCNT. Reprinted from ref.[148] with permission.

The doping effects of other elements on carbon materials for PMS activation have also been probed. It turned out that simply doping B, P and S atoms on graphene showed no apparent beneficial effect for activating PMS.[152] The performance of B-N co-doped graphene depended on the loading amount of boron. Trace amount of B could improve the catalytic activity of N-graphene, whereas higher B content could lead to a lower catalytic efficiency.[153] Duan *et al.* reported that the additional S doping on N-graphene could further enhance the catalytic activity of N-graphene because the S atoms could increase the spin density of the neighboring C (adjacent to N), thus enhancing the PMS

adsorption and activation.[154]

Despite of the immense investigations of heterogeneous catalytic activated PMS in the environmental remediation processes, little attention has been paid to its potential in organic synthesis. Furthermore, the mechanistic understanding of the PMS activation and the organic oxidation pathways with carbo-catalysts are not fully unveiled due to the complicated chemical and morphological nature of carbon materials. The identification of some reactive oxidation species is not convincing and contradictory among the literatures because of the limited techniques and knowledge.

2.5 Opportunities for carbo-catalysis in selective oxidation with PMS

Though the application of carbo-catalyzed PMS is focused on water remediation processes, aiming to mineralize the organic contaminants, this system is highly promising to be extended into the liquid phase selective oxidation reactions to produce high-valued fine chemicals. First of all, the oxidation *via* catalytic activated PMS is free from high temperature, high pressure and hazardous homogeneous additives. Oxone is more stable compared with the liquid peroxide oxidants, and cleaner than the heavy metal-based stoichiometric oxidants in the production of fine chemicals. Secondly, the multiple oxidation pathways enabled by activated PMS provide possibilities for its use in selective oxidation reactions, especially the non-radical processes which are milder and more selective than the radical ones.[155] Even though the free radicals are regarded as nonselective oxidizing species for aqueous contaminant degradation, the oxidation behaviour of radicals could be tuned by engineering of the reaction process. In the reported work, the PMS/organics ratio is usually high (e.g., PMS/phenol=30 mol/mol[147]) to establish highly oxidative environment for the mineralization of pollutants. By lowering the PMS dosage, the oxidation extent of organic chemicals by radicals could be controlled as many selective oxidation reactions are believed to undergo radical chain reactions. Thirdly, there are

still some debates against the mechanism understanding of the PMS activation over carbo-catalysts, especially the non-radical oxidation route due to the limited characterization techniques. Further study on the catalytic and oxidation behaviour of carbo-catalysts and organics with PMS is demanded. Finally, the use of catalytic activated PMS in selective oxidation will expand the fundamental knowledge of this reaction system and provide a new reaction strategy for liquid phase selective oxidation reactions.

2.6 Conclusions

The development of facile and environmentally benign strategies to carry out liquid phase selective oxidation reactions is always highly desired. In this chapter, the present methods for liquid phase selective oxidation reactions have been reviewed. The evolution of oxidants for selective oxidation starts from the hazardous stoichiometric heavy metals to liquid and gaseous clean oxidants. The heterogeneous carbo-catalysts possess advantages including sustainability, durability and recyclability compared with metal-based catalysts. Solid PMS oxidant could react with homogeneous promoters to generate oxidative species for selective oxidations, but the selectivity controlling remains an unsolved problem. This chapter also summarised the catalytic activation of PMS for the use in water remediation process. The catalytic activated PMS could oxidize organics under mild conditions without any homogeneous additives. Carbo-catalysts with tuned structure and surface chemistry could afford highly efficient activation of PMS and endow the mineralization of organic pollutants by both radical and non-radical pathways. Since there is little research on the feasibility of using heterogeneous catalyst-activated PMS in selective oxidation, the objective of this study is to probe the oxidation behaviour of alcohols and hydrocarbons over carbo-catalysts with activated PMS, thus providing an alternative route of liquid phase selective oxidation reactions.

References

1. Guo, Z.; Liu, B.; Zhang, Q.; Deng, W.; Wang, Y.; Yang, Y., Recent advances in heterogeneous selective oxidation catalysis for sustainable chemistry. *Chem. Soc. Rev.* **2014,** *43* (10), 3480-3524.

2. Sheng, S. D.; Guodong, W.; Shuchang, W.; Feng, P.; Robert, S., Carbocatalysis in Liquid-Phase Reactions. *Angew. Chem. Int. Ed.* **2017,** *56* (4), 936-964.

3. Hermans, I.; Spier, E. S.; Neuenschwander, U.; Turrà, N.; Baiker, A., Selective Oxidation Catalysis: Opportunities and Challenges. *Top. Catal.* **2009,** *52* (9), 1162-1174.

4. Su, D. S.; Perathoner, S.; Centi, G., Nanocarbons for the Development of Advanced Catalysts. *Chem. Rev.* **2013,** *113* (8), 5782-5816.

5. Fabrizio, C.; Henrique, T. J., Sustainability in Catalytic Oxidation: An Alternative Approach or a Structural Evolution? *ChemSusChem* **2009,** *2* (6), 508-534.

6. Davis, S. E.; Ide, M. S.; Davis, R. J., Selective oxidation of alcohols and aldehydes over supported metal nanoparticles. *Green Chemistry* **2013,** *15* (1), 17-45.

7. Sankar, M.; Nowicka, E.; Carter, E.; Murphy, D. M.; Knight, D. W.; Bethell, D.; Hutchings, G. J., The benzaldehyde oxidation paradox explained by the interception of peroxy radical by benzyl alcohol. *Nat. Commun.* **2014,** *5* (1), 3332.

8. Yamaguchi, K.; Mizuno, N., Supported Ruthenium Catalyst for the Heterogeneous Oxidation of Alcohols with Molecular Oxygen. *Angew. Chem. Int. Ed.* **2002,** *41* (23), 4538-4542.

9. Jørgensen, B.; Egholm Christiansen, S.; Dahl Thomsen, M. L.; Christensen, C. H., Aerobic oxidation of aqueous ethanol using heterogeneous gold catalysts: Efficient routes to acetic acid and ethyl acetate. *J. Catal.* **2007,** *251* (2), 332-337.

10. Prati, L.; Villa, A.; Campione, C.; Spontoni, P., Effect of gold addition on Pt and Pd catalysts in liquid phase oxidations. *Top. Catal.* **2007,** *44* (1), 319-324.

11. Dimitratos, N.; Villa, A.; Wang, D.; Porta, F.; Su, D.; Prati, L., Pd and Pt catalysts modified by alloying with Au in the selective oxidation of alcohols. *J. Catal.* **2006,** *244* (1), 113-121.

12. Carrettin, S.; McMorn, P.; Johnston, P.; Griffin, K.; Hutchings, G. J., Selective oxidation of glycerol to glyceric acid using a gold catalyst in aqueous sodium hydroxide. *Chem. Commun.* **2002,** (7), 696-697.

13. Jin, L.; Feng, P.; Hao, Y.; Hongjuan, W.; Wenxu, Z., Aerobic Liquid-Phase Oxidation of Ethylbenzene to Acetophenone Catalyzed by Carbon Nanotubes. *ChemCatChem* **2013,** *5* (6), 1578-1586.

14. Xie, R.; Fan, G.; Yang, L.; Li, F., Hierarchical flower-like Co–Cu mixed metal oxide microspheres as highly efficient catalysts for selective oxidation of ethylbenzene. *Chem. Eng. J.* **2016,** *288*, 169-178.

15. Li, X.-H.; Wang, X.; Antonietti, M., Solvent-Free and Metal-Free Oxidation of Toluene Using O2 and g-C3N4 with Nanopores: Nanostructure Boosts the Catalytic Selectivity. *ACS Catal.* **2012,** *2* (10), 2082-2086.

16. Guo, C.-C.; Liu, Q.; Wang, X.-T.; Hu, H.-Y., Selective liquid phase oxidation of toluene with air. *Appl. Catal. A-Gen.* **2005,** *282* (1), 55-59.

17. Conte, M.; Liu, X.; Murphy, D. M.; Whiston, K.; Hutchings, G. J., Cyclohexane oxidation using Au/MgO: an investigation of the reaction mechanism. *PCCP* **2012,** *14* (47), 16279-16285.

18. Schuchardt, U.; Cardoso, D.; Sercheli, R.; Pereira, R.; da Cruz, R. S.; Guerreiro, M. C.; Mandelli, D.; Spinacé, E. V.; Pires, E. L., Cyclohexane oxidation continues to be a challenge. *Appl. Catal. A-Gen.* **2001,** *211* (1), 1-17.

19. Lee, D. G.; Spitzer, U. A. J. T. J. o. O. C., Aqueous dichromate oxidation of primary alcohols. *The Journal of Organic Chemistry* **1970,** *35* (10), 3589-3590.

20. Menger, F. M.; Lee, C., Synthetically useful oxidations at solid sodium permanganate surfaces. *Tetrahedron Lett.* **1981,** *22* (18), 1655-1656.

21. Lou, J.-D.; Xu, Z.-N., Selective solvent-free oxidation of alcohols with potassium dichromate. *Tetrahedron Lett.* **2002,** *43* (49), 8843-8844.

22. Meyer, T. J.; Huynh, M. H. V., The Remarkable Reactivity of High Oxidation State Ruthenium and Osmium Polypyridyl Complexes. *Inorg. Chem.* **2003,** *42* (25), 8140-8160.

23. Borah, P.; Ma, X.; Nguyen, K. T.; Zhao, Y., A Vanadyl Complex Grafted to Periodic Mesoporous Organosilica: A Green Catalyst for Selective Hydroxylation of Benzene to Phenol. *Angew. Chem. Int. Ed.* **2012,** *51* (31), 7756-7761.

24. Hermans, I.; Jacobs, P. A.; Peeters, J., Understanding the autoxidation of hydrocarbons at the molecular level and consequences for catalysis. *J. Mol. Catal. A: Chem.* **2006,** *251* (1), 221-228.

25. Ive, H.; Lam, N. T.; A., J. P.; Jozef, P., Autoxidation of Cyclohexane: Conventional Views Challenged by Theory and Experiment. *ChemPhysChem* **2005,** *6* (4), 637-645.

26. Ive, H.; A., J. P.; Jozef, P., To the Core of Autocatalysis in Cyclohexane Autoxidation. *Chemistry* **2006,** *12* (16), 4229-4240.

27. Hao, Y.; Feng, P.; Jun, T.; Xiaowei, H.; Hongjuan, W.; Jian, Y.; Wenxu, Z., Selective Catalysis of the Aerobic Oxidation of Cyclohexane in the Liquid Phase by Carbon Nanotubes. *Angew. Chem.* **2011,** *123* (17), 4064-4068.

28. Shiraishi, Y.; Shiota, S.; Hirakawa, H.; Tanaka, S.; Ichikawa, S.; Hirai, T., Titanium Dioxide/Reduced Graphene Oxide Hybrid Photocatalysts for Efficient and Selective Partial Oxidation of Cyclohexane. *ACS Catal.* **2017,** *7* (1), 293-300.

29. Brink, G.-J. t.; Arends, I. W. C. E.; Sheldon, R. A., Green, Catalytic Oxidation of Alcohols in Water. *Science* **2000,** *287* (5458), 1636.

30. Bilgrien, C.; Davis, S.; Drago, R. S., The selective oxidation of primary alcohols to aldehydes by oxygen employing a trinuclear ruthenium carboxylate catalyst. *J. Am. Chem. Soc.* **1987,** *109* (12), 3786-3787.

31. Gao, J.; Ren, Z.-G.; Lang, J.-P., Oxidation of benzyl alcohols to benzaldehydes in water catalyzed by a Cu(II) complex with a zwitterionic calix[4]arene ligand. *J. Organomet. Chem.* **2015,** *792*, 88-92.

32. Hoover, J. M.; Ryland, B. L.; Stahl, S. S., Mechanism of Copper(I)/TEMPO-Catalyzed Aerobic Alcohol Oxidation. *J. Am. Chem. Soc.* **2013,** *135* (6), 2357-2367.

33. Qi, J.-Y.; Ma, H.-X.; Li, X.-J.; Zhou, Z.-Y.; Choi, M. C. K.; Chan, A. S. C.; Yang, Q.-Y., Synthesis and characterization of cobalt(iii) complexes containing 2-pyridinecarboxamide ligands and their application in catalytic oxidation of ethylbenzene with dioxygen. *Chem. Commun.* **2003,** (11), 1294-1295.

34. Morimoto, Y.; Bunno, S.; Fujieda, N.; Sugimoto, H.; Itoh, S., Direct Hydroxylation of Benzene to Phenol Using Hydrogen Peroxide Catalyzed by Nickel Complexes Supported by Pyridylalkylamine Ligands. *J. Am. Chem. Soc.* **2015,** *137* (18), 5867-5870.

35. Yang, G.; Ma, Y.; Xu, J., Biomimetic Catalytic System Driven by Electron Transfer for Selective Oxygenation of Hydrocarbon. *J. Am. Chem. Soc.* **2004,** *126* (34), 10542-10543.

36. Parmeggiani, C.; Matassini, C.; Cardona, F., A step forward towards sustainable aerobic alcohol oxidation: new and revised catalysts based on transition metals on solid supports. *Green Chemistry* **2017,** *19* (9), 2030-2050.

37. Enache, D. I.; Edwards, J. K.; Landon, P.; Solsona-Espriu, B.; Carley, A. F.; Herzing, A. A.;

Watanabe, M.; Kiely, C. J.; Knight, D. W.; Hutchings, G. J., Solvent-Free Oxidation of Primary Alcohols to Aldehydes Using Au-Pd/TiO_2 Catalysts. *Science* **2006,** *311* (5759), 362.

38. Kesavan, L.; Tiruvalam, R.; Rahim, M. H. A.; bin Saiman, M. I.; Enache, D. I.; Jenkins, R. L.; Dimitratos, N.; Lopez-Sanchez, J. A.; Taylor, S. H.; Knight, D. W.; Kiely, C. J.; Hutchings, G. J., Solvent-Free Oxidation of Primary Carbon-Hydrogen Bonds in Toluene Using Au-Pd Alloy Nanoparticles. *Science* **2011,** *331* (6014), 195.

39. Hughes, M. D.; Xu, Y.-J.; Jenkins, P.; McMorn, P.; Landon, P.; Enache, D. I.; Carley, A. F.; Attard, G. A.; Hutchings, G. J.; King, F.; Stitt, E. H.; Johnston, P.; Griffin, K.; Kiely, C. J., Tunable gold catalysts for selective hydrocarbon oxidation under mild conditions. *Nature* **2005,** *437* (7062), 1132-1135.

40. Carrettin, S.; McMorn, P.; Johnston, P.; Griffin, K.; Kiely, C. J.; Hutchings, G. J., Oxidation of glycerol using supported Pt, Pd and Au catalysts. *PCCP* **2003,** *5* (6), 1329-1336.

41. Wang, H.; Wang, C.; Yan, H.; Yi, H.; Lu, J., Precisely-controlled synthesis of Au@Pd core–shell bimetallic catalyst via atomic layer deposition for selective oxidation of benzyl alcohol. *J. Catal.* **2015,** *324*, 59-68.

42. Yamada, Y. M. A.; Arakawa, T.; Hocke, H.; Uozumi, Y., A Nanoplatinum Catalyst for Aerobic Oxidation of Alcohols in Water. *Angew. Chem. Int. Ed.* **2007,** *46* (5), 704-706.

43. Matsumoto, T.; Ueno, M.; Wang, N.; Kobayashi, S., Recent Advances in Immobilized Metal Catalysts for Environmentally Benign Oxidation of Alcohols. *Chemistry – An Asian Journal* **2008,** *3* (2), 196-214.

44. Yamaguchi, K.; Mori, K.; Mizugaki, T.; Ebitani, K.; Kaneda, K., Creation of a Monomeric Ru Species on the Surface of Hydroxyapatite as an Efficient Heterogeneous Catalyst for Aerobic Alcohol Oxidation. *J. Am. Chem. Soc.* **2000,** *122* (29), 7144-7145.

45. Khenkin, A. M.; Neumann, R., Low-Temperature Activation of Dioxygen and Hydrocarbon Oxidation Catalyzed by a Phosphovanadomolybdate: Evidence for a Mars–van Krevelen Type Mechanism in a Homogeneous Liquid Phase. *Angew. Chem. Int. Ed.* **2000,** *39* (22), 4088-4090.

46. Makwana, V. D.; Son, Y.-C.; Howell, A. R.; Suib, S. L., The Role of Lattice Oxygen in Selective Benzyl Alcohol Oxidation Using OMS-2 Catalyst: A Kinetic and Isotope-Labeling Study. *J. Catal.* **2002,** *210* (1), 46-52.

47. Ma, H.; Xu, J.; Chen, C.; Zhang, Q.; Ning, J.; Miao, H.; Zhou, L.; Li, X., Catalytic aerobic oxidation of ethylbenzene over Co/SBA-15. *Catal. Lett.* **2007,** *113* (3), 104-108.

48. Fu, X.; Feng, J.; Wang, H.; Ng, K. M., Morphological and structural evolution of α-MnO2 nanorods synthesized via an aqueous route through MnO4−/Mn2+ reaction. *J. Solid State Chem.* **2010,** *183* (4), 883-889.

49. Mondelli, C.; Ferri, D.; Grunwaldt, J.-D.; Ravasio, N.; Baiker, A., Redox properties of supported copper catalysts studied in liquid and gas phase by in situ ATR-IR and XAS. *Catal. Today* **2011,** *178* (1), 124-131.

50. Wu, G.; Wang, X.; Li, J.; Zhao, N.; Wei, W.; Sun, Y., A new route to synthesis of sulphonato-salen-chromium(III) hydrotalcites: Highly selective catalysts for oxidation of benzyl alcohol to benzaldehyde. *Catal. Today* **2008,** *131* (1), 402-407.

51. Lounis, Z.; Riahi, A.; Djafri, F.; Muzart, J., Chromium-exchanged zeolite (CrE-ZSM-5) as catalyst for alcohol oxidation and benzylic oxidation with t-BuOOH. *Appl. Catal. A-Gen.* **2006,** *309* (2), 270-272.

52. Nagashima, K.; Mitsudome, T.; Mizugaki, T.; Jitsukawa, K.; Kaneda, K., Creation of a high-valent manganese species on hydrotalcite and its application to the catalytic aerobic oxidation of alcohols. *Green Chemistry* **2010,** *12* (12), 2142-2144.

53. Mahyari, M.; Shaabani, A., Graphene oxide-iron phthalocyanine catalyzed aerobic oxidation of alcohols. *Appl. Catal. A-Gen.* **2014,** *469*, 524-531.

54. Chen, Y.; Chen, W.; Tang, Q.; Guo, Z.; Yang, Y.; Su, F., Aerobic Oxidation of Benzyl Alcohol over Activated Carbon Supported Manganese and Vanadium Catalysts: Effect of Surface Oxygen-Containing Groups. *Catal. Lett.* **2011,** *141* (1), 149-157.

55. Hummers, W. S.; Offeman, R. E., Preparation of Graphitic Oxide. *J. Am. Chem. Soc.* **1958,** *80* (6), 1339-1339.

56. Yongbo, K.; M., I. N.; Yuta, N.; Teruaki, H.; Masa-aki, K., Selective Aerobic Oxidation of Benzylic Alcohols Catalyzed by Carbon-Based Catalysts: A Nonmetallic Oxidation System. *Angew. Chem. Int. Ed.* **2010,** *49* (2), 436-440.

57. Luo, J.; Peng, F.; Yu, H.; Wang, H., Selective liquid phase oxidation of benzyl alcohol catalyzed by carbon nanotubes. *Chem. Eng. J.* **2012,** *204-206*, 98-106.

58. Yongbo, K.; Hodaka, R.; Yuta, N.; Teruaki, H.; Masa-aki, K., A Nitric Acid-Assisted Carbon-Catalyzed Oxidation System with Nitroxide Radical Cocatalysts as an Efficient and Green Protocol for Selective Aerobic Oxidation of Alcohols. *Adv. Synth. Catal.* **2010,** *352* (14-15), 2635-2642.

59. R., D. D.; Hong-Peng, J.; W., B. C., Graphene Oxide: A Convenient Carbocatalyst for Facilitating Oxidation and Hydration Reactions. *Angew. Chem.* **2010,** *122* (38), 6965-6968.

60. Boukhvalov, D. W.; Dreyer, D. R.; Bielawski, C. W.; Son, Y.-W., A Computational Investigation of the Catalytic Properties of Graphene Oxide: Exploring Mechanisms by using DFT Methods. *ChemCatChem* **2012,** *4* (11), 1844-1849.

61. Presolski, S.; Pumera, M., Graphene Oxide: Carbocatalyst or Reagent? *Angew. Chem. Int. Ed.* **2018,** *57* (51), 16713-16715.

62. Blanco, M.; Mosconi, D.; Otyepka, M.; Medveď, M.; Bakandritsos, A.; Agnoli, S.; Granozzi, G., Combined high degree of carboxylation and electronic conduction in graphene acid sets new limits for metal free catalysis in alcohol oxidation. *Chem. Sci.* **2019,** *10* (41), 9438-9445.

63. Luo, J.; Yu, H.; Wang, H.; Wang, H.; Peng, F., Aerobic oxidation of benzyl alcohol to benzaldehyde catalyzed by carbon nanotubes without any promoter. *Chem. Eng. J.* **2014,** *240*, 434-442.

64. Long, J.; Xie, X.; Xu, J.; Gu, Q.; Chen, L.; Wang, X., Nitrogen-Doped Graphene Nanosheets as Metal-Free Catalysts for Aerobic Selective Oxidation of Benzylic Alcohols. *ACS Catal.* **2012,** *2* (4), 622-631.

65. Jeyaraj, V. S.; Kamaraj, M.; Subramanian, V., Generalized Reaction Mechanism for the Selective Aerobic Oxidation of Aryl and Alkyl Alcohols over Nitrogen-Doped Graphene. *The Journal of Physical Chemistry C* **2015,** *119* (47), 26438-26450.

66. Watanabe, H.; Asano, S.; Fujita, S.-i.; Yoshida, H.; Arai, M., Nitrogen-Doped, Metal-Free Activated Carbon Catalysts for Aerobic Oxidation of Alcohols. *ACS Catal.* **2015,** *5* (5), 2886-2894.

67. Lin, Y.; Su, D., Fabrication of Nitrogen-Modified Annealed Nanodiamond with Improved Catalytic Activity. *ACS Nano* **2014,** *8* (8), 7823-7833.

68. Patel, M. A.; Luo, F.; Khoshi, M. R.; Rabie, E.; Zhang, Q.; Flach, C. R.; Mendelsohn, R.; Garfunkel, E.; Szostak, M.; He, H., P-Doped Porous Carbon as Metal Free Catalysts for Selective Aerobic Oxidation with an Unexpected Mechanism. *ACS Nano* **2016,** *10* (2), 2305-2315.

69. Jia, H.-P.; Dreyer, D. R.; Bielawski, C. W., C–H oxidation using graphite oxide. *Tetrahedron* **2011,** *67* (24), 4431-4434.

70. Li, X.-H.; Chen, J.-S.; Wang, X.; Sun, J.; Antonietti, M., Metal-Free Activation of Dioxygen by Graphene/g-C3N4 Nanocomposites: Functional Dyads for Selective Oxidation of Saturated Hydrocarbons. *J. Am. Chem. Soc.* **2011,** *133* (21), 8074-8077.

71. Yongjun, G.; Gang, H.; Jun, Z.; Zujin, S.; Yuanshuai, Z.; Sheng, S. D.; Jianguo, W.; Xinhe, B.; Ding, M., Nitrogen-Doped sp2-Hybridized Carbon as a Superior Catalyst for Selective Oxidation. *Angew. Chem. Int. Ed.* **2013,** *52* (7), 2109-2113.

72. Ricca, C.; Labat, F.; Russo, N.; Adamo, C.; Sicilia, E., Oxidation of Ethylbenzene to Acetophenone with N-Doped Graphene: Insight from Theory. *The Journal of Physical Chemistry C* **2014,** *118* (23), 12275-12284.

73. Yang, X.; Wang, H.; Li, J.; Zheng, W.; Xiang, R.; Tang, Z.; Yu, H.; Peng, F., Mechanistic Insight into the Catalytic Oxidation of Cyclohexane over Carbon Nanotubes: Kinetic and In Situ Spectroscopic Evidence. *Chemistry* **2013,** *19* (30), 9818-9824.

74. Wang, J.; Liu, H.; Gu, X.; Wang, H.; Su, D. S., Synthesis of nitrogen-containing ordered mesoporous carbon as a metal-free catalyst for selective oxidation of ethylbenzene. *Chem. Commun.* **2014,** *50* (65), 9182-9184.

75. Chen, A.; Yu, Y.; Wang, R.; Yu, Y.; Zang, W.; Tang, P.; Ma, D., Nitrogen-doped dual mesoporous carbon for the selective oxidation of ethylbenzene. *Nanoscale* **2015,** *7* (35), 14684-14690.

76. Huang, R.; Cao, C.; Liu, J.; Sun, D.; Song, W., N-Doped carbon nanofibers derived from bacterial cellulose as an excellent metal-free catalyst for selective oxidation of arylalkanes. *Chem. Commun.* **2019,** *55* (13), 1935-1938.

77. Hu, X.; Liu, Y.; Huang, H.; Huang, B.; Chai, G.; Xie, Z., Template-free synthesis of graphene-like carbons as efficient carbocatalysts for selective oxidation of alkanes. *Green Chemistry* **2020,** *22* (4), 1291-1300.

78. Wang, Z.; Jiang, Y.; Huo, H.; Hu, Y.; Xu, X.; Wang, P.; Yang, Y.; Lin, K., Synthesis of three-dimensional nitrogen doped meso/macroporous carbon beads for heterogeneous catalytic solvent-free oxidation of ethylbenzene. *Carbon* **2020,** *158*, 226-237.

79. Yong, W.; Jinshui, Z.; Xinchen, W.; Markus, A.; Haoran, L., Boron- and Fluorine-Containing Mesoporous Carbon Nitride Polymers: Metal-Free Catalysts for Cyclohexane Oxidation. *Angew. Chem. Int. Ed.* **2010,** *49* (19), 3356-3359.

80. Wang, Y.; Li, H.; Yao, J.; Wang, X.; Antonietti, M., Synthesis of boron doped polymeric carbon nitride solids and their use as metal-free catalysts for aliphatic C–H bond oxidation. *Chem. Sci.* **2011,** *2* (3), 446-450.

81. Cao, Y.; Yu, H.; Tan, J.; Peng, F.; Wang, H.; Li, J.; Zheng, W.; Wong, N.-B., Nitrogen-,

phosphorous- and boron-doped carbon nanotubes as catalysts for the aerobic oxidation of cyclohexane. *Carbon* **2013,** *57*, 433-442.

82. Liu, M.; Liu, Y.; Gao, Z.; Wang, C.; Ye, W.; Lu, R.; Zhang, S., Nitrogen and sulfur co-doped carbon nanospheres for highly efficient oxidation of ethylbenzene. *New J. Chem.* **2018,** *42* (19), 15962-15967.

83. Hussain, H.; Green, I. R.; Ahmed, I., Journey Describing Applications of Oxone in Synthetic Chemistry. *Chem. Rev.* **2013,** *113* (5), 3329-3371.

84. Edwards, J. O.; Pater, R. H.; Curclf, R.; Furia, F. D., ON THE FORMATION AND REACTIVITY OF DIOXIRANE INTERMEDIATES IN THE REACTION OF PEROXOANIONS WITH ORGANIC SUBSTRATES*. *Photochem. Photobiol.* **1979,** *30* (1), 63-70.

85. Curci, R.; D'Accolti, L.; Fusco, C., A Novel Approach to the Efficient Oxygenation of Hydrocarbons under Mild Conditions. Superior Oxo Transfer Selectivity Using Dioxiranes. *Acc. Chem. Res.* **2006,** *39* (1), 1-9.

86. Cassidei, L.; Fiorentino, M.; Mello, R.; Sciacovelli, O.; Curci, R., Oxygen-17 and carbon-13 identification of the dimethyldioxirane intermediate arising in the reaction of potassium caroate with acetone. *The Journal of Organic Chemistry* **1987,** *52* (4), 699-700.

87. Mello, R.; Fiorentino, M.; Sciacovelli, O.; Curci, R., On the isolation and characterization of methyl (trifluoromethyl) dioxirane. *The Journal of Organic Chemistry* **1988,** *53* (16), 3890-3891.

88. Murray, R. W.; Jeyaraman, R.; Mohan, L., Chemistry of dioxiranes. 4. Oxygen atom insertion into carbon-hydrogen bonds by dimethyldioxirane. *J. Am. Chem. Soc.* **1986,** *108* (9), 2470-2472.

89. Koo, B.-S.; Lee, C. K.; Lee, K.-J., OXIDATION OF BENZYL ALCOHOLS WITH OXONE® AND SODIUM BROMIDE. *Synth. Commun.* **2002,** *32* (14), 2115-2123.

90. Mello, R.; Fiorentino, M.; Fusco, C.; Curci, R., Oxidations by methyl(trifluoromethyl)dioxirane. 2. Oxyfunctionalization of saturated hydrocarbons. *J. Am. Chem. Soc.* **1989,** *111* (17), 6749-6757.

91. Mello, R.; Cassidei, L.; Fiorentino, M.; Fusco, C.; Huemmer, W.; Jaeger, V.; Curci, R., Oxidations by methyl(trifluoromethyl)dioxirane. 5. Conversion of alcohols into carbonyl compounds. *J. Am. Chem. Soc.* **1991,** *113* (6), 2205-2208.

92. Hull, L. A.; Budhai, L., Thermal decomposition of dimethyldioxirane. *Tetrahedron Lett.* **1993,** *34* (32), 5039-5042.

93. Dinoi, A.; Curci, R.; Carloni, P.; Damiani, E.; Stipa, P.; Greci, L., On the Reaction of Aminoxyls with Dioxiranes. *Eur. J. Org. Chem.* **1998,** *1998* (5), 871-876.

94. Glukhovtsev, M. N.; Canepa, C.; Bach, R. D., The Nature of the Transition Structure for the Oxidation of Alkanes with Dioxiranes. *J. Am. Chem. Soc.* **1998,** *120* (40), 10528-10533.

95. Thottumkara, A. P.; Bowsher, M. S.; Vinod, T. K., In Situ Generation of o-Iodoxybenzoic Acid (IBX) and the Catalytic Use of It in Oxidation Reactions in the Presence of Oxone as a Co-oxidant. *Org. Lett.* **2005,** *7* (14), 2933-2936.

96. Schulze, A.; Giannis, A., Oxidation of Alcohols with Catalytic Amounts of IBX. *Synthesis* **2006,** *2006* (02), 257-260.

97. Uyanik, M.; Akakura, M.; Ishihara, K., 2-Iodoxybenzenesulfonic Acid as an Extremely Active Catalyst for the Selective Oxidation of Alcohols to Aldehydes, Ketones, Carboxylic Acids, and Enones with Oxone. *J. Am. Chem. Soc.* **2009,** *131* (1), 251-262.

98. Uyanik, M.; Ishihara, K., Hypervalent iodine-mediated oxidation of alcohols. *Chem. Commun.* **2009,** (16), 2086-2099.

99. Lang, P. T.; Harned, A. M.; Wissinger, J. E., Oxidation of Borneol to Camphor Using Oxone and Catalytic Sodium Chloride: A Green Experiment for the Undergraduate Organic Chemistry Laboratory. *J. Chem. Educ.* **2011,** *88* (5), 652-656.

100. Wu, S.; Ma, H.; Lei, Z., AlCl3-catalyzed oxidation of alcohol. *Tetrahedron* **2010,** *66* (45), 8641-8647.

101. Tanaka, M.; Anan, K.; Demizu, Y.; Kurihara, M.; Doi, M.; Suemune, H., Side-Chain Chiral Centers of Amino Acid and Helical-Screw Handedness of Its Peptides. *J. Am. Chem. Soc.* **2005,** *127* (33), 11570-11571.

102. Lee, J.; von Gunten, U.; Kim, J.-H., Persulfate-Based Advanced Oxidation: Critical Assessment of Opportunities and Roadblocks. *Environmental Science & Technology* **2020,** *54* (6), 3064-3081.

103. Anipsitakis, G. P.; Dionysiou, D. D., Degradation of Organic Contaminants in Water with Sulfate Radicals Generated by the Conjunction of Peroxymonosulfate with Cobalt. *Environmental Science & Technology* **2003,** *37* (20), 4790-4797.

104. Antoniou, M. G.; de la Cruz, A. A.; Dionysiou, D. D., Degradation of microcystin-LR using sulfate radicals generated through photolysis, thermolysis and e− transfer mechanisms. *Appl. Catal. B-Environ.* **2010,** *96* (3), 290-298.

105. Guan, Y.-H.; Ma, J.; Li, X.-C.; Fang, J.-Y.; Chen, L.-W., Influence of pH on the Formation of Sulfate and Hydroxyl Radicals in the UV/Peroxymonosulfate System. *Environmental Science &*

Technology **2011,** *45* (21), 9308-9314.

106. Anipsitakis, G. P.; Dionysiou, D. D., Radical Generation by the Interaction of Transition Metals with Common Oxidants. *Environmental Science & Technology* **2004,** *38* (13), 3705-3712.

107. Zou, J.; Ma, J.; Chen, L.; Li, X.; Guan, Y.; Xie, P.; Pan, C., Rapid Acceleration of Ferrous Iron/Peroxymonosulfate Oxidation of Organic Pollutants by Promoting Fe(III)/Fe(II) Cycle with Hydroxylamine. *Environmental Science & Technology* **2013,** *47* (20), 11685-11691.

108. Chen, X.; Qiao, X.; Wang, D.; Lin, J.; Chen, J., Kinetics of oxidative decolorization and mineralization of Acid Orange 7 by dark and photoassisted Co2+-catalyzed peroxymonosulfate system. *Chemosphere* **2007,** *67* (4), 802-808.

109. Kim, J.; Edwards, J. O., A study of cobalt catalysis and copper modification in the coupled decompositions of hydrogen peroxide and peroxomonosulfate ion. *Inorg. Chim. Acta* **1995,** *235* (1), 9-13.

110. Ahn, Y.-Y.; Yun, E.-T.; Seo, J.-W.; Lee, C.; Kim, S. H.; Kim, J.-H.; Lee, J., Activation of Peroxymonosulfate by Surface-Loaded Noble Metal Nanoparticles for Oxidative Degradation of Organic Compounds. *Environmental Science & Technology* **2016,** *50* (18), 10187-10197.

111. Ahn, Y.-Y.; Bae, H.; Kim, H.-I.; Kim, S.-H.; Kim, J.-H.; Lee, S.-G.; Lee, J., Surface-loaded metal nanoparticles for peroxymonosulfate activation: Efficiency and mechanism reconnaissance. *Appl. Catal. B-Environ.* **2019,** *241*, 561-569.

112. Xie, M.; Tang, J.; Kong, L.; Lu, W.; Natarajan, V.; Zhu, F.; Zhan, J., Cobalt doped g-C3N4 activation of peroxymonosulfate for monochlorophenols degradation. *Chem. Eng. J.* **2019,** *360*, 1213-1222.

113. Duan, X.; Su, C.; Miao, J.; Zhong, Y.; Shao, Z.; Wang, S.; Sun, H., Insights into perovskite-catalyzed peroxymonosulfate activation: Maneuverable cobalt sites for promoted evolution of sulfate radicals. *Appl. Catal. B-Environ.* **2018,** *220*, 626-634.

114. Zhu, S.; Ho, S.-H.; Jin, C.; Duan, X.; Wang, S., Nanostructured manganese oxides: natural/artificial formation and their induced catalysis for wastewater remediation. *Environmental Science: Nano* **2020,** *7* (2), 368-396.

115. Zhang, T.; Zhu, H.; Croué, J.-P., Production of Sulfate Radical from Peroxymonosulfate Induced by a Magnetically Separable CuFe2O4 Spinel in Water: Efficiency, Stability, and Mechanism. *Environmental Science & Technology* **2013,** *47* (6), 2784-2791.

116. Tan, C.; Gao, N.; Deng, Y.; Deng, J.; Zhou, S.; Li, J.; Xin, X., Radical induced degradation of acetaminophen with Fe3O4 magnetic nanoparticles as heterogeneous activator of peroxymonosulfate. *J. Hazard. Mater.* **2014,** *276*, 452-460.

117. Liang, C.; Guo, Y.-y., Mass Transfer and Chemical Oxidation of Naphthalene Particles with Zerovalent Iron Activated Persulfate. *Environmental Science & Technology* **2010,** *44* (21), 8203-8208.

118. Oh, S.-Y.; Kim, H.-W.; Park, J.-M.; Park, H.-S.; Yoon, C., Oxidation of polyvinyl alcohol by persulfate activated with heat, Fe2+, and zero-valent iron. *J. Hazard. Mater.* **2009,** *168* (1), 346-351.

119. Liu, H.; Bruton, T. A.; Doyle, F. M.; Sedlak, D. L., In Situ Chemical Oxidation of Contaminated Groundwater by Persulfate: Decomposition by Fe(III)- and Mn(IV)-Containing Oxides and Aquifer Materials. *Environmental Science & Technology* **2014,** *48* (17), 10330-10336.

120. Saputra, E.; Muhammad, S.; Sun, H.; Ang, H.-M.; Tadé, M. O.; Wang, S., Shape-controlled activation of peroxymonosulfate by single crystal α-Mn2O3 for catalytic phenol degradation in aqueous solution. *Appl. Catal. B-Environ.* **2014,** *154-155*, 246-251.

121. Zhang, T.; Chen, Y.; Wang, Y.; Le Roux, J.; Yang, Y.; Croué, J.-P., Efficient Peroxydisulfate Activation Process Not Relying on Sulfate Radical Generation for Water Pollutant Degradation. *Environmental Science & Technology* **2014,** *48* (10), 5868-5875.

122. Yao, Y.; Yang, Z.; Sun, H.; Wang, S., Hydrothermal Synthesis of Co3O4–Graphene for Heterogeneous Activation of Peroxymonosulfate for Decomposition of Phenol. *Ind. Eng. Chem. Res.* **2012,** *51* (46), 14958-14965.

123. Ding, Y.; Zhu, L.; Wang, N.; Tang, H., Sulfate radicals induced degradation of tetrabromobisphenol A with nanoscaled magnetic CuFe2O4 as a heterogeneous catalyst of peroxymonosulfate. *Appl. Catal. B-Environ.* **2013,** *129*, 153-162.

124. Liang, H.; Sun, H.; Patel, A.; Shukla, P.; Zhu, Z. H.; Wang, S., Excellent performance of mesoporous Co3O4/MnO2 nanoparticles in heterogeneous activation of peroxymonosulfate for phenol degradation in aqueous solutions. *Appl. Catal. B-Environ.* **2012,** *127*, 330-335.

125. Yang, Q.; Choi, H.; Al-Abed, S. R.; Dionysiou, D. D., Iron–cobalt mixed oxide nanocatalysts: Heterogeneous peroxymonosulfate activation, cobalt leaching, and ferromagnetic properties for environmental applications. *Appl. Catal. B-Environ.* **2009,** *88* (3), 462-469.

126. Anipsitakis, G. P.; Stathatos, E.; Dionysiou, D. D., Heterogeneous Activation of Oxone Using Co3O4. *The Journal of Physical Chemistry B* **2005,** *109* (27), 13052-13055.

127. Shukla, P.; Wang, S.; Singh, K.; Ang, H. M.; Tadé, M. O., Cobalt exchanged zeolites for heterogeneous catalytic oxidation of phenol in the presence of peroxymonosulphate. *Appl. Catal. B-Environ.* **2010,** *99* (1), 163-169.

128. Liang, H.; Ting, Y. Y.; Sun, H.; Ang, H. M.; Tadé, M. O.; Wang, S., Solution combustion synthesis of Co oxide-based catalysts for phenol degradation in aqueous solution. *J. Colloid Interface Sci.* **2012,** *372* (1), 58-62.

129. Shukla, P. R.; Wang, S.; Sun, H.; Ang, H. M.; Tadé, M., Activated carbon supported cobalt catalysts for advanced oxidation of organic contaminants in aqueous solution. *Appl. Catal. B-Environ.* **2010,** *100* (3), 529-534.

130. Chen, Q.; Ji, F.; Guo, Q.; Fan, J.; Xu, X., Combination of heterogeneous Fenton-like reaction and photocatalysis using Co–TiO2 nanocatalyst for activation of KHSO5 with visible light irradiation at ambient conditions. *Journal of Environmental Sciences* **2014,** *26* (12), 2440-2450.

131. Shi, P.; Su, R.; Wan, F.; Zhu, M.; Li, D.; Xu, S., Co3O4 nanocrystals on graphene oxide as a synergistic catalyst for degradation of Orange II in water by advanced oxidation technology based on sulfate radicals. *Appl. Catal. B-Environ.* **2012,** *123-124*, 265-272.

132. Shi, P.; Dai, X.; Zheng, H.; Li, D.; Yao, W.; Hu, C., Synergistic catalysis of Co3O4 and graphene oxide on Co3O4/GO catalysts for degradation of Orange II in water by advanced oxidation technology based on sulfate radicals. *Chem. Eng. J.* **2014,** *240*, 264-270.

133. Hu, P.; Long, M., Cobalt-catalyzed sulfate radical-based advanced oxidation: A review on heterogeneous catalysts and applications. *Appl. Catal. B-Environ.* **2016,** *181*, 103-117.

134. Kang, J.; Duan, X.; Wang, C.; Sun, H.; Tan, X.; Tade, M. O.; Wang, S., Nitrogen-doped bamboo-like carbon nanotubes with Ni encapsulation for persulfate activation to remove emerging contaminants with excellent catalytic stability. *Chem. Eng. J.* **2018,** *332*, 398-408.

135. Kang, J.; Zhou, L.; Duan, X.; Sun, H.; Ao, Z.; Wang, S., Degradation of Cosmetic Microplastics via Functionalized Carbon Nanosprings. *Matter* **2019,** *1* (3), 745-758.

136. Chen, F.; Wu, X.-L.; Yang, L.; Chen, C.; Lin, H.; Chen, J., Efficient degradation and mineralization of antibiotics via heterogeneous activation of peroxymonosulfate by using graphene supported single-atom Cu catalyst. *Chem. Eng. J.* **2020,** *394*, 124904.

137. Qi, Y.; Li, J.; Zhang, Y.; Cao, Q.; Si, Y.; Wu, Z.; Akram, M.; Xu, X., Novel lignin-based single atom catalysts as peroxymonosulfate activator for pollutants degradation: Role of single cobalt and

electron transfer pathway. *Appl. Catal. B-Environ.* **2021,** *286*, 119910.

138. Qian, K.; Chen, H.; Li, W.; Ao, Z.; Wu, Y.-n.; Guan, X., Single-Atom Fe Catalyst Outperforms Its Homogeneous Counterpart for Activating Peroxymonosulfate to Achieve Effective Degradation of Organic Contaminants. *Environmental Science & Technology* **2021,** *55* (10), 7034-7043.

139. Yu, J.; Feng, H.; Tang, L.; Pang, Y.; Zeng, G.; Lu, Y.; Dong, H.; Wang, J.; Liu, Y.; Feng, C.; Wang, J.; Peng, B.; Ye, S., Metal-free carbon materials for persulfate-based advanced oxidation process: Microstructure, property and tailoring. *Prog. Mater Sci.* **2020,** *111*, 100654.

140. Duan, X.; Sun, H.; Wang, S., Metal-Free Carbocatalysis in Advanced Oxidation Reactions. *Acc. Chem. Res.* **2018,** *51* (3), 678-687.

141. Sun, H.; Liu, S.; Zhou, G.; Ang, H. M.; Tadé, M. O.; Wang, S., Reduced Graphene Oxide for Catalytic Oxidation of Aqueous Organic Pollutants. *ACS Appl. Mater. Interfaces* **2012,** *4* (10), 5466-5471.

142. Wang, Y.; Ao, Z.; Sun, H.; Duan, X.; Wang, S., Activation of peroxymonosulfate by carbonaceous oxygen groups: experimental and density functional theory calculations. *Appl. Catal. B-Environ.* **2016,** *198*, 295-302.

143. Duan, X.; Sun, H.; Ao, Z.; Zhou, L.; Wang, G.; Wang, S., Unveiling the active sites of graphene-catalyzed peroxymonosulfate activation. *Carbon* **2016,** *107*, 371-378.

144. Duan, X.; Ao, Z.; Zhou, L.; Sun, H.; Wang, G.; Wang, S., Occurrence of radical and nonradical pathways from carbocatalysts for aqueous and nonaqueous catalytic oxidation. *Appl. Catal. B-Environ.* **2016,** *188*, 98-105.

145. Duan, X.; Ao, Z.; Zhang, H.; Saunders, M.; Sun, H.; Shao, Z.; Wang, S., Nanodiamonds in sp2/sp3 configuration for radical to nonradical oxidation: Core-shell layer dependence. *Appl. Catal. B-Environ.* **2018,** *222*, 176-181.

146. Duan, X.; Tian, W.; Zhang, H.; Sun, H.; Ao, Z.; Shao, Z.; Wang, S., sp2/sp3 Framework from Diamond Nanocrystals: A Key Bridge of Carbonaceous Structure to Carbocatalysis. *ACS Catal.* **2019,** *9* (8), 7494-7519.

147. Duan, X.; Ao, Z.; Sun, H.; Indrawirawan, S.; Wang, Y.; Kang, J.; Liang, F.; Zhu, Z. H.; Wang, S., Nitrogen-Doped Graphene for Generation and Evolution of Reactive Radicals by Metal-Free Catalysis. *ACS Appl. Mater. Interfaces* **2015,** *7* (7), 4169-4178.

148. Duan, X.; Sun, H.; Wang, Y.; Kang, J.; Wang, S., N-Doping-Induced Nonradical Reaction on

Single-Walled Carbon Nanotubes for Catalytic Phenol Oxidation. *ACS Catal.* **2015,** *5* (2), 553-559.

149. Li, D.; Duan, X.; Sun, H.; Kang, J.; Zhang, H.; Tade, M. O.; Wang, S., Facile synthesis of nitrogen-doped graphene via low-temperature pyrolysis: The effects of precursors and annealing ambience on metal-free catalytic oxidation. *Carbon* **2017,** *115*, 649-658.

150. Wang, C.; Kang, J.; Sun, H.; Ang, H. M.; Tadé, M. O.; Wang, S., One-pot synthesis of N-doped graphene for metal-free advanced oxidation processes. *Carbon* **2016,** *102*, 279-287.

151. Liang, P.; Zhang, C.; Duan, X.; Sun, H.; Liu, S.; Tade, M. O.; Wang, S., N-Doped Graphene from Metal–Organic Frameworks for Catalytic Oxidation of p-Hydroxylbenzoic Acid: N-Functionality and Mechanism. *ACS Sustain. Chem. Eng.* **2017,** *5* (3), 2693-2701.

152. Duan, X.; Indrawirawan, S.; Sun, H.; Wang, S., Effects of nitrogen-, boron-, and phosphorus-doping or codoping on metal-free graphene catalysis. *Catal. Today* **2015,** *249*, 184-191.

153. Sun, H.; Wang, Y.; Liu, S.; Ge, L.; Wang, L.; Zhu, Z.; Wang, S., Facile synthesis of nitrogen doped reduced graphene oxide as a superior metal-free catalyst for oxidation. *Chem. Commun.* **2013,** *49* (85), 9914-9916.

154. Duan, X.; O'Donnell, K.; Sun, H.; Wang, Y.; Wang, S., Sulfur and Nitrogen Co-Doped Graphene for Metal-Free Catalytic Oxidation Reactions. *Small* **2015,** *11* (25), 3036-3044.

155. Duan, X.; Sun, H.; Shao, Z.; Wang, S., Nonradical reactions in environmental remediation processes: Uncertainty and challenges. *Appl. Catal. B-Environ.* **2018,** *224*, 973-982.

Chapter 3 Understanding of the Oxidation Behaviour of Benzyl Alcohol by Peroxymonosulfate *via* Carbon Nanotubes Activation

Abstract

Selective oxidation of benzyl alcohol (BzOH) into benzaldehyde (BzH) is very important in synthetic chemistry. Peroxymonosulfate (PMS) is a cheap, stable and soluble solid oxidant, holding promise for organic oxidation reactions. Herein, we report the catalytic PMS activation *via* carbon nanotubes (CNTs) for the selective oxidation of BzOH under mild conditions without other additives. A remarkable promotion of BzH yield with a selectivity over 80% was achieved on modified CNTs, i.e., O-CNTs *via* the radical oxidation process, and the oxygen functionalities for catalysis were comprehensively investigated by experimental study and theoretical exploration. To understand the different surface oxygen species on CNTs for the activation of PMS, density functional theory (DFT) calculations were performed to investigate the adsorption behaviour of PMS on various CNTs. The electrophilic oxygen was identified as the electron captor to activate PMS by O-O bond cleavage to form $SO_5^{\bullet-}$ and $SO_4^{\bullet-}$ radicals. The nucleophilic carbonyl groups can also induce a redox cycle to generate $^{\bullet}OH$ and $SO_4^{\bullet-}$ radicals, but phenolic hydroxyl groups impede the radical process with antioxidative functionality. The carbocatalysis-assisted PMS activation may provide a cheap process for the selective oxidation of alcohols into aldehydes or ketones. The insight achieved from this fundamental study may be further applied to other organic synthesis *via* selective oxidation.

The content of this chapter is published in ACS Catalysis 2020. 10 (6), 3516-3525.

3.1 Introduction

Selective oxidation of alcohols into aldehydes or ketones is one of the most important reactions in synthesis of organic compounds.[1] Benzyl alcohol (BzOH) oxidation has attracted extensive attention because the produced benzaldehyde (BzH) can serve as a versatile intermediate in the manufacture of many fine chemicals.[2] A variety of reaction routes have been developed based on different catalysts and oxidants. Stoichiometric metal oxides (chromates and permanganates) and peroxides (hydrogen peroxide and t-butylhydroperoxide) are frequently employed as the oxidants,[3-5] where the former oxidants cause pollution by the nature of heavy metals and the latter suffer from the poor stability in storage and transportation. In view of green chemistry, molecular oxygen as an oxidant has economical and environmental advantages over other oxidants. Noble metals such as Au and Pd can catalyze BzOH oxidation with high efficiency under moderate conditions, but large-scale applications are hampered by the scarcity and high cost of the catalysts.[6-7] Transitional metal-[8-9] and nanocarbon-[10] based catalysts are developed as substitutes for noble metals, but high reaction temperatures or extra additives/co-catalysts are the major issues impeding the application of O_2 as an oxidant.

Peroxymonosulfate (PMS, HSO_5^-), as a chemically stable and inexpensive solid oxidant, has received continuous attention in the oxidation of alcohols and can afford high ketone/aldehyde yields.[11] Nevertheless, PMS in these cases only serves as the precursor to generate the actual oxidizing agents through the reaction between PMS and some additives such as ketones,[12] *o*-iodoxybenzoic acid,[13-15] 2-iodoxybenzensulfonic acid[16-17] and Cl^-/Br^-[18] instead of using as an oxidant in the alcohol oxidation. Recently, it has been reported that PMS can be activated by carbon catalysts and present superior activity in advanced oxidation processes (AOPs) for aqueous contaminant degradation. Metal-free carbon materials such as carbon nanotubes (CNTs), reduced graphene oxides, and nanodiamonds can afford high

activity in phenol degradation under mild conditions and the carbonyl groups would facilitate the electron transfer from an sp^2 carbon network to PMS to generate highly reactive radicals.[19-24] However, there is still a lack of systematic investigation on the catalytic roles of other oxygenated functional groups in PMS activation with solid experimental evidence. In addition, to the best of our knowledge, the feasibility and efficiency of carbocatalyst-activated PMS in the selective oxidation of BzOH have never been reported.

In this paper, we present a novel process of selective oxidation of BzOH with CNT-activated PMS as the terminal oxidant. PMS was activated by annealed O-CNTs under benign conditions without any additives for BzOH oxidation. Experimental and theoretical studies on the catalytic roles of different surface oxygen species on CNTs, including carbonyl, phenolic hydroxyl, carboxylic acid and electrophilic peroxide/superoxide were comprehensively conducted. The oxidizing species responsible for BzH formation were identified in detail.

3.2. Results and discussion

Commercial multiwalled carbon nanotubes (MWCNTs) were first sonicated in a mixture of nitric acid and sulfuric acid to remove metal residuals and introduce oxygen species onto the carbon surface to obtain O-CNT. Then, the O-CNT was annealed in N_2 at different temperatures between 400 and 1000 ºC for the removal and redistribution of surface oxygen groups. The samples obtained are noted as OCNT-400, OCNT-600, OCNT-800, and OCNT-1000. According to transmission electron microscopy (TEM) images (Figure 3-1), both O-CNT and OCNT-800 are rich in crooked tubular segments and amorphous carbon fragments on the outer layer of the tubes, contributing to the structural and topological defects. The ratio I_D/I_G from Raman spectra (Figure 3-2) reflects the defectiveness of CNTs samples,[25] and the I_D/I_G value increased from 0.97 to 1.57 after the oxidation of original MWCNT due to acid

etching and tube shortening. The I_D/I_G value further increased as the annealing temperature increased, and I_D/I_G of OCNT-1000 can reach 1.91. The results indicate that the high-temperature annealing treatment introduces numerous defect sites from the decomposition of oxygen groups.

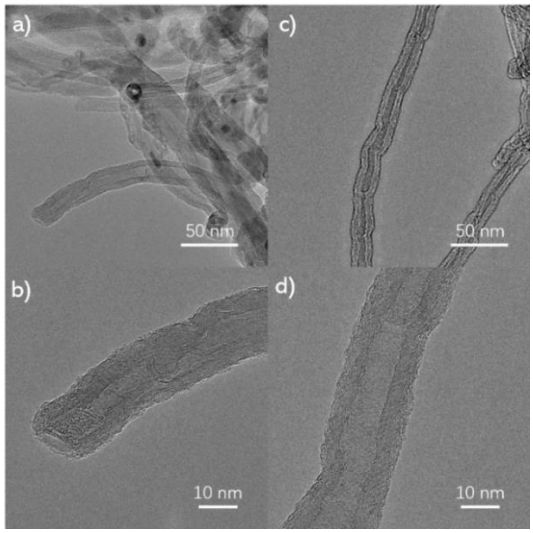

Figure 3-1. TEM images of defect-rich O-CNT (a, b), and OCNT-800 (c, d).

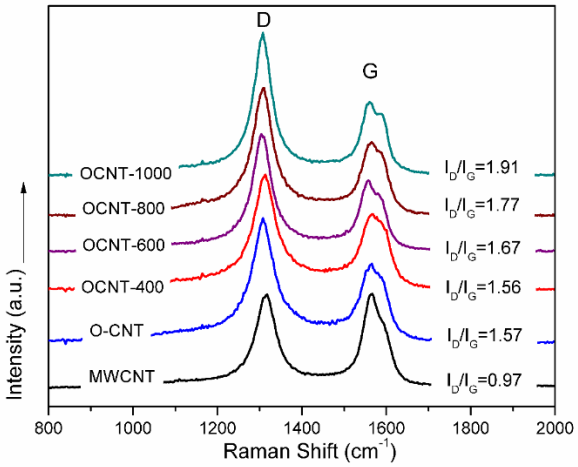

Figure 3-2. Raman spectra of pristine MWCNT, O-CNT, and various annealed O-CNTs.

Catalyst performance tests were conducted in aqueous acetonitrile to afford adequate solubility for both aromatic compounds and PMS. Table 3-1 lists the catalytic performances of various catalysts in BzOH oxidation by PMS. The reaction

temperature was controlled at 50 ºC, much lower than the typical selective oxidation by O_2.[2, 26] Without catalyst addition, only 14.7% conversion of BzOH and a very minimal BzH yield (1%) were observed (entry 1) through the self-activation of PMS. After adding MWCNT, BzOH conversion and BzH yield were increased, but to a very limited degree. The presence of oxygen species on the carbon surface (O-CNT) immediately conferred the catalytic system a higher reaction efficiency up to 22.8% BzH yield, due to the generation of active oxygen species on the CNT surface. After annealing of O-CNT, the catalytic activity of the O-CNT was further enhanced and the BzH selectivity/yield was significantly increased with the highest values up to 80.1/46.2% for OCNT-800 (at an annealing temperature of 800 ºC). To shed some light on the reaction pathway, an oxygen-free process was conducted by removing the dissolved oxygen from the solvent *via* flowing N_2 through the reaction solution (entry 7). There was no decline in BzH yield in O_2-free solution, indicating that the activation of PMS and selective oxidation process are independent of the dissolved O_2. In comparison to metal-free CNT catalysts, a noble-metal material (commercial Pt@Al_2O_3, 1 wt % of Pt, entry 9) and a transitional-metal oxide (commercial Fe_3O_4, entry 10) were tested under the similar reaction conditions, but their oxidation efficiencies were much lower than the annealed CNTs. Notably, neither benzoic acid nor other byproducts were found in the above cases according to gas chromatography–mass spectrometry (GC–MS) results, indicating that BzOH was either partially oxidized into BzH or fully oxidized into CO_2/H_2O in this reaction system.

Table 3-1. Selective oxidation of benzyl alcohol by various catalysts.[a]

Entry	Catalyst	BzOH conversion (%)	BzH selectivity (%)	BzH yield (%)
1	--	14.7	6.8	1.0
2	MWCNT	22.2	62.6	13.9
3	O-CNT	39.1	58.3	22.8
4	OCNT-400	47.0	80.9	38.1
5	OCNT-600	57.9	72.2	41.8
6	OCNT-800	57.6	80.1	46.2
7[b]	OCNT-800	59.2	79.1	46.9
8	OCNT-1000	60.3	75.3	45.4

9	$Pt@Al_2O_3$	17.9	71.2	12.8
10	Fe_3O_4	10.9	21.7	2.4

[a] Reaction conditions: 10 mg catalyst, 0.2 mmol BzOH, 0.22 mmol PMS, 10 mL acetonitrile/water (1:1, volume ratio), 50 ºC, 5 h.

[b] The dissolved oxygen in the solvent was removed before reaction by continuous N_2 bubbling, and the reaction was carried out under N_2 protection.

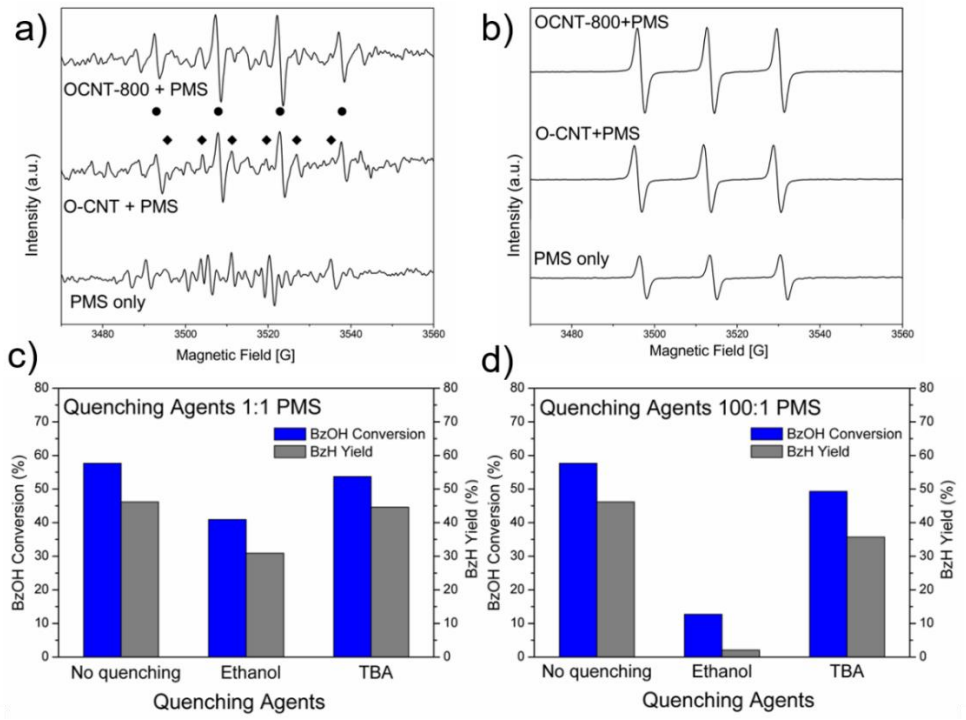

Figure 3-3. EPR spectra of O-CNT and OCNT-800 catalyzed PMS activation in the presence of (a) DMPO (DMPO-$^{\bullet}$OH-●, DMPO-$SO_4^{\bullet-}$-♦) and (b) TMP (c, d) Quenching effects on selective oxidation of benzyl alcohol. Reaction conditions: 10 mg OCNT-800, 0.2 mmol BzOH, 0.22 mmol PMS, 10 mL acetonitrile/water (1:1, volume ratio), 50 ºC, 5 h.

Previous studies reveal that carbon-based catalysts can activate PMS to generate hydroxyl radicals ($^{\bullet}$OH) and sulfate radicals ($SO_4^{\bullet-}$) for the degradation of aqueous organics. A non-radical proccess also exists in AOPs through adsorption/chemical bonding between the organic substrates/O-O bond of PMS and sp^2 hybridized carbon network after N heteroatom doping, where the carbon catalyst acts as a bridge to enable the electron transfer from the organic compounds to PMS.[27] The radical generation routes of $^{\bullet}$OH, $SO_4^{\bullet-}$ and $SO_5^{\bullet-}$ from PMS are presented in Eqs. (3-1) to (3-4). The

$SO_4^{\bullet-}$ radicals are reported to have a higher oxidation potential (2.5-3.1 V) than $^{\bullet}OH$ (2.7 V) and $SO_5^{\bullet-}$ (1.1 V).[28] In addition, $SO_5^{\bullet-}$ radicals can produce $SO_4^{\bullet-}$ radicals and singlet oxygen ($^1O_2$) by self-decomposition (Eq. 3-5).[28-30] The evolution of $^{\bullet}OH/SO_4^{\bullet-}$ radicals (Figure 3-3(a)) and $^1O_2$ (Figure 3-3(b)) during the reactions was recorded by in situ electron paramagnetic resonance (EPR) using 5,5-dimethyl-1-pyrroline *N*-oxide (DMPO) and 2,2,6,6-tetramethyl-4-piperidinol (TMP) to trap the radicals and singlet oxygen, respectively.[31-34] The peak intensities of the $^{\bullet}OH/SO_4^{\bullet-}$ radicals and singlet oxygen induced by CNTs followed the sequence of OCNT-800 > O-CNT > free PMS, demonstrating that the annealed O-CNT produced more radicals and $^1O_2$ species than the O-CNT without annealing.

$$HSO_5^- + e^- \rightarrow {}^{\bullet}OH + SO_4^{2-} \quad (3\text{-}1)$$

$$HSO_5^- + e^- \rightarrow OH^- + SO_4^{\bullet-} \quad (3\text{-}2)$$

$$^{\bullet}OH + SO_4^{2-} \leftrightarrow OH^- + SO_4^{\bullet-} \quad (3\text{-}3)$$

$$HSO_5^- - e^- \rightarrow H^+ + SO_5^{\bullet-} \quad (3\text{-}4)$$

$$2SO_5^{\bullet-} \rightarrow SO_4^{\bullet-}O_2SO_4^{\bullet-} \rightarrow {}^1O_2 + 2SO_4^{\bullet-} \quad (3\text{-}5)$$

To identify the intrinsic oxidizing components that are responsible for the conversion of BzOH and the formation of BzH, we further conducted a series of quenching experiments. Ethanol and *tert*-butanol (TBA) were adopted as quenching agents owing to their different scavenging abilities. Ethanol is used to quench $^{\bullet}OH$ and $SO_4^{\bullet-}$ radicals with high reaction rates.[35-36] *Tert*-butanol (TBA) is an effective $^{\bullet}OH$ scavenger but less effective in scavenging $SO_4^{\bullet-}$.[36] A comparison of quenching effects in low (1 equivalent of PMS) and high (100 times of PMS) dosage of the quenching agents on the oxidation efficiency with OCNT-800 is displayed in Figure 3-3 (c) and (d). The dosage of TBA did not cause severe decrease of the oxidation efficiency and there is only 10% loss of BzH yield with 100 times of TBA loading, indicating that the $^{\bullet}OH$ radicals play a minor role in BzH formation. A substantial decrease in BzH yield was observed when ethanol was added, with only 2% BzH yield remained at 100 times of

ethanol dosage. The quenching results reveal that $SO_4^{\bullet-}$ radicals with a high oxidative potential dominantly contribute to the selective oxidation of BzOH into BzH whereas the radical formation processes *via* Equations (3-1) to (3-4) suggest that the electron transfer between PMS and carbo-catalysts plays a pivotal role in radical generation by either electron gain or loss. The oxygenated functional groups and defect sites on CNTs can break the inertness of highly stable sp^2 graphitic structure and act as catalytic active sites. A wide range of oxygen species, including ketonic carbonyl (C=O), phenolic hydroxyl (C−OH) and carboxylic acid (COOH) groups, coexist on CNTs.[37] In the view of electroaffinity, there are electrophilic (peroxides and superoxides) and nucleophilic (e.g., C=O) oxygen species on carbocatalysts.[38-39] The electrophilic peroxide (O_2^{2-}) and superoxide (O_2^{-}) species are electron-deficient and tend to attack electron-rich molecules. The electron-rich C=O groups can serve as an electron donor. In general, both nucleophilic C=O and electrophilic groups can activate PMS to generate reactive radicals through electron transfer between PMS and oxygen functional groups. Meanwhile, in the field of polymer materials, it is known that hindered phenolic antioxidants are able to prevent the degradation of polymers since the phenolic groups can give H atoms to stop the free-radical chain reaction.[40-41] Therefore, phenolic hydroxyl groups on a carbocatalyst may possess similar functionality to capture the generated radicals and impede the selective oxidation of BzOH.

Table 3-2. Concentrations of surface oxygen groups determined by XPS survey and electrophilic oxygen determined by iodometric titration.

Catalyst	Total oxygen (fresh, at.%)	Oxygen species (% of total oxygen content)			Total oxygen (used, at.%)	Electrophilic oxygen (10^{-4} mol/g cat.)
		C-O	O=C−O	C=O		
MWCNT	0.83	32.4	47.9	19.7	1.82	0.9
O-CNT	7.43	42.8	45.8	11.4	7.33	1.3
OCNT-400	4.96	49.3	36.7	14.0	6.30	2.8
OCNT-600	3.06	51.3	35.9	12.7	4.90	5.0
OCNT-800	2.23	47.6	41.1	11.3	4.88	8.7
OCNT-1000	2.58	49.2	44.2	6.5	4.75	3.5

In this study, the iodometric titration method was used to quantitatively determine the amount of surface electrophilic oxygen species from the peroxides or superoxides on the CNT catalysts.[42-43] The derived amount of I_2 by $Na_2S_2O_3$ titration can quantitatively reflect the presence of the electrophilic oxygen species. Such an iodometric oxidation method can be specifically used to deactivate the electrophilic oxygen groups, which will be discussed in the reaction mechanism. The contents of the surface oxygen before and after the catalytic reaction and the amount of electrophilic oxygen derived from pristine MWCNT and O-CNTs annealed at different temperatures are presented in Table 3-2. After acid etching/oxidation, a remarkable increase of total oxygen content and electrophilic oxygen was observed on MWCNT. As the annealing temperature increased, the total oxygen content reduced due to the decomposition of the oxygen species with different thermal stabilities. Meanwhile, the amount of electrophilic oxygen increased with the rising annealing temperature because the desorption of oxygen groups (carboxyl, lactone, ether, etc.) in thermal treatment leads to the exposure of highly active defect sites, on which the oxygen species including electrophilic oxygen can be formed in an oxygen-containing atmosphere. Notably, the content of the electrophilic oxygen (8.7×10^{-4} mol/g cat.) was observed to be the highest on OCNT-800 and at a lower amount on OCNT-1000. At the temperature exceeding 1000 ºC, the phenolic hydroxyl and carbonyl groups started to decompose accompanied by the vanishing of some structural defects.[44] The deconvolution of O 1s X-ray photoelectron spectroscopy (XPS) (Table 3-2 and Figure 3-4) of different annealed O-CNT shows the coexistence of C=O, O=C−O and C−O groups on CNTs.[37, 42] OCNT-1000 contained less C=O groups but more O=C−O and C−O groups than OCNT-800, indicating the defect sites on OCNT-1000 were more likely to generate O=C−O/C−O instead of C=O. As a result, the regeneration of C=O and electrophilic oxygen are impeded on OCNT-1000.

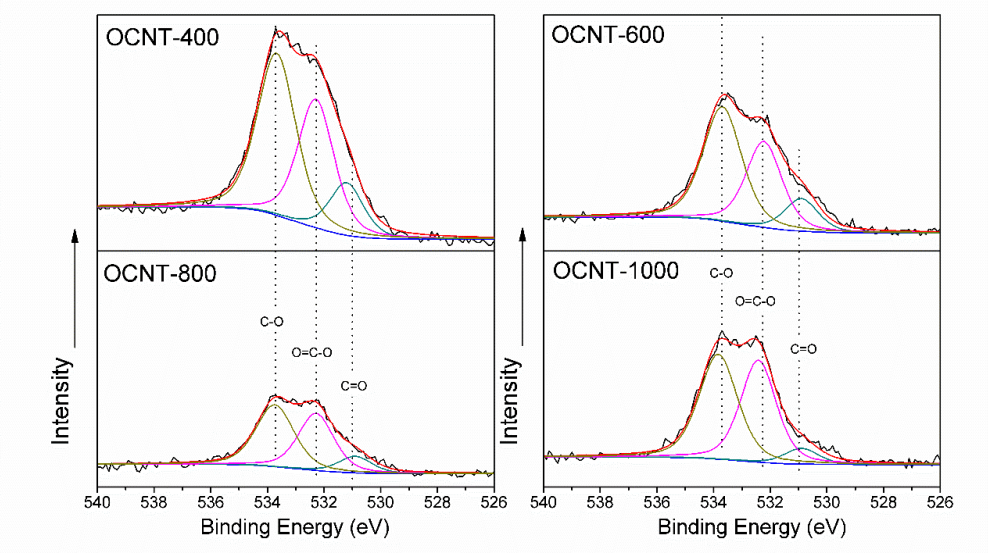

Figure 3-4. Deconvolution of O1s XPS spectra of OCNT-400, OCNT-600, OCNT-800 and OCNT-1000 assigned to C=O (~531.2 eV), O=C−O (~532.4 eV) and C−O (~533.7 eV).

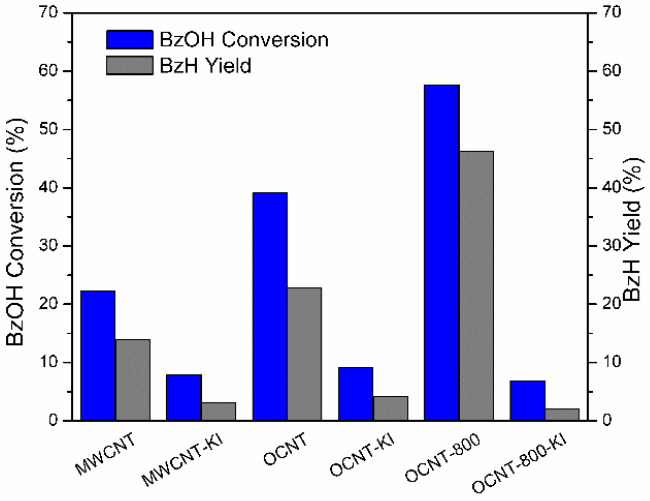

Figure 3-5. Selective oxidation of benzyl alcohol on CNT catalysts before and after the elimination of surface electrophilic oxygen species by KI. Reaction conditions: 10 mg catalyst, 0.2 mmol BzOH, 0.22 mmol PMS, 10 mL acetonitrile/water (1:1, volume ratio), 50 ºC, 5 h.

The electrophilic oxygen groups on MWCNT, O-CNT, and OCNT-800 were then selectively deactivated (MWCNT-KI, OCNT-KI, and OCNT-800-KI) by iodometric

oxidation to unveil the catalytic role of the electrophilic oxygen in PMS activation. The catalytic performances of those samples before and after the titration are displayed in Figure 3-5. Though the activity of MWCNT, O-CNT, and OCNT-800 varied greatly in PMS activation, the samples showed consistent performances after the electrophilic oxygen groups were eliminated. The BzOH conversion and BzH yield dramatically decreased to approximately the same level after the titration treatment for the three samples. Notably, OCNT-800-KI gave even slightly lower activity than OCNT-KI, agreeing well with the peak intensity variation in EPR (Figure 3-6). We can infer that the enhanced catalytic performance after annealing of O-CNT mainly originates from the generation of electrophilic oxygen species, which contribute to the effective production of $SO_5^{\bullet-}$ and $SO_4^{\bullet-}$ radicals.

Table 3-3. Selective oxidation of benzyl alcohol by O-CNT derivatives and small molecular mimics.[a]

Entry	Catalyst	BzOH conversion (%)	BzH selectivity (%)	BzH yield (%)
1[b]	OCNT-c	42.6	52.3	22.3
2	OCNT-PH	22.2	25.4	5.6
3	OCNT-BA	48.2	55.6	26.8
4	OCNT-BrPE	42.5	49.2	20.9
5[c]	--	14.7	6.8	1.0
6[d]	C=O	24.6	50.6	12.5
7[e]	C-OH	14.1	7.0	0.8
8[f]	COOH	15.4	9.1	1.4

[a] Reaction conditions: 10 mg catalyst, 0.2 mmol BzOH, 0.22 mmol PMS, 10 mL acetonitrile/water (1:1, volume ratio), 50 ºC, 5 h.

[b] O-CNT underwent the solvent-only treatment (OCNT-c) to control variables with the derivatives.

[c] No catalyst was loaded.

[d] *p*-benzoquinone (0.4 mmol) was used to mimic carbonyl group.

[e] 1,2-dihydroxybenzene (0.4 mmol) was used to mimic hydroxyl group.

[f] 1,4-dicarboxybenzene (0.4 mmol) was used to mimic carboxyl group.

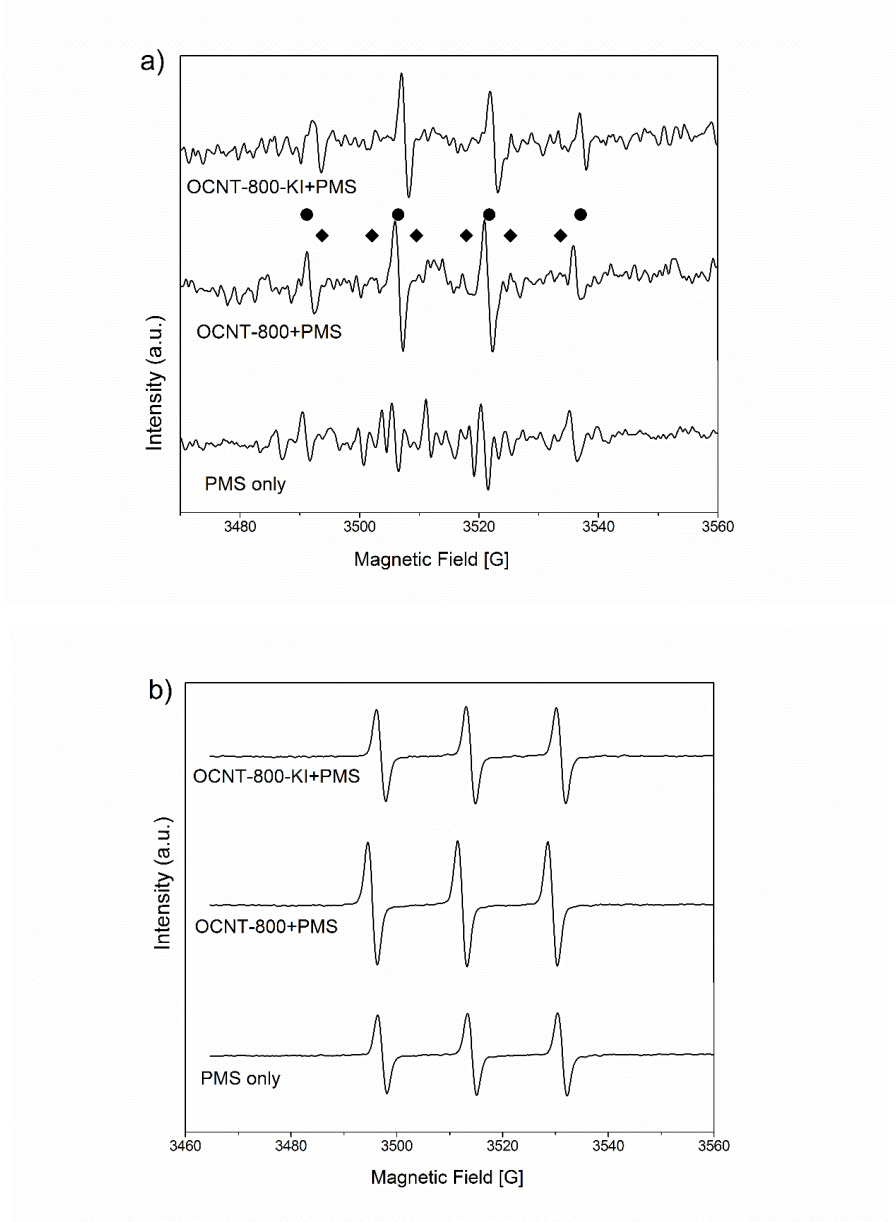

Figure 3-6. *In-situ* EPR spectra of OCNT-800 and OCNT-800-KI catalyzed PMS activation in the presence of a) DMPO (DMPO-˙OH-●, DMPO- $SO_4^{\bullet-}$-♦) and b) TMP. Conditions: 10 mg catalyst, 0.2 mmol BzOH, 0.22 mmol PMS, 10 mL acetonitrile/water (1:1, volume ratio), 50 ºC

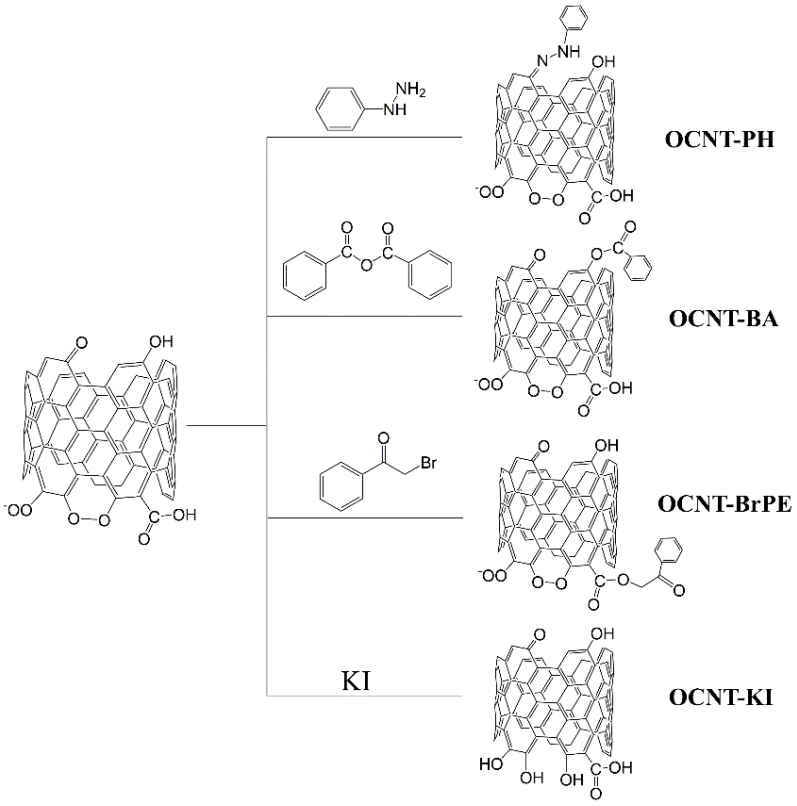

Scheme 3-1. Selective deactivation pathways of a) carbonyl b) phenol c) carbonxyl acid and d) electrophilic oxygen on O-CNT by phenylhydrazine (PH), benzoic anhydride (BA), 2-bromo-1-phenylethanone (BrPE) and KI.

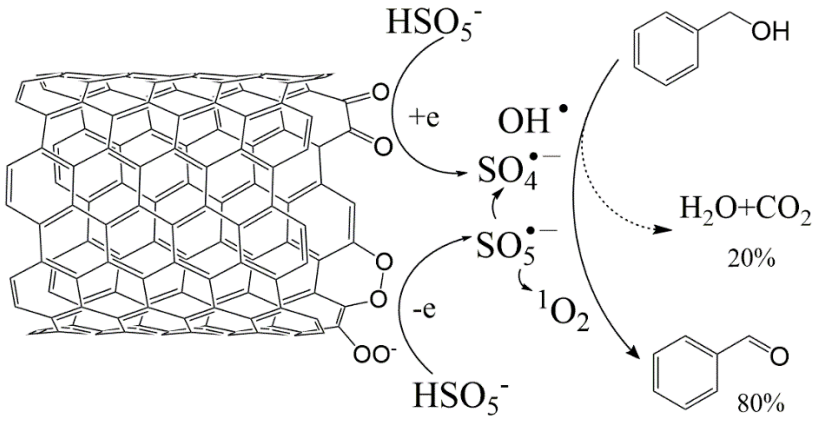

Scheme 3-2. Proposed mechanism of PMS activation on OCNT-800 and the oxidation of benzyl alcohol into benzaldehyde.

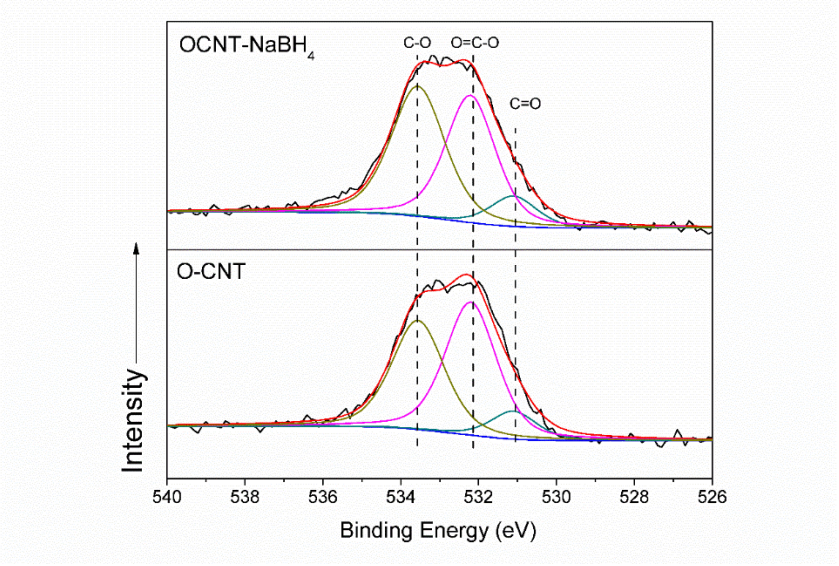

Figure 3-7. Deconvolution of O1s XPS spectra of O-CNT and OCNT-$NaBH_4$ (O-CNT after wet chemical reduction by $NaBH_4$)

The catalytic behaviour of the C=O, C−OH and COOH groups in the oxidation of BzOH was further explored by selective deactivation and small-molecule mimics of each group. The three target oxygen groups (C=O, C−OH and COOH) on O-CNT were deactivated by phenylhydrazine (PH), benzoic anhydride (BA), and 2-bromo-1-phenylethanone (BrPE), respectively, to obtain the relevant derivatives through highly specific reactions between the titrants and oxygen groups (Scheme 3-1).[37] The derived samples were referred to as OCNT-PH, OCNT-BA, and OCNT-BrPE. Meanwhile, *p*-benzoquinone, 1,2-dihydroxybenzene, and 1,4-dicarboxybenzene were used to mimic C=O, C−OH and COOH in the absence of catalysts. The selective oxidation results are listed in Table 3-3. After the C=O groups on O-CNT were deactivated (entry 2), both the BzOH conversion and BzH yield decreased evidently. Meanwhile, adding *p*-benzoquinone as the mimic of C=O leads to a considerable increase in conversion/yield (entries 5 and 6), confirming that C=O played an essential role as the electron donor in PMS activation. The removal of C−OH on O-CNT slightly enhanced the conversion/yield (entry 3), while the additional C−OH mimics lead to a reduced BzH yield (entry 7). To further confirm the role of C−OH groups, a larger amount of C−OH was produced on O-CNT by wet chemical reduction using $NaBH_4$. The

conversion of O=C−O into C−OH groups (XPS, Figure 3-7) leads to a significant decrease in the BzH yield from 22.8 to 6.9 % on O-CNT (Figure 3-8). Thus, it can be inferred that the phenolic hydroxyl groups are impediments during the radical evolution. As for carboxyl groups, entries 4 and 8 showed a subtle but still beneficial effect of COOH on the reactions, which might be owing to the C=O in COOH groups. The EPR tests showed that the radical signals induced by OCNT-PH/PMS were remarkably weakened compared to O-CNT/PMS (Figure 3-9). The other two derivates showed no apparent difference in radical generation compared to O-CNT, which also agrees with the results in Table 3-3 that the catalytic activity of O-CNT was not profoundly altered after C-OH/COOH deactivation. The results provide convincing experimental verifications to the above-mentioned hypothesis, identifying the roles of carbonyl and phenolic hydroxyl groups in the PMS activation and the selective oxidation processes. The proposed mechanism of CNT-facilitated PMS activation to transform BzOH to BzH is summarised in Scheme 3-2. The HSO_5^- can attract electrons from electron-rich C=O groups on CNTs to generate $^{\bullet}OH$ and $SO_4^{\bullet-}$ radicals. The electrophilic peroxide and superoxide species on CNTs are able to gain electrons from HSO_5^- and produce $SO_5^{\bullet-}$ radicals, which can be further transformed into $SO_4^{\bullet-}$ radicals. Thus, the selective oxidation of BzOH to BzH is significantly enabled by the radical process.

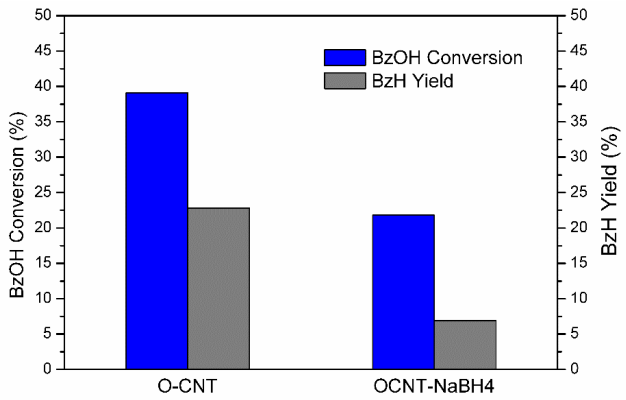

Figure 3-8. Selective oxidation of benzyl alcohol on O-CNT and OCNT-$NaBH_4$. Reaction conditions: 10 mg catalyst, 0.2 mmol BzOH, 0.22 mmol PMS, 10 mL acetonitrile/water (1:1, volume ratio), 50 ºC, 1 atm, 5 h.

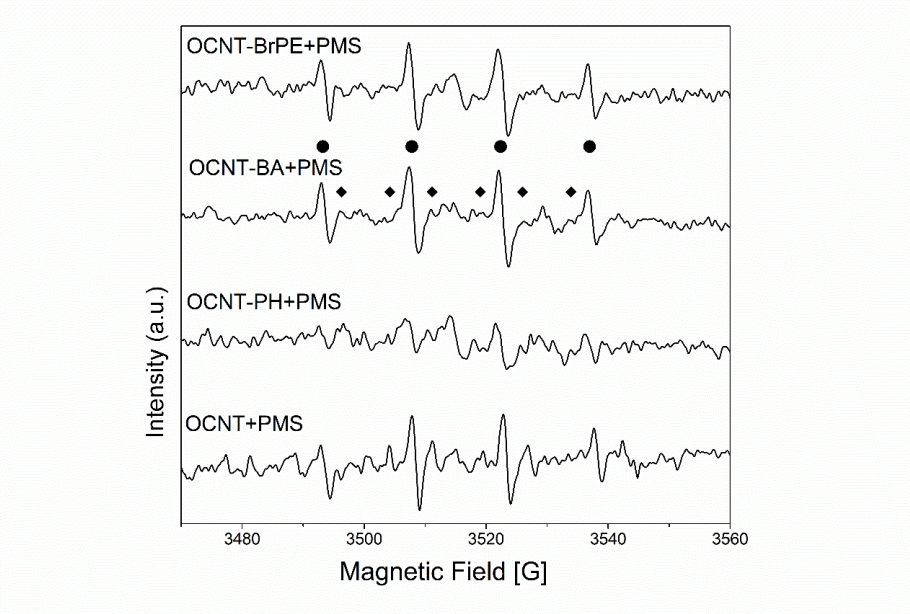

Figure 3-9. *In-situ* EPR spectra of OCNT and OCNT derivatives catalyzed PMS activation in the presence of DMPO (DMPO-$^{\bullet}$OH-●, DMPO- $SO_4^{\bullet-}$-♦). Conditions: 10 mg catalyst, 0.2 mmol BzOH, 0.22 mmol PMS, 10 mL acetonitrile/water (1:1, volume ratio), 50 ºC

The stability of OCNT-800 in successive tests was investigated, and both the BzOH conversion and BzH yield decreased after each run (Figure 3-10(a)). The BzH yield decreased from 47.4% in the first run to 28.1% in the second run and further reduced to 5.6 % after the fourth run. Then, the catalyst after the fourth run was annealed at 800 ºC (Recovered OCNT-800) and a full recovery was observed (47.6% BzH yield). The deactivation of the carbocatalyst was also found in aqueous contaminant degradation processes using PMS, and our catalyst showed a better recovery ability.[21, 45] The XPS survey spectra and O 1s deconvolution demonstrate that the surface oxygen content on the catalyst increased after each run (Figure 3-10(b)). The oxidative environment during the reaction mainly induced the regeneration of C−O and O=C−O groups on the carbon surface, while the C=O groups showed no obvious change (Figure 3-11). The determination of electrophilic oxygen on the catalysts after each run by the iodometric titration (Figure 3-10(b)) reveals almost a total consumption of the electrophilic oxygen from the fresh catalyst (8.7×10^{-4} mol/g cat.) to the fourth run (0.7×10^{-4} mol/g cat.). After the annealing recovery treatment, the amount of

electrophilic oxygen increased back to 5.2×10^{-4} mol/g cat. It can be inferred that the electrophilic oxygen groups were consumed during the reaction, which is responsible for the fast deactivation of the catalyst. This consumption also confirms the occurrence of electron transfer from PMS to electrophilic oxygen. As a result, the electrophilic oxygen is reduced to enable the radical process for the BzOH oxidation instead of the nonradical process in which the carbon catalyst serves as an electron bridge. The C=O groups stay unchanged after the catalytic reaction because of a reversible conversion between C=O and C−O groups thus forming a redox cycle.[21, 38, 46]

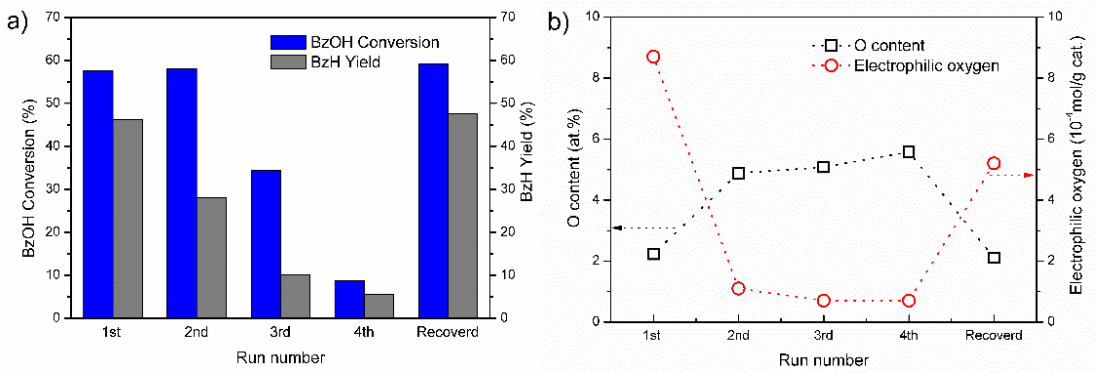

Figure 3-10. Stability test of OCNT-800 for 4 cycles and recovering OCNT-800 after the 4th run by post-annealing at 800 ºC. a) selective oxidation of benzyl alcohol, b) Total oxygen and electrophilic oxygen species obtained from XPS survey and iodometric titration. Reaction conditions: 10 mg catalyst, 0.2 mmol BzOH, 0.22 mmol PMS, 10 mL acetonitrile/water (1:1, volume ratio), 50 ºC, 5 h.

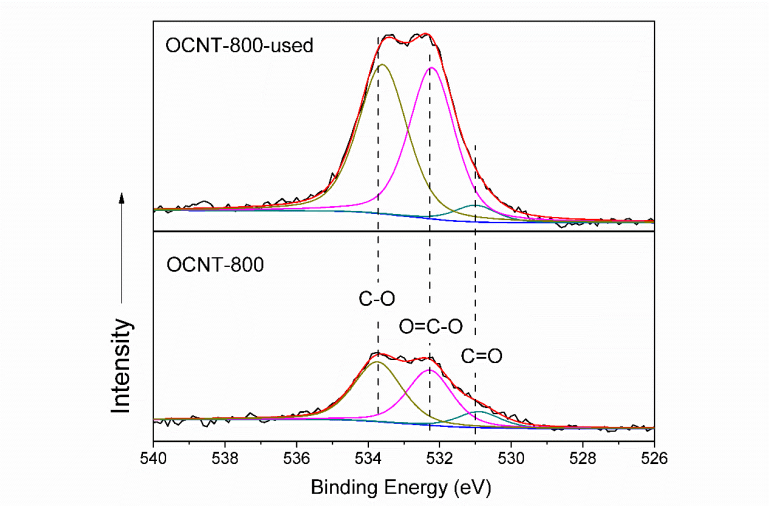

Figure 3-11. Deconvolution of O1s XPS spectra of OCNT-800 and used OCNT-800.

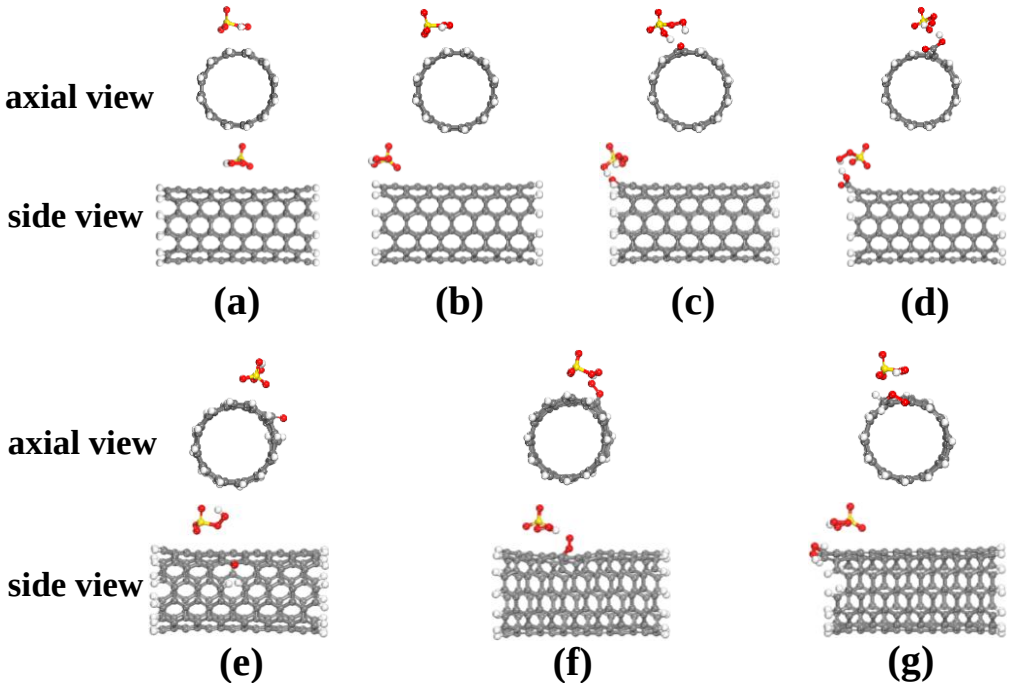

Figure 3-12. Structure of PMS molecules adsorbed on pristine CNT and CNT with different oxygen functional groups: (a) PMS on pristine CNT, (b) PMS on pristine CNT edge, (c) PMS on O-CNT with –OH, (d) PMS on O-CNT with –COOH, (e) PMS on O-CNT with –C=O, (f) PMS on O-CNT with –O=O, and (g) PMS on O-CNT with –O–O–. The gray, white, red, and yellow atoms are C, H, O, and S, respectively

Table 3-4. Adsorption energy (E_{ads}) of PMS on CNT, the O-O bond length (l_{O-O}) of PMS ($HO-OSO_3$), and the O-H bond length (l_{O-H}) of PMS ($H-OOSO_3$) in different density functional theory (DFT) models shown in Figure 3-12.

Configuration	E_{ads}(eV)	l_{O-O}(Å)	l_{O-H}(Å)
Free PMS	-	1.326	1.037
(a)	-1.17	1.434	1.004
(b)	-1.13	1.434	1.008
(c)	-1.66	1.466	0.997
(d)	-1.07	1.458	1.006
(e)	-1.12	1.426	1.005
(f)	-1.13	1.425	1.014
(g)	-1.25	1.438	0.998

To fully understand the roles of different oxygen-containing functional groups in promoting the PMS activation, all possible adsorption of PMS molecules (HSO_5^-) on

various CNT sites with the lowest energy configuration is described in Figure 3-12. The corresponding data of the adsorption energy and bond length (O-O: l_{O-O} and O-H: l_{O-H}) are listed in Table 3-4. For -OH, -COOH and -C=O groups, their behaviour in affecting the O-O bond in PMS ($HO-OSO_3$) was investigated. For electrophilic -O-O-/-O=O groups on CNTs, we focused on their abilities to stretch and cleave the O-H in PMS ($H-OOSO_3$) to echo the experimental results. As summarised in Table 3-4, the bond length l_{O-O} of free PMS molecules is 1.326 Å,[20] whereas l_{O-O} was remarkably stretched when PMS was adsorbed on pristine CNT and nucleophilic O-CNT, implying the potential to be transformed into HO and SO_4. The adsorption energies of PMS on CNTs ranged from -1.07 to -1.66 eV, among which the maximum E_{ads} of PMS on HO-CNT was -1.66 eV with the longest lo-o of 1.466 Å. It should be noted that in the case of HO-CNT, the H atom in the -OH group was separated from the O atom and was bonded to the PMS molecule, while the -OH group on CNT was transferred to the C=O group, which helps to explain the highest E_{ads} and longest lo-o in the HO-CNT system. This process implies that the PMS activation on -OH is not feasible from the thermodynamic perspective according to a previous report.[22]

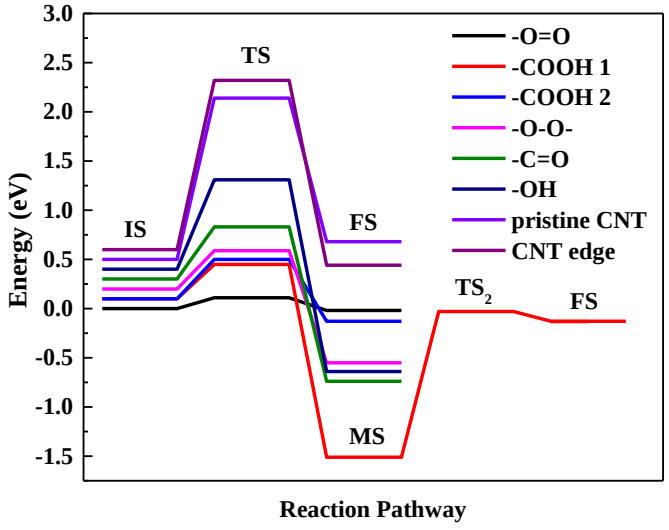

Figure 3-13. Reaction pathway of the activation of PMS on pristine CNT and CNT with different oxygen functional groups, where IS, TS, MS, and FS represent the initial structure, transition structure, intermediate product structure, and final structure, respectively.

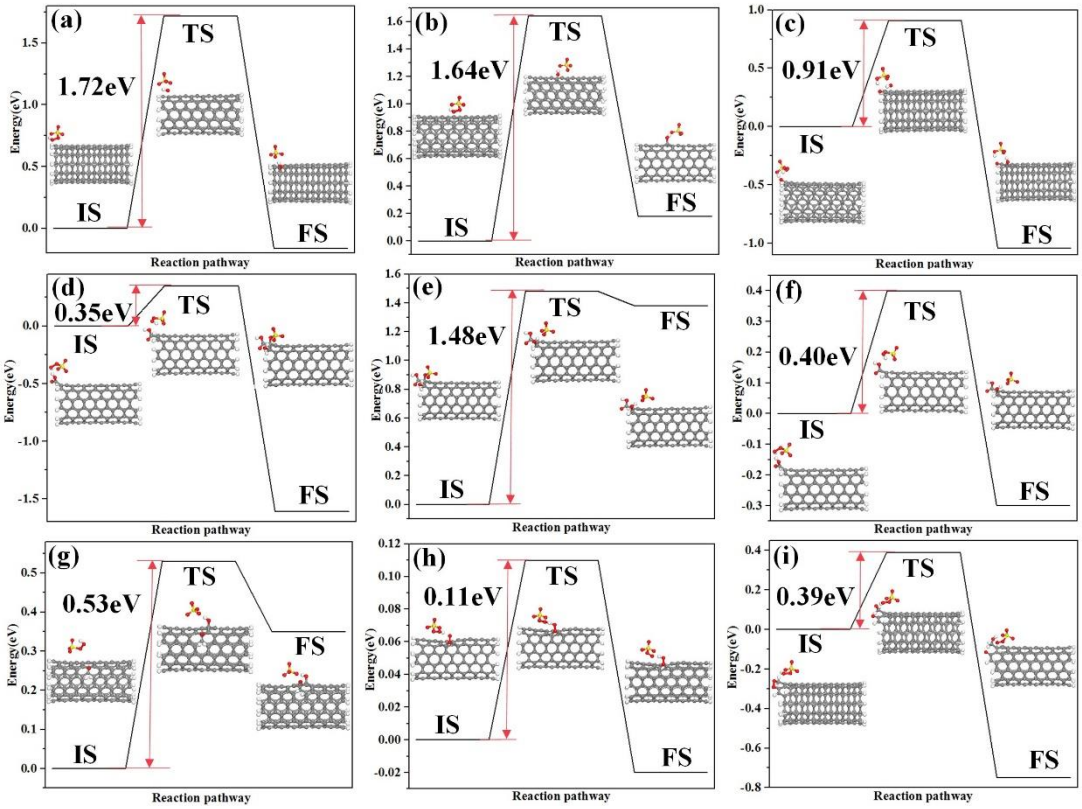

Figure 3-14. The reaction pathway and relevant reaction energy barriers E_b of activation of PMS on pristine CNT and CNT with different oxygen functional groups: (a) CNT edge pathway, (b) pristine CNT pathway, (c) –OH pathway, (d) –COOH pathway1, (e) –COOH pathway1 desorption of SO_4 group, (f) –COOH pathway 2, (g) –C=O pathway, (h) –O=O pathway, and (i) –O–O– pathway, where IS, TS, and FS with structure diagrams represent initial structure, transition structure, and final structure, respectively.

Particularly, there is no obvious change in l_{O-O} of PMS when adsorbed by -O-O-/-O=O on the CNTs with comparable adsorption energy to pristine CNT, implying a different activation mechanism for PMS activation in -O-O-/-O=O systems. Thus, based on the experimental results, the cleavage of O-O and O-H bonds of PMS on nucleophilic and electrophilic O-CNTs was investigated using transition-state searching method. The possible energy potential profiles of these reactions are shown in Figure 3-13. The reaction energy barriers E_b corresponding to different paths are displayed in Figure 3-

14. For the pristine CNT, despite the O-O bond stretching, the E_b value of the O-O bond cleavage to produce $SO_4^{\bullet-}$ was 1.64 and 1.72 eV at bulk carbon and edge sites, respectively. As previously reported, the critical energy barrier of 0.9 eV would determine the possibility of a chemical reaction at room temperature.[47-48] Thus, it is difficult to generate radicals through PMS activation by pristine CNT. For PMS activated by nucleophilic O-CNT, the O-O bond cleavage and the energy barrier E_b follow the order of OH > COOH > C=O. The highest E_b of 0.91 eV in the HO-CNT@PMS system demonstrates the ultralow degradation rate of PMS for radical formation. Meanwhile, it was found that in all of these three systems, the generated $^{\bullet}OH$ was directly bonded to the carbon atoms on the CNT, implying the possible quenching of $^{\bullet}OH$ by CNT itself. The binding between $^{\bullet}OH$ and CNT results in the decrease of the yield of free $^{\bullet}OH$ radicals, which explains the ultrashort lifetime of $^{\bullet}OH$ in comparison to $SO_4^{\bullet-}$.[49] Particularly, in the case of HOOC-CNT@PMS system, we found that the $SO_4^{\bullet-}$ can be feasibly bonded to the α-C (the C atom directly bonded to -COOH) of COOH function to form C-SO_4 in geometry optimization. Thus, two pathways of PMS activation by COOH function should be taken into consideration: pathway 1, $HSO_5^- + CNT \rightarrow C\text{-}OH + C\text{-}SO_4$; pathway 2, $HSO_5^- + CNT \rightarrow C\text{-}OH + SO_4^{\bullet-}$. The calculated E_b values for breaking the O-O bond are 0.35 and 0.40 eV in pathways 1 and 2, respectively. The energy barriers of the two pathways are slightly different, manifesting that they can occur simultaneously on the HOOC-CNT. In addition, the desorption of the SO_4 group from C-SO_4 generated in pathway 1 was investigated to evaluate the possibility of the regeneration of reactive SO_4 radicals (MS to FS for the case of –COOH in Figure 3-13). The extremely high E_b of 1.48 eV for this process implies that the $SO_4^{\bullet-}$ regeneration is impossible. Thus, the generated $SO_4^{\bullet-}$ radicals from PMS is easily inactivated by the α-C of the COOH function. Therefore, the COOH groups on CNT do not play a dominant role in activating PMS. The rather low E_b of 0.53 eV in O=C-CNT@PMS system manifests that the activation of PMS is efficient to break the O-O bond and to produce free radicals, in good consistency with the experimental observation. For electrophilic –O-O- and –C-O=O, the H-O bond is broken to produce $SO_5^{\bullet-}$, and the energy barrier was calculated to be

0.39 and 0.11 eV respectively, implying that the nucleophilic –C=O and electrophilic groups can promote the activation of PMS but in different mechanisms. The ultralow E_b value in electrophilic groups manifests the ultrafast formation rate of $SO_5^{\bullet-}$ which can subsequently transfer into $^1O_2$. These simulation results fit perfectly with our experimental observation.

Finally, the effects of different reaction conditions (reaction time, temperature, PMS dosage, catalyst dosage, and solvent) on catalytic efficiency were studied using OCNT-800 as a representative catalyst (Table 3-5). At increased reaction time (entries 1, 2, 3), temperature (entries 2, 4, 5), and PMS loading (entries 2, 9, 10), both the BzOH conversion and BzH yield increased but the BzH selectivity decreased due to the over-oxidation. Notably, the BzH yield reached 56.9% with 92.2% BzOH conversion when the PMS loading was doubled. On the other hand, doubling the catalyst dosage (entry 11) slightly increased the conversion, selectivity, and BzH yield. The reaction is also strongly influenced by the composition of the solvent. Acetonitrile/water turned out to be the best solvent (Table 3-6), and the catalytic efficiency was enhanced with a higher proportion of acetonitrile in the solvent (entries 2, 6, 7), which is possibly due to the limited aqueous solubility of BzOH and the hydrophobic nature of CNTs.[50] A higher acetonitrile/water ratio facilitates the adsorption of BzOH and PMS on CNTs' surface for further reactions, whereas the overhigh acetonitrile/water ratio (entry 8) leads to poor solubility of PMS and hinders the reaction. Comparing the results in entry 7 with reported work *via* different reaction systems (summarised in Table 3-7),[18, 26, 51-52] BzOH can be oxidized by O_2 with precious metals or nanocarbon catalysts to obtain over 90 % BzOH conversion/BzH selectivity at temperatures larger than 100 ºC. Peroxide oxidants, including H_2O_2 and PMS can afford a high BzH yield (>87%) in homogeneous environment with extra additives at low temperatures. Herein, we report a much more favourable reaction route to be performed under benign conditions without any additives, for which the reaction system can still be optimized to further improve the BzH yield.

Table 3-5. Selective oxidation of BzOH under various reaction conditions.[a]

Entry	Temperature (ºC)	Time (h)	PMS/BzOH[b]	AN/W[c]	BzOH conversion (%)	BzH selectivity (%)	BzH yield (%)
1	50	2	1.1	1	44.3	73.4	32.5
2	50	5	1.1	1	57.6	80.1	46.2
3	50	10	1.1	1	64.5	70.5	45.5
4	30	5	1.1	1	33.4	70.5	23.5
5	70	5	1.1	1	69.7	72.6	50.6
6	50	5	1.1	0.3	60.1	58.4	35.1
7	50	5	1.1	3	57.1	84.3	48.1
8	50	5	1.1	5	24.8	55.3	13.7
9	50	5	0	1	3.5	13.1	0.4
10	50	5	2	1	92.2	52.5	56.9
11[d]	50	5	1.1	1	57.9	83.2	48.2

[a] OCNT-800 (10 mg) was employed as catalyst and 0.2 mmol BzOH was added in 5 mL solvent.

[b] Molar ratio of PMS and BzOH.

[c] The volume ratio of acetonitrile (AN)/water (W).

[d] 20 mg catalyst was loaded.

Table 3-6. Selective oxidation of BzOH in different solvents.[a]

Solvent[b]	BzOH conversion (%)	BzH selectivity (%)	BzH yield (%)
AN/W-1	57.6	80.1	46.2
A/W-0.5	53.2	77.8	41.4
A/W-1	57.1	79.4	45.3
A/W-2	58.2	79.2	46.1
A/W-3	59.5	79.4	47.3
DMF/W-1	43.6	57.4	25.0
THF/W-1	11.4	24.6	2.8
MeOH/W-1	6.1	34.4	2.1
EtOH/W-1	8.2	14.6	1.2

[a] OCNT-800 was employed as catalyst and 0.2 mmol BzOH/0.22 mmol PMS was added. The reaction was conducted at 50 ºC for 5 h.

[b] 10 mL solvent mixture of solvent a/solvent b-x, where x = volume ratio of a:b (AN = acetonitrile, A = acetone, DMF = dimethylformamide, THF = tetrahydrofuran, MeOH = methanol, EtOH = ethanol, W = water).

Table 3-7. Comparison of benzyl alcohol oxidation *via* different reaction systems.

Catalyst	Oxidant	T/ ºC	t/h	Additive	BzOH conversion/%	BzH selectivity/%	BzH yield/%	Ref
Graphene oxide	O_2	100	24	N/A	N/A	N/A	92	[26]
Pd_3Pb nanocubes	O_2	130	1	N/A	91.3	91.0	N/A	[51]
Cu(II) complex, soluable	H_2O_2	60	24	TEMPO	N/A	N/A	99	[52]
N/A	PMS	N/A	3	NaBr	N/A	N/A	87	[18]
MWCNT	PMS	50	5	N/A	57.1	84.3	48.1	This work

3.3 Experimental section

Preparation of annealed CNT samples. Multiwalled carbon nanotubes (MWCNTs) were purchased from Timesnano, Chengdu, China. The length, inner diameter, and purity of the MWCNT are 10-30 μm, 10-20 nm, and 95%, respectively. The other chemicals used in this study were supplied by Sigma-Aldrich. To prepare the annealed CNTs, first, 5 g MWCNT was mixed with 250 mL of an acid mixture composed of 1:3 volume ratio of HNO_3 (65-68%) and H_2SO_4 (95-98%), which was sonicated at 50 ºC for 5 h. Then, the acid mixture was diluted and cooled down to room temperature. The oxidized MWCNT was filtered and washed with ultrapure water until the pH of the filtrate reached 7. The precipitate was dried at 60 ºC for 48 h and ground to obtain the oxidized carbon nanotubes (O-CNT). Then, O-CNT (0.5 g) was annealed in a N_2 atmosphere at 400, 600, 800 or 1000 ºC for 1.5 h at a heating rate of 5 ºC/min to obtain OCNT-400, OCNT-600, OCNT-800 and OCNT-1000, respectively.

Iodometric titration of electrophilic oxygen on carbons. A CNT sample (50 mg) was added to a mixture containing 5 mL KI (40 g/L), 5 mL H_2SO_4 (0.05 mol/L), and two drops of $(NH_4)_6Mo_7O_{24}$ (30 g/L). The reactions between electrophilic oxygen on the CNT surface and KI are shown in Eqs. 6-7. For convenience, the amount of detected I_2 was designated as the total amount of electrophilic oxygen. After 5 min sonication

followed by 1 h stirring at room temperature in the dark, I^- was oxidized to I_2. Then, the precipitate was filtered out and washed with ultrapure water to remove the adsorbed ion and dried at 60 ºC for 12 h. All of the filtrate was collected and then 0.3 g of the soluble starch indicator was added to the solution. The I_2 in the filtrate was titrated by $Na_2S_2O_3$ (2×10^{-4} mol/L) as demonstrated in (Eq. 8) until the blue color disappeared. The total concentration of the electrophilic oxygen (mol/g cat.) on the sample was calculated by Eq. 9, where *c* (mol/g), *V* (mL) and *m* (g) represent for the electrophilic oxygen concentration, volume consumption of the $Na_2S_2O_3$ solution, and mass loading of the CNTs sample, respectively.

$$O_2^{2-} + 2KI + 2H_2SO_4 \rightarrow O^{2-} + 2KHSO_4 + I_2 + H_2O \quad (3\text{-}6)$$

$$2O_2^{-} + 6KI + 6H_2SO_4 \rightarrow O^{2-} + 6KHSO_4 + 3I_2 + 3H_2O \quad (3\text{-}7)$$

$$I_2 + 2Na_2S_2O_3 \rightarrow 2NaI + Na_2S_4O_6 \quad (3\text{-}8)$$

$$c\ (\text{electrophilic oxygen}) = 1\times10^{-7}\ V/m \quad (3\text{-}9)$$

Selective deactivation of oxygenated groups on O-CNT. In the preparation of OCNT-PH, 0.2 g O-CNT, 0.5 g phenylhydrazine (PH), and 100 μL HCl (38%) were mixed in 10 mL $CHCl_3$ solvent and stirred at 60 ºC for 72 h in a N_2 atmosphere in the dark. The precipitate was filtered out, washed with $CHCl_3$ several times, and then dried at 60 ºC for 24 h to obtain OCNT-PH.

For the synthesis of OCNT-BA, 0.2 g O-CNT and 1 g benzoic anhydride (BA) were mixed in 10 mL $CHCl_3$ solvent and stirred at 60 ºC for 24 h with N_2 protection. The precipitate was filtered out, washed with $CHCl_3$ several times, and then dried at 60 ºC for 24 h to obtain OCNT-BA.

OCNT-BrPE was prepared as follows: 0.2 g O-CNT and 0.5 g 2-bromo-1-phenylethanone (BrPE) were mixed in 10 mL $CHCl_3$ solvent and stirred at room temperature for 10 h in a N_2 atmosphere in the dark. The precipitate was filtered out,

washed with $CHCl_3$ several times, and then dried at 60 ºC for 24 h to obtain OCNT-BrPE.

The wet chemial reduction of O-CNT was conducted using $NaBH_4$ to transform the surface C=O into C−OH groups. For the reduction, 0.1 g O-CNT and 1 g $NaBH_4$ were dissolved in 10 mL ethanol and stirred in a N_2 atmosphere at 50 ºC for 12 h. The precipitate was filtered out, washed with HCl and water, and then dried at 60 ºC for 24 h to obtain OCNT-$NaBH_4$.

Catalytic selective oxidation of BzOH. In a typical reaction process for the selective oxidation of benzyl alcohol, 10 mg catalyst was added into 10 mL solvent mixture (acetonitrile/water = 1:1, volume ratio) in a 25 mL flask and sonicated for 5 min. Then, 0.2 mmol BzOH and 0.22 mmol PMS (oxone, $KHSO_5 \cdot 0.5KHSO_4 \cdot 0.5K_2SO_4$) were added to initiate the oxidation. The solution was stirred at 50 ºC for 5 h. After the flask was cooled down, 0.2 mmol anisole was injected into the flask as an internal standard. A certain volume (1 mL) of the solution was withdrawn by a syringe, and the precipitate was filtered by a Millipore film. The organic compounds in the solution were extracted by 6 mL of toluene for three times and the organic phase was collected. The composition of the products was analysed by GC/MS using a 30 m × 0.25 mm×0.25 μm HP-5MS capillary column and FID detector.

Characterization measurements. Transmission electron microscopy (TEM) imaging was conducted on a JEOL 2100 microscope. Raman spectra were obtained under ambient conditions on a Renishaw Raman spectrometer with a 785 nm laser beam. X-ray photoelectron spectroscopy (XPS) data were obtained with a Kratos AXIS Ultra DLD system using Al Kα radiation. The base pressure was about 1×10^{-8} torr. The binding energy value was referenced to the C1s line at 284.6 eV from defect-free graphite. Deconvolution of O 1s spectra was performed using mixed Gaussian-Lorentzian component profiles after subtraction of a Shirley background using XPSPEAK41 software. The electron paramagnetic resonance (EPR) was conducted

on a Bruker EMS-plus instrument to record the evolution of free radicals during the selective oxidation, and the data were analysed by Xeon software. 5,5-Dimethyl-1-pyrroline *N*-oxide (DMPO) and 2,2,6,6-tetramethyl-4-piperidinol (TMP) were used as spin-trapping agents.

Computational methods. To understand the role of different surface oxygen species on CNTs, including ketonic carbonyl (–C=O), phenolic hydroxyl (C−OH), carboxylic acid (−COOH) and electrophilic peroxide (-O-O-) /superoxide (C-O=O) in the activation of PMS, density functional theory (DFT) calculations were performed to investigate the adsorption behaviour of PMS on CNTs (include pristine CNT and O-CNTs). The spin-unrestricted DFT calculations were conducted in Dmol3 package using general gradient approximation (GGA) with the Perdew-Burke-Ernzerhof (PBE) exchange-correlation functional.[53] An all-electron double numerical plus polarization (DNP) was employed as the basis set.[54] The convergence tolerance of energy was assumed at 10^{-5} Hartree (1 Hartree = 27.21 eV) and the maximal allowed force and displacement were 0.002 Hartree/Å and 0.005 Å, respectively. The DFT-D method within the TS scheme was used in all calculations to take the van der Waals forces into account.[55] In the simulations, a nonperiodic cluster model was used for (5, 5) single-walled carbon nanotubes (SWCNTs) with dangling bonds saturated by H atoms. Noteworthy that SWCNT was adopted to simplify the model structure because the electronic properties of perfect MWCNTs are rather similar to these perfect SWCNTs and the number of CNT walls slightly affected the adsorption.[56-59] For the PMS molecule adsorbed on CNTs, the adsorption energy E_{ads} is defined as

$$E_{ads} = E_{PMS/CNT} - (E_{PMS} + E_{CNT})$$

where $E_{PMS/CNT}$, E_{PMS}, E_{CNT} are the total energies of the PMS/CNT system, the isolated PMS molecule, and CNT in the same slab, respectively. To further investigate the activation mechanism of PMS on different CNTs, linear synchronous transit/quadratic synchronous transit (LST/QST) tools in Dmol3 package were used, which have been

well validated to determine the structure of the transition state and the minimum-energy reaction pathway.[60]

3.4 Conclusions

We presented a novel approach for the selective oxidation of BzOH to BzH using CNTs/PMS and explored the reaction pathways. The catalytic roles played by surface carbonyl, phenolic hydroxyl, carboxylic acid, and electrophilic peroxide/superoxide groups on CNTs were fundamentally investigated by selective deactivation and small-molecule mimics. Electrophilic oxygen species on CNTs were quantitatively determined and correlated to be the consumable active sites for the generation of $SO_5^{\bullet-}$ and $SO_4^{\bullet-}$ radicals. The thermal annealing treatment conferred highly active defect sites on CNTs for the attachment of electrophilic oxygen. The carbonyl groups served as electron donors to activate PMS into $^{\bullet}OH$ and $SO_4^{\bullet-}$ radicals. The phenolic hydroxyl groups on CNTs impeded the BzOH oxidation due to the antioxidation nature that inhibits the radical process. Density functional theory (DFT) calculations confirm that the nucleophilic –C=O groups can cleave O-O bonds in PMS molecules, while the electrophilic peroxide/superoxide groups would generate $SO_5^{\bullet-}$ by the O-H bond cleavage from PMS. However, the $SO_4^{\bullet-}$ generated by the O-O bond cleavage is easily quenched by the α-C atom on the carboxylic acid group, resulting in a nonsignificant effect of the carboxylic acid groups on the PMS activation. The highly active radicals generated from PMS dominantly contributed to the selective oxidation of BzOH to BzH with over 80% selectivity. The annealed O-CNT at 800 ºC possessed the largest amount of electrophilic oxygen groups and thus afforded the highest BzH yield in this work. In contrast to the conventional synthesis using precious metals as the catalysts, this study provides a new perspective for the selective oxidation of organics with carbon-based catalysts and PMS oxidant under benign conditions without other promoters or expensive additives. The current catalytic system (CNTs/PMS) for free-radical generation can also be applied to other organic synthesis *via* the selective

oxidation scheme. However, awareness should be raised on the correlation between the oxidation potential of the radicals and the energy barrier of different oxidative reactions to ensure the selective transformation without over-oxidizing.

References

1. Yongbo, K.; Hodaka, R.; Yuta, N.; Teruaki, H.; Masa-aki, K., A Nitric Acid-Assisted Carbon-Catalyzed Oxidation System with Nitroxide Radical Cocatalysts as an Efficient and Green Protocol for Selective Aerobic Oxidation of Alcohols. *Adv. Synth. Catal.* **2010,** *352* (14-15), 2635-2642.

2. Luo, J.; Yu, H.; Wang, H.; Wang, H.; Peng, F., Aerobic oxidation of benzyl alcohol to benzaldehyde catalyzed by carbon nanotubes without any promoter. *Chem. Eng. J.* **2014,** *240*, 434-442.

3. Wu, G.; Gao, Y.; Ma, F.; Zheng, B.; Liu, L.; Sun, H.; Wu, W., Catalytic oxidation of benzyl alcohol over manganese oxide supported on MCM-41 zeolite. *Chem. Eng. J.* **2015,** *271*, 14-22.

4. Ma, W.; Tong, Q.; Wang, J.; Yang, H.; Zhang, M.; Jiang, H.; Wang, Q.; Liu, Y.; Cheng, M., Synthesis and characterization of titanium(iv)/graphene oxide foam: a sustainable catalyst for the oxidation of benzyl alcohol to benzaldehyde. *RSC Adv.* **2017,** *7* (11), 6720-6723.

5. Choudhary, V. R.; Dumbre, D. K., Solvent-free selective oxidation of benzyl alcohol to benzaldehyde by tert-butyl hydroperoxide over U3O8-supported nano-gold catalysts. *Appl. Catal. A-Gen.* **2010,** *375* (2), 252-257.

6. Choudhary, V. R.; Dhar, A.; Jana, P.; Jha, R.; Uphade, B. S., A green process for chlorine-free benzaldehyde from the solvent-free oxidation of benzyl alcohol with molecular oxygen over a supported nano-size gold catalyst. *Green Chemistry* **2005,** *7* (11), 768-770.

7. Wang, H.; Wang, C.; Yan, H.; Yi, H.; Lu, J., Precisely-controlled synthesis of Au@Pd core–shell bimetallic catalyst via atomic layer deposition for selective oxidation of benzyl alcohol. *J. Catal.* **2015,** *324*, 59-68.

8. Makwana, V. D.; Son, Y.-C.; Howell, A. R.; Suib, S. L., The Role of Lattice Oxygen in Selective Benzyl Alcohol Oxidation Using OMS-2 Catalyst: A Kinetic and Isotope-Labeling Study. *J. Catal.* **2002,** *210* (1), 46-52.

9. Parmeggiani, C.; Matassini, C.; Cardona, F., A step forward towards sustainable aerobic alcohol oxidation: new and revised catalysts based on transition metals on solid supports. *Green Chemistry* **2017,** *19* (9), 2030-2050.

10. Long, J.; Xie, X.; Xu, J.; Gu, Q.; Chen, L.; Wang, X., Nitrogen-Doped Graphene Nanosheets as Metal-Free Catalysts for Aerobic Selective Oxidation of Benzylic Alcohols. *ACS Catal.* **2012,** *2* (4), 622-631.

11. Hussain, H.; Green, I. R.; Ahmed, I., Journey Describing Applications of Oxone in Synthetic Chemistry. *Chem. Rev.* **2013,** *113* (5), 3329-3371.

12. Mello, R.; Cassidei, L.; Fiorentino, M.; Fusco, C.; Hummer, W.; Jager, V.; Curci, R., OXIDATIONS BY METHYL(TRIFLUOROMETHYL)DIOXIRANE .5. CONVERSION OF ALCOHOLS INTO CARBONYL-COMPOUNDS. *J. Am. Chem. Soc.* **1991,** *113* (6), 2205-2208.

13. Thottumkara, A. P.; Bowsher, M. S.; Vinod, T. K., In Situ Generation of o-Iodoxybenzoic Acid (IBX) and the Catalytic Use of It in Oxidation Reactions in the Presence of Oxone as a Co-oxidant. *Org. Lett.* **2005,** *7* (14), 2933-2936.

14. Schulze, A.; Giannis, A., Oxidation of Alcohols with Catalytic Amounts of IBX. *Synthesis* **2006,** *2006* (02), 257-260.

15. Page, P. C. B.; Appleby, L. F.; Buckley, B. R.; Allin, S. M.; McKenzie, M. J., In Situ Generation of 2-Iodoxybenzoic Acid (IBX) in the Presence of Tetraphenylphosphonium Monoperoxysulfate (TPPP) for the Conversion of Primary Alcohols into the Corresponding Aldehydes. *Synlett* **2007,** *2007* (10), 1565-1568.

16. Uyanik, M.; Ishihara, K., Hypervalent iodine-mediated oxidation of alcohols. *Chem. Commun.* **2009,** (16), 2086-2099.

17. Uyanik, M.; Akakura, M.; Ishihara, K., 2-Iodoxybenzenesulfonic Acid as an Extremely Active Catalyst for the Selective Oxidation of Alcohols to Aldehydes, Ketones, Carboxylic Acids, and Enones with Oxone. *J. Am. Chem. Soc.* **2009,** *131* (1), 251-262.

18. Koo, B.-S.; Lee, C. K.; Lee, K.-J., OXIDATION OF BENZYL ALCOHOLS WITH OXONE® AND SODIUM BROMIDE. *Synth. Commun.* **2002,** *32* (14), 2115-2123.

19. Indrawirawan, S.; Sun, H.; Duan, X.; Wang, S., Nanocarbons in different structural dimensions (0–3D) for phenol adsorption and metal-free catalytic oxidation. *Appl. Catal. B-Environ.* **2015,** *179*, 352-362.

20. Duan, X.; Ao, Z.; Zhang, H.; Saunders, M.; Sun, H.; Shao, Z.; Wang, S., Nanodiamonds in sp2/sp3 configuration for radical to nonradical oxidation: Core-shell layer dependence. *Appl. Catal. B-Environ.* **2018,** *222*, 176-181.

21. Sun, H.; Liu, S.; Zhou, G.; Ang, H. M.; Tadé, M. O.; Wang, S., Reduced Graphene Oxide for Catalytic Oxidation of Aqueous Organic Pollutants. *ACS Appl. Mater. Interfaces* **2012,** *4* (10), 5466-5471.

22. Duan, X.; Sun, H.; Ao, Z.; Zhou, L.; Wang, G.; Wang, S., Unveiling the active sites of graphene-catalyzed peroxymonosulfate activation. *Carbon* **2016,** *107*, 371-378.

23. Duan, X.; Ao, Z.; Zhou, L.; Sun, H.; Wang, G.; Wang, S., Occurrence of radical and nonradical pathways from carbocatalysts for aqueous and nonaqueous catalytic oxidation. *Appl. Catal. B-Environ.* **2016,** *188*, 98-105.

24. Peng, W.; Liu, S.; Sun, H.; Yao, Y.; Zhi, L.; Wang, S., Synthesis of porous reduced graphene oxide as metal-free carbon for adsorption and catalytic oxidation of organics in water. *J. Mater. Chem. A* **2013,** *1* (19), 5854-5859.

25. Tuinstra, F.; Koenig, J. L., Raman Spectrum of Graphite. *The Journal of Chemical Physics* **1970,** *53* (3), 1126-1130.

26. R., D. D.; Hong-Peng, J.; W., B. C., Graphene Oxide: A Convenient Carbocatalyst for Facilitating Oxidation and Hydration Reactions. *Angew. Chem.* **2010,** *122* (38), 6965-6968.

27. Duan, X.; Sun, H.; Wang, Y.; Kang, J.; Wang, S., N-Doping-Induced Nonradical Reaction on Single-Walled Carbon Nanotubes for Catalytic Phenol Oxidation. *ACS Catal.* **2015,** *5* (2), 553-559.

28. Anipsitakis, G. P.; Dionysiou, D. D., Degradation of Organic Contaminants in Water with Sulfate Radicals Generated by the Conjunction of Peroxymonosulfate with Cobalt. *Environmental Science & Technology* **2003,** *37* (20), 4790-4797.

29. Liang, P.; Zhang, C.; Duan, X.; Sun, H.; Liu, S.; Tade, M. O.; Wang, S., An insight into metal organic framework derived N-doped graphene for the oxidative degradation of persistent contaminants: formation mechanism and generation of singlet oxygen from peroxymonosulfate. *Environmental Science: Nano* **2017,** *4* (2), 315-324.

30. Montgomery, R. E. J. J. o. t. A. C. S., Catalysis of peroxymonosulfate reactions by ketones. **1974,** *96* (25), 7820-7821.

31. Huang, Z.; Bao, H.; Yao, Y.; Lu, W.; Chen, W., Novel green activation processes and mechanism of peroxymonosulfate based on supported cobalt phthalocyanine catalyst. *Appl. Catal. B-Environ.* **2014,** *154-155*, 36-43.

32. Li, H.-R.; Wu, L.-Z.; Tung, C.-H., Reactions of Singlet Oxygen with Olefins and Sterically Hindered Amine in Mixed Surfactant Vesicles. *J. Am. Chem. Soc.* **2000,** *122* (11), 2446-2451.

33. Zhou, C.; Lai, C.; Huang, D.; Zeng, G.; Zhang, C.; Cheng, M.; Hu, L.; Wan, J.; Xiong, W.; Wen, M.; Wen, X.; Qin, L., Highly porous carbon nitride by supramolecular preassembly of monomers for photocatalytic removal of sulfamethazine under visible light driven. *Appl. Catal. B-Environ.* **2018,** *220*, 202-210.

34. Zhou, C.; Xu, P.; Lai, C.; Zhang, C.; Zeng, G.; Huang, D.; Cheng, M.; Hu, L.; Xiong, W.; Wen, X.; Qin, L.; Yuan, J.; Wang, W., Rational design of graphic carbon nitride copolymers by molecular doping for visible-light-driven degradation of aqueous sulfamethazine and hydrogen evolution. *Chem. Eng. J.* **2019,** *359*, 186-196.

35. Buxton, G. V.; Greenstock, C. L.; Helman, W. P.; Ross, A. B., Critical Review of rate constants for reactions of hydrated electrons, hydrogen atoms and hydroxyl radicals (·OH/·O− in Aqueous Solution. *J. Phys. Chem. Ref. Data* **1988,** *17* (2), 513-886.

36. Anipsitakis, G. P.; Dionysiou, D. D., Radical Generation by the Interaction of Transition Metals with Common Oxidants. *Environmental Science & Technology* **2004,** *38* (13), 3705-3712.

37. Qi, W.; Liu, W.; Zhang, B.; Gu, X.; Guo, X.; Su, D., Oxidative Dehydrogenation on Nanocarbon: Identification and Quantification of Active Sites by Chemical Titration. *Angew. Chem. Int. Ed.* **2013,** *52* (52), 14224-14228.

38. Zhang, J.; Liu, X.; Blume, R.; Zhang, A.; Schlögl, R.; Su, D. S., Surface-Modified Carbon Nanotubes Catalyze Oxidative Dehydrogenation of *n*-Butane. *Science* **2008,** *322* (5898), 73.

39. Madeira, L. M.; Portela, M. F., Catalytic oxidative dehydrogenation of n-butane. *Catalysis Reviews* **2002,** *44* (2), 247-286.

40. Vulic, I.; Vitarelli, G.; Zenner, J. M., Structure-property relationships: phenolic antioxidants with high efficacy and low color contribution. *Macromolecular Symposia* **2001,** *176* (1), 1-16.

41. Tocháček, J., Effect of secondary structure on physical behaviour and performance of hindered phenolic antioxidants in polypropylene. *Polym. Degrad. Stab.* **2004,** *86* (2), 385-389.

42. Li, J.; Yu, P.; Xie, J.; Liu, J.; Wang, Z.; Wu, C.; Rong, J.; Liu, H.; Su, D., Improving the Alkene Selectivity of Nanocarbon-Catalyzed Oxidative Dehydrogenation of n-Butane by Refinement of Oxygen Species. *ACS Catal.* **2017,** *7* (10), 7305-7311.

43. Li, J.; Yu, P.; Xie, J.; Zhang, Y.; Liu, H.; Su, D.; Rong, J., Grignard reagent reduced nanocarbon material in oxidative dehydrogenation of n-butane. *J. Catal.* **2018,** *360*, 51-56.

44. Szymański, G. S.; Karpiński, Z.; Biniak, S.; Świątkowski, A., The effect of the gradual thermal decomposition of surface oxygen species on the chemical and catalytic properties of oxidized activated carbon. *Carbon* **2002,** *40* (14), 2627-2639.

45. Duan, X.; Sun, H.; Kang, J.; Wang, Y.; Indrawirawan, S.; Wang, S., Insights into Heterogeneous Catalysis of Persulfate Activation on Dimensional-Structured Nanocarbons. *ACS Catal.* **2015,** *5* (8), 4629-4636.

46. Frank, B.; Zhang, J.; Blume, R.; Schlögl, R.; Su, D. S., Heteroatoms Increase the Selectivity in Oxidative Dehydrogenation Reactions on Nanocarbons. *Angew. Chem. Int. Ed.* **2009,** *48* (37), 6913-6917.

47. Foresman, J. B., Computational Chemistry: A Practical Guide for Applying Techniques to Real World Problems By David Young (Cytoclonal Pharmaceutics Inc.). Wiley-Interscience: New York. 2001. xxvi + 382 pp. $69.95. ISBN: 0-471-33368-9. *J. Am. Chem. Soc.* **2001,** *123* (41), 10142-10143.

48. Jiang, Q. G.; Ao, Z. M.; Li, S.; Wen, Z., Density functional theory calculations on the CO catalytic oxidation on Al-embedded graphene. *RSC Adv.* **2014,** *4* (39), 20290-20296.

49. Duan, X.; Sun, H.; Shao, Z.; Wang, S., Nonradical reactions in environmental remediation processes: Uncertainty and challenges. *Appl. Catal. B-Environ.* **2018,** *224*, 973-982.

50. Hummer, G.; Rasaiah, J. C.; Noworyta, J. P., Water conduction through the hydrophobic channel of a carbon nanotube. *Nature* **2001,** *414* (6860), 188-190.

51. Tang, C.; Zhang, N.; Shao, Q.; Huang, X.; Xiao, X., Rational design of ordered Pd–Pb nanocubes as highly active, selective and durable catalysts for solvent-free benzyl alcohol oxidation. *Nanoscale* **2019,** *11* (12), 5145-5150.

52. Gao, J.; Ren, Z.-G.; Lang, J.-P., Oxidation of benzyl alcohols to benzaldehydes in water catalyzed by a Cu(II) complex with a zwitterionic calix[4]arene ligand. *J. Organomet. Chem.* **2015,** *792*, 88-92.

53. Perdew, J. P.; Ruzsinszky, A.; Csonka, G. I.; Vydrov, O. A.; Scuseria, G. E.; Constantin, L. A.; Zhou, X.; Burke, K., Restoring the Density-Gradient Expansion for Exchange in Solids and Surfaces. *Phys. Rev. Lett.* **2008,** *100* (13), 136406.

54. Perdew, J. P.; Burke, K.; Ernzerhof, M., Generalized Gradient Approximation Made Simple. *Phys. Rev. Lett.* **1996,** *77* (18), 3865-3868.

55. Tkatchenko, A.; Scheffler, M., Accurate Molecular Van Der Waals Interactions from Ground-State Electron Density and Free-Atom Reference Data. *Phys. Rev. Lett.* **2009,** *102* (7), 073005.

56. Baughman, R. H.; Zakhidov, A. A.; de Heer, W. A., Carbon Nanotubes--the Route Toward Applications. *Science* **2002,** *297* (5582), 787.

57. Wang, Z.; Zhang, K.; Zhao, J.; Liu, X.; Xing, B., Adsorption and inhibition of butyrylcholinesterase by different engineered nanoparticles. *Chemosphere* **2010,** *79* (1), 86-92.

58. Nie, C.; Dai, Z.; Meng, H.; Duan, X.; Qin, Y.; Zhou, Y.; Ao, Z.; Wang, S.; An, T., Peroxydisulfate activation by positively polarized carbocatalyst for enhanced removal of aqueous organic pollutants. *Water Res.* **2019,** *166*, 115043.

59. Duan, X.; Ao, Z.; Sun, H.; Zhou, L.; Wang, G.; Wang, S., Insights into N-doping in single-walled carbon nanotubes for enhanced activation of superoxides: a mechanistic study. *Chem. Commun.* **2015,** *51* (83), 15249-15252.

60. Halgren, T. A.; Lipscomb, W. N., The synchronous-transit method for determining reaction pathways and locating molecular transition states. *Chem. Phys. Lett.* **1977,** *49* (2), 225-232.

Chapter 4 Tailoring collaborative N-O functionalities of graphene oxide for enhanced selective oxidation of benzyl alcohol

Abstract

Benzaldehyde (BzH) is an important chemical for industrial feedstock. However, the conventional production processes heavily rely on precious metal catalysts and bring about unavoidable pollution issues. Here we report a new catalytic process to use N-doped graphene oxide (NGO) as the catalyst for oxidation of benzyl alcohol (BzOH) into BzH by an environmentally benign oxidant, peroxymonosulfate (PMS). Different approaches are developed to synthesize carbonylated NGO, which shows higher catalytic efficiency than C=O-deficient NGO. The optimized catalyst could achieve 96% BzOH conversion and unprecedented 82% BzH yield under mild temperature (50 ºC), superior to some precious metal catalysts reported. The indispensable roles of pyridinic N and ketonic C=O groups on the catalyst for such attractive performance are unveiled. The pyridinic N and C=O groups could either form an electron bridge between BzOH and the oxidant to enable electron transfer for non-radical BzOH oxidation, or separately induce the generation of free radicals from PMS to accomplish BzOH oxidation. The non-radical oxidation process is more selective in yielding BzH. Furthermore the yielded BzH was free from over-oxidation into benzoic acid under various reaction conditions, because the unreacted BzOH can quench the radicals and BzH can hardly adsorb on graphene sheets, thus inhibiting its further oxidation. This work provided a cheap material and mechanic understanding of carbocatalysis for green organic synthesis with environmental and economic perspectives.

The content of this chapter is published in Carbon 2021. 182, 715-724.

4.1 Introduction

Selective oxidation of benzyl alcohol (BzOH) to benzaldehyde (BzH) is an important route to manufacture high value-added organic products.[1-2] Excellent efficiency has been achieved using conventional catalysts such as noble metals in O_2. However, the noble metals are too expensive for real applications,[3-4] and due to the inertness of O_2 molecules, high reaction temperature or addition of promoters such as HNO_3 is required to attain an ideal BzH yield. In order to tackle those problems, low-cost transition metals and nanocarbons could be applied as alternative catalysts.[5-10] Also, peroxide oxidants such as *tert*-butyl hydroperoxide (TBHP), hydrogen peroxide (H_2O_2), and peroxymonosulfate (PMS, basically available as a triple salt of potassium $KHSO_5 \cdot 1/2KHSO_4 \cdot 1/2K_2SO_4$, oxone) have been studied for liquid-phase organic oxidation reactions to replace oxygen gas.[11-13] These peroxides can be activated under mild conditions for oxidative reactions. However, liquid H_2O_2 and TBHP may have safety issues and high cost in transportation and storage, and thus a stable crystal solid chemical, PMS, has received intensive attention for both selective and non-selective oxidation reactions.[14] PMS has an excellent potential for numerous fundamental reactions of synthetic chemistry such as selective oxidation of C-H bonds of olefins and alcohols to obtain the corresponding oxygenated compounds.[11] However, extra additives are required to activate PMS to form more reactive and selective oxidizing species to accomplish a high yield of target products in these cases.[15-21]

In recent years, activation of PMS by carbon-based metal-free catalysts have been proposed and extensively studied in the advanced oxidation processes (AOPs) for water treatment.[22] The sp^2 hybridized carbocatalysts with surface carbonyl groups can induce the generation of various radicals including $SO_4^{\bullet-}$ (2.5-3.1 V), $SO_5^{\bullet-}$ (1.1 V) and $^{\bullet}OH$ (2.7 V), which can non-selectively attack the aqueous organics.[23-26] Furthermore, non-radical AOPs owing to the direct electron transfer from the target organics to PMS *via* the sp^2 carbon framework has also been reported.[27] However, the

reported PMS activation by carbocatalysts was dominantly applied to wastewater treatment and rarely used for organic synthesis. Unlike the radical-based AOPs, the non-radical pathway sheds lights on the feasibility of applying PMS in the selective oxidation. *Via* catalyst modification, the electron transfer ability and oxidative potentials of the PMS-carbocatalyst-organics systems can be tailored to replace the precious metal catalysts and expensive/unstable oxidants, thus achieving the selective oxidations in an environmentally benign manner.

Previously, we reported carbon nanotubes for PMS activation toward BzOH selective oxidation.[28] Dominated by a radical process, this facile reaction could be conducted without adding any other co-catalysts or additives under benign conditions. However, the BzH yield was still not ideal due to minor mineralization of BzOH into inorganics by the highly oxidizing radicals, reducing the selectivity to BzH. Thus, it was inspiring to improve oxidative efficiency *via* non-radical routes. BzH was known to be unstable owing to the presence of the aldehyde group and readily suffers from autoxidation into benzoic acid (BzOOH) even under air exposure.[29] Therefore, over-oxidation was a major concern for BzH in the selective oxidation of BzOH. Very unexpectedly, no by-product of BzOOH was detected, mirroring that further oxidation of the BzH into BzOOH did not occur in the carbon nanotube/PMS system,[28] while the reason for the selectivity not reaching 100% should be that a minimum amount of BzOH completely oxidized into CO_2 as in most reported AOPs. The reaction behaviour of BzOH and BzH towards the radical/non-radical oxidation by PMS deserved further research to gain a comprehensive understanding of the intrinsic reaction mechanism and to provide guidance for the catalyst design.

Nitrogen-doped carbon materials have been reported as efficient metal-free catalysts for PMS activation in AOPs, especially *via* the non-radical pathway.[27] The nature of carbon catalysts, including the surface functional groups and the electrochemical properties, could be tailored for improved catalytic efficiency. However, the identification of active sites on doped graphene catalysts was usually focused on either

N or O species. while the study regarding the synergistic effect of integrated functional groups on the catalytic performance has rarely been reported.

Herein, we present an investigation on tailoring the integrated functionalities of N-doped graphene oxides (NGO) and their application in highly selective oxidation of BzOH to BzH. The non-radical oxidation process was significantly enhanced by tuning the surface functionalities to gain a high BzH selectivity. The different reaction pathways towards the oxidative NGO/PMS system were explored deeply. The underlined role of BzOH against the undesired over-oxidations was also clarified. Thus, the current work paved a new way for highly efficient and green carbocatalysis for more valuable chemical synthesis.

4.2. Experimental section

Materials. Graphite powder, active carbon (AC) and nanodiamond (ND) were purchased from Sigma Aldrich. Single-walled carbon nanotubes (SWCNTs) and multi-walled carbon nanotubes (MWCNTs) were purchased from Timesnano, China. Peroxide hydroxide (~30%) was obtained from Chem-supply. The other chemicals were supplied by Sigma Aldrich.

N-doped carbocatalyst synthesis. Graphene oxide (GO) was first synthesized from graphite using the Hummers' method. N-doped graphene (NGO) was then obtained by impregnation and annealing. In a typical process, 1 g GO was finely ground and mixed with 1 g urea in a certain amount of water. The mixture was maintained at room temperature for 12 h and then dried at 60 ºC. The product was annealed at 400 ºC for 2 h under N_2 protection in an electric furnace. Then the black powder was fully washed by water and ethanol and dried at 60 ºC for 24 h to obtain NGO.

Other carbon substrates were prepared by the following procedures. One gram MWCNTs (or SWCNTs/ND) were added into a mixture of 45 mL H_2SO_4 (95-98%) and 15 mL HNO_3 (65-68%) and sonicated for 5 h at 25 ºC. Then the precipitate was filtered and thoroughly washed by deionized water. The black carbon nanotubes were dried at 60 ºC for 48 h to obtain O-MWCNT (O-SWCNT or O-ND). Then the O-MWCNT, O-SWCNT, AC and O-ND were employed as different carbon sources to prepare the corresponding N-doped carbocatalysts with a similar process as NGO. In addition, N(Melamine)-GO and N(NH_4NO_3)-GO were also synthesized by replacing urea with the same mass loading of melamine and NH_4NO_3 as N precursors.

Hydrogen peroxide, PMS and $KMnO_4$ were then used as oxidants for the post-oxidation treatments of NGO, separately. For the synthesis of NGO-H_2O_2, 0.5 g NGO was added into 50 mL H_2O_2 and stirred under 50 ºC for 5 h. After cooling down, the solid was filtered, washed and dried at 60 ºC for 24 h. The formation of NGO-PMS and NGO-$KMnO_4$ were carried out with the similar method and the mixture was composed of 0.5 g NGO, 0.5 mol oxidant and 50 mL water.

In addition, preparation of C=O-rich NGO with inorganic additives (NGO-A/N, NGO-A/Cl, NGO-A/C, NGO-Mg/N, NGO-Fe/N and NGO-Ca/N) was conducted with the same procedure as NGO except that 3.8 mmol of inorganic salts were added into the mixture at the impregnation step.

The passivation of carbonyl groups. The elimination of carbonyl groups on NGO and NGO-H_2O_2 was conducted in the following process. Firstly, 100 μL HCl (38%) with 0.5 g phenylhydrazine (PH) were dissolved in 10 mL $CHCl_3$, followed by adding 0.1 g NGO. The mixture was stirred under N_2 atmosphere at 60 ºC for 48 h in dark. The precipitate was then thoroughly rinsed with $CHCl_3$ and ethanol to remove the residual PH. Then the solid was dried at 60 ºC for 24 h to obtain NGO-PH. The NGO-H_2O_2-PH was prepared in the similar procedure.

Selective oxidation of BzOH. The catalytic evaluations of selective oxidation of BzOH were performed as follows. In a typical catalytic process, 5 mg catalyst was mixed with 2.5 mL water and 2.5 mL acetonitrile in a flask and maintained under sonication for 5 min. Then, 0.11 mmol oxone and 0.1 mmol BzOH were added into the flask, which was sealed and maintained at 50 ºC. After 5 h, the reactor was cooled down and was injected of 0.1 mmol anisole as an internal standard. The mixture after the reaction was filtered and the organic phase was extracted by toluene and analysed with GC.

Materials characterizations. Transmission electron microscopy (TEM) was conducted on a JEOL 2100 microscope. Scanning electron microscopy (SEM) was carried out using a Zeiss Neon 40EsV FIBSEM. X-ray photoelectron spectroscopy (XPS) analysis was performed on a Kratos AXIS Ultra DLD system at a base pressure of 1×10^{-8} torr with Al Kα radiation. The binding energies were referenced to the C1s line at 284.6 eV. Raman spectra of graphene samples were obtained on a Renishaw Raman spectrometer under ambient conditions using a 785 nm laser beam. Fourier transforms infrared spectra (FTIR) were obtained on a Bruker spectrometer. In situ electron paramagnetic resonance (EPR) spectra were derived on a Bruker EMS-plus instrument using 5,5-dimethyl-1-pyrroline *N*-oxide (DMPO) as the radical trapping agent.

4.3 Results and discussion

For fundamentally understanding of the significant roles of the individual functional groups (i.e., N and O species) on the catalysts in the catalytic reactions, a series of techniques were employed to modify graphene with varying functionalities and contents. In addition, a variety of designed reactions were performed to fully understand the oxidation behaviour.

4.3.1 Design and synthesis of carbocatalysts with tailored N-O functionalities

Urea was chosen in this work as it was one of the superior N precursors for the preparation of N-doped carbocatalysts in PMS activation.[30] The selective oxidation reaction of BzOH was performed in acetonitrile/water solution at moderate temperature (50 ºC) in the presence of PMS. Several carbon substrates were also employed including GO, MWCNTs, SWCNTs, AC and ND. Their corresponding N-doped catalysts were synthesized by an incipient impregnation and thermal decomposition method. The effects of the N doping into different carbon materials on the catalytic performance were investigated (Table 4-1). N doped GO achieved 22-fold enhancement of BzH yield (33.6%) compared with N-free GO (1.5%), while for the other carbon materials, the enhancement was below 3-fold. The information of N content on the catalysts was obtained from an elemental analysis of the XPS survey. With equal urea loading (urea: carbon source =1, mass ratio), the surface N content in N-doped GO reached 9.6% while for the other carbons, the N content was less than 3.1%, indicating that the structural nature of GO was superior to the other carbons in attaining more surface N species. The influence of the N precursor loading (urea, from 10 to 200 wt.%) suggested that, at the weight ratio of urea/GO over 1, the content of N species on N-doped GO was saturated and the catalytic performance showed no obvious change by further increased urea dosage (Figure 4-1). Therefore, the N-doped GO prepared with an equal mass ratio of urea:GO (denoted as NGO) was selected as the catalyst for subsequent investigation and discussion.

Table 4-1. N content and catalytic performances of different carbon sources before and after N doping in the selective oxidation of benzyl alcohol.

Carbon source[a]	Treatment[b]	N content (at.%)[c]	BzOH conversion (%)[d]	BzH selectivity (%)[d]	BzH yield (%)[d]	Fold[e]
GO	N free	--	8.2	18.3	1.5	22.4
	N doped	9.6	42.9	78.3	33.6	
O-MWCNT	N free	--	51.7	42.3	21.9	1.1
	N doped	1.2	47.2	50.1	23.6	
O-SWCNT	N free	--	10.9	67.9	7.4	1.5
	N doped	1.1	16.1	46.1	11.2	

AC	N free	--	14.4	45.2	6.5	2.7
	N doped	3.2	20.8	84.6	17.6	
O-ND	N free	--	33.5	50.6	16.9	0.7
	N doped	1.9	19.2	64.1	12.3	

[a] The carbon sources include graphene oxide (GO), oxidized multi-walled carbon nanotubes (O-MWCNT), oxidized single-walled carbon nanotubes (O-SWCNT), activated carbon (AC) and oxidized nanodiamonds (O-ND).

[b] The N-free catalysts were prepared following the same procedure as N doped ones except that no urea was loaded as the N precursor.

[c] The N content of each catalyst was obtained from XPS survey.

[d] Reaction conditions: 5 mg catalyst, 0.1 mmol BzOH, 0.11 mmol PMS, 5 mL acetonitrile/water (1:1, volume ratio), 50 ºC, 5 h.

[e] The enhancement of BzH yield after N doping for each carbon source.

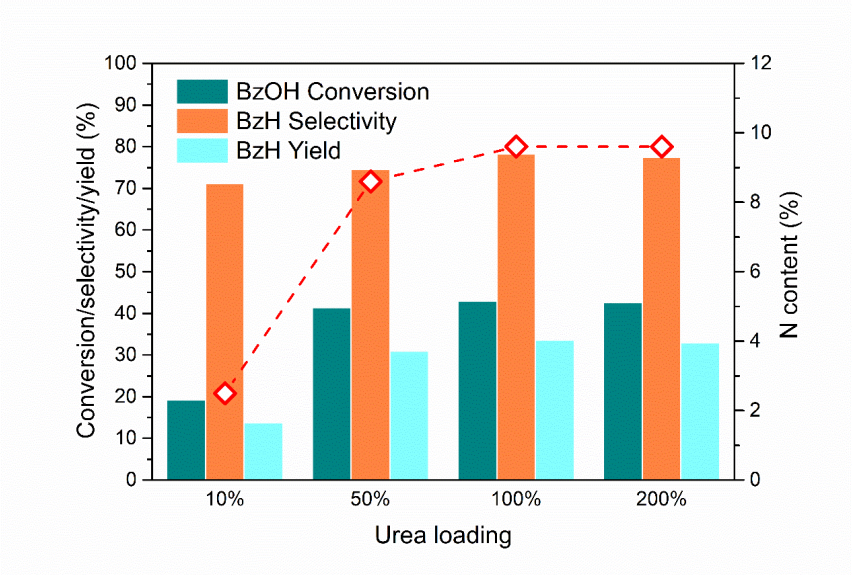

Figure 4-1. The surface N concentration and the selective oxidation of benzyl alcohol on the N-GO catalysts prepared with different urea loading amounts. Reaction conditions: 5 mg catalyst, 0.1 mmol BzOH, 0.11 mmol PMS, 5 mL acetonitrile/water (1:1, volume ratio), 50 ºC, 5 h.

After urea doping, the oxygen concentration on GO substantially dropped from 28.8 to 8.2%. In comparison, a control sample (GO-400) was prepared with the same procedure as NGO without urea loading. The oxygen concentration of GO-400 (15.0%) exceeded NGO (8.2%) by a large scale, indicating that the inserted N species led to the loss of oxygen groups. Notably, both BzOH conversion and BzH selectivity

increased with higher N dosage, indicating the incorporated N species might result in higher conversion/selectivity. SEM and TEM images (Figure 4-2 a, b) revealed the morphology of highly exfoliated graphene sheets with winkled structures, which were commonly observed on N-doped graphene.[24, 30] The nano-scaled thin layer structure enabled fast mass and charge transfer during the catalytic reactions. Further high-angle annular dark-field scanning (HAADF-STEM) images (Figure 4-2 c, left) and elemental mapping (Figure 4-2 c, right) indicated the uniform distributions of the abundant N and O species on NGO.

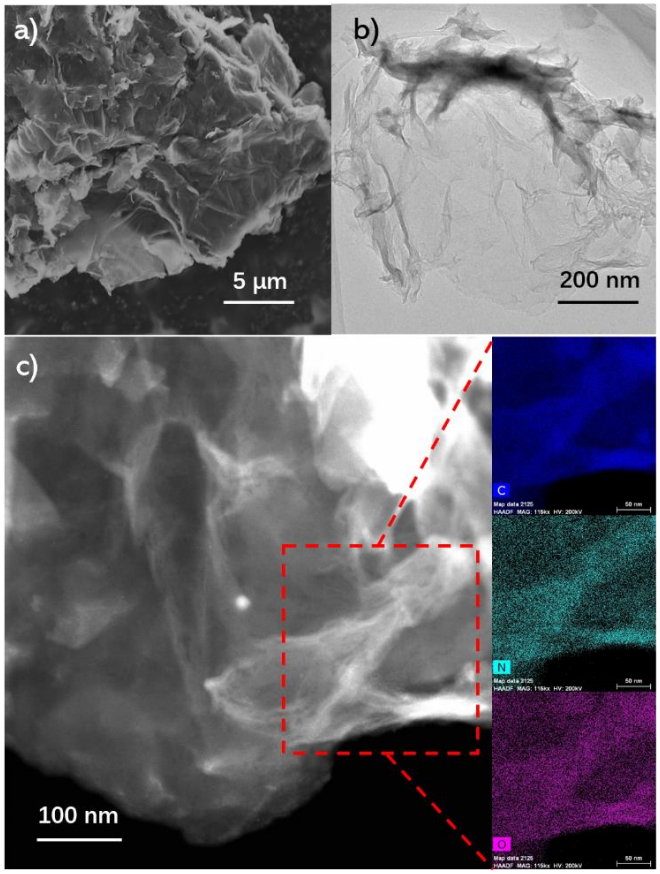

Figure 4-2. a) SEM and b) TEM image of NGO (urea as N precursor). c) HAADF-STEM image (left) and elemental mapping (right) of C, N and O in the selected area in the square of NGO.

The N species on carbon materials were composed of different types, such as graphitic or quaternary N, pyrrolic N, pyridinic N and amine. Previous research suggested that

the quaternary N served as the active site for PMS activation in AOPs, especially endowing the non-radical pathway.[27] Besides, the ketonic C=O groups on oxygenated carbo-catalysts also played an important role in PMS activation. The ketonic C=O groups were electron-rich and thus performed as nucleophilic active sites in various reactions.[31-33] However, there was still a lack of comprehensive understanding of the catalytic role of the other N species and the correlation between the surface N and O groups. It was recently found that the electron affinity (electrophilic and nucleophilic) of surface functionalities on the catalyst played a significant role in PMS activation for selective oxidation of BzOH by facilitating the electron transfer between the PMS and carbon catalysts.[28] In this regard, it was a logical consideration to develop highly active carbon catalysts with both electrophilic and nucleophilic groups to form an electron bridge to further promote the electron transfer from the target organics to PMS.

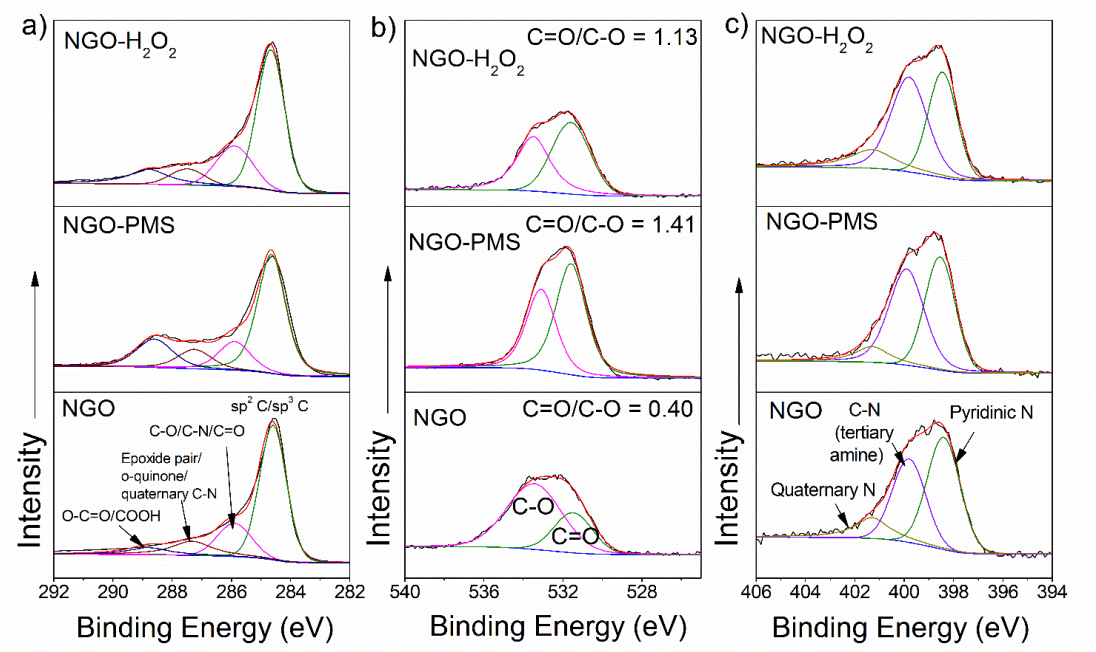

Figure 4-3. Deconvolution of a) C 1s, b) O 1s and c) N 1s XPS spectra of NGO, NGO-PMS and NGO-H_2O_2. The intensity scale was unified for the three samples in each spectra group (C1s, O1s and N1s).

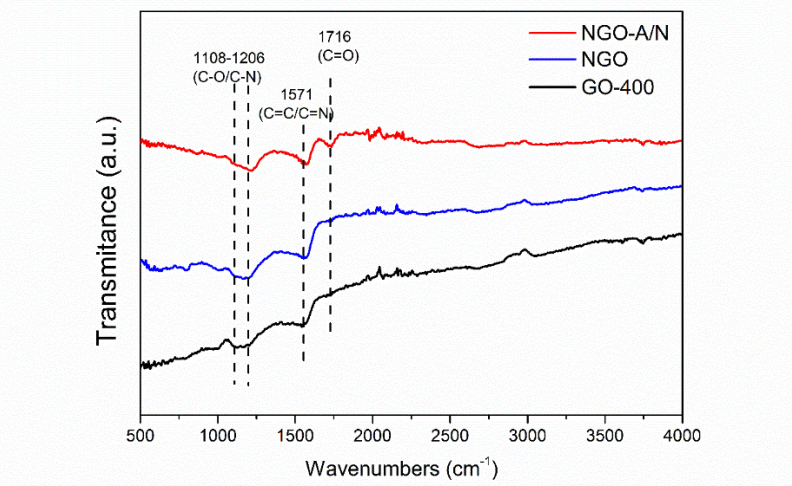

Figure 4-4. FTIR spectra of GO-400, NGO and NGO-A/N.

The surface chemistry of NGO was investigated by XPS (Figure 4-3). The deconvolution of N 1s spectra of NGO showed that 50% of the N species was pyridinic N (398.5 eV), whereas the quaternary N at around 401.3 eV only contributed 14% (Figure 4-3 (c), bottom). The peak around 400 eV could be assigned to pyrrolic or amine,[7, 34-35] but the N-H streching was not observed on FTIR spectra of NGO (Figure 4-4), so this peak was assignd to tertiary amine. It has been reported that the pyridinic N could induce *p*-type domains on graphene oxide[36] to withdraw electrons from the adsorbed electron-rich molecules. In this sense, the electron-withdrawing pyridinic N and the electron-rich C=O groups might facilitate adsorption of BzOH/PMS to form an electron tunnel for the electron transfer from BzOH to PMS. The O 1s XPS spectra of NGO could be fitted into two peaks of C-O and C=O species with a relatively low C=O/C-O ratio of 0.4 (Figure 4-3 (b), bottom), indicating that the surface oxygen functionalities on NGO were dominantly composed of C-O species. The C-O/C=O ratio of carbon materials significantly relied on the oxidizing environment,[31, 37] which provides possibilities to improve the catalytic performance *via* optimizing the N and O functionalities.

In order to increase the concentration of C=O groups on NGO, oxidation treatment was carried out using three typical oxidants (H_2O_2, $KMnO_4$ and PMS) and the samples

were denoted as NGO-H_2O_2, NGO-$KMnO_4$ and NGO-PMS, respectively. The N content of the catalysts and their catalytic activities in the selective oxidation of BzOH are summarised in Table 4-2. GO was ineffective in BzOH oxidation (entry 2) compared with the catalyst-free test (entry 1). Annealed GO without urea dopant (GO-400, entry 3) barely improved the catalytic performance. N doping on GO (NGO, entry 4) profoundly increased the BzOH conversion (42.9%) and BzH yield (33.6%) with a relatively high selectivity of 78.3%, indicating that the enhanced catalytic activity of NGO was attributed to the N doping. The post-oxidation of NGO further increased catalytic performances. Notably, the BzH selectivity kept over 90% for the three samples (entries 6,7,8). Among the three oxidized catalysts, NGO-$KMnO_4$ presented the lowest catalytic activity because $KMnO_4$ caused a severe loss of the surface N species (from 9.6 to 2.4%). The BzH yield of NGO-H_2O_2 reached 52.2%. However, GO-400-H_2O_2 presented no improvement in catalytic activity (entry 5), indicating that both N and O played crucial roles. BzH was the only organic product detected from GC-MS analysis, thus most of BzH was free from over-oxidation into BzOOH.

Table 4-2. Catalytic performances, N and O contents of various carbons in BzOH selective oxidation[a].

Entry	Catalyst	N/O content (at.%)[b]	BzOH conversion (%)	BzH selectivity (%)	BzH yield (%)
1	-	-	10.2	8.8	0.9
2	GO	-/28.8	9.7	8.2	0.8
3	GO-400	-/15.0	8.2	18.3	1.5
4	NGO	9.6/8.2	42.9	78.3	33.6
5	GO-400-H_2O_2	-/18.4	8.6	25.1	2.2
6	NGO-PMS	9.2/20.1	48.7	91.3	44.5
7	NGO-$KMnO_4$	2.4/27.5	45.8	93.2	42.7
8	NGO-H_2O_2	10.5/9.4	56.1	93.1	52.2
9	NGO-PH	10.8/8.0	31.2	60.5	18.9
10	NGO-H_2O_2-PH	13.6/7.7	30.7	55.7	17.1
11[c]	NGO-A/N	7.5/10.3	62.0	95.3	59.1
12[d]	NGO-A/N	7.5/10.3	96.0	85.4	82.0

[a] Reaction conditions: 0.1 mmol BzOH, 5 mg catalyst, 0.11 mmol PMS, 5 mL acetonitrile-water (volume ratio =1:1), 50 ºC, 5 h.

[b] Surface N and O concentrations on fresh catalysts derived from XPS.

[c] The reaction time was 3 h.

[d] The reaction time was 3 h and the PMS loading was 0.25 mmol.

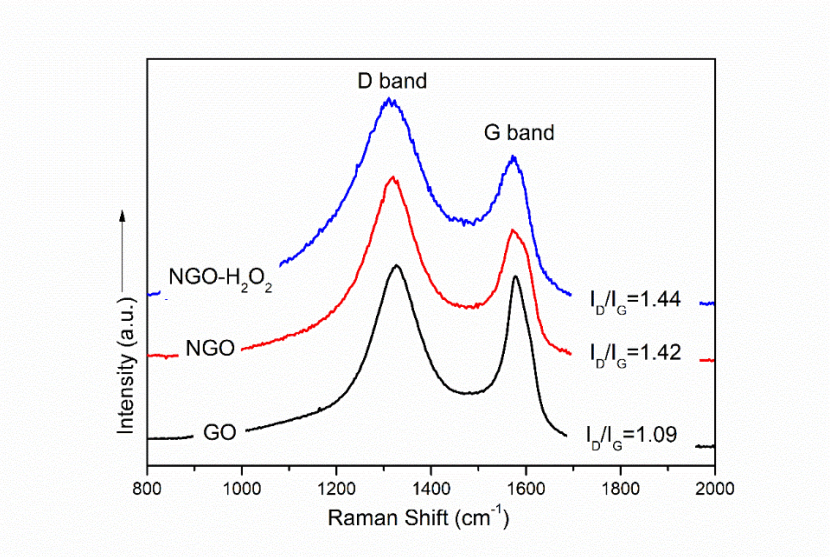

Figure 4-5. Raman spectra of GO, NGO and NGO-H_2O_2.

Raman spectra were adopted to evaluate the graphitic degree of the graphene-based catalysts with the peak intensity ratio of D and G (I_D/I_G) as an indicator (Figure 4-5).[38] After the N-doping, the I_D/I_G increases from 1.09 (GO) to 1.42, but the post-oxidation with H_2O_2 caused a negligible increase of I_D/I_G (1.44). It could be inferred that the enhanced catalysis after H_2O_2 treatment was not induced by the change of structural defects. The total oxygen content of NGO increased after post-oxidation treatments (Table 4-2) because more oxygen species were generated on NGO. The deconvolution of C 1s,[35, 39-41] O 1s [31] and N 1s [7, 34-35] XPS spectra revealed the evolution of the surface N and O states before and after the post-oxidation treatment. For the C 1s XPS spectra of NGO, NGO-PMS and NGO-H_2O_2 (Figure 4-3 (a)), the latter two samples had stronger intensity in the binding energy range of 286-290 eV than NGO, which was dominantly attributed to the generation of oxygenated groups. Then the O 1s and N 1s spectra were deconvoluted to gain detailed information of the composition of O and N species. The O 1s XPS spectra (Figure 4-3 (b)) further confirmed that the post-

oxidation treatment led to the conversion of C-O into C=O on NGO with a higher C=O/C-O ratio (NGO: 0.40, NGO-PMS: 1.41 and NGO-H_2O_2: 1.13) whereas there was no visible variation of the composition of N species (Figure 4-3 (c)). From the above results, the C=O groups were suggested to play a critical role in N-doped graphene catalysis and synergistically worked with the active N species for PMS activation.

4.3.2 Identification of active sites and mechanism of the catalytic routes

For identifying the catalytic roles of active N and O species and reaction pathway, different N precursors (melamine and NH_4NO_3) were used to prepare more NGO and H_2O_2 treated NGO samples. The XPS elemental analysis, N 1s deconvolution species and the catalytic performance of the relevant catalysts are presented in Table 4-3 and Figure 4-6. The N content on melamine derived N-GO was as high as 36.2%, dominantly composed of graphitic N (71%), with only 12% pyridinic N. The BzH yield over melamine derived N-GO reached 29.6%, slightly lower than that of urea derived NGO (33.6%). However, after post-oxidation by H_2O_2, the N content slightly reduced to 33.7% without apparent changes of the composition of N species, and the BzH yield decreased to 24.5%. For NH_4NO_3 derived N-GO, the total N concentration was 6.4% and was composed of 39% pyridinic N and 23% graphitic N. After H_2O_2 treatment, a considerable loss of pyridinic N occurred (graphitic N: 32%; pyridinic N: 26%; total N content: 4.2%), probably due to the unstable N-graphene configuration derived from NH_4NO_3. As a consequence, the BzH yield dramatically decreased from 16.7 to 4.2%. These results further confirmed the pivotal role of pyridinic N on NGO in PMS activation for BzOH oxidation.

Table 4-3. The N/O content and catalytic performances of N-doped GO samples prepared from different nitrogen precursors before and after H_2O_2 treatment in the selective oxidation of benzyl alcohol.

Catalyst[a]	N (at.%)[b]	O (at.%)[b]	BzOH conversion (%)[c]	BzH selectivity (%)[c]	BzH yield (%)[c]
N(Urea)-GO	9.6	8.9	42.9	78.3	33.6
N(Urea)-GO-H_2O_2	10.5	9.3	56.1	93.1	52.2
N(Melamine)-GO	36.2	8.5	40.5	73.1	29.6
N(Melamine)-GO-H_2O_2	33.7	10.6	38.5	63.6	24.5
N(NH_4NO_3)-GO	6.4	10.0	32.7	51.0	16.7
N(NH_4NO_3)-GO-H_2O_2	4.2	14.8	15.2	32.4	4.9

[a] The three different N precursors derived N-GO and N-GO-H_2O_2 were prepared following the same procedure.

[b] The N and O contents of each catalyst were obtained from XPS survey.

[c] Reaction conditions: 5 mg catalyst, 0.1 mmol BzOH, 0.11 mmol PMS, 5 mL acetonitrile/water (1:1, volume ratio), 50 ºC, 5 h.

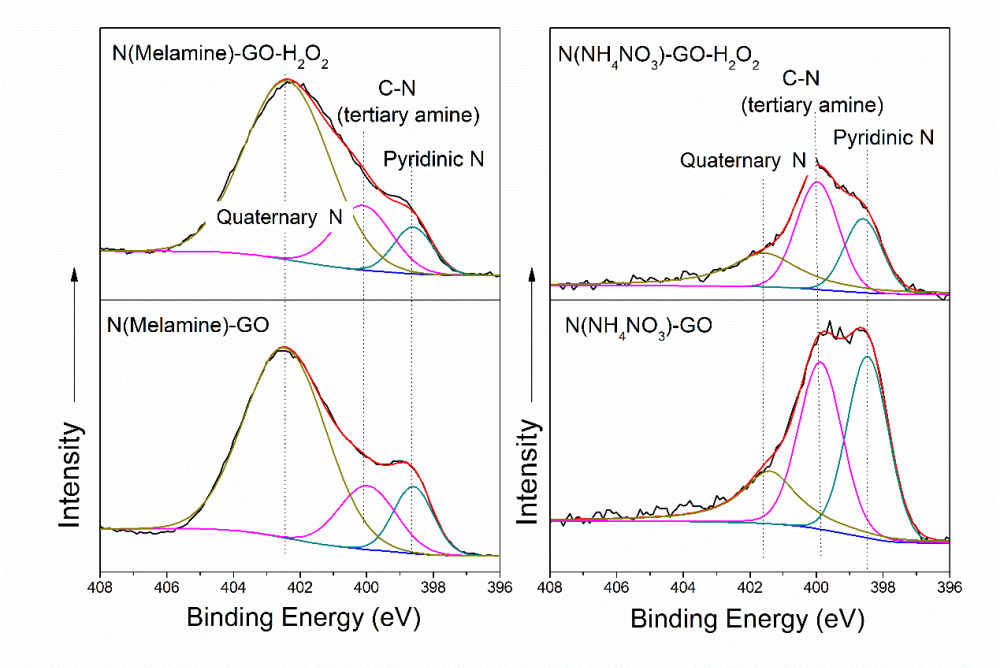

Figure 4-6. N 1s XPS spectra of N(Melamine)-GO, N(Melamine)-GO-H_2O_2, N(NH_4NO_3)-GO, and N(NH_4NO_3)-GO-H_2O_2.

The carbonyl groups on carbon materials could be selectively deactivated by phenylhydrazine (PH) *via* a specific reaction.[42] The C=O groups reacted with hydrazine to form a -C=N-N- structure, leading to the increased N concentration. The N and O contents of NGO and NGO-H_2O_2 before and after the C=O deactivation are

illustrated in Table 4-2, entries 9 and 10. For NGO-H_2O_2, the increase of N concentration (+3.1%) and decrease of O concentration (-1.7%) after the PH treatment was more significant than NGO (+1.2% and -0.2%), confirming that the C=O species on NGO were enriched after H_2O_2 post-oxidation. As expected, NGO and NGO-H_2O_2 suffered from a sharp decrease in both BzOH conversion and BzH selectivity owing to the deactivated C=O groups. Notably, the PH treated NGO and NGO-H_2O_2 showed similar catalytic efficiency, revealing that the enhanced catalytic performance by post-oxidation treatment was attributed to the created C=O groups. At this stage, the essential role of C=O species on NGO was verified and C=O was responsible for the improved conversion/selectivity.

The evolution of radicals during the activation of PMS was probed by EPR. Very weak signals of radicals were observed in EPR spectra without a catalyst and the generation of sulfate radicals and hydroxyl radicals were greatly enhanced upon the addition of NGO-H_2O_2 as suggested in Figure 4-7. A series of quenching tests were also performed for an in-depth understanding of the reaction pathways (radical/non-radical) in this system. Ethanol was employed as a strong quenching agent for both hydroxyl and sulfate radicals while *tert*-butanol (TBA) served as an effective $^{\bullet}OH$ scavenger.[28] The quenching effect of ethanol dosage on the reaction performances over NGO and NGO-H_2O_2 was presented in Figure 4-8 (a) and (b). A rapid drop of BzOH conversion and BzH yield was observed with increased dosage of ethanol, suggesting the importance of the radicals in selective oxidation of BzOH into BzH. When the acetonitrile solvent was completely replaced by ethanol, BzH selectivity increased remarkably and NGO-H_2O_2 possessed a higher BzH yield (29.1%) than NGO (14.1%). This suggests the BzOH oxidation was performed with both radical and non-radical routes and the non-radical oxidation route enables higher selectivity towards BzH. The addition of TBA only caused a slight decrease of reaction efficiency relative to ethanol (Figure 4-9). Therefore, sulfate radicals were suggested to be more effective for the selective oxidation of BzOH than hydroxyl radicals. Moreover, the different contributions of non-radical and radical processes to the BzH yield could also be

roughly determined by assuming that the BzH yield in the maximum ethanol dosage experiment was due to the non-radical reaction. Both the non-radical and radical processes were enhanced after post-oxidation of NGO and the non-radical reaction showed a more significant increase (Figure 4-10). It could be inferred that the radical and non-radical processes were simultaneously facilitated by the enriched C=O groups, and the non-radical oxidation route was more selective in BzOH oxidation. Likewise, the role of N species in the radical/non-radical process was investigated by altering the urea dosage during NGO preparation (from 10 to 100%, Figure 4-11). Similarly, both radical and non-radical reaction rates increased with a higher N content. These results revealed that the C=O and N species were actively involved in both radical and non-radical oxidation reactions.

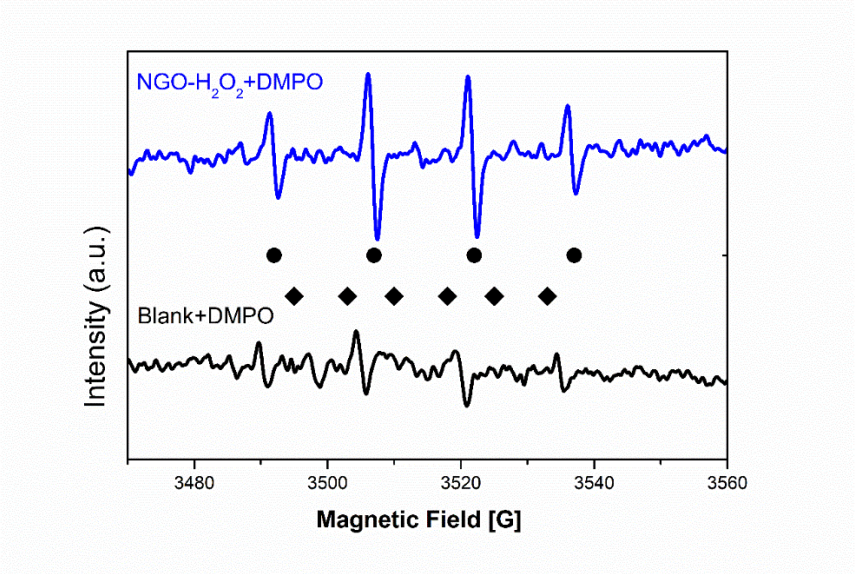

Figure 4-7. In-situ EPR spectra of NGO-H_2O_2 catalyzed PMS activation and blank control in the presence of DMPO (DMPO-$^{\bullet}$OH-●, DMPO- $SO_4^{\bullet-}$-♦). Conditions: 5 mg catalyst, 0.1 mmol BzOH, 0.11 mmol PMS, 5 mL acetonitrile/water (1:1, volume ratio), 50 ºC.

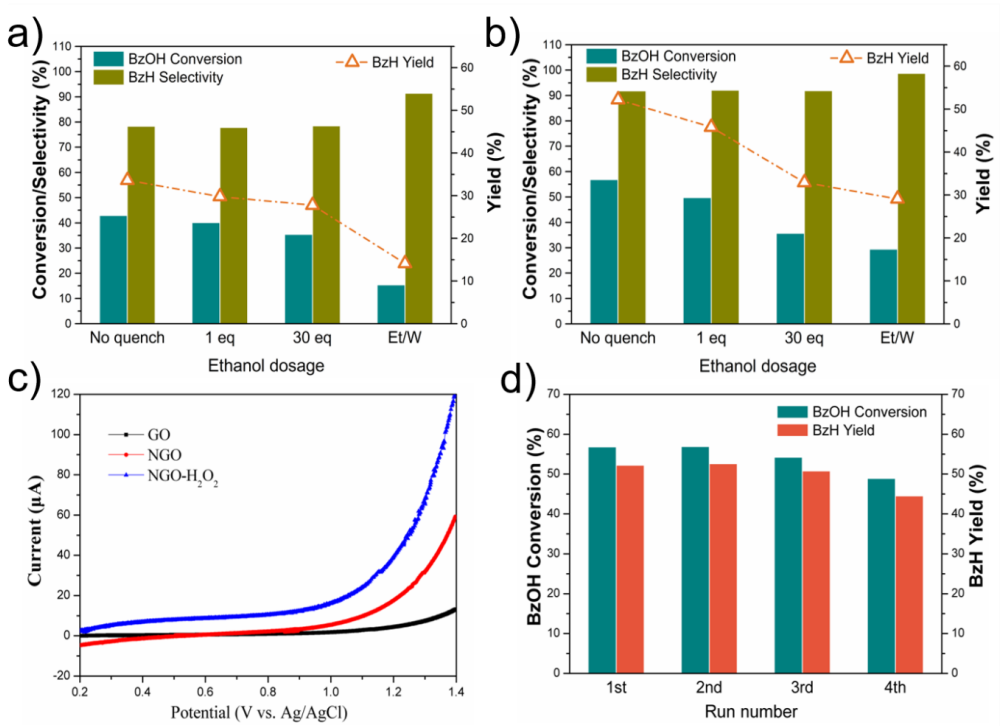

Figure 4-8. The influences of ethanol dosage on the selective oxidation of benzyl alcohol with a) NGO and b) NGO-H_2O_2. The ethanol dosages were set as 1 equivalent of PMS (1eq), 100-fold of PMS (100 eq) and replacing the acetonitrile solvent with ethanol (Et/W), respectively. c) Linear-sweep voltammograms of different catalysts ([Na_2SO_4]=0.1M). d) Stability and recycling test of NGO-H_2O_2. Reaction conditions of a), b) and d): 0.1 mmol BzOH, 5 mg catalyst, 0.11 mmol PMS, 5 mL acetonitrile/water (volume ratio =1:1,), 50 ºC, 5 h.

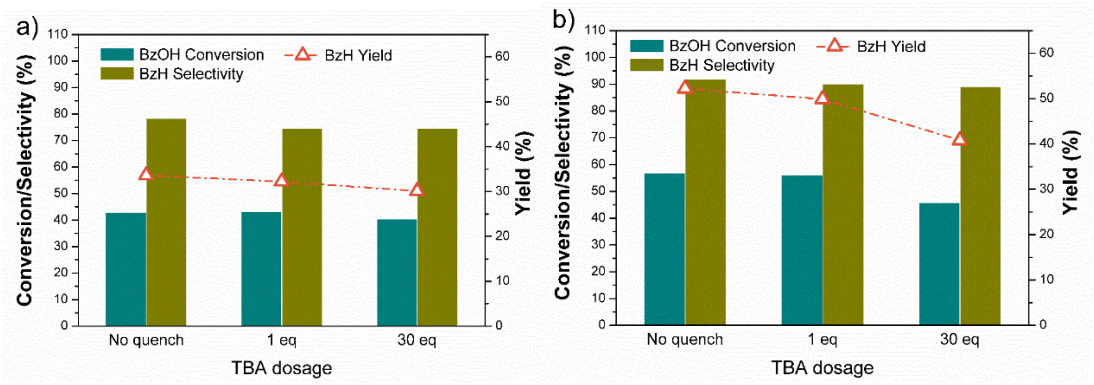

Figure 4-9. The influence of *tert*-butanol (TBA) dosage (no quench, 1 equivalent to PMS and 30 equivalent to PMS) on the selective oxidation of benzyl alcohol with a) NGO and b) NGO-H_2O_2.

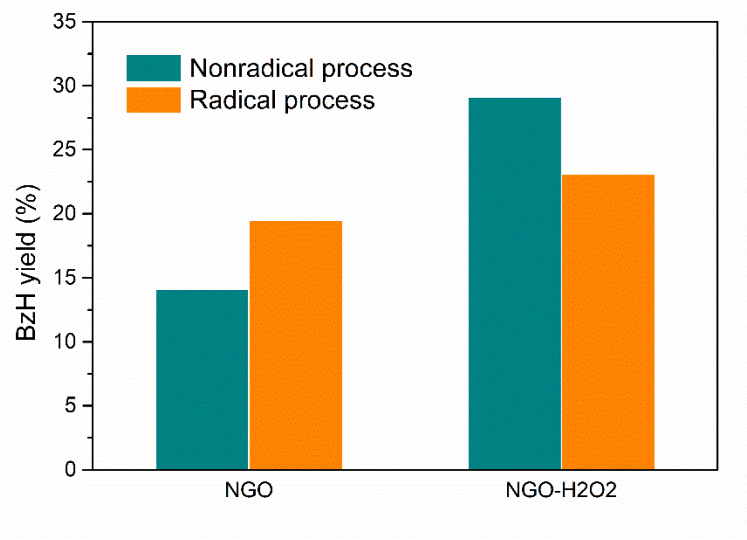

Figure 4-10. The radical/non-radical reaction contribution to the BzH yield of NGO and NGO-H_2O_2 catalyst. The contribution of non-radical process ($Y(BzH)_{ethanol}$) was obtained by replacing acetonitrile with ethanol in the solvent. The contribution of radical process was calculated as: $Y(BzH)-Y(BzH)_{ethanol}$, wherein Y(BzH) refers to the BzH yield of non-ethanol involved reaction.

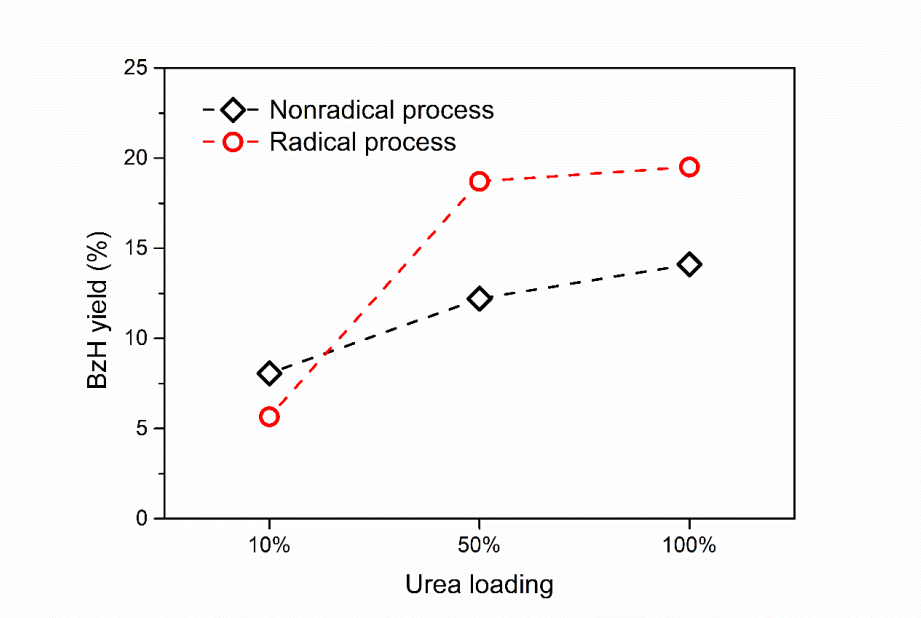

Figure 4-11. The radical/nonradical reaction contributions to the BzH yield of NGO derived from different urea dosage amount (10-100 wt.%).

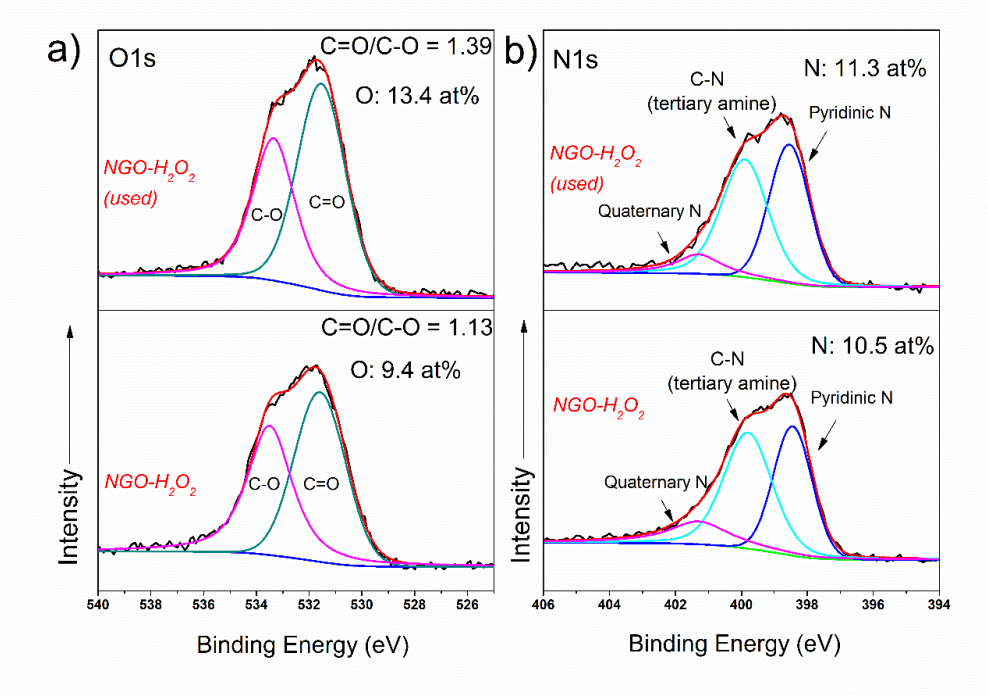

Figure 4-12. Deconvolution of O 1s and N 1s XPS spectra of fresh and used NGO-H_2O_2.

As the carbocatalyst-mediated electron transfer was crucial for the non-radical pathway, linear sweep voltammetry (LSV) tests were conducted to measure the electrochemical properties of the catalysts. As shown in Figure 4-8 (c), in the presence of PMS/BzOH, the electron transfer ability of the catalysts followed an order of NGO-H_2O_2 > NGO > GO, agreeing well with the catalytic performance especially the non-radical oxidation. In addition, NGO-H_2O_2 possessed better stability in comparison with our previously reported carbocatalysts,[28] with only 7.9% decrease in BzOH conversion and 7.7% decrease in BzH yield after 4 runs (Figure 4-8 (d)), indicating that most of the active sites were well maintained after the reaction. Figure 4-12 suggests that the oxygen content of the used catalyst (13.4 at.%) was slightly higher than the fresh one (9.4 at.%), due to the surface oxidation of catalyst in PMS environment (such as the transformation of C-O/C=O into O-C=O), which could possibly lead to the minor deactivation.[43]

4.3.3 Preparation of the C=O-rich NGO with inorganic additives

For further confirmation of the hypothesis, a one-step method was developed to prepare a C=O-rich NGO catalyst from GO by introducing additives during the preparation. A solid-state synthesis method has been reported, employing magnesium nitrate to produce reduced GO and annealed CNTs based MgO-nanocarbon hybrids with high C=O concentration.[44-45] In this work, both non-metallic salts including NH_4NO_3 (A/N), NH_4Cl (A/Cl), NH_4HCO_3 (A/C) and metallic nitrate salts were tested individually as additives with urea to prepare the C=O-rich NGO. The ketonic C=O content was greatly enhanced by the addition of non-metal salts (Figure 4-13 (a)). Likewise, similar results were observed when replacing the non-metal salts with $Mg(NO_3)_2$, $Ca(NO_3)_2$ and $Fe(NO_3)_3$ (Figure 4-13 (b)). The FTIR spectra of NGO-A/N exhibited an obvious increase of C=O groups at 1716 cm^{-1} compared with NGO,[46-48] confirming the successful generation of C=O (Figure 4-4). It was inferred that loading either non-metallic or metallic salts into the NGO preparation could enrich the ketonic C=O groups, possibly due to the etching of graphene sheets by the decomposition of the salt, which led to more defect sites for the selective generation of C=O. In terms of the catalyst evaluation, all the applied inorganic salts were able to enhance the catalytic efficiency (Table 4-4). The BzH selectivity and yield were raised to over 90% and 50% by the addition of salts in the catalyst preparation. NGO-A/N showed the best reactivity after 3 h reaction at the PMS/BzOH molar ratio of 1.1 to generate BzH in 59.1% yield and 95.3% selectivity, superior to NGO-H_2O_2 (Table 4-2, entries 8 and 11). The cycling/stability tests (Figure 4-14 (a)) and ethanol quenching results (Figure 4-14 (b)) on NGO-A/N were like these on NGO-H_2O_2. When the radicals were quenched with full ethanol dosage, 34.9% BzH yield was remained compared with 59.1% BzH yield from the no-quenching test, indicating that over half of the performed oxidation was originated from the non-radical reaction. These results provided convincing proofs to the previous conjecture that the N species and C=O were co-active sites for BzOH oxidation in PMS activation. Besides, the oxidation reaction performed under various conditions by adopting NGO-A/N as the representative

catalyst showed that the increased temperature, reaction time, catalyst and PMS dosage could lead to improved conversion of BzOH and yield of BzH (Table 4-5). The BzH selectivity remained almost at a similar level regardless of the change of reaction conditions, indicating that such a highly selective reaction system was robust and suitable for a wide range of working conditions. In this work, the highest BzH yield of 82% was obtained at a PMS/BzOH ratio of 2.5 with 96% BzOH conversion and 85.4% selectivity (Table 4-2, entry 12), which was even superior to that of a noble-metal (Pd/Pb) catalyst with higher conversion (96 versus 91.3%) and lower temperature (50 versus 130 ºC).[49]

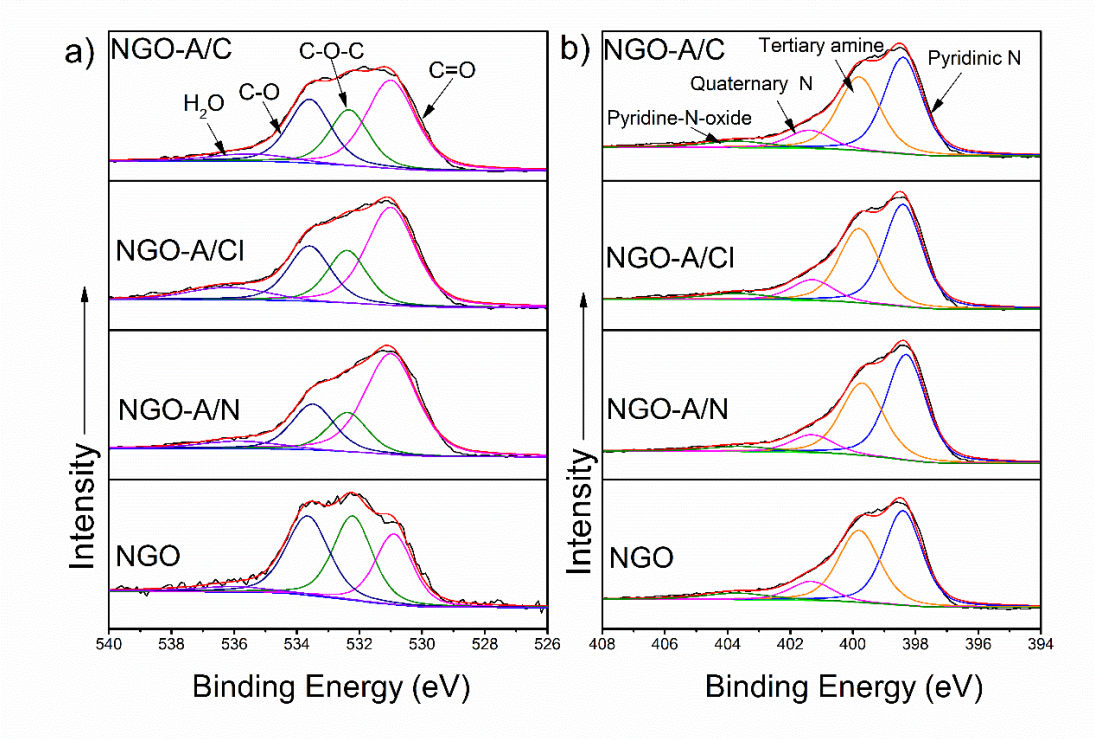

Figure 4-13. Deconvolution of O 1s XPS spectra of various NGO catalysts.

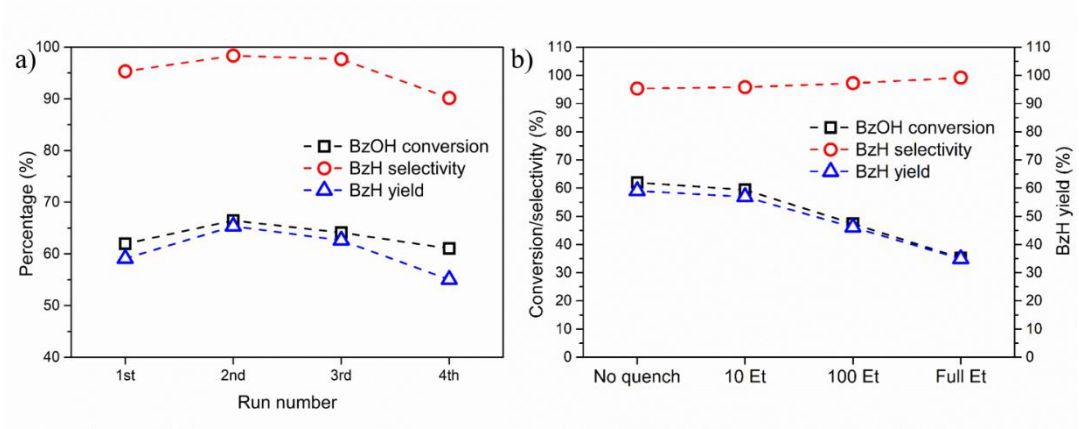

Figure 4-14. (a) Stability and recycling tests of NGO-A/N. (b) Effect of quenching agent (ethanol) on selective oxidation of BzOH by NGO-A/N.

Table 4-4. Composition of surface N and O species on catalysts and their catalytic activity in selective oxidation of BzOH. Reaction conditions: 5 mg catalyst, 0.1 mmol BzOH, 0.11 mmol PMS, 5 mL acetonitrile/water (1:1, volume ratio), 50 ºC, 3 h.

Catalyst	O/N content (at. %)	C-O content (at. %)	C-O-C content (at. %)	C=O content (at. %)	BzOH conversion (%)	BzH selectivity (%)	BzH yield (%)
NGO	7.8/9.3	2.7	2.6	2.0	46.2	81.3	37.5
NGO-A/N	7.5/10.3	1.6	1.3	4.3	62.0	95.3	59.1
NGO-A/Cl	7.2/9.9	1.7	1.5	3.5	60.3	96.0	57.9
NGO-A/C	7.7/9.3	2.1	1.7	3.5	59.2	95.1	56.3
NGO-Mg/N	8.4/10.2	2.1	2.3	3.1	59.7	94.1	56.2
NGO-Ca/N	8.2/9.4	1.6	2.0	4.2	59.4	93.9	55.8
NGO-Fe/N	7.2/10.8	1.7	1.7	3.4	55.1	93.4	51.5

Table 4-5. Selective oxidation of BzOH under different conditions by employing NGO-A/N as representative catalyst. The reactions were undertaken in 5 mL acetonitrile/water mixture containing 0.1 mmol BzOH.

Entry	Catalyst dosage (mg)	Reaction time (h)	Temperature (ºC)	PMS/BzOH (molar ratio)	BzOH conversion (%)	BzH selectivity (%)	BzH yield (%)
1	2.5	3	50	1.1	61.1	96.2	58.8
2	5	3	50	1.1	62.0	95.3	59.1
3	10	3	50	1.1	63.6	94.6	60.2
4	5	1	50	1.1	52.6	93.0	48.9
5	5	2	50	1.1	58.6	95.2	55.8

6	5	5	50	1.1	63.9	92.8	59.3
7	5	3	35	1.1	61.0	86.5	52.8
8	5	3	65	1.1	65.2	94.7	61.8
9	5	3	50	0.6	34.1	95.5	32.6
10	5	3	50	2	85.7	93.1	79.8
11	5	3	50	2.5	96.0	85.4	82.0
12	5	3	50	3	98.2	79.5	78.1

4.3.4 Catalytic mechanism elucidation

It is concluded from the above results that the pyridinic N and carbonyl C=O are dual active sites in both radical and non-radical oxidation of BzOH into BzH. We speculate the non-radical reaction was accomplished by mediated electron transfer *via* the surface complex based on the test of LSV curves (another proof will be provided in the next section). It has been reported that the electrophilic pyridinic N shows strong basicity against the other N species and is prone to adsorb the –OH groups from alcohols to facilitate the oxidation.[50] Besides, PMS molecules could be activated on both electrophilic and nucleophilic functional groups. The adsorption of PMS on nucleophilic C=O led to the rupture of O-O bond to deliver $SO_4^{\bullet-}$ and $^{\bullet}OH$ radicals,[25] while the adsorption of PMS on electrophilic species could result in the O-H bond cleavage (H-$OOSO_3$) to generate $SO_5^{\bullet-}$ radicals for subsequent oxidations.[28]

Based on that, a possible mechanism of the reaction pathways using the prepared NGO was schematically shown in Figure 4-15. The modified NGO was equipped with abundant pyridinic N and carbonyl species and could activate PMS for the selective oxidation of BzOH into BzH *via* both radical and non-radical processes. When the pyridinic N and C=O species were located closely on the edges of graphene planes, the pyridinic N could induce electrophilic domains on adjacent graphene layers and attract the electron-saturated branch in BzOH whereas the electron-rich C=O groups were related to the -O-O- configuration in PMS. The electron transfer from BzOH to PMS occurred subsequently through the highly conjugated π system of graphene to accomplish the non-radical pathway. BzH was produced from BzOH by donating two

electrons to PMS and releasing two H atoms to the solvent. On the other hand, the isolated N and C=O could adsorb and activate PMS by capturing electrons from PMS to generate $SO_5^{\bullet-}$ radicals which could further decompose into $SO_4^{\bullet-}$ radicals, or donating an electron to PMS to form $SO_4^{\bullet-}$ and $^{\bullet}OH$ radicals. The generated reactive radicals would subsequently react with BzOH to generate BzH. A plausible reaction pathway between BzOH and radicals is provided assuming that the radicals firstly attract an α–H from BzOH to derive the $PhCHOH^{\bullet}$ radical, since the α–H from the BzOH molecules was reported to quench the radicals [29] (will be further verified in the next section). The catalyst maintained the electron balance and stability *via* the transfer of delocalized electrons in both radical and non-radical processes.

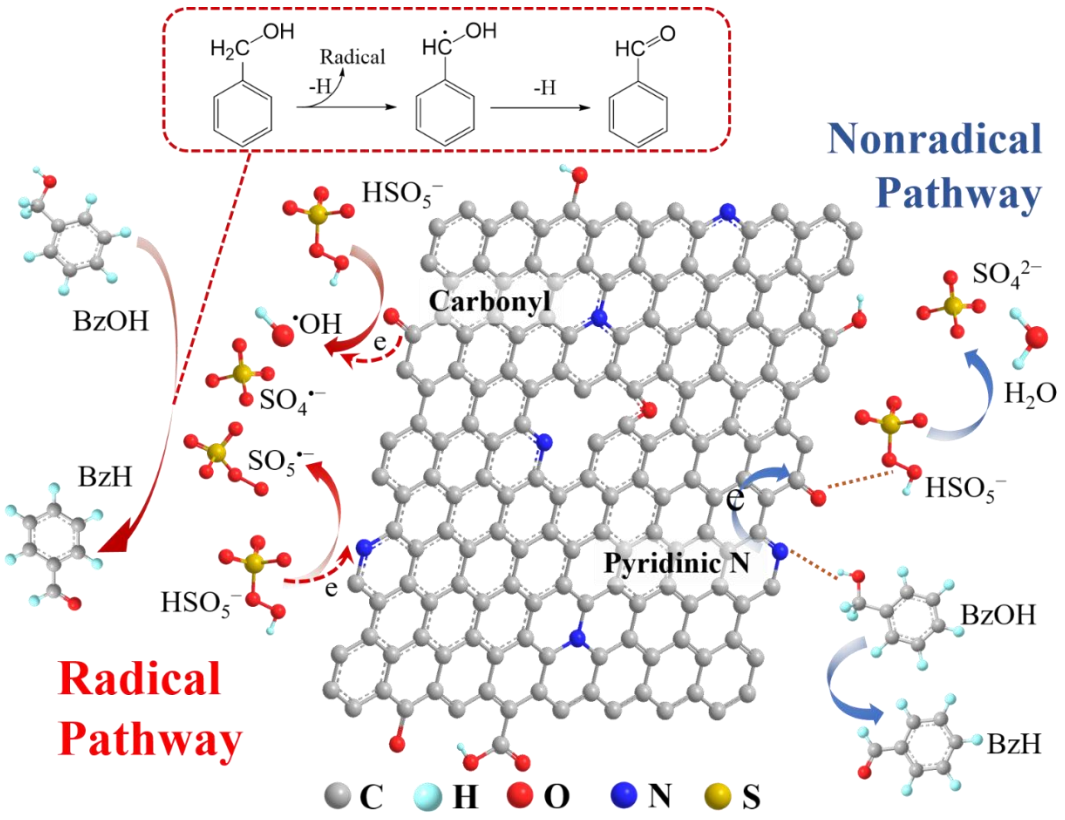

Figure 4-15. Proposed mechanism of the radical/non-radical pathways for selective oxidation of BzOH over the optimized NG.

4.3.5 Underlined mechanism for BzH without deep-oxidation

In theory, the oxidation of BzOH could result in the formation of BzH (marked by the blue arrow), or further oxidation product of BzOOH (marked by the red arrow) as displayed in Figure 4-16 (a). However, in this NGO/PMS system, the deep-oxidation of BzH into BzOOH was not observed as mentioned above. To fully understand the oxidation behaviour, especially why BzH was free from deep-oxidation, the individual and competitive reactions of BzOH and BzH towards the PMS/NGO system were performed. Firstly, BzOH and BzH were individually loaded into the reaction system with different PMS dosage. When BzOH was the only reactant, its conversion was remarkably increased with higher PMS dosage (Figure 4-16 (b)). BzH was detected as the only organic product even at the 2.5-fold PMS dosage, and no BzOOH was found in the product. However, when BzH was the oxidation substrate, BzH was selectively oxidized into BzOOH with 70-80% selectivity (Figure 4-16 (c)). A nearly linear relationship was observed between the BzH conversion and the PMS concentration. Ethanol quenching tests were performed to probe the oxidation pathway of BzH, and the result was shown in the inset of Figure 4-16 (c). The BzH conversion was sharply reduced from 61.4% to 3.5% after adding ethanol. Therefore, the BzH to BzOOH reaction route in the PMS/NGO system was only applicable *via* radical processes in the absence of BzOH. The absence of non-radical oxidation of BzH is possibly because the aldehyde groups have weaker acidity than alcohols, thus the adsorption of benzaldehyde on pyridinic N is hard to occur. Moreover, this observation suggests that the non-radical oxidation of BzOH was attributed to the electron-transfer *via* the surface-adsorbed chemicals instead of the widely reported singlet oxygen ($^1O_2$). The $^1O_2$ was proven to be generated *via* the interaction of the catalyst and PMS, regardless of the organic reactant,[51] thus the fact that BzH could only be oxidized by the radicals ruled out the possibility of the oxidation of BzOH by $^1O_2$ since BzH possessed a more oxidizable nature than BzOH. When an identical amount of BzOH and BzH co-existed in the system, the ascending curve of BzOH conversion with the increased PMS dosage was observed (Figure 4-16 (d)), similar to Figure 4-16 (b). However, the conversion

of BzH was kept below 2% (calculated according to the selectivity level of Figure 4-16 (b)), indicating that BzH can hardly be oxidized due to the presence of BzOH. Therefore, it was suggested that BzH is free from deep-oxidation during the selective oxidation of BzOH due to the unreacted BzOH serving as the terminating agent.

It has been reported that the α–H from the BzOH molecules could quench the radicals and minimize the autoxidation of BzH,[29] which might help explain the inhibitive effect of BzOH on the radical-based BzH oxidation. To prove that, identical amount of 1-phenylethanol, toluene and ethylbenzene were added to the BzH oxidation system individually to demonstrate the influence of the α–H-containing benzylic alcohol on BzH oxidation. The results demonstrated that all the added chemicals could inhibit the BzH oxidation, but the inhibition influence was associated with the chemical structures. The 1-phenylethanol molecule with one α–H was less effective in suppressing the BzH conversion compared with BzOH with two α–H (Figure 4-17 and Figure 4-16 (d)), but still more inhibitive than toluene and ethylbenzene containing no hydroxyl α–H. Based on these observations, it was suggested that the benzylic alcohols with α–H was more reactive than aliphatic C-H towards the radicals and could inhibit the radical-chain oxidation of BzH. Overall, the selectivity of the BzOH to BzH in PMS/NGO reaction system could naturally reach a high level and the over-oxidation of BzH was blocked *via* both non-radical and radical routes.

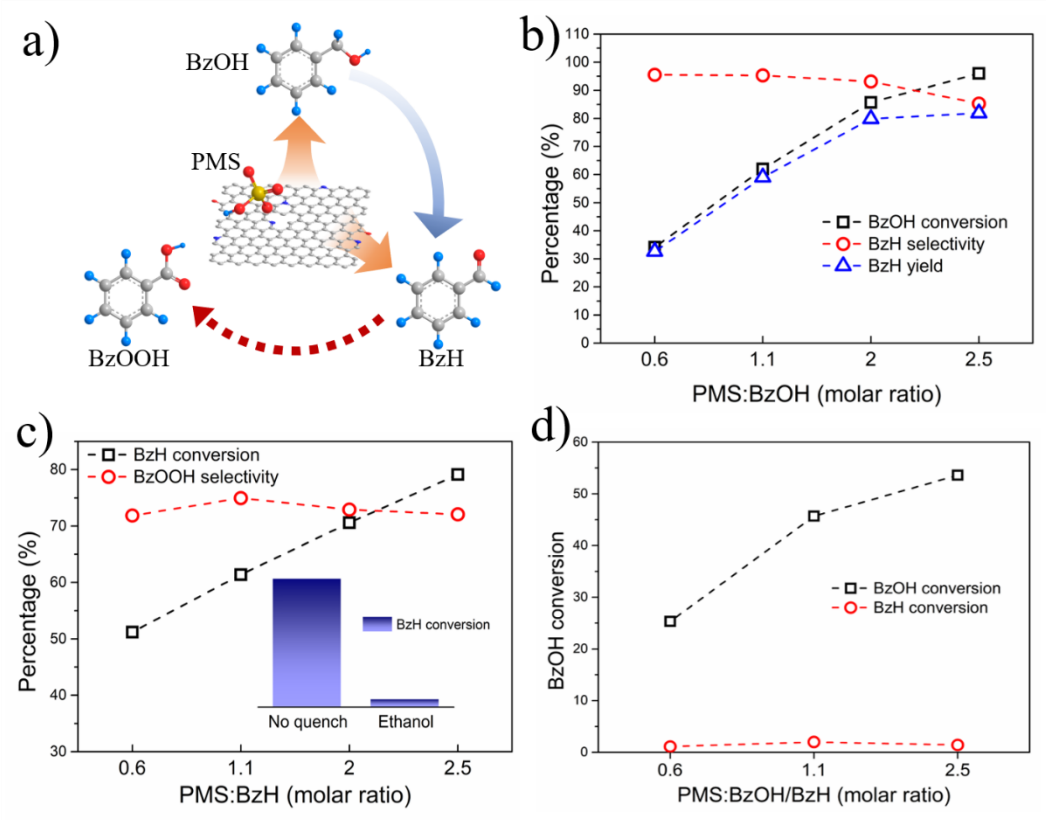

Figure 4-16. a) The oxidation behaviour of BzOH in PMS/graphene system. b) Oxidation of only BzOH with different PMS dosage. c) Oxidation of only BzH with different PMS dosage (the inset showed the decrease of BzH conversion when the acetonitrile in the solvent was replaced with ethanol). d) Oxidation with the co-existence of BzOH and BzH. Reaction conditions: 0.1 mmol BzOH (applicable to (b) and (d)), 5 mg NGO-A/N, 0.1 mmol BzH (applicable to (c) and (d)), 5 mL acetonitrile-water (volume ratio =1:1), 50 ºC, 3 h.

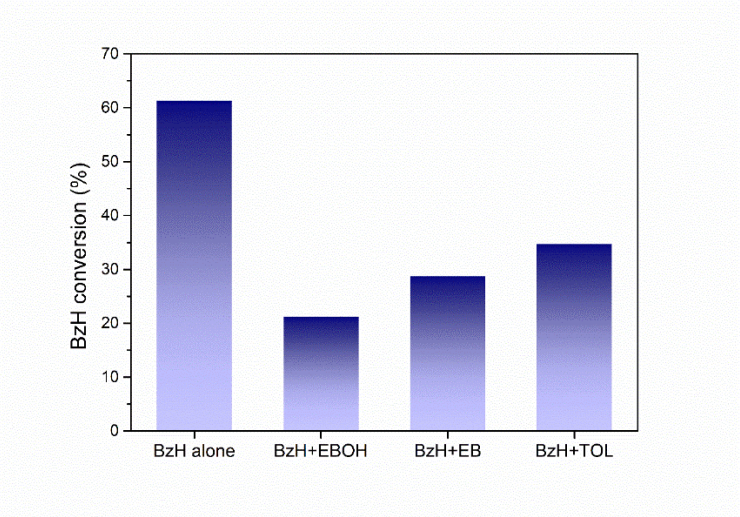

Figure 4-17. The inhibition effect of different benzylic chemicals including 1-phenylethanol (EBOH), ethylbenzene (EB) and toluene (TOL) on the oxidation of BzH. Reaction conditions: 5 mg NGO-A/N, 0.1 mmol BzH, 0.1 mmol benzylic compound, 0.11 mmol PMS, 5 mL acetonitrile/water (1:1, volume ratio), 50 ºC, 3 h.

4.4 Conclusions

We report the development of carbonylated N-doped graphene catalysts for the selective conversion of BzOH into BzH by PMS with high efficiency under benign conditions. The surface C=O groups were enriched by either post-oxidation treatment of NGO or adding inorganic salts during the preparation of NGO. A BzOH conversion of 96% and BzH selectivity of 85.4% were achieved on an optimized carbocatalyst *via* both non-radical and radical processes. The experimental results indicated that the doped N species and carbonyl groups (C=O) made joint contributions to the enhanced radical and non-radical activities, of which the non-radical oxidation could afford higher BzH selectivity. The electron-withdrawing pyridinic N sites were integrated with the PMS molecules to build a bridge for the electron transfer from the adsorbed BzOH to PMS to accomplish the non-radical oxidation process. For the isolated pyridinic N and C=O, each of these two functional groups could adsorb and activate PMS to generate various radicals for subsequent BzOH oxidation. Sulfate radicals played the dominant role for the radical-based BzOH oxidation. BzH remained to be

the sole product under the testing conditions as the deep-oxidation of BzH into BzOOH could neither occur in radical nor non-radical route due to the presence of unreacted BzOH. The presence of BzOH would inhibit the over-oxidation of BzH by radicals by quenching the radicals at its α–H to cease the autooxidation of BzH. This study revealed the intrinsic nature of the selective reaction *via* PMS/NGO system for BzOH conversion to BzH, which might provide a versatile strategy using such functionalized graphene catalysts for the selective oxidation of other organics.

References

1. Luo, J.; Yu, H.; Wang, H.; Wang, H.; Peng, F., Aerobic oxidation of benzyl alcohol to benzaldehyde catalyzed by carbon nanotubes without any promoter. *Chem. Eng. J.* **2014,** *240*, 434-442.

2. Luo, L.; Wang, Z.-j.; Xiang, X.; Yan, D.; Ye, J., Selective Activation of Benzyl Alcohol Coupled with Photoelectrochemical Water Oxidation via a Radical Relay Strategy. *ACS Catal.* **2020,** *10* (9), 4906-4913.

3. Choudhary, V. R.; Dhar, A.; Jana, P.; Jha, R.; Uphade, B. S., A green process for chlorine-free benzaldehyde from the solvent-free oxidation of benzyl alcohol with molecular oxygen over a supported nano-size gold catalyst. *Green Chemistry* **2005,** *7* (11), 768-770.

4. Wang, H.; Wang, C.; Yan, H.; Yi, H.; Lu, J., Precisely-controlled synthesis of Au@Pd core–shell bimetallic catalyst via atomic layer deposition for selective oxidation of benzyl alcohol. *J. Catal.* **2015,** *324*, 59-68.

5. Makwana, V. D.; Son, Y.-C.; Howell, A. R.; Suib, S. L., The Role of Lattice Oxygen in Selective Benzyl Alcohol Oxidation Using OMS-2 Catalyst: A Kinetic and Isotope-Labeling Study. *J. Catal.* **2002,** *210* (1), 46-52.

6. Parmeggiani, C.; Matassini, C.; Cardona, F., A step forward towards sustainable aerobic alcohol oxidation: new and revised catalysts based on transition metals on solid supports. *Green Chemistry* **2017,** *19* (9), 2030-2050.

7. Long, J.; Xie, X.; Xu, J.; Gu, Q.; Chen, L.; Wang, X., Nitrogen-Doped Graphene Nanosheets as Metal-Free Catalysts for Aerobic Selective Oxidation of Benzylic Alcohols. *ACS Catal.* **2012,** *2* (4), 622-631.

8. Yongbo, K.; M., I. N.; Yuta, N.; Teruaki, H.; Masa-aki, K., Selective Aerobic Oxidation of Benzylic Alcohols Catalyzed by Carbon-Based Catalysts: A Nonmetallic Oxidation System. *Angew. Chem. Int. Ed.* **2010,** *49* (2), 436-440.

9. R., D. D.; Hong-Peng, J.; W., B. C., Graphene Oxide: A Convenient Carbocatalyst for Facilitating Oxidation and Hydration Reactions. *Angew. Chem.* **2010,** *122* (38), 6965-6968.

10. Sheng, S. D.; Guodong, W.; Shuchang, W.; Feng, P.; Robert, S., Carbocatalysis in Liquid-Phase Reactions. *Angew. Chem. Int. Ed.* **2017,** *56* (4), 936-964.

11. Hussain, H.; Green, I. R.; Ahmed, I., Journey Describing Applications of Oxone in Synthetic Chemistry. *Chem. Rev.* **2013,** *113* (5), 3329-3371.

12. Neyens, E.; Baeyens, J., A review of classic Fenton's peroxidation as an advanced oxidation technique. *J. Hazard. Mater.* **2003,** *98* (1), 33-50.

13. Choudhary, V. R.; Dumbre, D. K., Solvent-free selective oxidation of benzyl alcohol to benzaldehyde by tert-butyl hydroperoxide over U3O8-supported nano-gold catalysts. *Appl. Catal. A-Gen.* **2010,** *375* (2), 252-257.

14. Hu, P.; Long, M., Cobalt-catalyzed sulfate radical-based advanced oxidation: A review on heterogeneous catalysts and applications. *Appl. Catal. B-Environ.* **2016,** *181*, 103-117.

15. Mello, R.; Cassidei, L.; Fiorentino, M.; Fusco, C.; Hummer, W.; Jager, V.; Curci, R., OXIDATIONS BY METHYL(TRIFLUOROMETHYL)DIOXIRANE .5. CONVERSION OF ALCOHOLS INTO CARBONYL-COMPOUNDS. *J. Am. Chem. Soc.* **1991,** *113* (6), 2205-2208.

16. Thottumkara, A. P.; Bowsher, M. S.; Vinod, T. K., In Situ Generation of o-Iodoxybenzoic Acid (IBX) and the Catalytic Use of It in Oxidation Reactions in the Presence of Oxone as a Co-oxidant. *Org. Lett.* **2005,** *7* (14), 2933-2936.

17. Schulze, A.; Giannis, A., Oxidation of Alcohols with Catalytic Amounts of IBX. *Synthesis* **2006,** *2006* (02), 257-260.

18. Page, P. C. B.; Appleby, L. F.; Buckley, B. R.; Allin, S. M.; McKenzie, M. J., In Situ Generation of 2-Iodoxybenzoic Acid (IBX) in the Presence of Tetraphenylphosphonium

Monoperoxysulfate (TPPP) for the Conversion of Primary Alcohols into the Corresponding Aldehydes. *Synlett* **2007,** *2007* (10), 1565-1568.

19. Uyanik, M.; Ishihara, K., Hypervalent iodine-mediated oxidation of alcohols. *Chem. Commun.* **2009,** (16), 2086-2099.

20. Uyanik, M.; Akakura, M.; Ishihara, K., 2-Iodoxybenzenesulfonic Acid as an Extremely Active Catalyst for the Selective Oxidation of Alcohols to Aldehydes, Ketones, Carboxylic Acids, and Enones with Oxone. *J. Am. Chem. Soc.* **2009,** *131* (1), 251-262.

21. Koo, B.-S.; Lee, C. K.; Lee, K.-J., OXIDATION OF BENZYL ALCOHOLS WITH OXONE® AND SODIUM BROMIDE. *Synth. Commun.* **2002,** *32* (14), 2115-2123.

22. Duan, X.; Sun, H.; Kang, J.; Wang, Y.; Indrawirawan, S.; Wang, S., Insights into Heterogeneous Catalysis of Persulfate Activation on Dimensional-Structured Nanocarbons. *ACS Catal.* **2015,** *5* (8), 4629-4636.

23. Sun, H.; Liu, S.; Zhou, G.; Ang, H. M.; Tadé, M. O.; Wang, S., Reduced Graphene Oxide for Catalytic Oxidation of Aqueous Organic Pollutants. *ACS Appl. Mater. Interfaces* **2012,** *4* (10), 5466-5471.

24. Duan, X.; Ao, Z.; Sun, H.; Indrawirawan, S.; Wang, Y.; Kang, J.; Liang, F.; Zhu, Z. H.; Wang, S., Nitrogen-Doped Graphene for Generation and Evolution of Reactive Radicals by Metal-Free Catalysis. *ACS Appl. Mater. Interfaces* **2015,** *7* (7), 4169-4178.

25. Duan, X.; Sun, H.; Ao, Z.; Zhou, L.; Wang, G.; Wang, S., Unveiling the active sites of graphene-catalyzed peroxymonosulfate activation. *Carbon* **2016,** *107*, 371-378.

26. Duan, X.; Ao, Z.; Zhou, L.; Sun, H.; Wang, G.; Wang, S., Occurrence of radical and nonradical pathways from carbocatalysts for aqueous and nonaqueous catalytic oxidation. *Appl. Catal. B-Environ.* **2016,** *188*, 98-105.

27. Duan, X.; Sun, H.; Wang, Y.; Kang, J.; Wang, S., N-Doping-Induced Nonradical Reaction on Single-Walled Carbon Nanotubes for Catalytic Phenol Oxidation. *ACS Catal.* **2015,** *5* (2), 553-559.

28. Li, J.; Li, M.; Sun, H.; Ao, Z.; Wang, S.; Liu, S., Understanding of the Oxidation Behaviour of Benzyl Alcohol by Peroxymonosulfate via Carbon Nanotubes Activation. *ACS Catal.* **2020,** *10* (6), 3516-3525.

29. Sankar, M.; Nowicka, E.; Carter, E.; Murphy, D. M.; Knight, D. W.; Bethell, D.; Hutchings, G. J., The benzaldehyde oxidation paradox explained by the interception of peroxy radical by benzyl alcohol. *Nat. Commun.* **2014,** *5* (1), 3332.

30. Li, D.; Duan, X.; Sun, H.; Kang, J.; Zhang, H.; Tade, M. O.; Wang, S., Facile synthesis of nitrogen-doped graphene via low-temperature pyrolysis: The effects of precursors and annealing ambience on metal-free catalytic oxidation. *Carbon* **2017,** *115*, 649-658.

31. Zhang, J.; Liu, X.; Blume, R.; Zhang, A.; Schlögl, R.; Su, D. S., Surface-Modified Carbon Nanotubes Catalyze Oxidative Dehydrogenation of *n*-Butane. *Science* **2008,** *322* (5898), 73.

32. Frank, B.; Zhang, J.; Blume, R.; Schlögl, R.; Su, D. S., Heteroatoms Increase the Selectivity in Oxidative Dehydrogenation Reactions on Nanocarbons. *Angew. Chem. Int. Ed.* **2009,** *48* (37), 6913-6917.

33. Sun, H.; Kwan, C.; Suvorova, A.; Ang, H. M.; Tadé, M. O.; Wang, S., Catalytic oxidation of organic pollutants on pristine and surface nitrogen-modified carbon nanotubes with sulfate radicals. *Appl. Catal. B-Environ.* **2014,** *154-155*, 134-141.

34. Kato, T.; Yamada, Y.; Nishikawa, Y.; Ishikawa, H.; Sato, S., Carbonization mechanisms of polyimide: Methodology to analyze carbon materials with nitrogen, oxygen, pentagons, and heptagons. *Carbon* **2021,** *178*, 58-80.

35. Yamada, Y.; Yasuda, H.; Murota, K.; Nakamura, M.; Sodesawa, T.; Sato, S., Analysis of heat-treated graphite oxide by X-ray photoelectron spectroscopy. *J. Mater. Sci.* **2013,** *48* (23), 8171-8198.

36. Yang, H. B.; Miao, J.; Hung, S.-F.; Chen, J.; Tao, H. B.; Wang, X.; Zhang, L.; Chen, R.; Gao, J.; Chen, H. M.; Dai, L.; Liu, B., Identification of catalytic sites for oxygen reduction and oxygen evolution in N-doped graphene materials: Development of highly efficient metal-free bifunctional electrocatalyst. *Science Advances* **2016,** *2* (4), e1501122.

37. Li, J.; Yu, P.; Xie, J.; Liu, J.; Wang, Z.; Wu, C.; Rong, J.; Liu, H.; Su, D., Improving the Alkene Selectivity of Nanocarbon-Catalyzed Oxidative Dehydrogenation of n-Butane by Refinement of Oxygen Species. *ACS Catal.* **2017,** *7* (10), 7305-7311.

38. Tuinstra, F.; Koenig, J. L., Raman Spectrum of Graphite. *The Journal of Chemical Physics* **1970,** *53* (3), 1126-1130.

39. Fujimoto, A.; Yamada, Y.; Koinuma, M.; Sato, S., Origins of sp3C peaks in C1s X-ray Photoelectron Spectra of Carbon Materials. *Anal. Chem.* **2016,** *88* (12), 6110-6114.

40. Yamada, Y.; Kim, J.; Matsuo, S.; Sato, S., Nitrogen-containing graphene analyzed by X-ray photoelectron spectroscopy. *Carbon* **2014,** *70*, 59-74.

41. Senda, T.; Yamada, Y.; Morimoto, M.; Nono, N.; Sogabe, T.; Kubo, S.; Sato, S., Analyses of oxidation process for isotropic pitch-based carbon fibers using model compounds. *Carbon* **2019,** *142*, 311-326.

42. Qi, W.; Liu, W.; Zhang, B.; Gu, X.; Guo, X.; Su, D., Oxidative Dehydrogenation on Nanocarbon: Identification and Quantification of Active Sites by Chemical Titration. *Angew. Chem. Int. Ed.* **2013,** *52* (52), 14224-14228.

43. Wang, Y.; Ao, Z.; Sun, H.; Duan, X.; Wang, S., Activation of peroxymonosulfate by carbonaceous oxygen groups: experimental and density functional theory calculations. *Appl. Catal. B-Environ.* **2016,** *198*, 295-302.

44. Zhang, Y.; Wang, J.; Rong, J.; Diao, J.; Zhang, J.; Shi, C.; Liu, H.; Su, D., A Facile and Efficient Method to Fabricate Highly Selective Nanocarbon Catalysts for Oxidative Dehydrogenation. *ChemSusChem* **2017,** *10* (2), 353-358.

45. Diao, J.; Zhang, Y.; Zhang, J.; Wang, J.; Liu, H.; Su, D. S., Fabrication of MgO–rGO hybrid catalysts with a sandwich structure for enhanced ethylbenzene dehydrogenation performance. *Chem. Commun.* **2017,** *53* (82), 11322-11325.

46. Pytlakowska, K.; Kozik, V.; Matussek, M.; Pilch, M.; Hachuła, B.; Kocot, K., Glycine modified graphene oxide as a novel sorbent for preconcentration of chromium, copper, and zinc ions from water samples prior to energy dispersive X-ray fluorescence spectrometric determination. *RSC Adv.* **2016,** *6* (49), 42836-42844.

47. Hosseini, M.-S.; Masteri-Farahani, M.; Shahsavarifar, S., Chemical modification of reduced graphene oxide with sulfonic acid groups: Efficient solid acids for acetalization and esterification reactions. *Journal of the Taiwan Institute of Chemical Engineers* **2019,** *102*, 34-43.

48. Lam, E.; Chong, J. H.; Majid, E.; Liu, Y.; Hrapovic, S.; Leung, A. C. W.; Luong, J. H. T., Carbocatalytic dehydration of xylose to furfural in water. *Carbon* **2012,** *50* (3), 1033-1043.

49. Tang, C.; Zhang, N.; Shao, Q.; Huang, X.; Xiao, X., Rational design of ordered Pd–Pb nanocubes as highly active, selective and durable catalysts for solvent-free benzyl alcohol oxidation. *Nanoscale* **2019,** *11* (12), 5145-5150.

50. Wang, J.; Huang, R.; Zhang, Y.; Diao, J.; Zhang, J.; Liu, H.; Su, D., Nitrogen-doped carbon nanotubes as bifunctional catalysts with enhanced catalytic performance for selective oxidation of ethanol. *Carbon* **2017,** *111*, 519-528.

51. Jawad, A.; Zhan, K.; Wang, H.; Shahzad, A.; Zeng, Z.; Wang, J.; Zhou, X.; Ullah, H.; Chen, Z.; Chen, Z., Tuning of Persulfate Activation from a Free Radical to a Nonradical Pathway through the Incorporation of Non-Redox Magnesium Oxide. *Environmental Science & Technology* **2020,** *54* (4), 2476-2488.

Chapter 5 Selective oxidation of alcohols by graphene-like carbon with electrophilic oxygen and integrated pyridinic nitrogen active sites

Abstract

The selective oxidations of alcohols into the corresponding aldehydes or ketones are essential reactions for organic synthesis. The development of facile, green and cost-effective protocols to accomplish the selective oxidation is highly attractive. Here we present the selective oxidation of aromatic alcohols by peroxymonosulfate (PMS) oxidant with N-doped graphene-like carbon (NG) synthesized *via* a metal-free approach without producing a large amount of hazardous wastes. In the tested selective oxidation reaction, over 96% of benzyl alcohol (BzOH) was converted into benzaldehyde (BzH) with high selectivity under mild conditions. The synthesized NG catalyst contains abundant electrophilic oxygen species, serving as the major active sites for the generation of reactive radicals from PMS to endow the selective oxidation of BzOH in the radical pathway. The N species, especially the integrated pyridinic N create electron-withdrawing and electron-donating regions for BzOH and PMS adsorption, enabling the non-radical oxidation of BzOH *via* the electron transfer through the surface coordinated complex. This work opens a new avenue to convert metal-free raw materials into effectively functionalized carbon materials, coupled with their potential applications in the selective oxidation of alcohols.

The content of this chapter is published in Nanoscale: 2021, 13, 12979-12990.

5.1 Introduction

Cost-effective and environmentally benign synthesis of aldehydes and ketones from the selective oxidations of their corresponding alcohols is of great importance in the manufacture of pharmaceuticals, dyes and perfumes, or direct use as solvents.[1] The traditional oxidation methods using stoichiometric oxidants suffer from high cost, toxicity and poorly controlled selectivity. To overcome these shortcomings, heterogeneous catalytic systems with environment-friendly catalysts/oxidants have been explored. The majority of the established oxidation strategies depend on the expensive noble-metal catalysts to overcome the high oxidation potentials of many alcohol substrates, usually under thermal conditions.[2-5] To avoid the issue of scarcity or toxicity of the metal-based catalysts and attain better sustainability, metal-free materials, especially nanocarbon catalysts underwent fast development in the past decade.[6-7] For instance, tremendous efforts have been devoted to the synthesis of functionalized graphene and carbon nanotubes (CNT) for selective oxidation of alcohols, with some nanocarbon catalysts showing comparable activity to the metal catalysts in oxidative reactions with superior recyclability and recoverability.[8-11]

Graphene-based materials have stimulated immense research enthusiasm as either multifunctional catalysts or catalyst supports owing to their tunable chemical and mechanical properties.[12-13] Chemical exfoliation is one of the most important protocols for large-scale preparation of graphene oxide and its derivatives, especially the widely used Hummer's method,[14] but this process produces a large amount of hazardous and corrosive liquid waste *via* complex procedures, which is against the eco- and environmental considerations. High-quality graphene nanosheets can be manufactured with the chemical vapor deposition on metal catalysts such as Cu and Ni,[15-16] whereas the use of gaseous carbon source is unfavourable for the facile synthesis of graphene with widely available feedstock. Nitrogen-doped graphene-like carbon can be produced through a pyrolysis method from biomass either with or without metal

catalysts.[17-18] The doped N species on graphene have been proven as active sites in a variety of reactions, leading to substantially enhanced catalytic performances.[8, 19-21] For the metal-free synthesis of graphene, glucose is frequently used as the carbon precursor and N-rich organics such as urea and dicyandiamide as N precursors.[19, 22] The graphitization degree increases with higher N precursor/C precursor mass ratio ($M_{N/C}$), hence the $M_{N/C}$ is normally over 10 in these cases. It's noteworthy that the catalytic performances of graphene-based catalysts are linked to a variety of factors besides the graphitization degree, including the chemical composition of N and O species, thus the scientific understanding and identification of the individual role of the functionalities are at the core of the target catalytic reactions.

In this work, we reported the metal-free synthesis of N-doped graphene-like carbon (NG) using starch as the carbon precursor and urea as the N precursor with low $M_{N/C}$, as well as a minor loading of ammonium nitrate to facilitate the formation of thin-layered graphene film. The prepared NG delivered advanced activity in the selective oxidation of aromatic alcohols including benzyl alcohol (BzOH) and 1-phenylethanol (1-PE) by the activated peroxymonosulfate (PMS, HSO_5^-) oxidant. Compared with the frequently employed gas and liquid oxidants such as oxygen,[23] hydrogen peroxide [24] and *tert*-butyl hydroperoxide (TBHP),[25] PMS as a low-cost and stable solid oxidant can avoid the safety issues such as transportation and storage and is energy-effective to produce reactive oxidizing species in mild environment. PMS has been dominantly devoted to the non-selective oxidative removal of aqueous contaminants[26-27] while its feasibility in selective oxidation *via* the catalytic activation is rarely reported. Herein, the fabricated NG samples endowed highly selective transformation of BzOH into benzaldehyde (BzH) with 96.1% BzOH conversion and 81.9% BzH yield by the activated PMS through the combination of radical and non-radical processes. The electrophilic oxygen (peroxides and superoxide species) and integrated pyridinic N species were identified as dual active sites for the selective oxidation. Our work offers a facile way to the fabrication of carbonaceous material for selective oxidation of alcohols.

5.2. Experimental section

Materials and chemicals. The chemicals used for the NG synthesis and selective oxidation reactions were all purchased from Sigma-Aldrich. Potassium peroxymonosulfate (oxone, $KHSO_5 \cdot 1/2KHSO_4 \cdot 1/2K_2SO_4$) was applied as the PMS oxidant.

Synthesis of N-doped graphene-like carbon (NG). For the fabrication of NG, 1 g starch (soluble, ACS reagent), 4 g urea and 2 g ammonium nitrate (AN) were dissolved in 20 mL ethanol and stirred at 45 ºC until fully vaporized. The obtained white solid was ground into powder and annealed at the target temperature (600, 700, 800, 900 and 1000 ºC) for 2 h at a heating rate of 1 ºC/min under N_2 protection. After naturally cooled down, the carbonized black solid was ground to powder and then mixed with 10 mL HNO_3 (70%, ACS reagent) to remove the impurities and to stablize the carbonaceous material in oxidative environment to aviod the catalyst consuming oxidant in the subsequent catalytic reactions. Finally the solid catalyst was filtered out, washed with water and ethanol and dried overnight in an oven at 60 ºC. The obtained catalyst was denoted as NG-x (x=600, 700, 800, 900 and 1000, respectivly according to the pyrolysis temperatures). For comparison, the samples prepared with identical mole amount of magnesium nitrate, ammonium chloride and no additive salt instead of AN at 800 ºC were denoted as NG-800(MgN), NG-800(ACl) and NG-800(blank), respectively. NG-800(10:1) was prepared with the mass ratio of urea:starch=10:1 without additive salt.

Determination and deactivation of electrophilic functionalities on NG samples. The electrophilic oxygen species (peroxide O_2^{2-} and superoxide O_2^{-}) on NG samples were determined *via* the iodometric titration method, as depicted in Equations (5-1) to (5-4). Both the peroxide and superoxied species could oxidize I^- into I^0 which was subsequently titrated with $Na_2S_2O_3$. For convenient calculation, the amount of titrated

I_2 was used to reflect the sum of electrophilic oxygen species. Taking NG-800 for example, 5 mg NG-800 was mixed with 10 mL solution containing KI (20 g/L), H_2SO_4 (0.025 mol/L) and $(NH_4)_6Mo_7O_{24}$ (0.3 g/L). The mixture was sonicated for 5 min then stirred for 1 h under room temperature. The whole operation was performed in the darkness to prevent the degradation of I^- by the light. The precipitate was filtered and washed with ultra-pure water for several times and the filtrate was collected. The precipitate was dried in an oven at 60 ºC overnight to obtain NG-800(KI). For the titration of I_2, 0.3 g starch indicator was loaded in the filtrate to obtain the blue suspension, followed by the titration with $Na_2S_2O_3$ (2×10^{-4} mol/L) (Equation (5-3)). The amount of electrophilic oxygen (mol/g cat.) on NG-800 was calculated from Equation (5-4), where *c* (mol/g), *V* (mL) and *m* (g) represent for the concentration of the electrophilic oxygen (normalized by the amount of I_2), the volume of $Na_2S_2O_3$ solution and the mass loading of NG-800, respectively.

$$O_2^{2-} + 2I^- \rightarrow 2O^{2-} + I_2 \qquad (5\text{-}1)$$

$$2O_2^- + 6I^- \rightarrow 4O^{2-} + 3I_2 \qquad (5\text{-}2)$$

$$I_2 + 2Na_2S_2O_3 \rightarrow 2NaI + Na_2S_4O_6 \qquad (5\text{-}3)$$

$$c = 1\times10^{-7}\ V/m \qquad (5\text{-}4)$$

Catalytic oxidation of alcohols. The selective oxidation of alcohols was carried out in a 50 mL three-necked flask. Firstly, 10 mg catalyst was mixed with 10 mL solvent containing 5 mL acetonitrile and 5 mL water, followed by sonication for several minutes until the catalyst was scattered throughout the solvent. Then a certain amount of oxone and 0.2 mmol alcohol substrate were added into the mixture to start the reaction. The flask was sealed and stirred in an oil bath at the aimed temperature for 5 h. After the reaction, 0.2 mmol anisole was injected into the reactant as internal standard. The catalyst was filtered out and the organic reactants/products in the solution were extracted with toluene for three times (the volume ratio of toluene and

reaction solution was 6:1 totally). The whole organic phase was collected and analysed by gas chromatography (GC). The quenching experiments were performed with different dose of *tert*-butanol or ethanol in the solvent.

Characterization. Transmission electron microscopy (TEM) imaging, scanning transmission electron microscopy (STEM) imaging and energy-dispersive x-ray spectroscopy (EDS) elemental mapping were conducted on a FEI TALOS FS200X G2 FEG TEM. Scanning electron microscopy (SEM) imaging was performed on a NEON FIB-SEM instrument. Raman spectra were obtained on a Renishaw Raman spectrometer with a laser beam of 785 nm. X-ray photoelectron spectra (XPS) were obtained on a Kratos AXIS Ultra DLD fitted with AlKα source. The pressure of the sample analyse chamber was around 1×10^{-8} torr. The binding energies were adjusted by shifting the C 1s peak to 284.6 eV. The deconvolution of XPS spectra were performed using XPSPEAK41 software applying Gaussian-Lorentzian component profiles after subtraction of a Shirley background. The X-ray diffraction (XRD) was measured on a Bruker D8 Advance diffractometer using Cu-Kα radiation with λ=1.5406 Å. The 2θ range was between 5 to 90º at a scanning rate of 2º/min. The N_2 adsorption and desorption isotherms were conducted on a Tristar II 3020 instrument (Micromeritics) in liquid nitrogen environment (−196 ºC) to obtain the specific surface area of different NG samples using BET method.

5.3 Results and discussion

5.3.1 Characterizations of catalysts

The SEM images reveal the morphology of NG samples prepared at different annealing temperatures (600-100 ºC) with ammonium nitrate additive as depicted in Figure 5-1. At 600 ºC, layered carbon nitride was formed due to the condensation of urea [22] confined with the carbonized intermediate of starch. The graphene-like flakes began to appear at the temperature of 700 ºC, and the stacked carbon nitride layers

were fully exfoliated and pyrolysed into graphene sheets at 800 and 900 ºC. NG-800 demonstrated thin-layered graphene with many wrinkles as suggested from SEM and TEM imaging (Figure 5-2 (a) and (b)), which was usually observed on N-doped graphene.[28-29] HAADF-STEM and elemental mappings confirmed the uniformly scattered N and O species over the graphene sheets (Figure 5-2 (c)). At the annealing temperature of 1000 ºC, the graphene flakes started to decompose which led to the formation of hollow structure (Figure 5-1). For comparison, the NG samples were also prepared without additive salt (blank) and with magnesium nitrate (MgN) and ammonium chloride (ACl), respectively, to distinguish the role of ammonium nitrate (AN) in the catalyst preparation. Small carbon flakes grown on the bulk-size amorphous carbonaceous basement were found when the additive salt was absent (Figure 5-3), indicating that low mass loading of urea ($M_{N/C}$ =4) was unable to form graphene structure and the addition of AN contributed to the formation of large graphene platelets. Compared with AN, NG prepared from MgN showed similar morphology while the NG flakes derived from ACl were smaller with partially aggregated graphene sheets. It can be inferred that the nitrate salts are superior to the other salts possibly because the decomposed nitrate salts can produce NOx thus forming a pre-etched carbonaceous precursor for the generation of thin-layered graphene-like structure.

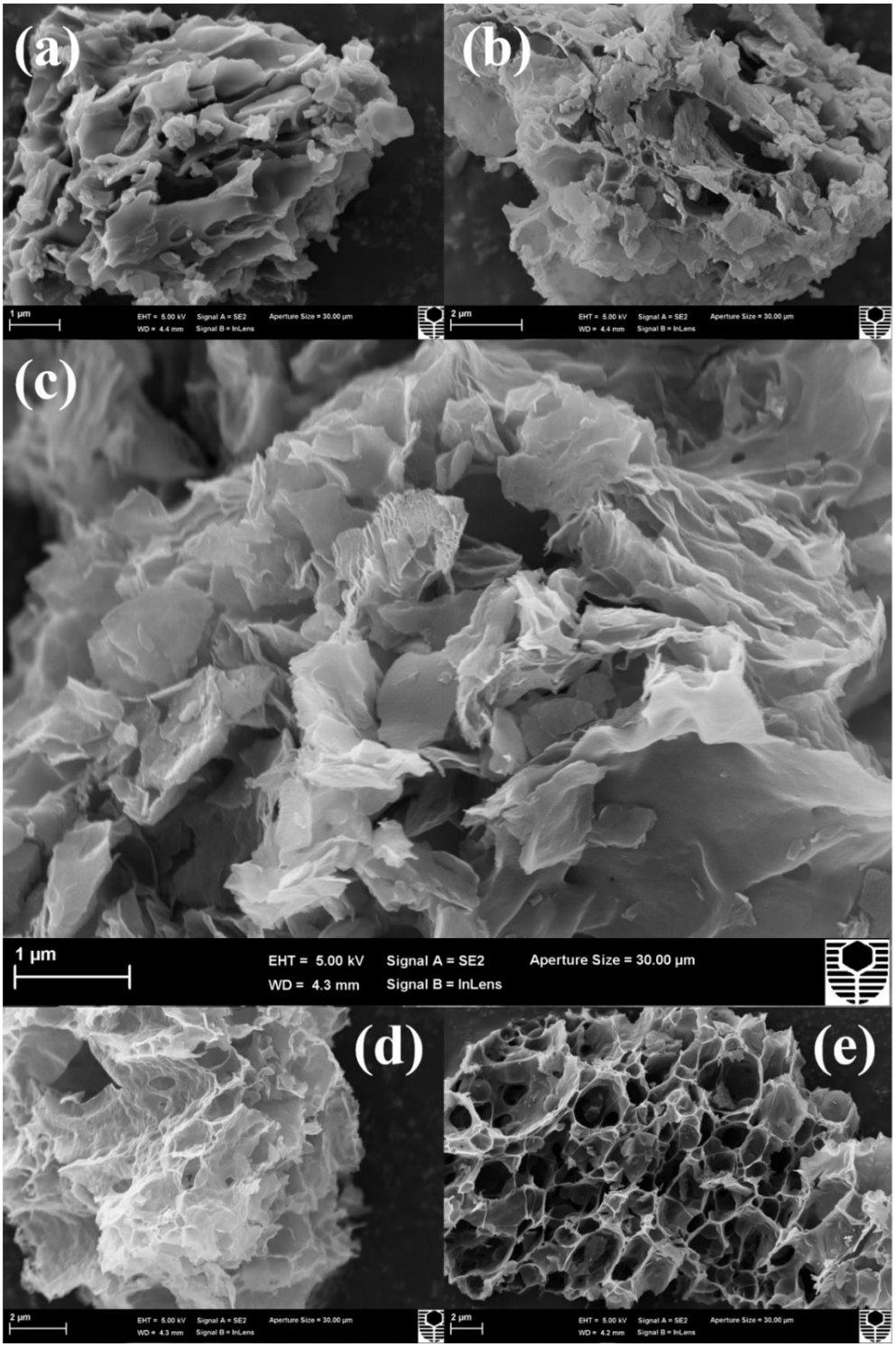

Figure 5-1. SEM images of (a) NG-600, (b) NG-700, (c) NG-800, (d) NG-900 and (e) NG-1000.

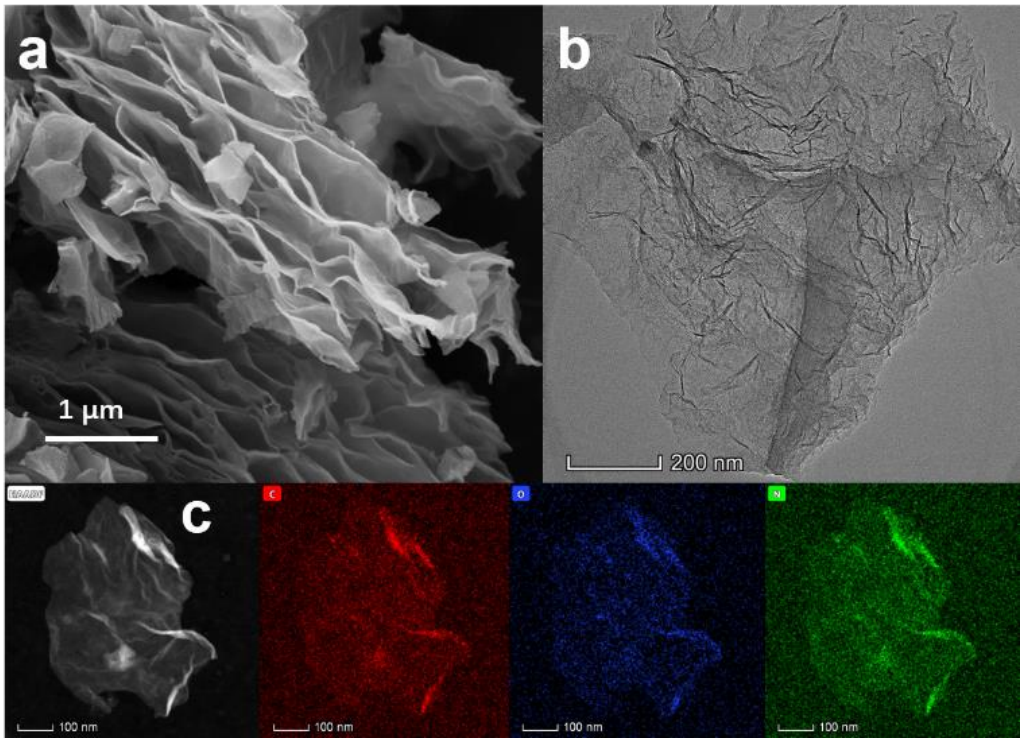

Figure 5-2. Structural characterizations of NG-800. (a) SEM image (b) TEM image (c) STEM image and EDS mapping of NG-800.

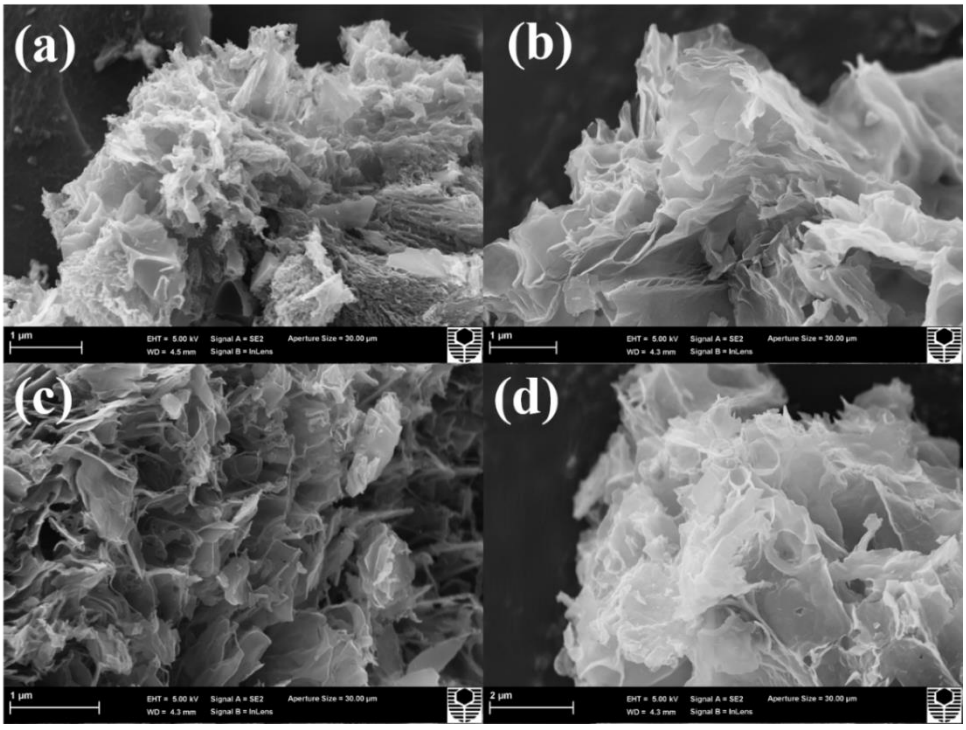

Figure 5-3. SEM images of (a) NG(blank), (b) NG(AN), (c) NG(ACl) and (d) NG(MgN)

As shown in Figure 5-4 (a) and (b), all the NG samples presented (002) graphitic diffraction peaks in the XRD patterns. The peak intensities of the NG prepared from different salts follow the sequence of NG-800(AN) < NG-800(MgN) < NG-800(ACl) < NG-800(blank), implying that the thickness of the graphene layers of NG(AN) was thinner than the other samples. Therefore, AN salt can be selected for the synthesis of thin-layered graphene sheets following a metal-free manner. For the NG prepared with AN under different temperatures (Figure 5-4 (b)), 900 ºC derived NG showed the weakest (002) intensity, followed closely by 800 and 1000 ºC, which was in accordance with the SEM results. This is further supported by the high-resolution C 1s XPS spectra (Figure 5-4 (c)) because the full width at half maximum (FWHM) of C 1s spectra reflects the ordering of the graphene structure.[30] The FWHM of C 1s for the NG samples decreased with higher pyrolysing temperatures, with NG-900 showing the lowest FWHM. The NG samples obtained within 800-1000 ºC were presenting typical sp^2 graphitic C 1s spectra, confirming the formation of graphene-like structure. Raman spectra were employed to probe the defective degree of the NG samples with the intensity of the D band and G band (I_D/I_G) mirroring the defectiveness.[31] For the NG-800, 900 and 1000 with well-established graphene layers, NG-800 and NG-900 presented identical I_D/I_G of 1.36 while NG-1000 presented a slightly higher I_D/I_G (1.38) (Figure 5-5), which also agreed with the XPS results. The specific surface area (SSA) of NG was measured by nitrogen sorption experiments (Figure 5-4 (d)). The SSA of NG samples increased with higher annealing temperatures in the range of 600-900 ºC, with NG-800 and NG-900 reaching 673 and 1019 m^2/g, respectively. The SSA of NG-1000 (733 m^2/g) was lower than NG-900, which proved the decomposition of thin-layered graphene at the temperature over 900 ºC.

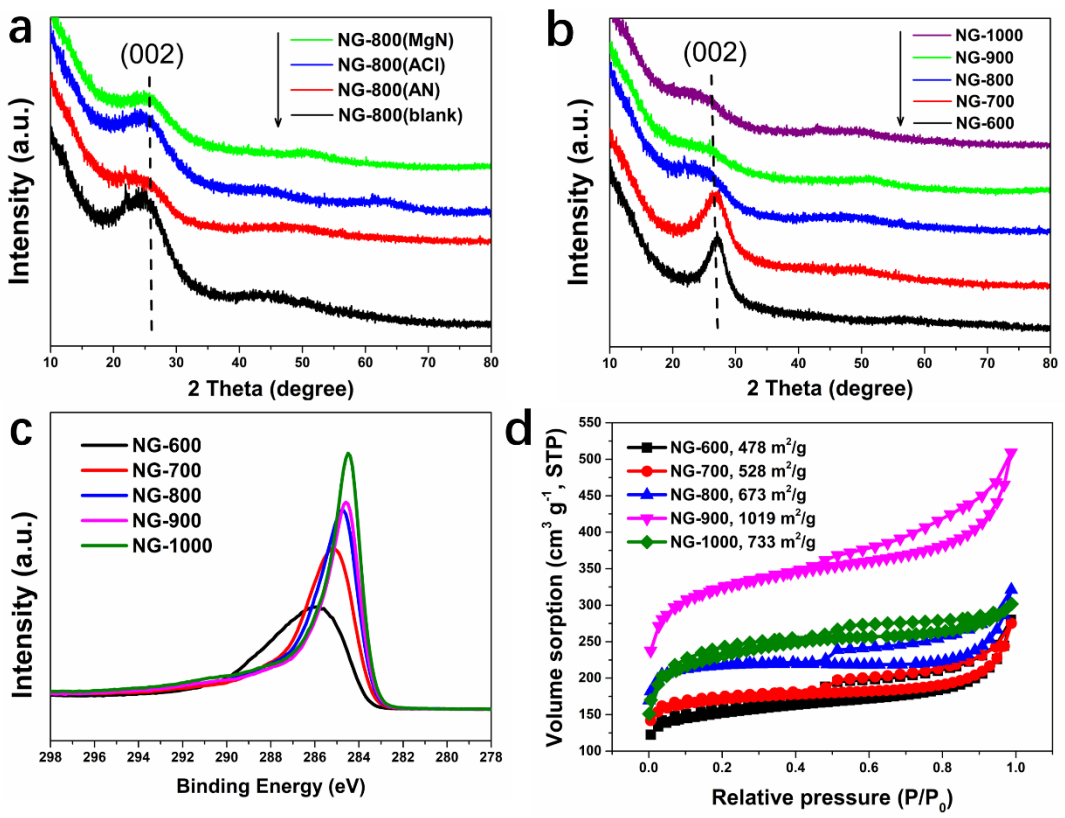

Figure 5-4. XRD patterns of (a) NG derived at different temperatures and (b) NG derived with different additive salts. (c) High resolution C 1s XPS spectra. (d) Nitrogen sorption isotherms and BET specific surface area of NG-600, NG-700, NG-800, NG-900 and NG-1000.

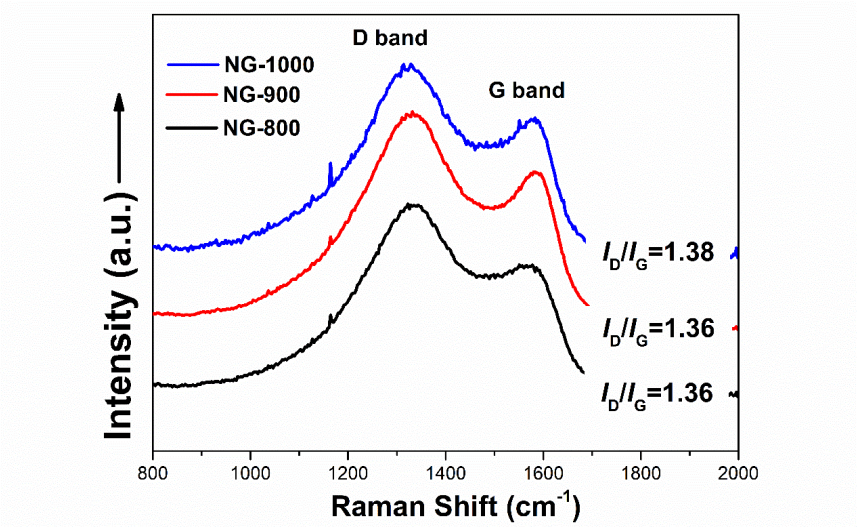

Figure 5-5. Raman spectra of NG samples.

The N and O contents obtained by XPS were summarised in Table 5-1. The N concentration decreased with the increasing annealing temperatures from 23.3 at% of NG-600 to 12.4 at% of NG-800, witnessing the transformation from carbon nitride intermediate to N-doped graphene-like carbon. For NG-900 and NG-1000, the N content further decreased to 7.3 and 4.8 at%, respectively, due to the collapse of N-rich carbonaceous fragments. The N species on NG samples were dominantly composed with three types according to the deconvolution of N 1s XPS spectra, namely pyridinic N, pyrrolic N and graphitic N. The amount of each N component was summarised in Table 5-2. All the three N species were synchronously decomposed with the increased annealing temperature. Specifically, when the annealing temperature was elevated from 800 ºC to 1000 ºC, the loss of pyridinic (3.6 to 0.8 at%) and pyrrolic N (5.6 to 1.5 at%) was more significant than the reduction of graphitic N (1.4 to 1.2 at%). On the contrary, there was no severe variation of the concentration and composition of oxygen groups for the NGs prepared with different temperatures (Table 5-1 and Table 5-2), which could be possibly due to the regeneration of oxygen during the acid-purification and stabilization treatment.

5.3.2 Catalytic oxidation of benzyl alcohol

The catalytic performances of the synthesized NG samples were firstly probed in the selective oxidation of BzOH, a widely explored alcohol oxidation reaction. The reaction was carried out at a moderate temperature (50 ºC), preferable to the most reported cases. The mixed acetonitrile/water was selected as the solvent based on our previous work.[32] BzH was the target product and served as an indicator of the oxidation selectivity of this reaction system. The reaction outcomes over different NG samples were displayed in Table 5-1. In the non-catalyst experiment, only 10.1 % BzOH conversion and 2.5 % BzH yield were obtained, implying that the inactivated PMS oxidant was almost unable to react with BzOH. NG-600 showed the minimum catalytic activity in BzOH oxidation with 9.7 % BzH yield because no graphene-like structure was formed at low pyrolysing temperature. Along with the increased

annealing temperature, the graphene flakes were created and the corresponding catalytic performance exhibited substantial improvement. The highest oxidation efficiency was observed on NG-800, enabling 96.1% BzOH conversion, 85.2% BzH selectivity and 81.9% BzH yield. Surprisingly, NG-900 possessed the highest SSA and thinner-layered graphene sheets whereas its catalytic activity was slightly lower than NG-800, which was possibly due to the loss of N species (NG-900: 7.3% vs NG-800: 12.4%, Table 5-1). As for NG-1000, the further reduced N content (4.8%) and decomposed graphene structure led to lower BzH yield of 61.5%. The NG-800(blank) and NG-800(ACl) afforded 20.4 and 23.9% BzH yield, respectively, owing to the failed formation of thin-layered large graphene sheets. On the contrary, the NG-800(MgN) presented almost identical catalytic performance as NG-800(AN) to achieve 81.2% BzH yield. Furthermore, the N contents of AN (12.4%) and MgN (13.9%) derived NG were higher than that on NG-800(blank) (8.9%) and NG-800(ACl) (10.5%), indicating the additive nitrate salts not only contributed to the formation of thin-layered graphene flakes but also facilitated the immobilization of N species to gain a higher N content. In comparison, another NG sample was prepared with high $M_{N/C}$=10 denoted as NG-800(10:1). The NG-800 was superior to NG-800(10:1) in both the BzOH conversion and BzH selectivity and the BzH yield of NG-800 surpassed NG-800(10:1) by 13.6%. Hence the NG produced with low urea loading and additive nitrate salt was more effective in BzOH oxidation with PMS than the one prepared with solely high $M_{N/C}$.

Table 5-1. The N/O content of NG samples and the catalytic performance in BzOH oxidation.[a]

Entry	Catalyst	N content (at.%)[b]	O content (at.%)[b]	BzOH conversion (%)	BzH selectivity (%)	BzH yield (%)
1	Blank	-	-	10.1	24.8	2.5
2	NG-600	23.3	9.1	12.4	78.2	9.7
3	NG-700	17.8	10.1	72.3	77.6	56.1

4	NG-800	12.4	9.3	96.1	85.2	81.9
5	NG-900	7.3	9.7	90.4	82.1	74.2
6	NG-1000	4.8	8.8	74.2	82.9	61.5
7	NG-800(blank)	8.9	9.5	29.5	69.1	20.4
8	NG-800(MgN)	13.9	8.5	94.4	86.1	81.2
9	NG-800(ACl)	10.5	8.5	29.8	80.1	23.9
10	NG-800(10:1)	11.8	9.7	89.6	76.1	68.3

[a] Reaction conditions: 10 mg catalyst, 0.2 mmol BzOH, 0.6 mmol PMS, 10 mL acetonitrile/water (1:1, volume ratio), 50 ºC, 5 h.

[b] The N and O contents (atomic percentage) were obtained by XPS spectra.

Table 5-2. Composition of O and N species on NG-600, NG-700, NG-800, NG-900 and NG-1000 derived from deconvolution of XPS spectra.[a]

Samples	Pyridinic N	Pyrrolic N	Graphitic N	Pyridine−N−oxide	NO_2	C=O	O=C−O	C−O	H_2O
NG-600	5.5	9.1	6.9	1.2	0.6	1.7	3.2	3.3	1.0
NG-700	6.7	7.9	1.7	0.5	1.1	3.1	4.6	2.2	0.2
NG-800	3.6	5.6	1.4	0.8	1.0	2.8	4.4	1.6	0.4
NG-900	1.7	2.5	1.1	0.6	1.3	2.9	4.3	2.0	0.6
NG-1000	0.8	1.5	1.2	0.2	1.1	2.1	4.5	1.7	0.5

[a] The content of each N or O component is provided in atomic percentage.

The effect of the reaction conditions on the oxidation efficiency of BzOH was investigated using NG-800 as a representative catalyst. The BzOH conversion was significantly influenced by the PMS concentration, showing a continuous increase with higher PMS loading (Figure 5-6). Conversely, the BzH selectivity dropped from 99.4% to 85.2% when multiplying the PMS loading by three times, indicating that the excess PMS could lead to a slight over-oxidation of the BzOH/BzH. However, no organic by-products such as benzoic acid and benzyl benzoate were detected in these cases. Known that the carbo-activated PMS in advanced oxidation processes could lead to the mineralization of organic contaminants where a high molar ratio of

PMS/contaminant was applied, we suppose that the overloading of PMS may cause a minor deep-oxidation of BzOH into CO_2. The reaction was also performed under different temperatures (Figure 5-7). The reaction efficiency was remarkably enhanced during the elevation of the temperature from 30 ºC to 60 ºC free from the decrease of selectivity, with 97.3% conversion and 85.0% BzH selectivity obtained at 60 ºC. This suggests that the selective oxidation of BzOH by NG activated PMS is viable in a facile and benign process. The reaction efficiency was further monitored as a function of reaction time to obtain a kinetic view of the selective oxidation process (Figure 5-8). At a PMS/BzOH (mol/mol) ratio of 3, around 50% of BzOH was converted within the first hour, delivering over 90% BzH selectivity. As the consumption of PMS and BzOH reactant and the accumulation of BzH, the reaction rate gradually decreased and it cost two hours for the conversion of 91.5% to reach 96%. A minor drop of BzH selectivity was observed from 92.4% at the first hour to 85.2% after 5 hours reaction.

Beyond that, the catalytic efficiency of the BzOH oxidation in this work is compared with the relative reaction systems in the literatures as summarised in Table 5-3.[8, 10, 23, 32-34] Nanocarbons catalyzed BzOH oxidation by O_2 gas was normally performed with high temperature (>100 ºC), high catalyst loading and long reaction time, due to the triplet ground state structure of O_2. At temperatures lower than 100 ºC, the O_2 activation efficiency was greatly suppressed, leading to low BzOH conversion rates. The BzOH oxidation was accomplished with higher reaction rate and under a milder environment in this work compared with the reported cases by the nanocarbons/O_2 reaction system. Our results are also superior to those of Au catalysed BzOH oxidation by TBHP, a liquid peroxide oxidant, achieving a slightly higher reaction rate with a much lower temperature (50 vs. 125 ºC). Catalyst-free BzOH oxidation has also been reported by PMS with good efficiency, but extra homogeneous additives were required to generate the actual oxidizing species. Moreover, this work profoundly enhanced the BzOH oxidation efficiency ralative to the one from CNT activated PMS (81.9% to 48.1% BzH yield).

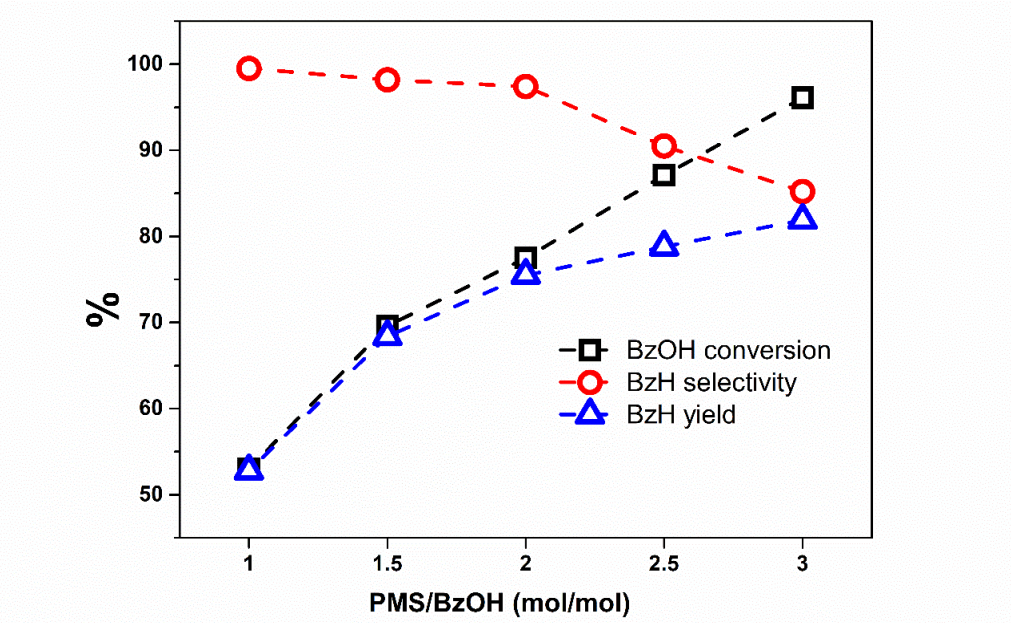

Figure 5-6. The effect of PMS concentration on the catalytic efficiency of BzOH oxidation with NG-800. Reaction conditions: 5 mg catalyst, 0.1 mmol BzOH, 5 mL acetonitrile/water (1:1, volume ratio), 50 ºC, 5 h.

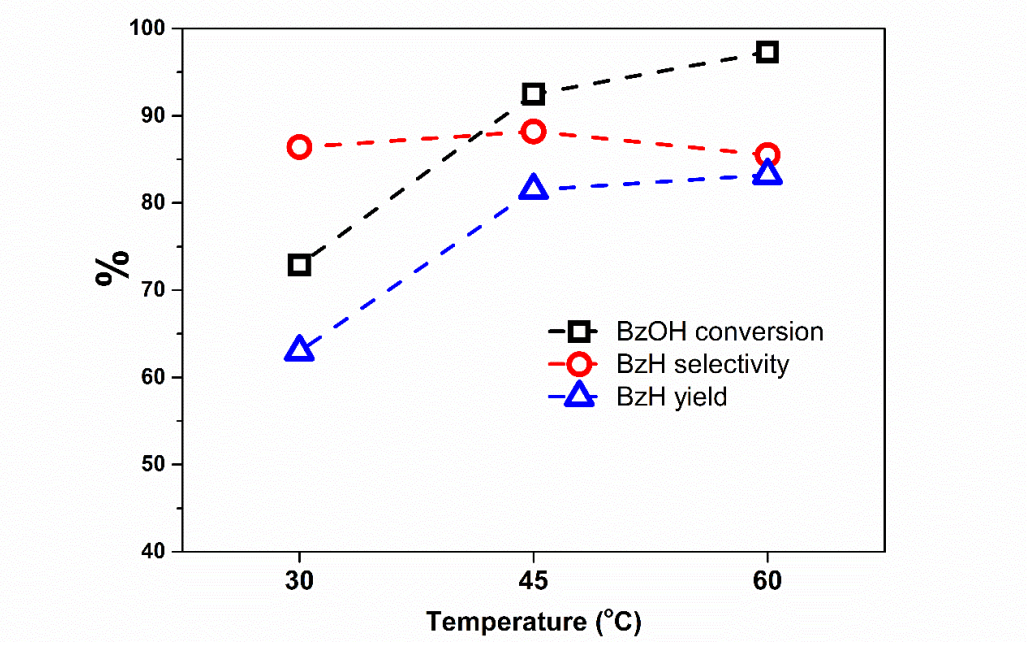

Figure 5-7. The effect of reaction temperature on the catalytic efficiency of BzOH oxidation with NG-800. Reaction conditions: 5 mg catalyst, 0.1 mmol BzOH, 0.3 mmol PMS, 5 mL acetonitrile/water (1:1, volume ratio), 5 h.

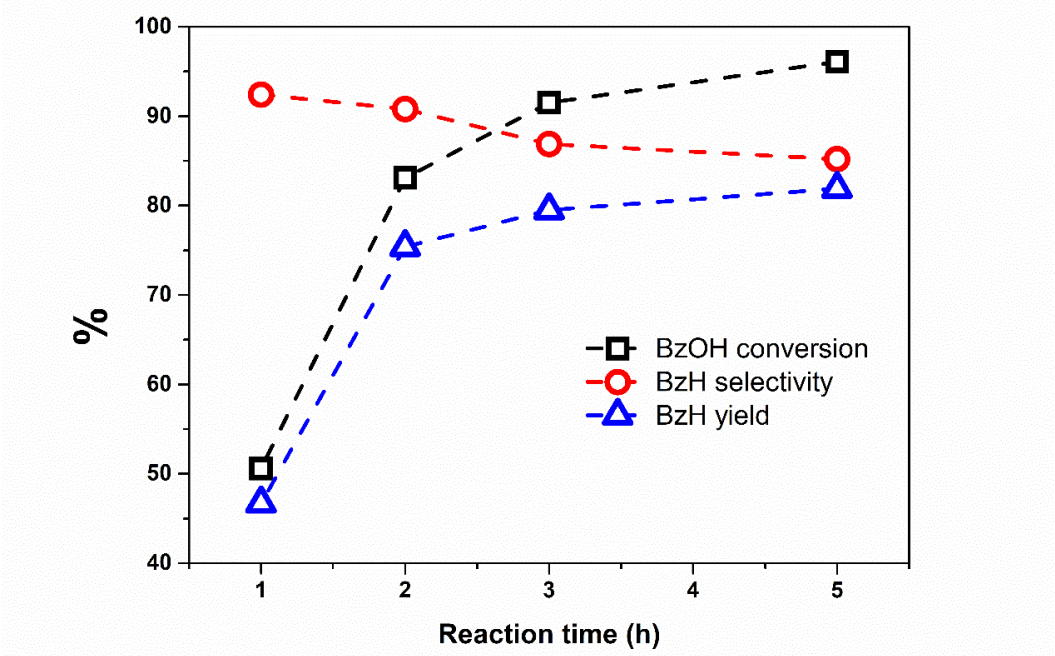

Figure 5-8. The effect of reaction time on the catalytic efficiency of BzOH oxidation with NG-800. Reaction conditions: 5 mg catalyst, 0.1 mmol BzOH, 0.3 mmol PMS, 5 mL acetonitrile/water (1:1, volume ratio), 50 ºC.

Table 5-3. Comparison of the oxidation efficiency of benzyl alcohol in this work with the reported literatures.

Entry	Catalyst loading (relative to the mass of BzOH)	Oxidant	T/ ºC	t/h	Additive	BzOH conversion/ %	BzH selectivity /%	BzH yield/%	Ref
1	Graphene oxide (200%)	O_2/1 atm	100	24	–	–	–	92	[23]
2	NCNT (2%)	O_2/15 atm	130	8	–	44.7	94.1	–	[10]
3	N-graphene (300%)	O_2/1 atm	70	10	–	12.8	100	–	[8]
4	Au/Al_2O_3 (2.5%)	TBHP	125	5	–	89.9	89.2	–	[33]
5	–	PMS	–	3	NaBr	–	–	87	[34]
6	Carbon nanotubes (50%)	PMS	50	5	–	57.1	84.3	48.1	[32]
7	NG (50%)	PMS	50	5	–	96.1	85.2	81.9	Herein

5.3.3 Identification of the reaction routes

For the oxidation reactions induced by catalytic activated PMS, both radical and non-radical processes could occur in a broad variety of reaction systems. The reactive radicals produced from PMS include $^{\bullet}OH$, $SO_4^{\bullet-}$ and $SO_5^{\bullet-}$, with $SO_4^{\bullet-}$ radicals have been widely accepted as the dominant oxidizing species in many advanced oxidation reactions because of the high redox potential and long half time period.[35-36] The generation processes of the radicals were illustrated in Equations (5-5) to (5-9) with PMS serving as either electron donor or acceptor. The understanding of non-radical oxidation mainly focus on either surface complex mediated electron transfer or singlet oxygen ($^1O_2$).[37-38] Equation (5-8) demonstrates a possible way for the generation of singlet oxygen *via* the decomposition of $SO_5^{\bullet-}$.[39-40] The effect of radicals on the selective oxidation of BzOH was probed by quenching experiments, adopting *tert*-butanol (TBA) as effective scavenger of hydroxyl radicals and ethanol (EtOH) as quencher for both hydroxyl and sulfate radicals.[41-42] The selective oxidation efficiency of BzOH over NG-800 with the added TBA and EtOH in different concentrations was displayed in Figure 5-9 (a), indicated by the BzH yield. The individual dose of either TBA or EtOH could cause reduction of BzH yield. Thus both the hydroxyl and sulfate radicals were responsible for the selective conversion of BzOH into BzH. Specifically, TBA caused a minor decrease of BzH yield while the effect of EtOH was more significant, implying the sulfate radicals played a more important role in the selective transformation of BzOH into BzH. At the maximum EtOH loading (replacing the entire organic solvent with EtOH), almost all the radicals could be captured and over half of the original BzH yield remained, attributed to the non-radical oxidation route. Therefore, the selective oxidation of BzOH was accomplished by both radical and non-radical processes in this system.

$$HSO_5^- + e^- \rightarrow {}^{\bullet}OH + SO_4^{2-} \qquad (5\text{-}5)$$

$$HSO_5^- + e^- \rightarrow OH^- + SO_4^{\bullet-} \qquad (5\text{-}6)$$

$$HSO_5^- - e^- \rightarrow H^+ + SO_5^{\bullet -} \quad (5\text{-}7)$$

$$2SO_5^{\bullet -} \rightarrow {}^1O_2 + 2SO_4^{\bullet -} \quad (5\text{-}8)$$

$$^{\bullet}OH + SO_4^{2-} \rightarrow OH^- + SO_4^{\bullet -} \quad (5\text{-}9)$$

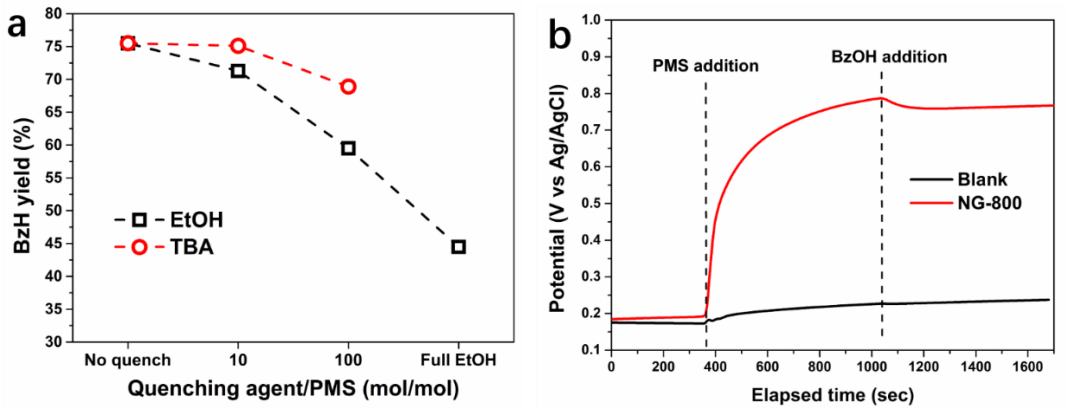

Figure 5-9. (a) The effect of *tert*-butanol (TBA) and ethanol (EtOH) dose of different concentrations on the BzH yield (NG-800 as catalyst). Reaction conditions: 10 mg catalyst, 0.2 mmol BzOH, 0.4 mmol PMS, 50 ºC, 5 h, 10 mL acetonitrile/water (1:1, volume ratio). Full EtOH test was performed by replacing the acetonitrile solvent with ethanol. (b) The open circuit potential of NG-800 upon the addition of PMS (1.5 mM) and BzOH (1.5 mM) in Na_2SO_4 solution (100 mM).

To identify the non-radical pathway in this reaction system, open circuit potential test was employed to probe the electron transfer behaviour among the NG-800, PMS and BzOH molecules as presented in Figure 5-9 (b). For NG-800, there was a rapid increase of potential from +0.19 to +0.78 V (vs Ag/AgCl) after the addition of PMS, whereas the potential only increased from +0.17 to +0.22 V in the absence of NG-800. This could be due to the charge redistribution between PMS and NG-800 by the physisorption of PMS on the surface of NG-800.[43] The subsequent addition of BzOH resulted in a reverse potential shift from +0.78 to +0.76 V because of the electron transfer from BzOH to PMS mediated by NG-800. The potential of the blank test was not influenced by the BzOH addition. To further exclude the participation of $^1O_2$ in the

non-radical oxidation of BzOH, another selective oxidation experiment was conducted using BzH as the oxidation substrate instead of BzOH with NG-800 activated PMS. BzH is a readily oxidizable substrate which can be oxidized into benzoic acid simply by the exposure to the atmosphere.[44] From the previously reported results and Equations (5-7) to (5-8), the generation of $^1O_2$ fully relies on the interaction of catalyst and PMS.[45] Therefore, if the non-radical oxidation pathway of BzOH was caused by $^1O_2$, the more oxidizable BzH should undergo the similar oxidation process with $^1O_2$. As shown in Figure 5-10, the conversion of BzH (79.8%) caused by NG-800/PMS was even higher than the conversion of BzOH under the same reaction conditions (77.5%). Then the BzH oxidation was performed in full EtOH environment, affording only 16.8% BzH conversion, much lower than the proportion of non-radical contribution in BzOH oxidation as discussed above. Based on these results, we infer that the non-radical route in the selective oxidation of BzOH was accomplished *via* the surface coordinated complex rather than the singlet oxygen.

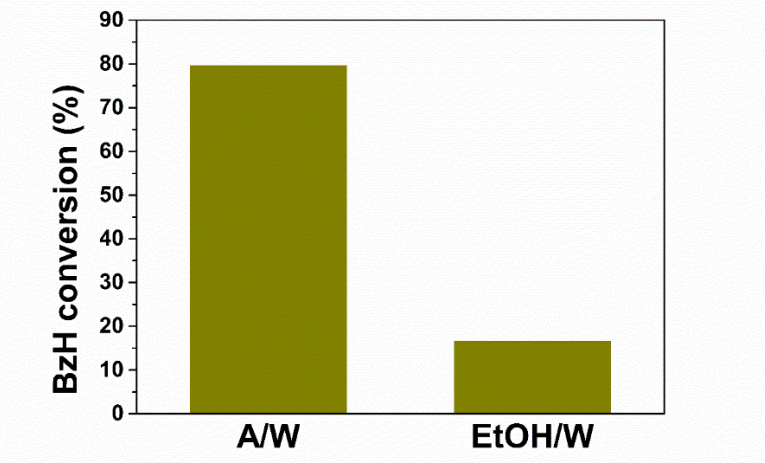

Figure 5-10. The oxidation of BzH with NG-800 in acetonitrile/water 1:1 solvent (A/W) and ethanol/water 1:1 solvent (EtOH/W). Reaction conditions: 5 mg catalyst, 0.1 mmol BzH, 0.2 mmol PMS, 5 mL acetonitrile/water (1:1, volume ratio), 50 ºC, 5 h.

5.3.4 Active sites for PMS activation

In our previous work, the electrophilic oxygen species (peroxides and superoxides) attached on modified carbon nanotubes (CNTs) were verified as the major active sites for PMS activation to endow a radical-based process for BzOH oxidation.[32] Herein we looked into the influence of surface electrophilic oxygen species on the catalytic properties of the NG samples. First, the concentrations of electrophilic oxygen on NG samples by different annealing temperatures were determined *via* iodometric titration method [46-47] as displayed in Figure 5-11 (a). The amount of electrophilic oxygen increased with higher annealing temperature, which could be due to the joint effect of increased SSA and defect degree as discussed earlier, since the electrophilic oxygen is prone to form on the defect sites on sp^2 hybridized carbon.[48] For high temperature annealed NG, we believe the existence of electrophilic oxygen was dominantly due to the capture and activation of oxygen by NG surface when it was exposed to oxidative environment such as atmosphere and acid washing. Specifically, NG-800 contained more electrophilic oxygen than NG-800(10:1), indicating that the additive AN salt contributed to the formation of graphene structure with abundant electrophilic oxygen groups. Meanwhile, the electrophilic oxygen species on NG-800 was eliminated after the iodometric titration, and the obtained sample was denoted as NG-800(KI). It can be seen from the inset of Figure 5-11 (a) that the removal of electrophilic functionalities from NG-800 led to a significant drop of BzH yield from 75.5% to 28.6%. The full EtOH test over NG-800(KI) demonstrated a higher proportion of non-radical contribution (77%) compared with that of NG-800 (57%). However the actual BzH yield derived from radical (31.0%) and non-radical processes (44.5%) of NG-800 was still higher than that of NG-800(KI) (6.6 and 22.0%, respectively). Thus it can be inferred the electrophilic oxygen species made a greater contribution to the radical process whereas the N species dominantly enables the non-radical oxidation of BzOH. Another proof for the indispensable role of electrophilic oxygen in this reaction is displayed in Figure 5-11 (b). The cycling test of NG-800 manifested that the oxidation efficiency decreased during the four runs, and the electrophilic oxygen decreased

simultaneously, confirming the electrophilic oxygen was the active site for the PMS activation and its consumption was the main reason for the reduced activity. The catalyst after the fourth run was then re-annealed at 800 ºC for recovery. The obtained sample presented slightly higher catalytic efficiency as well as a larger amount of electrophilic oxygen than the fresh catalyst, exhibiting the excellent recovery ability of NG-800.

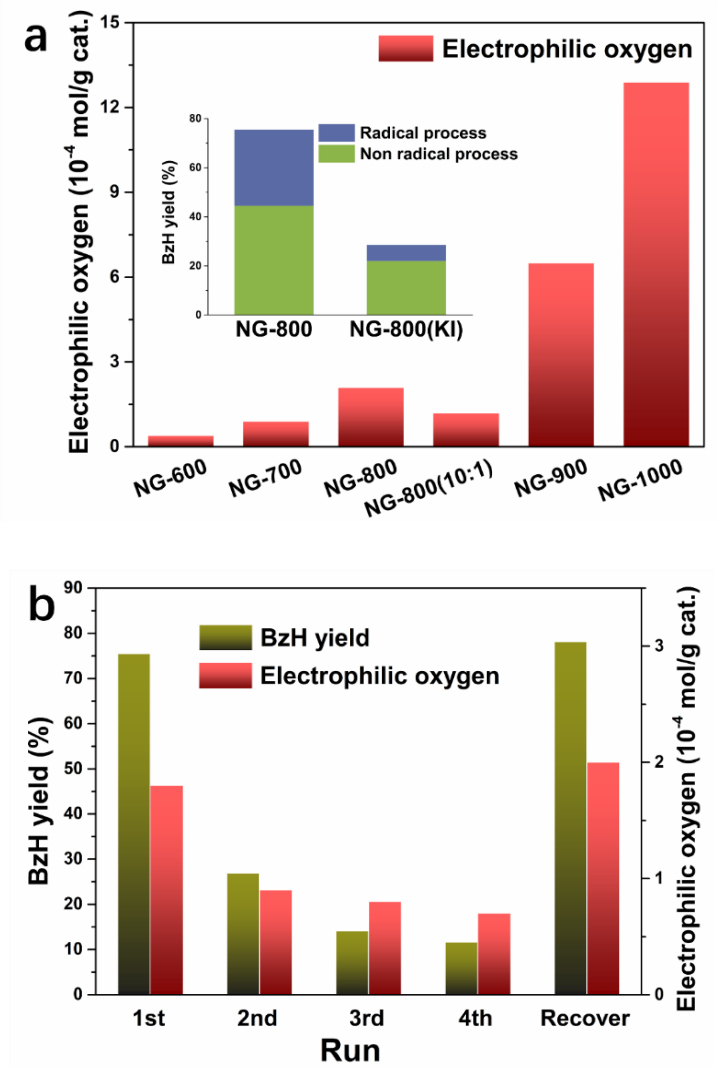

Figure 5-11. (a) Concentration of electrophilic oxygen on NG samples. The inset of (a) is the radical and non-radical contributions on the BzH yield over NG-800 and NG-800(KI). (b) Catalytic performance and concentration of electrophilic oxygen of NG-800 for 4 reaction cycles and recovering NG-800 after the 4th run by re-annealing at 800 ºC. Reaction conditions: 10 mg catalyst, 0.2 mmol BzOH, 0.4 mmol PMS, 50 ºC, 5 h, 10 mL acetonitrile/water (1:1, volume ratio).

Previous research suggests that the graphitic N (or quaternary N) coordinated with the sp^2 carbon network was active site for PMS activation *via* the adsorption of PMS at the positive-charged adjacent carbon atoms for non-radical oxidation of organics.[21, 49] However, the roles of pyridinic N and pyrrolic N were less studied. As discussed above, the decreased N species for higher-temperature annealed NG was dominantly attributed to the decomposition of pyridinic and pyrrolic N. In this regard, the catalytic role of the doped N on the NG could be attributed to the joint effect of different N species. To probe the impact of the less investigated N species, a series of N-containing organics free from oxygen groups were introduced into the selective oxidation reaction to mimic the pyridinic and pyrrolic N in different configurations as displayed in Figure 5-12. The pyridinic N was reported to be electron-withdrawing functionality,[50] but the addition of pyridine (PD) and 4-*tert*-butylpyridine (4-TPD) with single pyridinic N showed no beneficial effects to the selective oxidation of BzOH. Likewise, the BzOH oxidation was not enhanced by pyrimidine (PMD) additive which contains two N atoms in a single aromatic ring. In contrast, the addition of 4'-(4-methylphenyl)-2,2':6',2"-terpyridine (MPT-PD) tremendously improved the oxidation efficiency, delivering 50.4% BzOH conversion and 43.5% BzH yield, which were 10- and 27-fold as high as those from the blank test. We suppose that the single electron-withdrawing pyridinic N atoms in PD and 4-TPD are unable to conduct the electron transfer from BzOH to PMS due to the lack of electron mediator and PMS adsorption sites. The inactive behaviour of PMD is probably because of the spatial hindrance to simultaneously locate the PMS and BzOH molecules. The terpyridine compounds are equipped with both electron-donating and electron-withdrawing abilities by the conjugated pyridine rings,[51-52] thus provide possibilities for the formation of intermediate complex to accomplish the oxidation *via* electron transfer. In the case of the NG surface, the integrated pyridinic N atoms of different aromatic rings at the armchair edge of the graphene sheets could act as a bridge for electron transfer between the anchored PMS and BzOH molecules. Besides, the electron-rich BzOH attracted on pyridinic N might also cooperate with the PMS adsorbed on graphitic N site to endow the oxidation process. Pyrrole (PRL) was used to mimic the pyrrolic N, while no

promotion of reaction efficiency was observed after its addition. It's noteworthy that the pyrrole suffered from polymerization under acidic PMS environment to generate $(C_4H_2NH)_n$, but the polymerized pyrrole was still unable to facilitate the oxidation of BzOH, implying that neither single nor integrated pyrrolic N molecules could enable the PMS activation for BzOH oxidation. The results from the small molecule mimics indicate that the integrated pyridinic N species are active sites for the BzOH oxidation by PMS, while the pyrrolic N exhibits no obvious impact on the reaction.

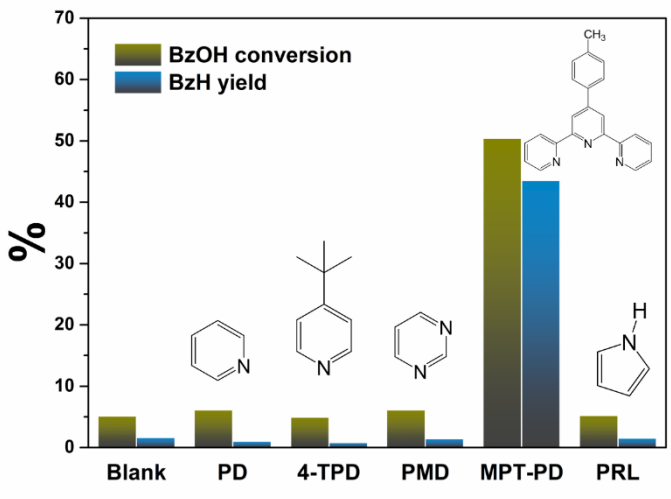

Figure 5-12. The selective oxidation of BzOH with small molecule mimics. The reaction conditions: 0.2 mmol BzOH, 0.4 mmol small molecule mimics, 0.3 mmol PMS, 50 ºC, 3 h, 10 mL acetonitrile/water (1:1, volume ratio).

5.3.5 Reaction mechanism

Based on the above experimental analysis, a possible mechanism for this NG/PMS/BzOH oxidation system was proposed in Figure 5-13. The radical-based oxidation mainly occurs over the electrophilic oxygen species on NG which are electron-deficient and can capture an electron from PMS to generate $SO_5^{\bullet-}$. The $SO_5^{\bullet-}$ radicals can subsequently decompose into $SO_4^{\bullet-}$ which has a higher redox potential for BzOH oxidation. Beyond that, the other functionalities such as nucleophilic C=O may

also make a minor contribution to produce •OH and $SO_4^{\bullet-}$ by serving as an electron donor to the PMS molecules as reported.[53] On the other hand, the N species dominantly endow the non-radical oxidation of BzOH by electron transfer through the conjugated graphene network. The integrated pyridinic N atoms located at different aromatic rings may create both electron-withdrawing and electron-donating districts to accommodate the adsorption of BzOH and PMS molecules, thus enabling the construction of coordinated complex for the non-radical BzOH oxidation. The graphitic N with high electronegativity can induce a higher charge density to the neighboring carbon atoms, which is prone to capture PMS by the superoxide -O-O- bond and to receive the electron transferred from the BzOH molecules. The electron transfer from BzOH to PMS through the adsorption complex eventually results in the formation of SO_4^{2-} and BzH.

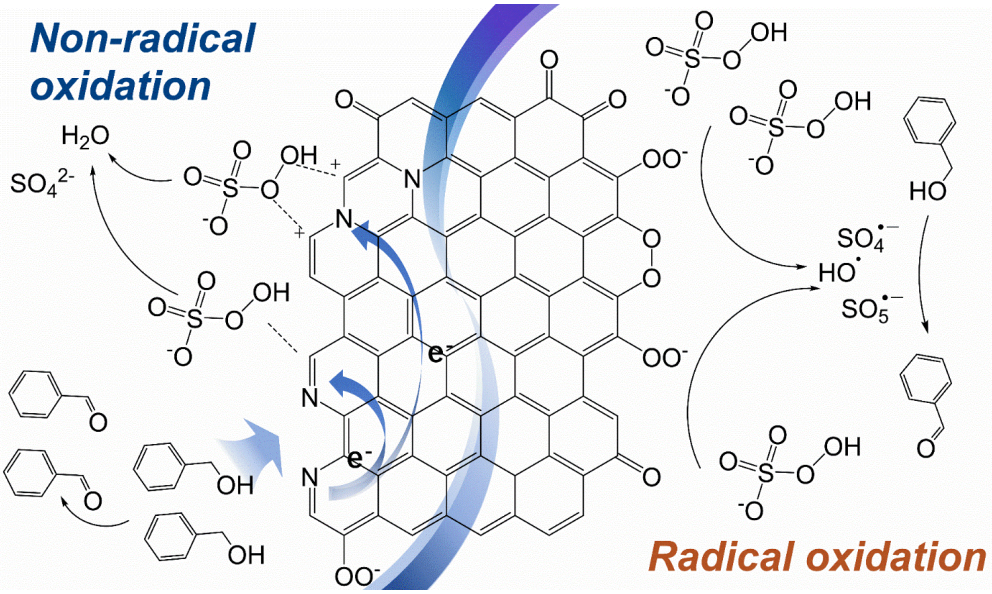

Figure 5-13. Proposed reaction mechanism of the PMS activation and BzOH oxidation over NG catalyst.

5.3.6 The selective oxidation of other alcohols.

The application of NG-800 activated PMS was then extended to other primary alcohols including the selective oxidation of 1-phenylethanol and cyclohexanol into acetophenone and cyclohexanone, respectively. The reaction results under different conditions are displayed in Table 5-4. Compared with BzOH, the NG-800/PMS system was less effective for the selective oxidation of 1-phenylethanol, which was probably caused by the spatial confinement of the secondary alcohol. Under the same reaction conditions, the conversion of 1-phenylethanol was 39.3%, in contrast with 96.1% conversion of BzOH in Table 1. By increasing the reaction time and temperature, a remarkable enhancement of 1-phenylethanol conversion was achieved. The highest conversion of 1-phenylethanol (80.1%) was obtained by increasing the temperature by 10 ºC and doubling the reaction time to 10 h with over 80% selectivity towards acetophenone. The oxidation of non-activated cyclohexanol by NG/PMS system was much slower relative to the aromatic alcohols. By increasing the temperature and reaction time, the conversion of cyclohexanol increased from 2.7 to 9.7%, while the cyclohexanone selectivity dropped from 75.3 to 55.5%. A higher concentration of catalyst or PMS is predicted to be essential to produce more reactive oxygen species or active reaction sites for the efficient oxidation of inactive alcohols.

Table 5-4. The oxidation of other alcohols over NG-800. Reaction conditions: 10 mg catalyst, 0.2 mmol substrate, 0.6 mmol PMS, 10 mL acetonitrile/water (1:1, volume ratio).

Substrate	Product	T (ºC)	Time (h)	Conversion (%)	Selectivity (%)
1-phenylethanol	Acetophenone	50	5	39.3	83.8
		60	5	50.9	81.3

		50	10	65.6	79.4
		60	10	80.1	81.2
Cyclohexanol	Cyclohexanone	50	5	2.7	75.3
		60	5	4.0	72.9
		50	10	7.5	58.9
		60	10	9.7	55.5

5.4 Conclusions

In summary, we reported a metal-free route to the synthesis of N-doped graphene-like carbon *via* a protocol with a low $M_{N/C}$, which does not produce a large amount of hazardous waste as encountered by conventional methods. The additive of ammonium nitrate salt played an indispensable role to the fabrication of thin-layered graphene sheets as well as the generation of electrophilic oxygen functionalities. The prepared NG catalyst was successfully used in the highly efficient oxidation of BzOH to produce BzH with PMS. Over 96% BzOH conversion and 85% BzH selectivity were obtained from the optimized reaction *via* both radical and non-radical processes. The electrophilic oxygen species dominantly contributed to the radical generation from PMS, with $SO_4^{\bullet-}$ playing a leading role to oxidize BzOH into BzH. The non-radical pathway is suggested to be performed by N active sites *via* the electron transfer within the surface coordinated complex and mediated electron transfer instead of singlet oxygen. Small molecule mimics imply that the integrated pyridinic N species are crucial for the oxidation of BzOH, providing both electron-withdrawing and electron-donating abilities. The NG/PMS oxidation system was also applicable to the selective oxidation of other aromatic alcohols such as 1-phenylethanol. This work provides a facile strategy to prepare the cost-effective carbo-catalysts with tailored functionalities

and reveals their catalytic pathways to effectively participate these organic selective reactions exemplified by the oxidation of BzOH to yield BzH.

References

1. Parmeggiani, C.; Matassini, C.; Cardona, F., A step forward towards sustainable aerobic alcohol oxidation: new and revised catalysts based on transition metals on solid supports. *Green Chemistry* **2017,** *19* (9), 2030-2050.

2. Enache, D. I.; Edwards, J. K.; Landon, P.; Solsona-Espriu, B.; Carley, A. F.; Herzing, A. A.; Watanabe, M.; Kiely, C. J.; Knight, D. W.; Hutchings, G. J., Solvent-Free Oxidation of Primary Alcohols to Aldehydes Using Au-Pd/TiO_2 Catalysts. *Science* **2006,** *311* (5759), 362.

3. Maity, P.; Gopinath, C. S.; Bhaduri, S.; Lahiri, G. K., Applications of a high performance platinum nanocatalyst for the oxidation of alcohols in water. *Green Chemistry* **2009,** *11* (4), 554-561.

4. Dong, L.; Gari, R. R. S.; Li, Z.; Craig, M. M.; Hou, S., Graphene-supported platinum and platinum–ruthenium nanoparticles with high electrocatalytic activity for methanol and ethanol oxidation. *Carbon* **2010,** *48* (3), 781-787.

5. Choudhary, V. R.; Dhar, A.; Jana, P.; Jha, R.; Uphade, B. S., A green process for chlorine-free benzaldehyde from the solvent-free oxidation of benzyl alcohol with molecular oxygen over a supported nano-size gold catalyst. *Green Chemistry* **2005,** *7* (11), 768-770.

6. Su, D. S.; Perathoner, S.; Centi, G., Nanocarbons for the Development of Advanced Catalysts. *Chem. Rev.* **2013,** *113* (8), 5782-5816.

7. Duan, X.; Sun, H.; Wang, S., Metal-Free Carbocatalysis in Advanced Oxidation Reactions. *Acc. Chem. Res.* **2018,** *51* (3), 678-687.

8. Long, J.; Xie, X.; Xu, J.; Gu, Q.; Chen, L.; Wang, X., Nitrogen-Doped Graphene Nanosheets as Metal-Free Catalysts for Aerobic Selective Oxidation of Benzylic Alcohols. *ACS Catal.* **2012,** *2* (4), 622-631.

9. Sheng, S. D.; Guodong, W.; Shuchang, W.; Feng, P.; Robert, S., Carbocatalysis in Liquid-Phase Reactions. *Angew. Chem. Int. Ed.* **2017,** *56* (4), 936-964.

10. Luo, J.; Yu, H.; Wang, H.; Wang, H.; Peng, F., Aerobic oxidation of benzyl alcohol to benzaldehyde catalyzed by carbon nanotubes without any promoter. *Chem. Eng. J.* **2014,** *240*, 434-442.

11. Luo, J.; Peng, F.; Yu, H.; Wang, H., Selective liquid phase oxidation of benzyl alcohol catalyzed by carbon nanotubes. *Chem. Eng. J.* **2012,** *204-206*, 98-106.

12. Navalon, S.; Dhakshinamoorthy, A.; Alvaro, M.; Antonietti, M.; García, H., Active sites on graphene-based materials as metal-free catalysts. *Chem. Soc. Rev.* **2017,** *46* (15), 4501-4529.

13. Navalon, S.; Dhakshinamoorthy, A.; Alvaro, M.; Garcia, H., Carbocatalysis by Graphene-Based Materials. *Chem. Rev.* **2014,** *114* (12), 6179-6212.

14. Hummers, W. S.; Offeman, R. E., Preparation of Graphitic Oxide. *J. Am. Chem. Soc.* **1958,** *80* (6), 1339-1339.

15. Li, X.; Cai, W.; An, J.; Kim, S.; Nah, J.; Yang, D.; Piner, R.; Velamakanni, A.; Jung, I.; Tutuc, E.; Banerjee, S. K.; Colombo, L.; Ruoff, R. S., Large-Area Synthesis of High-Quality and Uniform Graphene Films on Copper Foils. *Science* **2009,** *324* (5932), 1312.

16. Kim, K. S.; Zhao, Y.; Jang, H.; Lee, S. Y.; Kim, J. M.; Kim, K. S.; Ahn, J.-H.; Kim, P.; Choi, J.-Y.; Hong, B. H., Large-scale pattern growth of graphene films for stretchable transparent electrodes. *Nature* **2009,** *457* (7230), 706-710.

17. Chen, C.; Xu, G.; Wei, X.; Yang, L., A macroscopic three-dimensional tetrapod-separated graphene-like oxygenated N-doped carbon nanosheet architecture for use in supercapacitors. *J. Mater. Chem. A* **2016,** *4* (25), 9900-9909.

18. Wang, C.; Kang, J.; Sun, H.; Ang, H. M.; Tadé, M. O.; Wang, S., One-pot synthesis of N-doped graphene for metal-free advanced oxidation processes. *Carbon* **2016,** *102*, 279-287.

19. Wen, G.; Gu, Q.; Liu, Y.; Schlögl, R.; Wang, C.; Tian, Z.; Su, D. S., Biomass-Derived Graphene-like Carbon: Efficient Metal-Free Carbocatalysts for Epoxidation. *Angew. Chem. Int. Ed.* **2018,** *57* (51), 16898-16902.

20. Yongjun, G.; Gang, H.; Jun, Z.; Zujin, S.; Yuanshuai, Z.; Sheng, S. D.; Jianguo, W.; Xinhe, B.; Ding, M., Nitrogen-Doped sp2-Hybridized Carbon as a Superior Catalyst for Selective Oxidation. *Angew. Chem. Int. Ed.* **2013,** *52* (7), 2109-2113.

21. Duan, X.; Sun, H.; Wang, Y.; Kang, J.; Wang, S., N-Doping-Induced Nonradical Reaction on Single-Walled Carbon Nanotubes for Catalytic Phenol Oxidation. *ACS Catal.* **2015,** *5* (2), 553-559.

22. Li, X.-H.; Kurasch, S.; Kaiser, U.; Antonietti, M., Synthesis of Monolayer-Patched Graphene from Glucose. *Angew. Chem. Int. Ed.* **2012,** *51* (38), 9689-9692.

23. R., D. D.; Hong-Peng, J.; W., B. C., Graphene Oxide: A Convenient Carbocatalyst for Facilitating Oxidation and Hydration Reactions. *Angew. Chem.* **2010,** *122* (38), 6965-6968.

24. Gao, J.; Ren, Z.-G.; Lang, J.-P., Oxidation of benzyl alcohols to benzaldehydes in water catalyzed by a Cu(II) complex with a zwitterionic calix[4]arene ligand. *J. Organomet. Chem.* **2015,** *792*, 88-92.

25. Choudhary, V. R.; Dumbre, D. K., Solvent-free selective oxidation of benzyl alcohol to benzaldehyde by tert-butyl hydroperoxide over U3O8-supported nano-gold catalysts. *Appl. Catal. A-Gen.* **2010,** *375* (2), 252-257.

26. Ghanbari, F.; Moradi, M., Application of peroxymonosulfate and its activation methods for degradation of environmental organic pollutants: Review. *Chem. Eng. J.* **2017,** *310*, 41-62.

27. Duan, X.; Ao, Z.; Zhou, L.; Sun, H.; Wang, G.; Wang, S., Occurrence of radical and nonradical pathways from carbocatalysts for aqueous and nonaqueous catalytic oxidation. *Appl. Catal. B-Environ.* **2016,** *188*, 98-105.

28. Duan, X.; Ao, Z.; Sun, H.; Indrawirawan, S.; Wang, Y.; Kang, J.; Liang, F.; Zhu, Z. H.; Wang, S., Nitrogen-Doped Graphene for Generation and Evolution of Reactive Radicals by Metal-Free Catalysis. *ACS Appl. Mater. Interfaces* **2015,** *7* (7), 4169-4178.

29. Li, D.; Duan, X.; Sun, H.; Kang, J.; Zhang, H.; Tade, M. O.; Wang, S., Facile synthesis of nitrogen-doped graphene via low-temperature pyrolysis: The effects of precursors and annealing ambience on metal-free catalytic oxidation. *Carbon* **2017,** *115*, 649-658.

30. Lin, Y.; Pan, X.; Qi, W.; Zhang, B.; Su, D. S., Nitrogen-doped onion-like carbon: a novel and efficient metal-free catalyst for epoxidation reaction. *J. Mater. Chem. A* **2014,** *2* (31), 12475-12483.

31. Tuinstra, F.; Koenig, J. L., Raman Spectrum of Graphite. *The Journal of Chemical Physics* **1970,** *53* (3), 1126-1130.

32. Li, J.; Li, M.; Sun, H.; Ao, Z.; Wang, S.; Liu, S., Understanding of the Oxidation Behaviour of Benzyl Alcohol by Peroxymonosulfate via Carbon Nanotubes Activation. *ACS Catal.* **2020,** *10* (6), 3516-3525.

33. Ndolomingo, M. J.; Meijboom, R., Selective liquid phase oxidation of benzyl alcohol to benzaldehyde by tert-butyl hydroperoxide over γ-Al2O3 supported copper and gold nanoparticles. *Appl. Surf. Sci.* **2017,** *398*, 19-32.

34. Koo, B.-S.; Lee, C. K.; Lee, K.-J., OXIDATION OF BENZYL ALCOHOLS WITH OXONE® AND SODIUM BROMIDE. *Synth. Commun.* **2002,** *32* (14), 2115-2123.

35. Duan, X.; Su, C.; Miao, J.; Zhong, Y.; Shao, Z.; Wang, S.; Sun, H., Insights into perovskite-catalyzed peroxymonosulfate activation: Maneuverable cobalt sites for promoted evolution of sulfate radicals. *Appl. Catal. B-Environ.* **2018,** *220*, 626-634.

36. Huang, Z.; Bao, H.; Yao, Y.; Lu, W.; Chen, W., Novel green activation processes and mechanism of peroxymonosulfate based on supported cobalt phthalocyanine catalyst. *Appl. Catal. B-Environ.* **2014,** *154-155*, 36-43.

37. Duan, X.; Sun, H.; Shao, Z.; Wang, S., Nonradical reactions in environmental remediation processes: Uncertainty and challenges. *Appl. Catal. B-Environ.* **2018,** *224*, 973-982.

38. Lee, H.; Lee, H.-J.; Jeong, J.; Lee, J.; Park, N.-B.; Lee, C., Activation of persulfates by carbon nanotubes: Oxidation of organic compounds by nonradical mechanism. *Chem. Eng. J.* **2015,** *266*, 28-33.

39. Anipsitakis, G. P.; Dionysiou, D. D., Degradation of Organic Contaminants in Water with Sulfate Radicals Generated by the Conjunction of Peroxymonosulfate with Cobalt. *Environmental Science & Technology* **2003,** *37* (20), 4790-4797.

40. Liang, P.; Zhang, C.; Duan, X.; Sun, H.; Liu, S.; Tade, M. O.; Wang, S., An insight into metal organic framework derived N-doped graphene for the oxidative degradation of persistent contaminants: formation mechanism and generation of singlet oxygen from peroxymonosulfate. *Environmental Science: Nano* **2017,** *4* (2), 315-324.

41. Buxton, G. V.; Greenstock, C. L.; Helman, W. P.; Ross, A. B., Critical Review of rate constants for reactions of hydrated electrons, hydrogen atoms and hydroxyl radicals (·OH/·O− in Aqueous Solution. *J. Phys. Chem. Ref. Data* **1988,** *17* (2), 513-886.

42. Anipsitakis, G. P.; Dionysiou, D. D., Radical Generation by the Interaction of Transition Metals with Common Oxidants. *Environmental Science & Technology* **2004,** *38* (13), 3705-3712.

43. Ahn, Y.-Y.; Bae, H.; Kim, H.-I.; Kim, S.-H.; Kim, J.-H.; Lee, S.-G.; Lee, J., Surface-loaded metal nanoparticles for peroxymonosulfate activation: Efficiency and mechanism reconnaissance. *Appl. Catal. B-Environ.* **2019,** *241*, 561-569.

44. Sankar, M.; Nowicka, E.; Carter, E.; Murphy, D. M.; Knight, D. W.; Bethell, D.; Hutchings, G. J., The benzaldehyde oxidation paradox explained by the interception of peroxy radical by benzyl alcohol. *Nat. Commun.* **2014,** *5* (1), 3332.

45. Jawad, A.; Zhan, K.; Wang, H.; Shahzad, A.; Zeng, Z.; Wang, J.; Zhou, X.; Ullah, H.; Chen, Z.; Chen, Z., Tuning of Persulfate Activation from a Free Radical to a Nonradical Pathway through the Incorporation of Non-Redox Magnesium Oxide. *Environmental Science & Technology* **2020,** *54* (4), 2476-2488.

46. Li, J.; Yu, P.; Xie, J.; Liu, J.; Wang, Z.; Wu, C.; Rong, J.; Liu, H.; Su, D., Improving the Alkene Selectivity of Nanocarbon-Catalyzed Oxidative Dehydrogenation of n-Butane by Refinement of Oxygen Species. *ACS Catal.* **2017,** *7* (10), 7305-7311.

47. Li, J.; Yu, P.; Xie, J.; Zhang, Y.; Liu, H.; Su, D.; Rong, J., Grignard reagent reduced nanocarbon material in oxidative dehydrogenation of n-butane. *J. Catal.* **2018,** *360*, 51-56.

48. Zhang, J.; Liu, X.; Blume, R.; Zhang, A.; Schlögl, R.; Su, D. S., Surface-Modified Carbon Nanotubes Catalyze Oxidative Dehydrogenation of *n*-Butane. *Science* **2008,** *322* (5898), 73.

49. Chen, X.; Oh, W.-D.; Hu, Z.-T.; Sun, Y.-M.; Webster, R. D.; Li, S.-Z.; Lim, T.-T., Enhancing sulfacetamide degradation by peroxymonosulfate activation with N-doped graphene produced through delicately-controlled nitrogen functionalization via tweaking thermal annealing processes. *Appl. Catal. B-Environ.* **2018,** *225*, 243-257.

50. Yang, H. B.; Miao, J.; Hung, S.-F.; Chen, J.; Tao, H. B.; Wang, X.; Zhang, L.; Chen, R.; Gao, J.; Chen, H. M.; Dai, L.; Liu, B., Identification of catalytic sites for oxygen reduction and oxygen evolution in N-doped graphene materials: Development of highly efficient metal-free bifunctional electrocatalyst. *Science Advances* **2016,** *2* (4), e1501122.

51. Sauvage, J. P.; Collin, J. P.; Chambron, J. C.; Guillerez, S.; Coudret, C.; Balzani, V.; Barigelletti, F.; De Cola, L.; Flamigni, L., Ruthenium(II) and Osmium(II) Bis(terpyridine)

Complexes in Covalently-Linked Multicomponent Systems: Synthesis, Electrochemical Behaviour, Absorption Spectra, and Photochemical and Photophysical Properties. *Chem. Rev.* **1994,** *94* (4), 993-1019.

52. Barigelletti, F.; Flamigni, L., Photoactive molecular wires based on metal complexes. *Chem. Soc. Rev.* **2000,** *29* (1), 1-12.

53. Duan, X.; Sun, H.; Ao, Z.; Zhou, L.; Wang, G.; Wang, S., Unveiling the active sites of graphene-catalyzed peroxymonosulfate activation. *Carbon* **2016,** *107*, 371-378.

Chapter 6 Cobalt single atom catalysts on carbon supports for highly efficient selective oxidations with activated peroxymonosulfate

Abstract

The development of highly efficient strategy for the liquid phase selective oxidations is one of the most challenging tasks facing the chemical industries. The synthesis of novel catalysts with atomically dispersed active centres is highly desirable to achieve the maximised atom efficiency. In this work, Co-based single atom catalysts (SAC) on carbon-based materials are successfully synthesized and applied for the selective oxidation of benzyl alcohol (BzOH) and ethylbenzene (EB) to derive the corresponding aldehyde and ketone products *via* the activated peroxymonosulfate (PMS) oxidant. SAC catalysts with Co single atoms embedded in nitrogen-doped graphene (SACo@NG) and carbon nitride support (SACo@g-C_3N_4) are prepared with Co contents of 4.1 wt.% and 3.17 wt.%, respectively. Characterization results suggest that the monodispersed Co atoms are coordinated with N atoms to form robust and highly effective catalytic centre

s. The SACo@NG/PMS system shows high efficiency in BzOH oxidation to selectively yield benzaldehyde under mild conditions. Both radical and non-radical processes occur in the selective oxidation of BzOH. The SACo@g-C_3N_4 is applied to the selective oxidatioon of EB with over 95% conversion and acetophenone selectivity by activated PMS. The generated radicals, especially sulfate radicals ($SO_4^{\bullet-}$) can activate the C-H bond in EB. This work provides new insights to the preparation of efficient transition metal-based SACs and their potential application in PMS mediated selective oxidation of alcohols. This work uncovers facile and scalable approaches to prepare robust Co-based single atom catalysts and unveils their potential in the

oxidation of hydrocarbons *via* a highly efficient and environmentally benign PMS activation.

The first part of this chapter is published in Small 17 (16), 2004579.

The second part of this chapter is reprinted (adapted) with permission from Journal of Materials Chemistry A 9 (5), 3029-3035.

Part 1 Cobalt Single Atoms Embedded in Nitrogen-doped Graphene for Selective Oxidation of Benzyl Alcohol by Activated Peroxymonosulfate

6.1 Introduction

The selective transformation of alcohols into their corresponding aldehydes or ketones is among the most valuable reactions in organic chemistry.[1] Tremendous efforts have been devoted to the development of efficient reaction strategies.[2-4] Compared with the homogeneous oxidative reactions with stoichiometric toxic or expensive oxidants like hydrogen peroxide, heterogeneous catalysis has received more attention recently due to the merits of easy separation/recycling and achieving green reaction process.[5] Precious metals such as platinum, ruthenium, gold and palladium are found to afford excellent catalytic activity for the selective oxidation of alcohols,[2, 6-7] however, their scarcity and high cost hinder the real applications for chemical industry. As an alternative, the catalysts based on earth-abundant transition metals are investigated to activate different oxidants including molecular oxygen, ozone and liquid peroxides (i.e. hydrogen peroxide and *tert*-butylhydroperoxide) for oxidative applications.[8-10] The particle size and dispersion of the metal/metal oxides play a pivotal role in affecting the catalytic performance. Therefore, much attention has been focused on reducing the particle size and optimizing the coordination between the metals and supports. Graphene based materials are extensively studied as substrate to support highly dispersed metal particles owing to the high surface area and excellent chemical/electrochemical properties.[11-12]

Single-atom catalysts (SACs) consist of individual atoms dispersed on and/or bonded with the surface atoms of an appropriate support with high selectivity, catalytic activity and excellent atomic efficiency.[13-15] The catalysts with supported noble metals (such

as Pt, Au, Pd) or transition ones (such as Fe, Cu, Zn and Co) are fabricated with SACs and applied in various reaction systems.[16-18] Nevertheless, the aggregation tendency of single atoms hinders further enrichment of the metal active sites on the catalyst surface, thus for the reported SACs, the metal contents are usually limited within a relatively low level, despite many protocols attempted like metal–organic frameworks derived pyrolysis,[19] wet impregnation method,[20-22] impregnation followed with annealing method,[23-24] atomic layer deposition[25-26] and photochemical reduction.[27] For instance, the Co-based SACs prepared from Co-N complex,[28] impregnation combined with pyrolysis approach[29-30] normally present Co contents of less than 3 wt.%. Hence, efforts are still ongoing for the synthesis of robust and highly active transition metal-based SACs. Besides, our recent study suggests that the transition metal-based SACs are stable under acidic or oxidative environment,[31] thus the SACs are potentially applicable in liquid phase oxidation reactions without severe metal leaching.

Peroxymonosulfate (PMS, normally available as a triple salt $KHSO_5 \cdot 1/2KHSO_4 \cdot 1/2K_2SO_4$) is an inexpensive and soluble solid oxidant and has been widely applied in oxidative reactions in aqueous media.[32] Compared with other gaseous or explosive liquid phase oxidants, PMS combines the advantages of benign oxidation conditions and highly stabilized nature to reduce the storage and transportation cost. Supported transition metals were discovered effective for heterogeneous catalytic activation of PMS among which the supported Co (II) presented the best performance.[33-34] The Co-based catalysts can induce a redox cycle *via* the valence change of Co to generate reactive sulfate radicals ($SO_4^{\bullet-}$) for advanced oxidation processes (AOPs).[33-34] However, to the best of our knowledge, the selective oxidation by transition metal SACs activated PMS still remains unexplored.

In this study, we proposed a feasible approach to the synthesis of Co-based SAC on nitrogen-doped graphene support (SACo@NG) with 4.1 wt.% Co loading which was subsequently applied to the activation of PMS under mild conditions for aqueous oxidation reaction. The monodispersed Co atoms on the graphene framework were

bonded with N atoms and conferred high activity in activating PMS for the efficient conversion of benzyl alcohol (BzOH) into benzaldehyde (BzH). In comparison, graphene oxide (GO), nitrogen-doped graphene (NG) and Co nanoparticles loaded on NG (CoNP@NG) were synthesized and performed in BzOH oxidation as well. All these results clearly highlight that the catalytic efficiency of SACo@NG are far exceeding other catalysts. Mechanism exploration implies that the selective oxidation by PMS *via* SACo@NG activation involves both radical and non-radical processes.

6.2 Results and discussion

6.2.1 Characterizations of catalysts

Nitrogen adsorption/desorption isotherms were conducted to analyse the information on the porous structure and surface areas of the GO, NG, CoNP@NG and SACo@NG. The results reveal that there is an obvious decline in the specific surface areas of CoNP@NG (792.5. m^2g^{-1}) and SACo@NG (822.6 m^2g^{-1}) compared to NG with a value of 858.3 m^2g^{-1} (Figure 6-1). It may be due to the metal loading that reduced the value of surface area. Scanning electron microscopy (SEM) image indicates that SACo@NG retained the smooth morphology of graphene without the presence of nanoclusters (Figure 6-2 (a)). The SACo@NG can be fabricated with scalable character as shown in the inset of Figure 6-2 (a) with a mass of 1.3 g, revealing the great potential for practical applications. The mass loading of cobalt was confirmed by inductively coupled plasma-optical emission spectroscopy (ICP-OES) with the value around 4.1 wt.% for SACo@NG. In addition, transmission electron microscopy (TEM) images in Figure 6-2 (b) also reveals the absence of Co nanoparticles in SACo@NG, showing similar appearance as GO and NG but completely different from the morphology of CoNP@NG with visible Co particles (Figure 6-3). X-ray diffraction (XRD) results also indicate the absence of Co crystals as no corresponding characteristic peaks assigned were detected for SACo@NG (Figure 6-4 (a)).

Conversely, (200) and (220) lattice plane peaks appeared in CoNP@NG, revealing the formation of CoO particles. Raman spectra presented similar D and G band intensity ratios for the tested samples, indicating that there was no obvious change in the sp^2 carbon structure for SACo@NG compared with GO and NG (Figure 6-4 (b)). Furthermore, The EDS signals at 6.91 keV in Figure 6-2 (c) indicate the presence of cobalt on SACo@NG. It should be noted that the signal of Cu was sourced from the Cu grid instead of from the SACo@NG sample. EDS elemental mapping demonstrates that the C, N and Co elements are uniformly distributed throughout the SACo@NG (Figure 6-2 (c) and (d)). The high-resolution transmission electron microscopy (HRTEM) image provides further evidence that no Co-derived nanoparticles or clusters on the surface of SACo@NG were detected, consistent with the XRD results. Figure 6-2 (e) and the inset image display the existence of the defective non-C6 carbon ring structure in SACo@NG, which could be ascribed to the inserted Co atoms in the carbon matrix. It can be directly observed from the aberration-corrected scanning transmission electron microscopy (AC-STEM) that the individual Co atoms are randomly dispersed on the graphene support, benefiting from the higher Z-contrast of Co than N and C (Figure 6-2 (f)). The structural characterizations of SACo@NG showed solid evidence of the successful synthesis of single cobalt atoms on the surface of graphene.

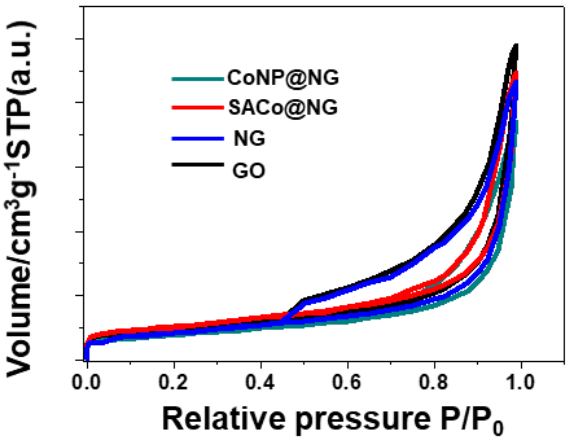

Figure 6-1. Nitrogen adsorption−desorption isotherms of GO, NG, CoNP@NG and SACo@NG.

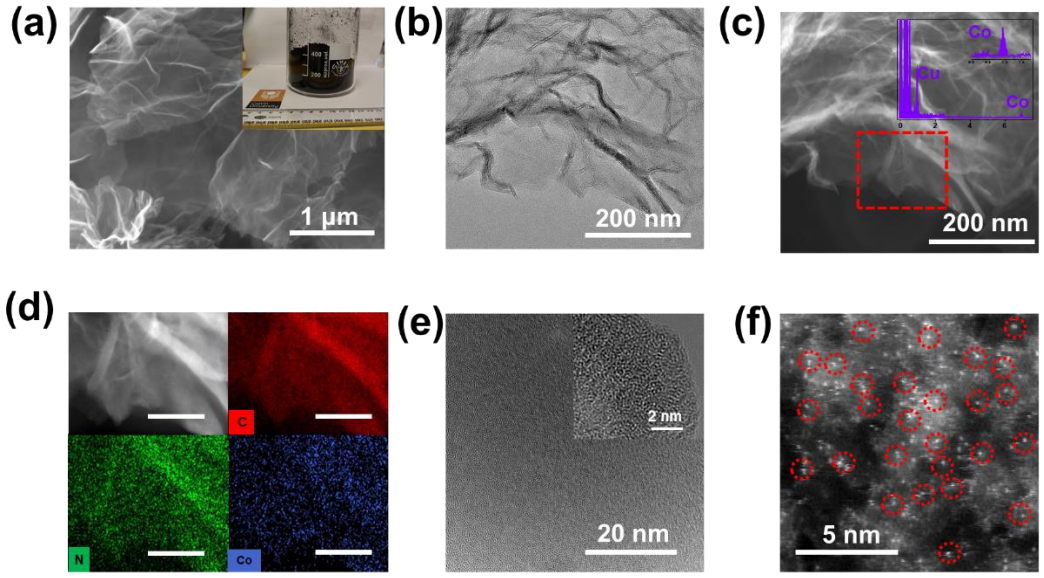

Figure 6-2. Structural characterizations of SACo@NG. (a) SEM image of SACo@NG. The inset is the optical image of 1.3g SACo@NG. (b) TEM image and (c) HAADF-STEM image of SACo@NG. The inset is the EDS spectroscopy of the selected area. (d) HAADF image and corresponding EDS mappings of SACo@NG. The scale bar is 60 nm. (e) HRTEM image and (f) AC-STEM-annular dark-field (ADF) image of SACo@NG.

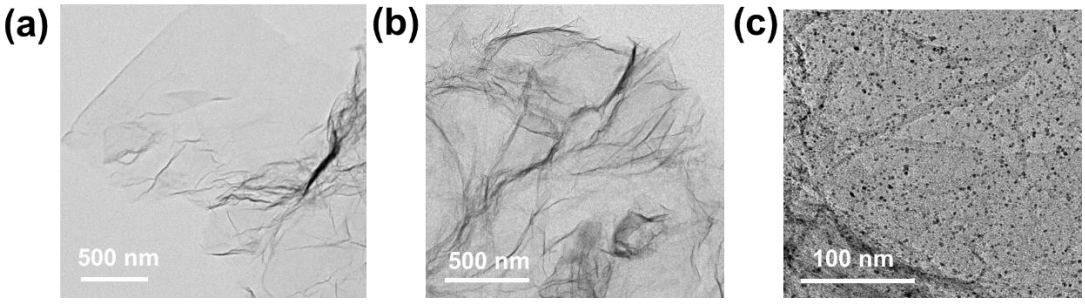

Figure 6-3. TEM images of a) GO b) NG and c) CoNP@NG.

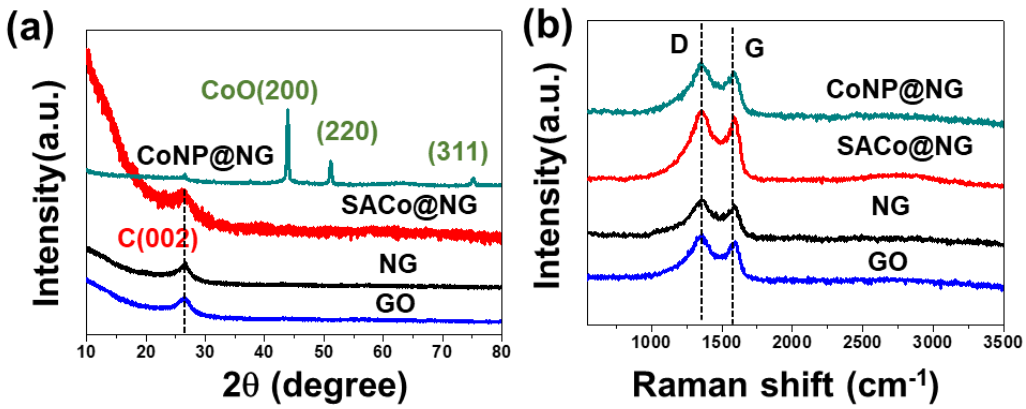

Figure 6-4. (a) XRD patterns and (b) Raman spectra of GO, NG, CoNP@NG and SACo@NG.

X-ray photoelectron spectroscopy (XPS) was conducted to investigate the valence states of Co, N and O in SACo@NG. The peak at around 398.1 eV in N 1s spectra shows that the N species were dominantly formed with pyridinic N (Figure 6-5), thus the Co atoms in the SACo@NG were mainly bonded to pyridinic N atoms. The Co 2p spectrum confirmed that the Co species in SACo@NG was in the state of Co^{2+} around 780.5 eV rather than metallic Co (0) (Figure 6-6 (a)), corresponding to the Co–N species.[35-36] In the near edge X-ray absorption structure (NEXAFS) spectra (Figure 6-6 (b)), the Co L-edge absorption spectra were divided into L_2 and L_3 regions, which correspond to $2p_{1/2}$ and $2p_{3/2}$ levels resulting from the 2p core–hole spin-orbital coupling.[36] The main Co L_2 edge features detected by the surface-sensitive total electron yield in SACo@NG were similar to these of CoPc, revealing that the valence states and chemical environment of cobalt of SACo@NG are close to CoPc but not the Co foil. The electronic structure and coordination environment were further investigated by X-ray absorption near-edge structure (XANES) (Figure 6-6 (c)). The Co K-edge of SACo@NG exhibited a similar near edge structure to that of CoPc. The corresponding Fourier transforms (FT) obtained from the extended X-ray absorption fine structure (EXAFS) showed that the main peak of SACo@NG was located at approximately 1.41 Å, suggesting the formation of Co–N bond, which is shorter than

the Co−O peak at 1.58 Å of standard CoO (Figure 6-6 (d)). In contrast, no Co−Co peaks at 2.18 Å or other high-shell peaks were observed.

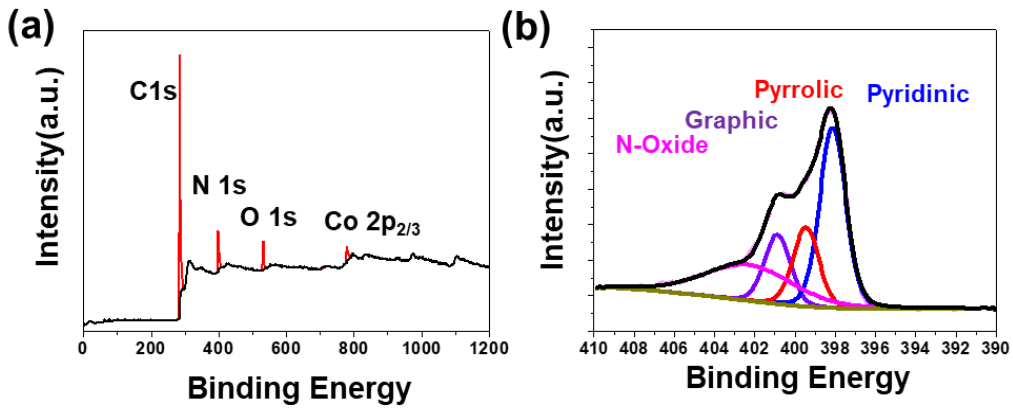

Figure 6-5. (a) XPS whole spectrum and (b) XPS N 1s of SACo@NG.

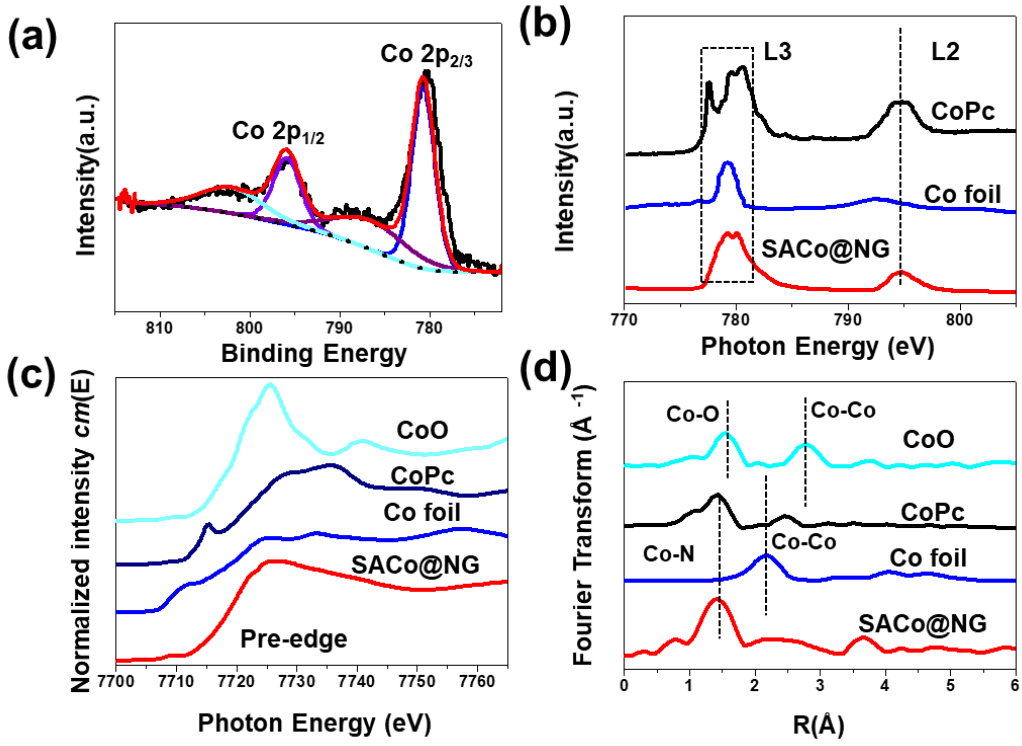

Figure 6-6. Chemical environment and composition of the SACo@NG. (a) XPS analysis of the SACo@NG composites. (b) Co L-edge of the NEXAFS spectra of SACo@NG, Co foil and CoPc. (c) XANES Co-edge and (d) Fourier transform of the EXAFS spectra of CoO, CoPc, Co foil and SACo@NG.

6.2.2 Selective oxidation of BzOH

The oxidation of BzOH to produce BzH was selected as a representative reaction for the evaluation of the catalytic performance of alcohols transformation. The reaction over various catalysts was performed under benign temperature of 50 ºC, much lower than the other reported Co-SAC catalyzed BzOH oxidation by O_2,[5] and the results are summarised in Table 6-1. The reaction conditions were determined based on our previous work.[37] The catalyst-free PMS could hardly oxidize BzOH, with the conversion lower than 5 % and the BzH yield around 1%. GO showed very limited enhancement of BzH yield (5.0 %) while the N doping effectively increased the BzH yield to 30.1 % with 86.3 % BzH selectivity, indicating that the N species on graphene can serve as active centres to activate PMS.[38] The BzH yield was further increased to 34.9 % over CoNP@NG (6.7 wt.% of Co nanoparticle loading with the average size of 2.1 nm), but apparently the reaction rate still needs to be accelerated. The catalytic efficiency was significantly promoted when 4.1 wt.% of Co was atomically dispersed on NG (SACo@NG) to achieve over 90 % BzOH conversion and BzH selectivity after 180 min reaction totally exhibiting 84.7 % BzH yield. Notably, the BzH selectivity (93.4 %) derived over SACo@NG was close to that of CoNP@NG (92.1 %) but higher than NG (86.3 %). Comparing the reaction result of SACo@NG with the reported *via* different catalytic systems (Table 6-2), the reaction efficiency in terms of BzH selectivity and yield herein is comparable to the metal-catalyst mediated BzOH oxidation by O_2. One obvious advantage of SACo@NG application for BzOH oxidation requires a much lower reaction temperature than literature (50 vs. 130 ºC).[5, 39] The sole PMS can yield 87 % BzH in homogeneous environment, while extra additives are still needed.[40] The selectivity of SACo@NG is also higher than radical based BzOH oxidation by carbon nanotubes activated PMS (80.1 %),[37] suggesting the intrinsic oxidation mechanism over SACo@NG may differ from the metal-free activated PMS oxidation. Compared with Co NPs, the Co SACs exposed more active sites for PMS activation thus the BzOH oxidation rate is greatly enhanced. A lower oxidation efficiency was derived from CoPc with 71.2 % BzOH conversion, 73.5 %

BzH selectivity and 52.3 % yield, possibly due to its poor electron transfer capability and low resistance against the oxidizing acidic environment of PMS activation. Besides, the catalytic performance of noble metal catalyst was also tested by employing a commercially available Pd@Al_2O_3 catalyst (1 wt.% of Pd) loaded with the similar metal mole amount of SACo@NG. The Pd@Al_2O_3 could merely afford 30.4 % conversion and 23.7 % yield, much lower than SACo@NG reflecting the extraordinarily high catalytic efficiency of single atom cobalt catalyst. It's noteworthy that in all the performed oxidation tests, no other organic species were detected, indicating BzH had not been further oxidized into benzoic acid. It could possibly due to the prior reactivity of BzOH towards the oxidant, especially the radicals produced, compared with the BzH in the catalytic system.[39]

Table 6-1. Selective oxidation of BzOH over different catalysts.[a)]

Catalyst	BzOH conversion	BzH selectivity	BzH yield
Blank[b)]	4.6	23.5	1.1
GO	14.3	34.6	5.0
NG	34.9	86.3	30.1
CoNP@NG	37.9	92.1	34.9
SACo@NG	90.6	93.4	84.7
CoPc[c)]	71.2	73.5	52.3
Pd@Al_2O_3[d)]	30.4	77.9	23.7

[a)] Reaction conditions: 5 mg catalyst, 0.1 mmol BzOH, 0.16 mmol PMS, 5 mL acetonitrile/water (1:1, volume ratio), 50 ºC, 3 h.

[b)] Control experiment without catalyst loading.

[c)] CoPc (2 mg) was loaded.

[d)] 36 mg of Pd@Al_2O_3 was loaded (the Pd content was 1 wt.%).

Table 6-2. Comparison of benzyl alcohol oxidation *via* different reaction systems.

Catalyst	Oxidant	*T*/ ºC	*t*/h	Additive	BzOH conversion/%	BzH selectivity/%	BzH yield/%	Ref
Single atom Co@NG	O_2	130	5	N/A	94.8	N/A	92.4	[5]
Pd_3Pb nanocubes	O_2	130	1	N/A	91.3	91.0	N/A	[39]

N/A	PMS	N/A	3	NaBr	N/A	N/A	87	[40]
Carbon nanotubes	PMS	50	5	N/A	57.6	80.1	46.2	[37]
SACo@NG	PMS	50	3	N/A	90.6	93.4	84.7	Herein

The influence of the reaction conditions on SACo@NG catalyzed oxidation was explored by varying the PMS dosage, temperature and reaction time. The BzOH conversion increased with higher PMS concentration while the BzH selectivity decreased (Figure 6-7), revealing that the excess PMS may induce the over-oxidation of BzOH directly into inorganic compounds. The peak of BzH yield appeared at the PMS/BzOH ratio of 1.6 and then suffered from sharp decrease with further increased PMS dosage. The catalytic performance was benignly affected by temperature and reaction time. In the range of 35-65 ºC, the BzH selectivity slightly decreased (from 99.6 to 96.5 %) with increasing temperature, indicating the over-oxidation was facilitated by a higher temperature (Figure 6-8). Accordingly, increasing the reaction temperature by 30 ºC would cause substantial improvement of BzOH conversion and BzH yield by 16 % and 14 %, respectively. Similar trends of conversion and yield were observed when increasing the reaction time, whereas the selectivity showed no significant change (Figure 6-9). The recycling test of SACo@NG reflected its excellent stability after four runs (Figure 6-10), thus the chemically bonded Co atoms with N are highly stable free from deactivation. Interestingly, the catalytic performance was slightly improved at the second run, which could possibly due to the oxidative environment causing the rearrangement of surface functionalities such as C-O to C=O conversion, since the presence of ketonic C=O is favourable for PMS activation.

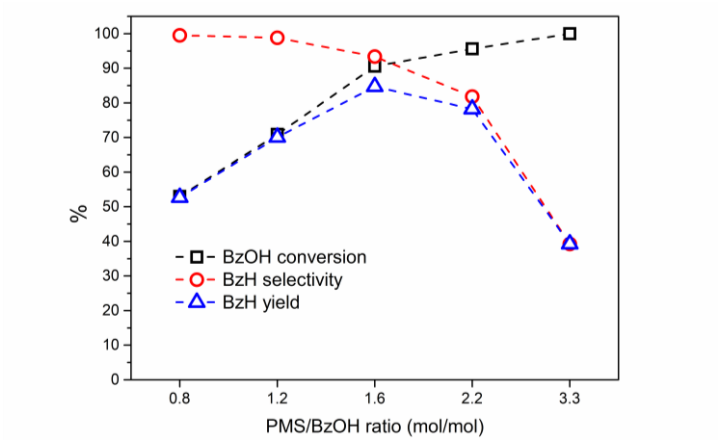

Figure 6-7. The effect of PMS loading on the selective oxidation of BzOH. Reaction conditions: 5 mg SACo@NG, 0.1 mmol BzOH, 5 mL acetonitrile/water (1:1, volume ratio), 50 ºC, 3 h.

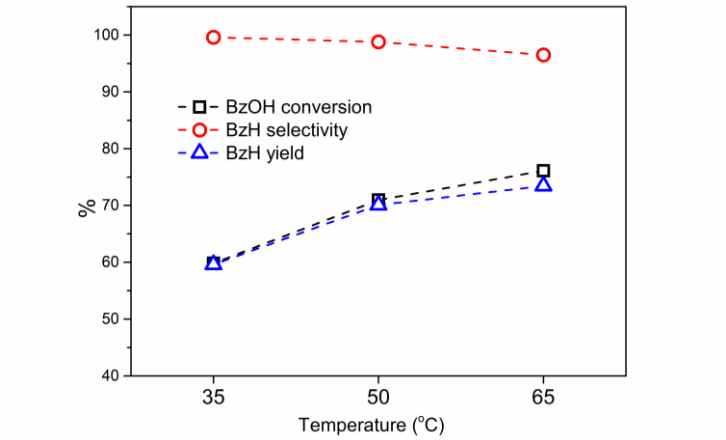

Figure 6-8. The effect of temperature on the selective oxidation of BzOH. Reaction conditions: 5 mg SACo@NG, 0.1 mmol BzOH, 0.12 mmol PMS, 5 mL acetonitrile/water (1:1, volume ratio), 3 h.

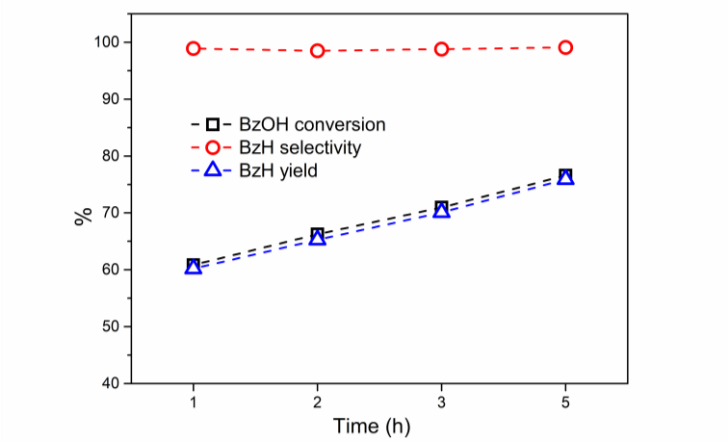

Figure 6-9. The effect of reaction time on the selective oxidation of BzOH. Reaction conditions: 5 mg SACo@NG, 0.1 mmol BzOH, 0.12 mmol PMS, 5 mL acetonitrile/water (1:1, volume ratio), 50 ºC.

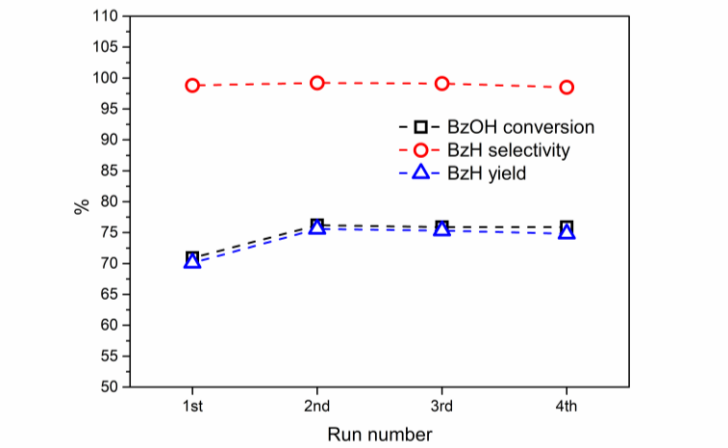

Figure 6-10. Recycling and stability test of SACo@NG. Reaction conditions: 5 mg SACo@NG, 0.1 mmol BzOH, 0.12 mmol PMS, 5 mL acetonitrile/water (1:1, volume ratio), 50 ºC, 3h.

6.2.3 Mechanism study of BzOH oxidation over SACo@NG by activated PMS

The reaction pathways for PMS activation and BzOH oxidation were identified by conducting a series of quenching tests to clarify the radical and non-radical contributions to the oxidation reactions. In regards to the radical-based oxidation process, the PMS activation routes with Co are hypothesized to occur *via* Equations (6-1) to (6-5) where the reactive $^{\bullet}OH$, $SO_4^{\bullet-}$ and $SO_5^{\bullet-}$ radicals are assumed to be

generated with PMS activation *via* the electron transfer among Co^{2+}, Co^{3+} and PMS.[41] The $^{\bullet}OH$ (1.8-2.7 V) and $SO_5^{\bullet-}$ (1.1 V) radicals can transform into $SO_4^{\bullet-}$ which possesses higher redox potential (2.5-3.1 V) and longer half-life period (30-40 μs *vs* $^{\bullet}OH$ 20 ns).[34, 42] The redox cycle of Co^{2+}/Co^{3+} ensures that the Co SACs continuously participate in the radical generation without deactivation.

$$Co^{2+} + HSO_5^- \rightarrow Co^{3+} + {}^{\bullet}OH + SO_4^{2-} \quad (6\text{-}1)$$

$$Co^{2+} + HSO_5^- \rightarrow Co^{3+} + OH^- + SO_4^{\bullet-} \quad (6\text{-}2)$$

$$Co^{3+} + HSO_5^- \rightarrow Co^{2+} + H^+ + SO_5^{\bullet-} \quad (6\text{-}3)$$

$$^{\bullet}OH + SO_4^{2-} \leftrightarrow OH^- + SO_4^{\bullet-} \quad (6\text{-}4)$$

$$2SO_5^{\bullet-} \rightarrow {}^1O_2 + 2SO_4^{\bullet-} \quad (6\text{-}5)$$

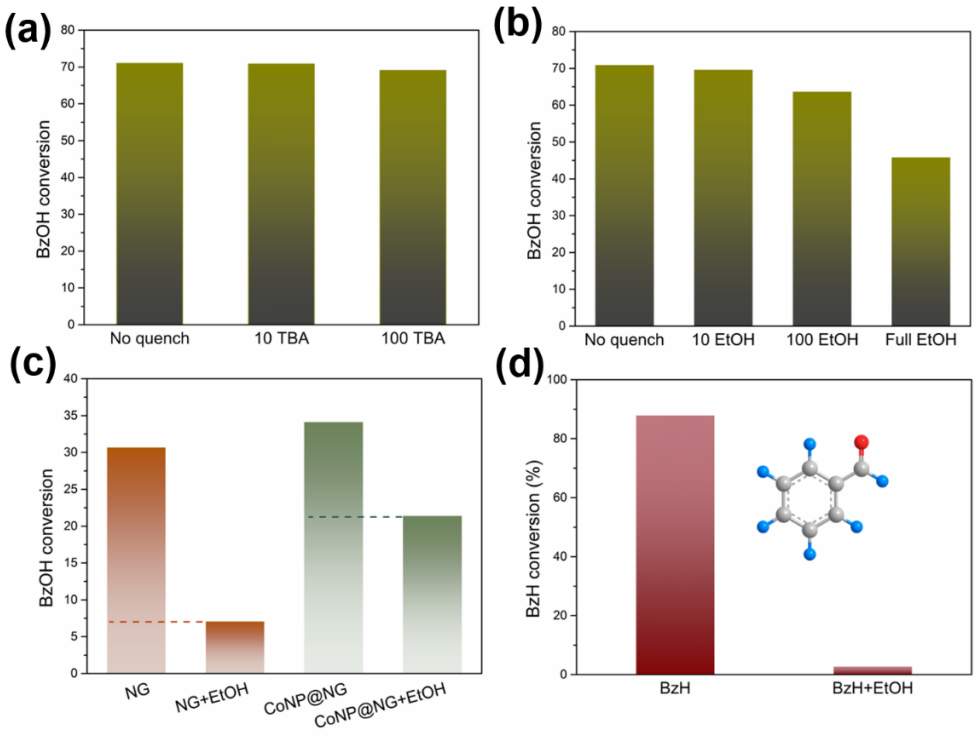

Figure 6-11. The influences of radical scavengers on the oxidation of BzOH over SACo@NG. a) *tert*-butanol dosage b) ethanol dosage. The scavenger/PMS (mol/mol) ratios were 10 and 100, respectively. Full EtOH test was performed by replacing the

acetonitrile solvent with ethanol. c) The influence of full EtOH dosage on the oxidation of BzOH over NG and CoNP@NG. d) The influence of full EtOH dosage on the oxidation of BzH over SACo@NG. Reaction conditions of no quenching tests: 5 mg catalyst, 0.1 mmol BzOH (0.1 mmol BzH in (d)), 0.12 mmol PMS, 5 mL acetonitrile/water (1:1, volume ratio), 50 ºC, 3 h.

To verify these reaction pathways, ethanol (EtOH) and *tert*-butanol (TBA) were employed as the radical scavengers for the following tests. TBA showed a higher reaction rate towards $^{\bullet}OH$ ($k=(3.8\text{-}7.6)\times10^5$ $M^{-1}s^{-1}$) compared with $SO_4^{\bullet-}$ ($k=(4.0\text{-}9.1)\times10^5$ $M^{-1}s^{-1}$) while EtOH is effective in scavenging both hydroxyl and sulfate radicals.[43-44] It can be seen from Figure 6-11 (a) and (b) that the reaction rate of BzOH oxidation over SACo@NG decreased with higher dosage of TBA and EtOH, but apparently EtOH played a more significant role than TBA. When the scavenger dosage was 100-folds to PMS, EtOH and TBA caused 7.3 % and 2.0 % decrease of BzOH conversion, respectively. It can be concluded that the sulfate radicals are dominantly responsible for BzOH oxidation within the radical process. The quenching effect was maximised by replacing the organic acetonitrile solvent with EtOH, in which the radical-based BzOH oxidation was almost ceased. There was 45.9 % conversion remained in that case compared with 71.0 % without quenching test, roughly reflecting that over 60 % out of the total BzOH oxidation on SACo@NG was attributed by nonradical-based process. Similarly, the non-radical oxidation over CoNP@NG accounts for 62 % of the total BzOH conversion, whereas for NG the non-radical process only contributed 23 % (Figure 6-11 (c)). Thus we can infer that the incorporation of Co into NG converted the PMS activation for BzOH oxidation from radical to non-radical dominated processes.

Recent mechanistic studies on the non-radical activation of PMS propose two popular pathways: the catalyst-mediated electron transfer by surface complexed substrate/PMS, and the singlet oxygen ($^1O_2$).[45-46] However, there is a great deal of uncertainty for the identification of non-radical route because the present characterization protocols are

still debatable.[47] Singlet oxygen can be created from the above Equation (6-5) or by self-decomposition of PMS.[48] Therefore, a critical task herein is to clarify whether or not $^1O_2$ is related to the selective oxidation of BzOH. The quenching experiments using BzH as the substrate instead of BzOH was performed. BzH is readily oxidized in less oxidative environment, even in atmosphere the BzH can be gradually oxidized into benzoic acid.[49] Thus it follows that if the $^1O_2$ is able to induce the non-radical oxidation of BzOH, BzH can also be oxidized by $^1O_2$. A higher BzH conversion (88 %) was achieved in no-scavenger test compared with the reacted BzOH under similar conditions (71 %), agreeing with the highly oxidizable nature of BzH (Figure 6-11 (d)). However, only 2.8 % BzH conversion remained after EtOH quenching, indicating that BzH was oxidized *via* radical pathway and $^1O_2$ seldom participated the oxidation. Accordingly, we infer that the $^1O_2$ is not involved in the non-radical oxidation of BzOH which instead is dominantly related to the surface adsorption and electron transfer through the graphene framework. The Co^{2+} and Co^{3+} atoms might be the main sites to attract PMS and BzOH molecules to form complex configuration, as well as the abundant surface N and nucleophilic C=O groups (Figure 6-12) which could potentially serve as the adsorption sites.

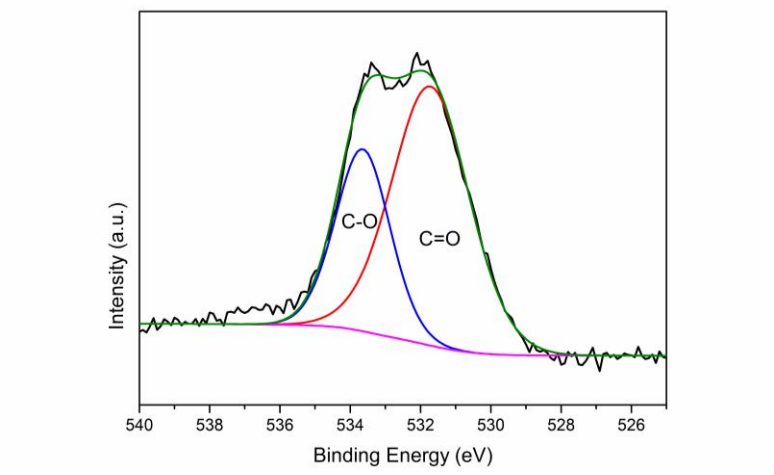

Figure 6-12. Deconvolution of O 1s XPS spectra of SACo@NG.

The proposed mechanism for the selective oxidation of BzOH over SACo@NG is further displayed in Figure 6-13. The Co atoms connected with N atoms on NG sheet are functioned as the main active sites for both radical and non-radical PMS activation for BzOH oxidation. The Co^{2+} and Co^{3+} can induce the formation of $^{\bullet}OH$, $SO_4^{\bullet-}$ and $SO_5^{\bullet-}$ radicals *via* the electron transfer between the Co atom and PMS. The BzOH molecules are subsequently attacked by these free radicals to form BzH. On the other hand, the PMS and BzOH molecules can be adsorbed on SACo@NG and the direct electron transfer from BzOH to PMS occurs *via* the highly delocalized π electrons from the graphene framework. Due to these jointly effects from desirable radical production, preferable adsorption and favourable electron transfer brought in by SACo@NG, BzOH could be more effectively converted into BzH.

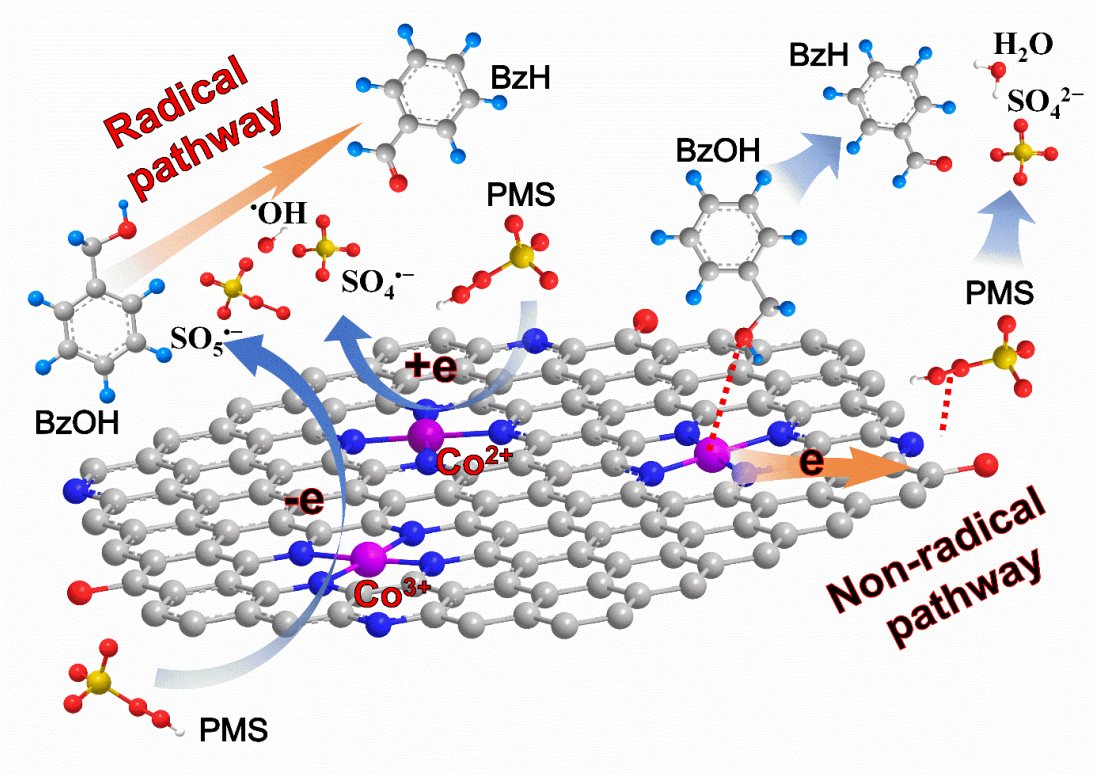

Figure 6-13. Proposed mechanism of PMS activation and BzOH oxidation over SACo@NG

6.3 Experimental Section

Chemicals and Materials. All chemicals purchased from Sigma-Aldrich were used without further purifying in this work. Melamine ($C_3H_6N_6$) was annealed at 500 °C (ramp rate, 5 °C min^{-1}) for 2 h in a covered alumina crucible placed inside the muffle furnace to get yellowish powder g-C_3N_4. The powder was used after being finely ground. Graphene oxide (GO) was prepared based on the modified thermally reduced method reported previously.[50] Briefly, the graphite oxide was obtained by Hummers' method, then 1 g graphite oxide was promptly placed into the furnace at 400 ºC under atmospheric pressure. After annealing for 2 min, the abrupt mass fluffy black powder was obtained as graphene oxide precursor. Subsequently, the graphene oxide precursor was annealed at 800 ºC for 1h under Ar flow of 50 sccm to get GO. The synthesis of nitrogen-doped graphene (NG) was performed by firstly mixing g-C_3N_4 with graphene oxide precursor and then annealing the mixture at 800 ºC for 1 h under Ar flow of 50 sccm. Then the annealed powder was activated by excess hydrogen peroxide (H_2O_2, 20-60 %) at room temperature for 3 h, then washed and dried at 60 ºC overnight.

The preparation of SACo@NG was as follows. Cobalt (II) acetylacetonate (40 mg) was resolved into ethanol solution (50 % acetone, with 20 mg/ml citric acid) and sonicated for 1 h. The above solution was added dropwise into the g-C_3N_4 powder (with cobalt content of 0.5 wt.% vs g-C_3N_4) when grinding. The powder was annealed at 665 ºC for 2 h and then grinded for 30 min. The sample was leached in the HCl (2 mol/L) for 2h at 60 ºC for 5 h, then filtered and washed for 5 times by deionized water. The above sample was noted as g-C_3N_4-Co. The g-C_3N_4-Co and graphene oxide precursor were mixed in the ethanol solution and sonicated for 10 mins. Then the poly ethyleneimine (PEI) solution (50 % (w/v) in H_2O) and polyvinylpyrrolid (PVP, average mol wt. 40000) (with mass ratio=1:1; 50 wt.% in total) were added into above solution and continuously sonicated for 1 h and stirred for 2 h. The mixture was further dried and ground to fine powder. The prepared sample was annealed at 800 ºC (ramp

rate, 10 °C min^{-1}) for 1 h. Then the annealed sample was activated by excess hydrogen peroxide at room temperature for 3 h, washed thoroughly with deionized water and ethanol and dried at 60 ºC for 24 h.

As for the CoNP@NG, graphene oxide precursor (70 mg) and PEI (10 mg) were ultrasonicated and dispersed in 50 mL ethylene glycol solution for 2 h. Furthermore, $Co(acac)_2$ (30 mg) was dispersed into 20 mg ethanol and dropped into above mixture. The dispersion was ultrasonicated for 20 min and then stirred for 1 h prior to be placed in a microwave oven (1000 W). The microwave treatment process was conducted inside the fume cupboard and continuously heated for 5 min and then stirred for 3 h. The dark solution was then filtered and washed with ethanol for 5 times. Then the above sample was mixed with g-C_3N_4 with the weight ratio of 1:1 and then annealed at 800 ºC for 1 h to obtain the final product. The final Co loading of CoNP@NG was 6.7 wt.%, investigated by ICP.

Selective oxidation reaction. A typical process for the selective oxidation of BzOH started with adding 5 mg catalyst in 5 mL acetonitrile/water solvent (1:1 volumn ratio) in a flask under sonication for several minutes until the catalyst was fully dispersed, then 0.1 mmol BzOH and 0.12 mmol oxone were added into the solution to start the reaction. The flask was maintained at 50 ºC for 3 h. After the finishing of the reaction, the flask was cooled down for approximately 2 min and 0.1 mmol anisole was injected into the reactant as an internal standard. Then 0.5 mL reaction mixture was withdrawn and the catalyst was filtered out. The organic compounds were fully extracted by toluene (1×3 mL), then the collected upper phase was analysed by GC/MS using a 30 m ×0.25 mm ×0.25 μm HP-5MS capillary column. The effects of reaction conditions were investigated by adjusting the relevant parameters (reaction temperature, reaction time and PMS dosage) as required.

Structural characterizations. The microstructure of SACo@NG was conducted by SEM (Zeiss Neon 40 EsB) and HRTEM (FEI Titan G2 80-200 TEM/STEM). High-

resolution aberration-corrected scanning transmission electron microscopy annular dark field images (AC-STEM, Nion UltraSTEM100 microscope) was obtained by operating at 60 kV at a beam current of 60 pA. ICP-OES was carried out on PerkinElmer Optima 7300 DV to determine the mass content of cobalt in SACo@NG. XRD was carried out with Bruker D8 Advance diffractometer with Cu Kα (λ = 1.5406 Å). XPS was collected in Kratos AXIS Ultra DLD system. The nitrogen absorption and desorption tests were done on an ASAP 2020 (Micromeritics) to obtain the specific surface area. Element loadings of C, N, O and H were obtained by the elemental analyser (Elementar, vario MICRO cube) at 950 ºC. The Raman patterns were conducted by one alpha300 RA Correlative Raman-AFM Microscope with a 532 nm He−Ne laser. NEXAFS spectroscopy measurements were collected at the Soft X-Ray beamline of the Australian Synchrotron. All spectra were obtained in partial electron yield (TEY) mode. All NEXAFS spectra were treated and normalized using the QANT software program developed at the Australian Synchrotron. X-ray absorption spectroscopy (XAS) data was collected at the XAS Beamline (12ID) at the Australian Synchrotron in Melbourne with the beamline optics employed (Si-coated collimating mirror and Rh-coated focusing mirror). The powder samples were mixed with cellulose binder then made into pellets by finely mechanical grinding. Both fluorescence and transmission spectra were collected based on the concentration of cobalt in each sample (the validity of this method was confirmed *via* comparing the fluorescence and transmission spectra intensity for one of the samples based on which both methods yielded comparable signal-to-noise data). All XAS data were processed with Athena software in Australian Synchrotron.

6.4 Conclusions

In summary, we firstly demonstrated the dynamically catalytic effect of single cobalt atoms embedded in nitrogen-doped graphene for selective oxidation of BzOH by activated peroxymonosulfate. Comprehensive characterizations of the SACo@NG

clearly confirm that the Co single atoms are chemically bonded with N atoms to form a stabilized configuration within the carbon matrix. The SACo@NG catalyst was successfully applied to the selective oxidation of BzOH into BzH by the activation of the environmentally benign PMS oxidant and showed superior catalytic performance compared to NG and CoNP@NG. More than 90 % of both BzOH conversion and BzH selectivity were accomplished over the SACo@NG with excellent cycling stability. The incorporated Co atoms function as active sites for PMS activation *via* both radical and non-radical pathways. The redox cycle between Co^{2+} and Co^{3+} enables the continuous activation of PMS *via* charge transfer to generate reactive $^{\bullet}OH$, $SO_4^{\bullet-}$ and $SO_5^{\bullet-}$ radicals for BzOH oxidation. Mechanism study verifies that the non-radical process contributed over 60 % to the total BzOH oxidation by the surface adsorption of PMS/BzOH on SACo@NG followed by electron transfer from BzOH to PMS, ruling out the oxidation by singlet oxygen. This work paves a new pathway to transferring the organic synthesis into a more sustainable and greener manner *via* the concept of the transition-metal single atom catalysis for PMS activation, which may expand to other alcohol selective oxidation systems.

Part 2 Atomically dispersed cobalt on graphitic carbon nitride as robust catalyst for selective oxidation of ethylbenzene by peroxymonosulfate

6.5 Introduction

The selective oxidation of abundant and cheap hydrocarbons into the corresponding higher-valued compounds, such as alcohols and aldehydes, is of great importance in organic synthesis.[51-52] Although various catalysts and oxidants have been developed, the activation of C-H bond in hydrocarbons still remains one of the most challenging reactions.[4] The liquid phase oxidative conversion of ethylbenzene (EB) is attracting substantial attention to produce acetophenone (AcPO) which is an important intermediate for chemical industries.[53] The conventional reactions exhibit advanced reaction efficiency by adopting stoichiometric oxidants such as permanganate and dichromate.[54] However, these processes produce a large amount of hazardous waste. As an alternative, heterogeneous catalysis with immobilized transition-metal active sites and environmentally benign oxidants has been extensively investigated. The catalytic efficiency of the reported metal-based catalyst heavily depends on the dispersion level and the stability of the metallic active sites. Nevertheless, the transition-metal based catalysts usually suffer from severe metal leaching during the liquid phase reactions, especially in acidic oxidative environment, which impedes their application as robust catalysts.

Recently, the development of single-atom catalyst (SAC) is one of the most active research fields, exhibiting superior efficiency and excellent selectivity in energy-related or environmental catalysis, far exceeding these of metal nanoparticles catalysts.[14, 18, 55] In addition, the atomic metal active sites are chemically bonded with the supporting materials, thus significantly enhancing the stability under harsh reaction

conditions compared with nanoclusters or nanoparticles.[56] Tremendous efforts have been made to anchor noble-metal or transition-metal single atoms on carbon-based materials such as graphene, carbon nanotubes and carbon nitride, since carbo-catalysts not only exhibit high resistance to acidic/basic environment but also hold unique chemical and electrochemical properties to enhance the electron transfer behaviour to accomplish the catalytic reactions.[13, 57] Specifically, g-C_3N_4 is a layered material, similar to graphene, which owns a medium band gap and serves as an effective catalyst for a broad variety of reactions.[58-59] It also possesses advantages including good chemical stability and low cost. Furthermore, the rich N environment can provide sufficient N atoms to coordinate with metal, allowing g-C_3N_4 as an excellent supporting material for metallic single atoms. Nevertheless, there are still many challenges remaining to overcome, for instance, how we can achieve one feasible, controllable, low-cost approach for single atom synthesis. The realisation of such an approach is highly attractive and will provide new possibilities of potential applications for efficient catalysis.[60]

Many oxidizing agents including oxygen, ozone, and liquid phase peroxides (i.e. hydrogen peroxide, *tert*-butyl hydroperoxide (TBHP) and halides) are employed as terminal oxidants to stimulate the C-H activation in a variety of hydrocarbon oxidative reactions.[61-66] In case of oxygen, the resultant hydrocarbon conversion is low due to the difficulty to activate O_2 owing to its triplet ground state structure, which usually requires high temperature/pressure or the presence of co-catalysts to assist the activation of the inert C-H bonds.[53, 67-68] On the other hand, the liquid oxidants and ozone are causing a big concern for transportation and storage. Therefore, the application of inexpensive and stable solid-phase oxidant is a good strategy to overcome the aforementioned disadvantages of gas/liquid oxidants and afford high efficiency under benign conditions. Peroxymonosulfate (PMS, HSO_5^-) is a cost-effective oxidant that has been widely applied in the degradation of various contaminants in water.[69] It is proven that PMS can be activated by a wide range of catalysts, including the supported transition-metals such as Mn, Fe and Co, among

which Co affords the best catalytic performance.[33-34] In most cases, the catalytic activation of PMS will lead to the generation of oxidative radicals ($^{\bullet}OH$, $SO_4^{\bullet-}$ and $SO_5^{\bullet-}$) which play a crucial role in the oxidation of stubborn organic pollutants.[42, 70-71] Despite PMS is receiving extensive attention in environmental remediation, its potential application in selective oxidation for fine chemical production is rarely explored.

Herein, we look at the Co-based single atom catalyst anchored on carbon nitride support with 3.17 wt.% Co dopant. To the best of our knowledge, for the first time this has been applied in the selective oxidation of ethylbenzene into acetophenone by PMS activation. The prepared Co SAC exhibited excellent catalytic efficiency as well as reusability, achieving over 97 % EB conversion and 95 % AcPO selectivity under 60 ºC and atmospheric pressure. The strong C-H bonds in EB molecules were activated by the generated free radicals. This work opens a new frontier for the fabrication of transition metal based single atom catalysts with their facile applications in C-H bond activation under mild conditions.

6.6 Results and discussion

6.6.1 Characterizations

Firstly, the structure of the prepared samples was systematically studied. As suggested from the XRD results of pure g-C_3N_4, SACo@g-C_3N_4 and CoNP@g-C_3N_4 (Figure 6-14), the characteristic peaks located at around 13.2 and 27.5 º correspond to the in-plane structural packing of tri-s-triazine units and the interlayer stacking of aromatic systems, which could be indexed to the (100) and (002) planes of hexagonal g-C_3N_4 (JCPDS 87-1526), respectively. SEM images (Figure 6-15 (a)) reveal the graphene-like smooth structure of SACo@g-C_3N_4 different from g-C_3N_4 with amorphous particle structure shown in Figure 6-16. The inset image confirms the scalable

synthesis of SACo@g-C_3N_4 with the mass of 1.1 g. The mass loading of cobalt was obtained through inductively coupled plasma-atomic emission spectroscopy (ICP-AES) with the value of 3.17 wt.%. Nitrogen adsorption/desorption isotherms were conducted to analyse the surface area of pristine g-C_3N_4, CoNP@g-C_3N_4 and SACo@g-C_3N_4. These results indicate that there is an obvious increase in the specific surface area of SACo@g-C_3N_4 (211 m^2g^{-1}) compared with g-C_3N_4 (33 mg m^2g^{-1}) and CoNP@g-C_3N_4 (28 mg m^2g^{-1}) as shown in Figure 6-17. Moreover, the TEM image in Figure 6-15 (b) indicates the absence of obvious Co particles on SACo@g-C_3N_4, consistent with the XRD results that only carbon plane peaks are observed in SACo@g-C_3N_4 without the characteristic peaks assigned to Co crystals. Conversely, for the XRD of CoNP@g-C_3N_4, characteristic peaks of Co crystals located at 2θ = 36.6, 42.5, 61.6 and 73.9º corresponding to (111), (200), (220) and (311) planes appeared (Figure 6-14), which fit with the XRD pattern (JCPDS #78-0431). The Co nanoparticles are also observed on CoNP@g-C_3N_4 with high resolution TEM (Figure 6-18). EDS elemental mapping demonstrates that the C, N and Co elements are uniformly distributed throughout the SACo@g-C_3N_4 (Figure 6-15 (c) and (d)). In addition, the HRTEM image (Figure 6-15 (e)) further confirms that no Co nanoparticles or clusters exist on SACo@g-C_3N_4. AC-STEM-annular dark-field (ADF) was employed to directly probe the atomic dispersion of individual Co atoms randomly dispersed on the g-C_3N_4 support, benefiting from the higher Z-contrast of Co than N and C (Figure 6-15 (f)). The structural investigation of SACo@g-C_3N_4 reveals the successful synthesis of single cobalt atoms embedded in g-C_3N_4.

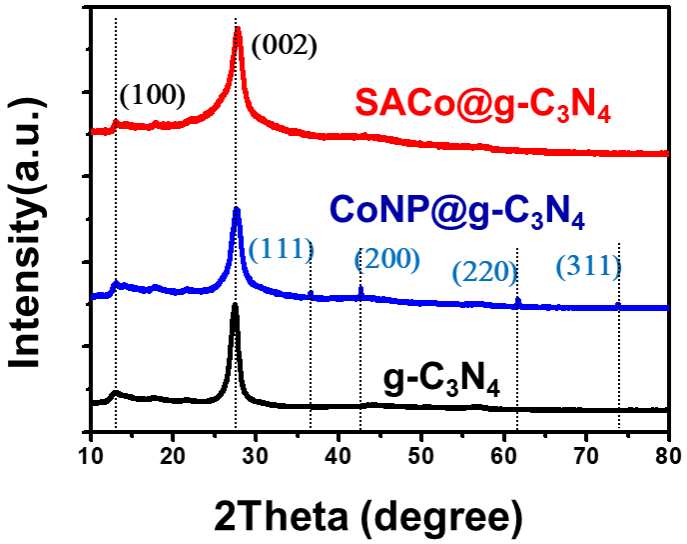

Figure 6-14. XRD patterns of g-C_3N_4, CoNP@g-C_3N_4 and SACo@g-C_3N_4.

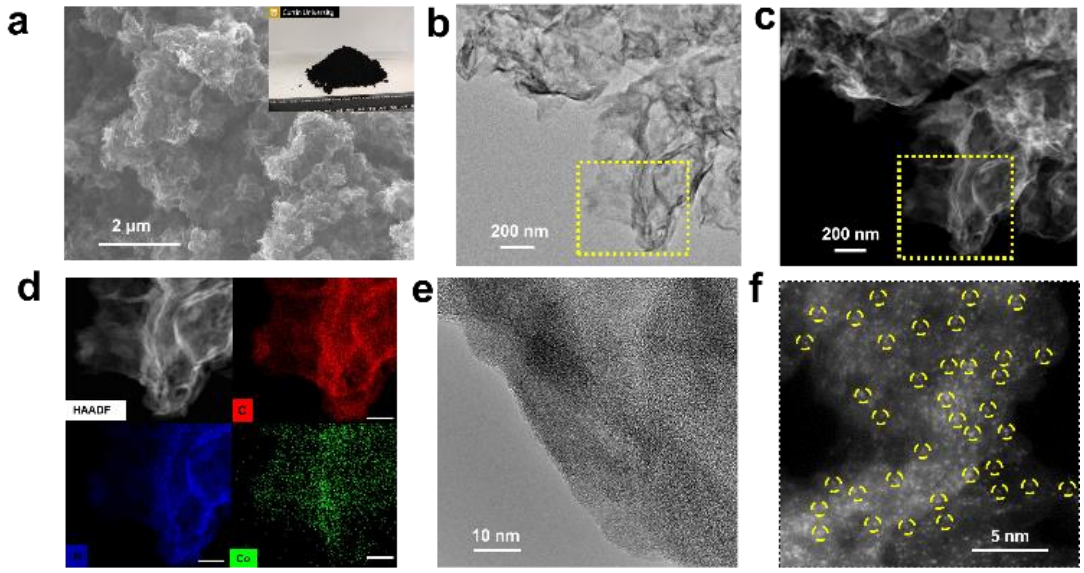

Figure 6-15. Characterizations of SACo@g-C_3N_4. a) SEM image of SACo@g-C_3N_4, inset is the optical image of 1.1 g SACo@g-C_3N_4. b) TEM image and c) HAADF-STEM image of SACo@g-C_3N_4. d) HAADF image and the corresponding EDS mappings of SACo@g-C_3N_4, the scale bar is 100 nm. e) HRTEM image and f) AC-STEM-annular dark-field (ADF) image of SACo@g-C_3N_4.

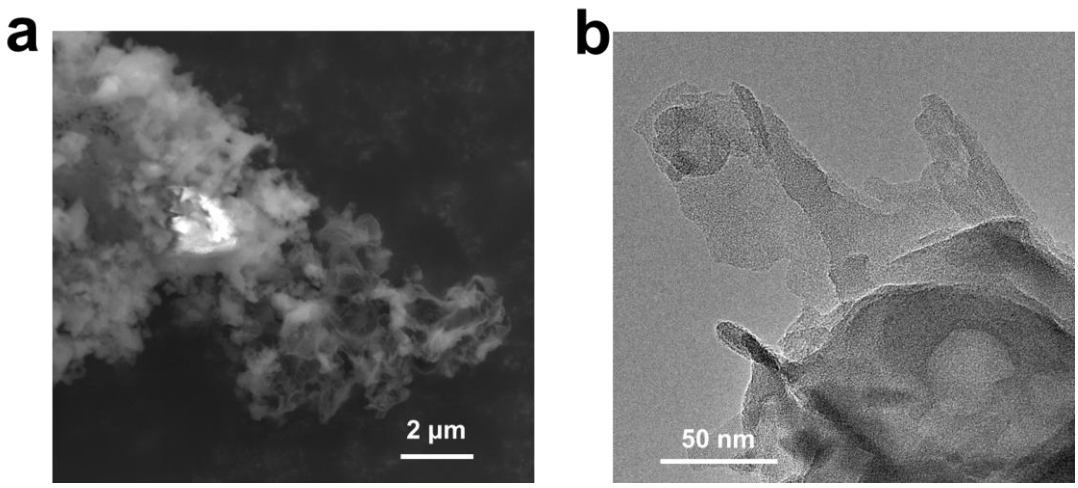

Figure 6-16. Characterizations of g-C_3N_4. a) SEM image; b) TEM image.

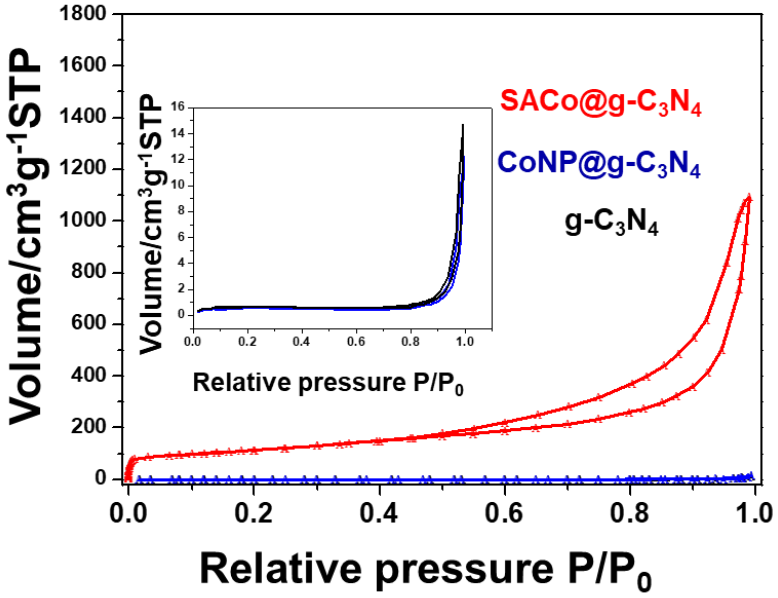

Figure 6-17. N_2 absorption and desorption curves of g-C_3N_4, CoNP@g-C_3N_4 and SACo@g-C_3N_4.The inset image is the magnified curves of g-C_3N_4 and CoNP@g-C_3N_4.

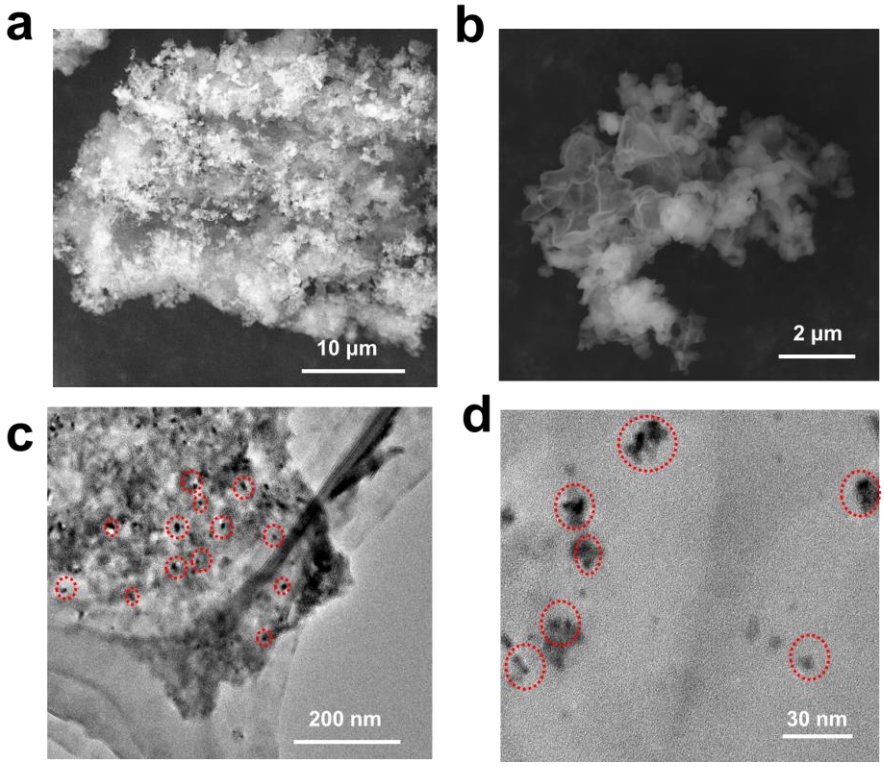

Figure 6-18. Characterizations of CoNP@g-C_3N_4. a,b) the SEM images; c,d) the low and high resolution TEM images.

X-ray photoelectron spectroscopy (XPS) was employed to probe the composition and status of the relevant elements. In the C 1s spectrum, the two peaks at 284.6 and 287.9 eV can be assigned to C-C and N-C=N, respectively (Figure 6-19 (b)). The N 1s spectrum were fitted into the three peaks of C-N=C (398.6 eV), N-C3(400.0 eV) and C-N-H (401.1 eV) (Figure 6-19 (c)). The synchrotron-based near-edge X-ray absorption fine structure (NEXAFS) was performed to further investigate the interfacial interaction of g-C_3N_4 and SACo@g-C_3N_4. In the carbon K-edge NEXAFS spectra (Figure 6-20 (a)), both g-C_3N_4 and SACo@g-C_3N_4 reveal the presence of characteristic resonances of carbon nitride: π *C=C at 286.2 eV, π *C–N–C at 288.1 eV, and long-range σ *C–C resonance occurring over the range of 292–300 eV.[72] In the nitrogen K-edge region (Figure 6-20 (b)), g-C_3N_4 and SACo@g-C_3N_4 shows two typical π* resonances at 399.7 (N1) and 402.5 eV (N2) corresponding to the aromatic C–N–C coordination in one tri-s-triazine heteroring (N1) and the N–3C bridging

among three tri-s-triazine moieties (N2).[73] The Co 2p spectrum (Figure 6-19 (d)) displays that the Co species in SACo@g-C_3N_4 were composed of Co^{2+} around 780.6 eV, which are indexed to the Co−N species instead of metallic Co (0).[36] For a better investigation of the electronic structure and coordination environment of Co in SACo@g-C_3N_4, X-ray absorption near-edge structure (XANES) was further conducted, where the presence of Co K-edge exhibits a similar pre-edge structure with that of CoPc (Figure 6-20 (c)). Moreover, the Fourier transforms (FT) obtained from the extended X-ray absorption fine structure (EXAFS) clearly indicated that the dominant peak of SACo@g-C_3N_4 was located at approximately 1.50 Å. This observation is due to the formation of Co−N bonds which are much shorter than the Co−O peak at 1.64 Å in standard Co_3O_4 and far different from the Co−Co peaks at 2.18 Å (Figure 6-20 (d)). It is a solid confirmation that the Co species in SACo@g-C_3N_4 were atomically dispersed and chemically coordinated in the Co-N bonds.

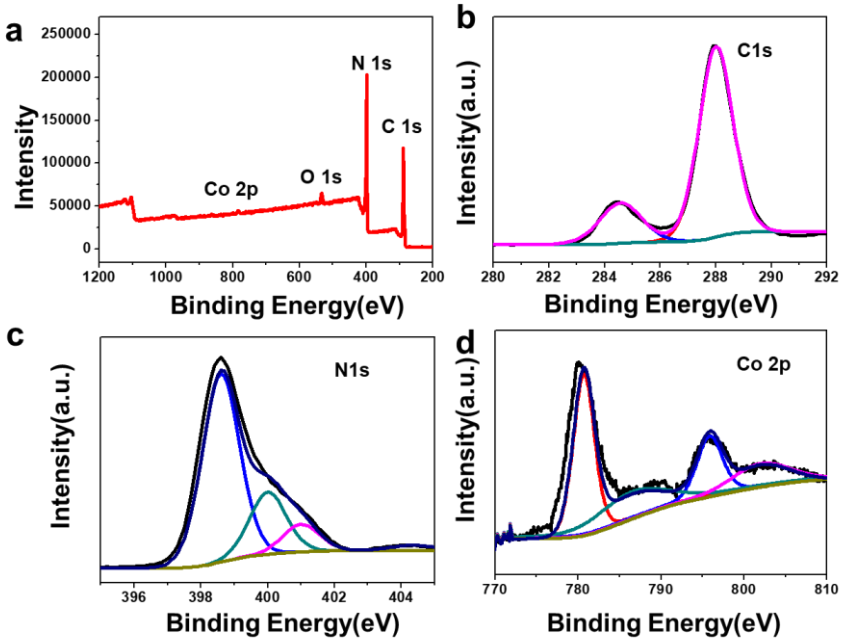

Figure 6-19. XPS spectra of SACo@g-C3N4. a) whole spectrum b) C 1s c) N 1s and d) Co 2p.

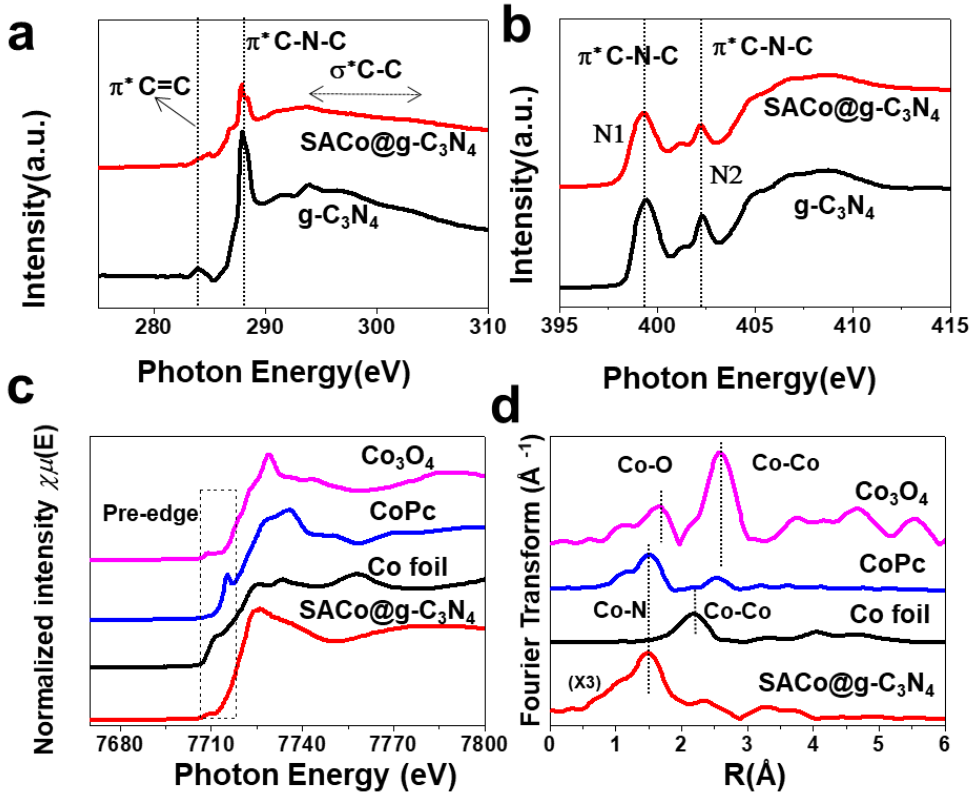

Figure 6-20. Chemical structure of SACo@g-C_3N_4. a, b) Carbon and nitrogen K-edge NEXAFS spectra of g-C_3N_4 and SACo@g-C_3N_4. c) XANES Co-edge and d) Fourier transform of the EXAFS spectra of Co_3O_4, CoPc, Co foil and SACo@ g-C_3N_4.

The chemical structures of g-C_3N_4 and SAAg@g-C_3N_4 were further investigated through the FTIR analysis. Figure 6-21 presents three main absorption regions in the FTIR spectra of g-C_3N_4 and SACo@g-C_3N_4. The broad peak at 3000–3500 cm^{-1} is assigned to the stretching vibration of N-H and surface water molecules. The peaks at 1343–1472 cm^{-1} are ascribed to the characteristic vibration of aromatic rings and the peaks at 1640 cm^{-1} are mainly due to the presence of C-N bonds.[74] The characteristic peaks over 1200–1700 cm^{-1} in SACo@g-C_3N_4 is weakened compared with pure g-C_3N_4, possibly due to the presence of amorphous carbon on the surface of SACo@g-C_3N_4 derived from decomposition of citric acid,[75] consistent with the dark color change shown in Figure 6-15 (a).

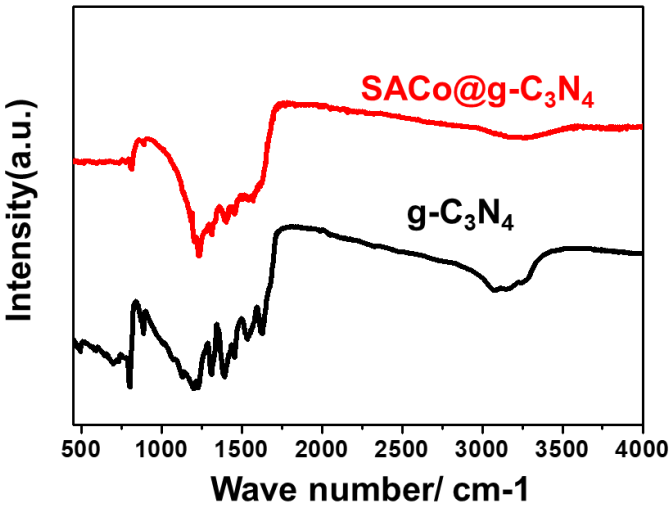

Figure 6-21. FTIR spectrum g-C_3N_4 and SACo@g-C_3N_4.

6.6.2 Catalyst evaluation

The selective oxidation of EB over different catalysts by PMS was carried out at 60 ºC, which is lower than most of the reported cases with O_2 or liquid peroxide oxidants (Table 6-4). The solvent selection and product analysis methodology were determined according to our reported work.[37] Without catalyst, a very low oxidation efficiency was obtained, affording only 10.8% EB conversion and 7.3% AcPO yield after reaction of 15 h (Table 6-3, entry 1). Hence the PMS molecules without activation can hardly oxidize the strong C-H bond in EB. The loading of Co-free g-C_3N_4 increased the EB conversion up to 27.4 %, which is in accordance with the previous research that the plain g-C_3N_4 have a certain but limited functionality for inducing the PMS activation.[33, 76] Upon insertion of Co nanoparticles in g-C_3N_4 (CoNP@g-C_3N_4), the EB conversion was remarkably improved to 90.6% with AcPO selectivity of 88.4% (Table 6-3, entry 3). However, the CoNP@g-C_3N_4 was almost completely deactivated after the reaction, giving merely 14.4% conversion at the second run. Meanwhile, the Co content on the spent CoNP@g-C_3N_4 dropped to 0.15 wt.% in comparison with 4.50 wt.% of fresh catalyst as detected by ICP-AES. Meanwhile, Co particles can seldom be seen from the SEM/TEM images on used CoNP@g-C_3N_4 which only had weak Co

signal sparsely distributed in the sample as observed by the EDS mappings (Figure 6-22). It can be inferred that the Co NPs are highly unstable in PMS solvent as the acidity of the solution was increased with the proceeding of the oxidation reaction; thus the activity of CoNP@g-C_3N_4 was stemmed from the enhanced homogeneous catalysis as result of the gradually leaching Co ions. The SACo@g-C_3N_4 achieved extraordinary oxidation efficiency of 97.5% EB conversion with 95.6% AcPO selectivity and 93.2% AcPO yield, dynamically confirming that Co single atoms are active sites for the PMS-mediated EB oxidation. Moreover, excellent catalytic stability and reusability were observed over SACo@g-C_3N_4 by conducting four recycling tests with each one running for 24 h (Figure 6-23 (a)). There is no obvious sign of activity loss within four runs and the Co content nearly kept unchanged for SACo@g-C_3N_4 throughout the oxidation process (3.12 wt.% after fourth run vs. 3.17 wt.% of fresh catalyst), demonstrating that the Co single atoms are strongly coordinated to the g-C_3N_4 support with adequate resistance against the long-time reaction in this acidic oxidizing solvent. It highlights the advantage of SACo@g-C_3N_4 as a robust catalyst to work in facile manners for PMS activation without the requirement of pH control and additional buffers. Besides the AcPO formed as the dominant product, a minimal amount of 1-phenylethanol (1-PA) was also produced during the EB oxidation. The selectivity of 1-PA was below 1.5% for all the tested catalysts in Table 6-3, which was further reduced below 0.2% for the SACo@g-C_3N_4 catalyzed EB oxidations regardless of different conditions such as PMS dosage and reaction time. This suggests that the C-H bond activation could directly lead to the formation ketone derivates instead of following a consecutive reaction route to yield 1-PA and subsequently AcPO. Overall, the catalytic performance of SACo@g-C_3N_4 is comparable to the level of the highest EB oxidation efficiency ever reported (Table 6-4). More specifically, this SACo@g-C_3N_4/PMS configuration demonstrated superior EB conversion rate and selectivity of AcPO in comparison with the reported oxidations using O_2, H_2O_2 and TBHP as the respective oxidant but the current system required much lower reaction temperature and shorter time.[53, 62-64, 67-68]

Table 6-3. Selective oxidation of EB on different catalysts.[a)]

Entry	Catalyst	Co (wt.%)	EB conversion (%)	Selectivity (%)		AcPO yield (%)
				AcPO	1-PA	
1	Blank	–	10.8	67.5	0.2	7.3
2	g-C_3N_4	–	27.4	69.6	1.5	19.1
3	CoNP@g-C_3N_4	4.50	90.6	88.4	0.1	80.1
4	CoNP@g-C_3N_4 (used)	0.15	14.4	99.6	0	14.3
5	SACo@g-C_3N_4	3.17	97.5	95.6	0.2	93.2

[a)] Reaction conditions: 5 mg catalyst, 0.1 mmol EB, 0.5 mmol PMS, 10 mL acetonitrile/water (1:1, volume ratio), 60 ºC, 15 h.

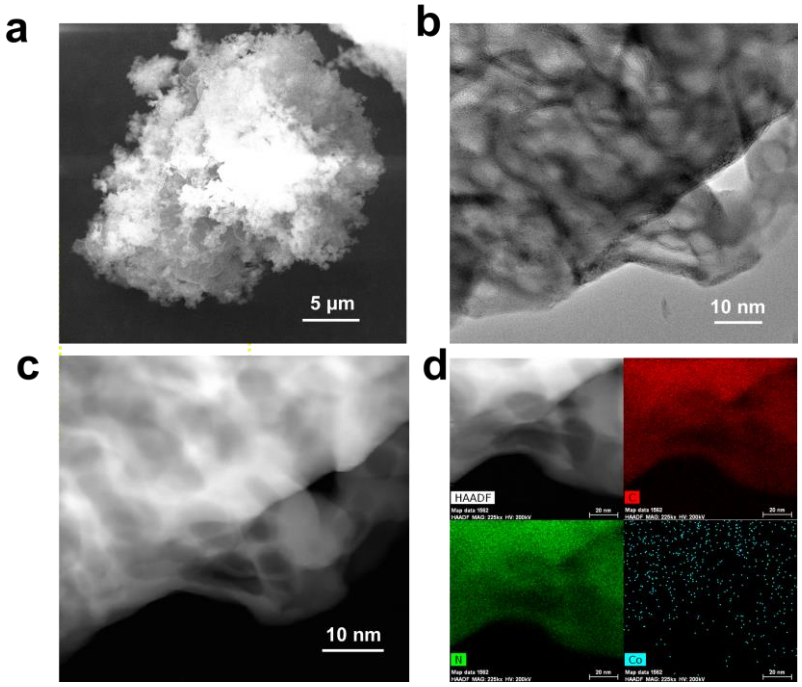

Figure 6-22. Characterizations of CoNP@g-C_3N_4. a) SEM image b) TEM image c,d) HAADF image and the corresponding EDS mappings.

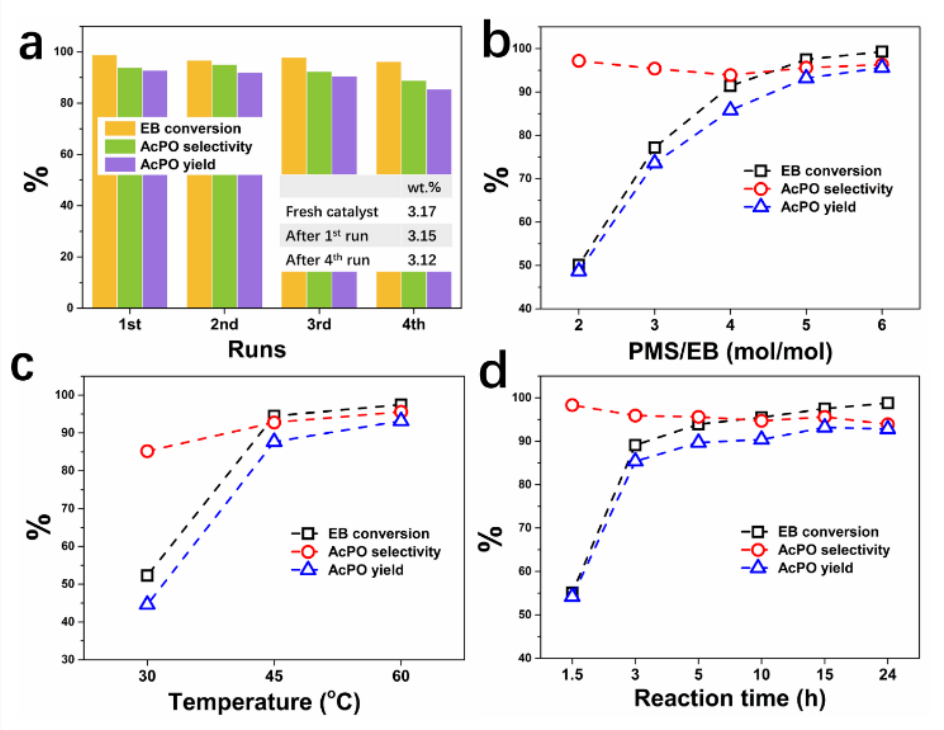

Figure 6-23. a) Recycling and stability test on SACo@g-C_3N_4 (Reaction conditions: 5 mg catalyst, 0.1 mmol EB, 0.5 mmol PMS, 10 mL acetonitrile 1:1 water, 60 ºC, 24 h). The effects of reaction conditions on the selective oxidation of EB with SACo@g-C_3N_4 (5 mg catalyst, 0.1 mmol EB and 10 mL acetonitrile 1:1 water). b) PMS dosage (0.5 mmol PMS, 60 ºC). c) Reaction temperature (0.5 mmol PMS, 15 h). d) Reaction time (60 ºC, 15 h).

Table 6-4. Comparison of ethylbenzene (EB) oxidation *via* different reaction systems.

Entry	Catalyst	Oxidant	T (ºC)[a]	Time (h)	EB conversion (%)	AcPO selectivity (%)	Ref
1	Pd@N-doped carbon	O_2/1 atm	120	20	14.2	94	[67]
2	Co@NCNT	O_2/0.8 MPa	120	5	68.1	93.2	[68]
3	Carbon nanotube	O_2/1.5 MPa	155	4	38.2	60.9	[53]
4	Mn(III) porphyrin	H_2O_2[c]	RT[b]	5.5	66	66	[62]
5	Co-Cu	TBHP[d] 3:1 EB(mol/mol)	120	12	92.8	89.4	[63]
6	N-porous carbon	TBHP 3:1 EB(mol/mol)	100	12	83.5	93.3	[64]
7	SACo@g-C_3N_4	PMS 5:1 EB(mol/mol)	60	5	93.9	89.7	Herein
8	SACo@g-C_3N_4	PMS 5:1 EB(mol/mol)	60	15	97.5	95.6	Herein

[a] Reaction temperature.

[b] Room temperature

[c] Aqueous hydrogen peroxide (30% w/w) was diluted in acetonitrile (2:5) and added to the reaction mixture in 37.5μl aliquots every 15min for the oxidation of 0.3mmol ethylbenzene.

[d] *Tert*-butyl hydroperoxide

To understand the influence of the oxidant loading, the oxidation efficiency over SACo@g-C_3N_4 as a function of PMS/EB ratio (from 2 to 6) was investigated. As shown in Figure 6-23 (b), the conversion and product yield increased rapidly with higher PMS dosage. Over 90 % EB was converted at PMS/EB ratio of >4, and the EB conversion was >99% when the PMS/EB ratio was 6. Surprisingly, there was no severe loss of AcPO selectivity with higher PMS loading, indicating that both the EB and the AcPO are not liable to be deeply oxidized in PMS solution. The reaction efficiency is also greatly affected by the reaction temperature (Figure 6-23 (c)). Increasing the temperature from 30 to 45 ºC contributed to a remarkable elevation of EB conversion by 40%, while further increment of temperature to 60 ºC was less effective to enhance the oxidation. Therefore, a minor input of energy is necessary to assist the highly efficient PMS activation and to overcome the energy barrier of C-H bond activation. Furthermore, the continuous oxidation reaction with time was displayed in Figure 6-23 (d). The conversion reached 89.1% at 3 h, manifesting that the SACo@g-C_3N_4/PMS system enables the C-H activation with high reaction rate. After 3 h of reaction, the conversion continued increasing but the reaction rate decreased and finally climbed up to 98.8% at 24 h. On the contrary, the AcPO selectivity slightly reduced with reaction time, but still showed a high selectivity of 93.9% at 24 h. The oxidation efficiency over the SACo@g-C_3N_4/PMS system at different conditions confirms its excellent catalytic performance, showing large potential in selective oxidation reactions.

6.6.3 Identification of the oxidation mechanism

Various reactive radicals such as $^{\bullet}OH$ (1.8-2.7 V), $SO_4^{\bullet-}$ (2.5-3.1 V) and $SO_5^{\bullet-}$ (1.1 V) can be generated from the PMS activation *via* electron-transfer between PMS and the

Co catalyst.[42] As illustrated in Equations (6-1) to (6-5) (in part 1), the continuous decomposition of PMS is accomplished with the redox cycle of Co(II)/Co(III), thereby forming free radicals. Sulfate radicals usually have a greater impact on the oxidation reaction than other radicals because of its higher redox potential and longer half-life period.[77] Apart from that, singlet oxygen and non-radical oxidation by catalyst-mediated electron transfer are also reported as possible pathways for PMS enabled oxidation process.[45-46, 78] To identify the intrinsic oxidative species responsible for the selective conversion of EB, both electron paramagnetic resonance (EPR) and radical scavenging tests were performed. It's suggested from Figure 6-24 (a) that SACo@g-C_3N_4 is superior to the metal-free g-C_3N_4 in generating the $^{\bullet}OH$ radicals. The signals of $SO_4^{\bullet-}$ radicals are not very distinct, whereas some ambiguous signals appeared between two adjacent signals of $^{\bullet}OH$ radicals. We assume that this phenomenon could be attributed to the presence of both DMPO-$SO_4^{\bullet-}$ and DMPOX,[79-81] an oxidation product of DMPO due to the excessive amount of oxidizing species such as $^{\bullet}OH$ and $SO_4^{\bullet-}$.

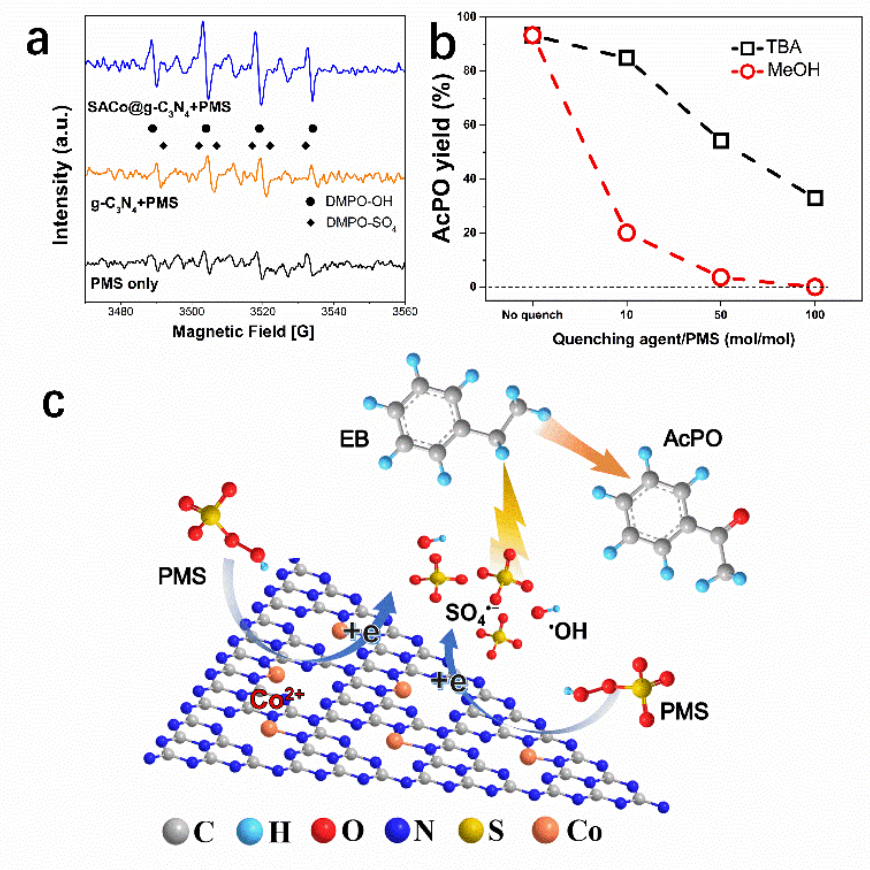

Figure 6-24. a) EPR spectra of g-C_3N_4 and SACo@g-C_3N_4 catalyzed PMS activation in the presence of 5,5-dimethyl-1-pyrroline N-oxide (DMPO). b) The influence of TBA and MeOH dosage on the formation of AcPO over SACo@g-C_3N_4. c) Proposed mechanism of SACo@g-C_3N_4-mediated PMS activation and selective conversion of EB.

The radical scavenging tests by *tert*-butanol (TBA) and methanol (MeOH) were then conducted to evaluate the functions of different radicals in C-H activation. MeOH is used as a quencher for both hydroxyl and sulfate radicals owing to the high reactivity towards these two radicals, whereas TBA without α-H shows a much weaker scavenging effect on $SO_4^{\bullet-}$ than $^{\bullet}OH$.[82] The influence of excess dosage of TBA or MeOH on the reaction efficiency over SACo@g-C_3N_4 catalyzed EB oxidation is displayed in Figure 6-24 (b). As expected, the addition of MeOH has a greater effect than TBA on suppressing the EB conversion and AcPO formation. Specifically, at 10-times dose of the quenching agents, 20.1 and 84.8 % AcPO yields were attained for

MeOH and TBA loaded experiments, respectively, compared with 93.2 % AcPO yield from no-quenching experiment. The AcPO yield decreased to 0 at the MeOH/PMS ratio of 100 while 32.9 % AcPO yield remained with the same dosage TBA. It can be concluded that the activation of C-H in EB is originated from the oxidative radicals and the sulfate radicals paly the dominant role in the C-H oxidation to fabricate AcPO with high selectivity, as illustrated in Figure 6-24 (c). Considering the Co atoms in SACo@g-C_3N_4 dominantly exist as Co (II), as mentioned above, the $SO_4^{\bullet-}$ radicals are readily generated *via* Equations (6-1) to (6-3). Noteworthy that in some oxidative reactions using Co-based catalysts, the oxidation of organic substrate by the Co catalyst/PMS system was accomplished *via* both radical and non-radical processes.[83-84] While in other cases with different organic substrates or supporting materials for Co active sites, the oxidation reaction was dominantly attributed to the sulfate radicals.[33, 71] Thus it follows that the intrinsic mechanism for PMS derived oxidation process is closely related to not only the catalyst category (especially the interactions of metal active centres and different supports) but also the adsorptive properties of the organic substrate.

6.7 Experimental Section

Synthesis of g-C_3N_4. The g-C_3N_4 was synthesized by annealing urea in the air. Firstly, urea (CON_2H_4, 90 g) was put into a covered alumina crucible and placed inside the muffle furnace. Then, the temperature was increased up to 600 ºC (ramp rate 10 ºC/min) and held for 2 h. Finally, around 7 g of g-C_3N_4 was collected. For safety, the annealing process was carried in the fume cardboard to ventilate the produced smoke. Before usage, the g-C_3N_4 was further ground for 20 min to get the uniform yellowish powder.

Synthesis of SACo@g-C_3N_4. The SACo@g-C_3N_4 (Co single atom doped g-C_3N_4) was synthesized as follows. Firstly, the citric acid ($C_6H_8O_7$, 2 g) was added into the mixed

solution of isopropanol and acetone (volume ratio of 2:1, 100 ml). After stirring for 10 min, the transparent solution was obtained followed by the addition of cobalt (II) phthalocyanine (CoPc, 100 mg). The violet solution was stirred for 2 h and the fine grinded g-C_3N_4 powder (5 g) was added into the above solution. The mixture was stirred and naturally evaporated to 10 mL volume. Then, the whole mixture was transferred into an agate mortar and ground to dry powder. The yellow powder was heated to 655 ºC at a ramp rate of 7 ºC/min and kept for 2 h under Ar at a flow rate of 50 mL/min. The obtained black powder was dispersed in excess oxone (peroxymonosulfate) solution (20 g/L) and stirred at 50 ºC for 24 h, then thoroughly washed and dried at 60 ºC overnight. The final black powder was noted as SACo@g-C_3N_4.

Synthesis of CoNP@g-C_3N_4. Cobalt (II) acetylacetonate ($C_{10}H_{16}CoO_4$, 50 mg) and g-C_3N_4 powder (200 mg) was firstly ultrasonicated for 10 min and dispersed in 30 mL ethanol then transferred into 100 mL ethylene glycol solution. The dispersion was stirred for 1 h before placed in a lab-use microwave oven (1000 W) in the fume cupboard and heated for 5 min. The solution was then filtered using the membrane film and washed with ethanol for 5 times. The final yellowish powder was dried in the oven at 80 ºC for 5 h and was noted as CoNP@g-C_3N_4.

Selective oxidation of ethylbenzene. In a typical EB oxidation reaction, 5 mg catalyst was added in 10 mL acetonitrile 1:1 water solvent in a three-necked flask and the mixture was sonicated for a few minutes to fully disperse the catalyst. The reaction started at the addition of 0.1 mmol EB and 0.5 mmol oxone ($KHSO_5 \cdot 1/2KHSO_4 \cdot 1/2K_2SO_4$) and was maintained at 60 ºC for 15 h in an oil bath. Then the flask was naturally cooled down for around 2 min, followed with the addition of 0.1 mmol anisole as the internal standard. The catalyst was filtered out and the aromatic compounds were extracted from the reactant by toluene for three times (the volume usage of toluene 6:1 the reaction solution), and the organic phase was analysed by gas chromatography (GC). The reactions performed under other conditions were

achieved with the same procedure except that the relevant parameters were adjusted as required. The radicals generated during the oxidation reaction were probed by electron paramagnetic resonance (EPR) on a Bruker EMS-plus instrument. The EPR data were analysed by Xeon software using 5,5-dimethyl-1-pyrroline N-oxide (DMPO, 0.08 M) as the spin-trapping agent.

6.8 Conclusions

In this study, we demonstrated a novel approach to the synthesis of cobalt-based catalysts with individually dispersed Co atoms doped on g-C_3N_4. Joint characterization proofs verify that the anchored Co atoms (3.17 wt.%) were coordinated with N species to form highly stable Co-N bonds. The maximised utility efficiency of Co and outstanding stability of such a robust catalyst can be utilized for the activation of C-H bond in EB by PMS, achieving 93.2% yield of AcPO at a low temperature of 60 ºC. The selective conversion of EB into AcPO relies on the rapid generation of free radicals from activated PMS, along with redox cycle of Co(II)/Co(III). Sulfate radicals, with a higher oxidation potential, plays a more significant role than other radicals to activate the inert C-H bonds. This work presented a novel synthesis strategy of Co-based single-atom catalyst that could be expanded to prepare SACs of other transition-metals. More importantly, the developed SAC displays a promising efficiency for selective oxidation of ethylbenzene to acetophenone by PMS activation, which opens a new way for the break-up of C-H bonds in various hydrocarbons for organic synthesis.

References

1. Parmeggiani, C.; Matassini, C.; Cardona, F., A step forward towards sustainable aerobic alcohol oxidation: new and revised catalysts based on transition metals on solid supports. *Green Chemistry* **2017,** *19* (9), 2030-2050.

2. Enache, D. I.; Edwards, J. K.; Landon, P.; Solsona-Espriu, B.; Carley, A. F.; Herzing, A. A.; Watanabe, M.; Kiely, C. J.; Knight, D. W.; Hutchings, G. J., Solvent-Free Oxidation of Primary Alcohols to Aldehydes Using Au-Pd/TiO_2 Catalysts. *Science* **2006,** *311* (5759), 362.

3. Higashimoto, S.; Kitao, N.; Yoshida, N.; Sakura, T.; Azuma, M.; Ohue, H.; Sakata, Y., Selective photocatalytic oxidation of benzyl alcohol and its derivatives into corresponding aldehydes by molecular oxygen on titanium dioxide under visible light irradiation. *J. Catal.* **2009,** *266* (2), 279-285.

4. Sheng, S. D.; Guodong, W.; Shuchang, W.; Feng, P.; Robert, S., Carbocatalysis in Liquid-Phase Reactions. *Angew. Chem. Int. Ed.* **2017,** *56* (4), 936-964.

5. Li, M.; Wu, S.; Yang, X.; Hu, J.; Peng, L.; Bai, L.; Huo, Q.; Guan, J., Highly efficient single atom cobalt catalyst for selective oxidation of alcohols. *Appl. Catal. A-Gen.* **2017,** *543*, 61-66.

6. Maity, P.; Gopinath, C. S.; Bhaduri, S.; Lahiri, G. K., Applications of a high performance platinum nanocatalyst for the oxidation of alcohols in water. *Green Chemistry* **2009,** *11* (4), 554-561.

7. Dong, L.; Gari, R. R. S.; Li, Z.; Craig, M. M.; Hou, S., Graphene-supported platinum and platinum–ruthenium nanoparticles with high electrocatalytic activity for methanol and ethanol oxidation. *Carbon* **2010,** *48* (3), 781-787.

8. Zhu, J.; Kailasam, K.; Fischer, A.; Thomas, A., Supported Cobalt Oxide Nanoparticles As Catalyst for Aerobic Oxidation of Alcohols in Liquid Phase. *ACS Catal.* **2011,** *1* (4), 342-347.

9. Wu, G.; Gao, Y.; Ma, F.; Zheng, B.; Liu, L.; Sun, H.; Wu, W., Catalytic oxidation of benzyl alcohol over manganese oxide supported on MCM-41 zeolite. *Chem. Eng. J.* **2015,** *271*, 14-22.

10. Behera, G. C.; Parida, K. M., Liquid phase catalytic oxidation of benzyl alcohol to benzaldehyde over vanadium phosphate catalyst. *Appl. Catal. A-Gen.* **2012,** *413-414*, 245-253.

11. Allen, M. J.; Tung, V. C.; Kaner, R. B., Honeycomb Carbon: A Review of Graphene. *Chem. Rev.* **2010,** *110* (1), 132-145.

12. Navalon, S.; Dhakshinamoorthy, A.; Alvaro, M.; Garcia, H., Carbocatalysis by Graphene-Based Materials. *Chem. Rev.* **2014,** *114* (12), 6179-6212.

13. Gawande, M. B.; Fornasiero, P.; Zbořil, R., Carbon-Based Single-Atom Catalysts for Advanced Applications. *ACS Catal.* **2020,** *10* (3), 2231-2259.

14. Xu, H.; Cheng, D.; Cao, D.; Zeng, X. C., A universal principle for a rational design of single-atom electrocatalysts. *Nature Catalysis* **2018,** *1* (5), 339-348.

15. Liu, J.-C.; Tang, Y.; Wang, Y.-G.; Zhang, T.; Li, J., Theoretical understanding of the stability of single-atom catalysts. *National Science Review* **2018,** *5* (5), 638-641.

16. Zhang, G.; Jia, Y.; Zhang, C.; Xiong, X.; Sun, K.; Chen, R.; Chen, W.; Kuang, Y.; Zheng, L.; Tang, H.; Liu, W.; Liu, J.; Sun, X.; Lin, W.-F.; Dai, H., A general route via formamide condensation to prepare atomically dispersed metal–nitrogen–carbon electrocatalysts for energy technologies. *Energy & Environmental Science* **2019,** *12* (4), 1317-1325.

17. Zhao, L.; Zhang, Y.; Huang, L.-B.; Liu, X.-Z.; Zhang, Q.-H.; He, C.; Wu, Z.-Y.; Zhang, L.-J.; Wu, J.; Yang, W.; Gu, L.; Hu, J.-S.; Wan, L.-J., Cascade anchoring strategy for general mass production of high-loading single-atomic metal-nitrogen catalysts. *Nat. Commun.* **2019,** *10* (1), 1278.

18. Zhao, S.; Chen, G.; Zhou, G.; Yin, L.-C.; Veder, J.-P.; Johannessen, B.; Saunders, M.; Yang, S.-Z.; De Marco, R.; Liu, C.; Jiang, S. P., A Universal Seeding Strategy to Synthesize Single Atom Catalysts on 2D Materials for Electrocatalytic Applications. *Adv. Funct. Mater.* **2020,** *30* (6), 1906157.

19. Jiao, L.; Wan, G.; Zhang, R.; Zhou, H.; Yu, S.-H.; Jiang, H.-L., From Metal–Organic Frameworks to Single-Atom Fe Implanted N-doped Porous Carbons: Efficient Oxygen Reduction in Both Alkaline and Acidic Media. *Angew. Chem. Int. Ed.* **2018,** *57* (28), 8525-8529.

20. Hackett, S. F. J.; Brydson, R. M.; Gass, M. H.; Harvey, I.; Newman, A. D.; Wilson, K.; Lee, A. F., High-Activity, Single-Site Mesoporous Pd/Al2O3 Catalysts for Selective Aerobic Oxidation of Allylic Alcohols. *Angew. Chem.* **2007,** *119* (45), 8747-8750.

21. Kwak, J. H.; Hu, J.; Mei, D.; Yi, C.-W.; Kim, D. H.; Peden, C. H. F.; Allard, L. F.; Szanyi, J., Coordinatively Unsaturated Al^{3+} Centers as Binding Sites for Active Catalyst Phases of Platinum on γ-Al_2O_3. *Science* **2009,** *325* (5948), 1670.

22. Qiao, B.; Wang, A.; Yang, X.; Allard, L. F.; Jiang, Z.; Cui, Y.; Liu, J.; Li, J.; Zhang, T., Single-atom catalysis of CO oxidation using Pt1/FeOx. *Nat. Chem.* **2011,** *3* (8), 634-641.

23. Zheng, Y.; Jiao, Y.; Zhu, Y.; Cai, Q.; Vasileff, A.; Li, L. H.; Han, Y.; Chen, Y.; Qiao, S.-Z., Molecule-Level g-C3N4 Coordinated Transition Metals as a New Class of Electrocatalysts for Oxygen Electrode Reactions. *J. Am. Chem. Soc.* **2017,** *139* (9), 3336-3339.

24. Li, J.-C.; Yang, Z.-Q.; Tang, D.-M.; Zhang, L.; Hou, P.-X.; Zhao, S.-Y.; Liu, C.; Cheng, M.; Li, G.-X.; Zhang, F.; Cheng, H.-M., N-doped carbon nanotubes containing a high concentration of single iron atoms for efficient oxygen reduction. *NPG Asia Materials* **2018,** *10* (1), e461-e461.

25. Yan, H.; Lin, Y.; Wu, H.; Zhang, W.; Sun, Z.; Cheng, H.; Liu, W.; Wang, C.; Li, J.; Huang, X.; Yao, T.; Yang, J.; Wei, S.; Lu, J., Bottom-up precise synthesis of stable platinum dimers on graphene. *Nat. Commun.* **2017,** *8* (1), 1070.

26. Sun, S.; Zhang, G.; Gauquelin, N.; Chen, N.; Zhou, J.; Yang, S.; Chen, W.; Meng, X.; Geng, D.; Banis, M. N.; Li, R.; Ye, S.; Knights, S.; Botton, G. A.; Sham, T.-K.; Sun, X., Single-atom Catalysis Using Pt/Graphene Achieved through Atomic Layer Deposition. *Scientific Reports* **2013,** *3* (1), 1775.

27. Liu, P.; Zhao, Y.; Qin, R.; Mo, S.; Chen, G.; Gu, L.; Chevrier, D. M.; Zhang, P.; Guo, Q.; Zang, D.; Wu, B.; Fu, G.; Zheng, N., Photochemical route for synthesizing atomically dispersed palladium catalysts. *Science* **2016,** *352* (6287), 797.

28. Wang, Z.-L.; Hao, X.-F.; Jiang, Z.; Sun, X.-P.; Xu, D.; Wang, J.; Zhong, H.-X.; Meng, F.-L.; Zhang, X.-B., C and N Hybrid Coordination Derived Co–C–N Complex as a Highly Efficient Electrocatalyst for Hydrogen Evolution Reaction. *J. Am. Chem. Soc.* **2015,** *137* (48), 15070-15073.

29. Zhao, C.; Dai, X.; Yao, T.; Chen, W.; Wang, X.; Wang, J.; Yang, J.; Wei, S.; Wu, Y.; Li, Y., Ionic Exchange of Metal–Organic Frameworks to Access Single Nickel Sites for Efficient Electroreduction of CO2. *J. Am. Chem. Soc.* **2017,** *139* (24), 8078-8081.

30. Fei, H.; Dong, J.; Feng, Y.; Allen, C. S.; Wan, C.; Volosskiy, B.; Li, M.; Zhao, Z.; Wang, Y.; Sun, H.; An, P.; Chen, W.; Guo, Z.; Lee, C.; Chen, D.; Shakir, I.; Liu, M.; Hu, T.; Li, Y.; Kirkland, A. I.; Duan, X.; Huang, Y., General synthesis and definitive structural identification of MN4C4 single-atom catalysts with tunable electrocatalytic activities. *Nature Catalysis* **2018,** *1* (1), 63-72.

31. Cheng, Y.; Zhao, S.; Li, H.; He, S.; Veder, J.-P.; Johannessen, B.; Xiao, J.; Lu, S.; Pan, J.; Chisholm, M. F.; Yang, S.-Z.; Liu, C.; Chen, J. G.; Jiang, S. P., Unsaturated edge-anchored Ni single atoms on porous microwave exfoliated graphene oxide for electrochemical CO2. *Appl. Catal. B-Environ.* **2019,** *243*, 294-303.

32. Hussain, H.; Green, I. R.; Ahmed, I., Journey Describing Applications of Oxone in Synthetic Chemistry. *Chem. Rev.* **2013,** *113* (5), 3329-3371.

33. Xie, M.; Tang, J.; Kong, L.; Lu, W.; Natarajan, V.; Zhu, F.; Zhan, J., Cobalt doped g-C3N4 activation of peroxymonosulfate for monochlorophenols degradation. *Chem. Eng. J.* **2019,** *360*, 1213-1222.

34. Duan, X.; Su, C.; Miao, J.; Zhong, Y.; Shao, Z.; Wang, S.; Sun, H., Insights into perovskite-catalyzed peroxymonosulfate activation: Maneuverable cobalt sites for promoted evolution of sulfate radicals. *Appl. Catal. B-Environ.* **2018,** *220*, 626-634.

35. Pan, Y.; Lin, R.; Chen, Y.; Liu, S.; Zhu, W.; Cao, X.; Chen, W.; Wu, K.; Cheong, W.-C.; Wang, Y.; Zheng, L.; Luo, J.; Lin, Y.; Liu, Y.; Liu, C.; Li, J.; Lu, Q.; Chen, X.; Wang, D.; Peng, Q.; Chen, C.; Li, Y., Design of Single-Atom Co–N5 Catalytic Site: A Robust Electrocatalyst for CO2 Reduction with Nearly 100% CO Selectivity and Remarkable Stability. *J. Am. Chem. Soc.* **2018,** *140* (12), 4218-4221.

36. Wu, Y.; Chen, Z.; Cheong, W.-C.; Zhang, C.; Zheng, L.; Yan, W.; Yu, R.; Chen, C.; Li, Y., Nitrogen-coordinated cobalt nanocrystals for oxidative dehydrogenation and hydrogenation of N-heterocycles. *Chem. Sci.* **2019,** *10* (20), 5345-5352.

37. Li, J.; Li, M.; Sun, H.; Ao, Z.; Wang, S.; Liu, S., Understanding of the Oxidation Behaviour of Benzyl Alcohol by Peroxymonosulfate via Carbon Nanotubes Activation. *ACS Catal.* **2020,** *10* (6), 3516-3525.

38. Li, D.; Duan, X.; Sun, H.; Kang, J.; Zhang, H.; Tade, M. O.; Wang, S., Facile synthesis of nitrogen-doped graphene via low-temperature pyrolysis: The effects of precursors and annealing ambience on metal-free catalytic oxidation. *Carbon* **2017,** *115*, 649-658.

39. Tang, C.; Zhang, N.; Shao, Q.; Huang, X.; Xiao, X., Rational design of ordered Pd–Pb nanocubes as highly active, selective and durable catalysts for solvent-free benzyl alcohol oxidation. *Nanoscale* **2019,** *11* (12), 5145-5150.

40. Koo, B.-S.; Lee, C. K.; Lee, K.-J., OXIDATION OF BENZYL ALCOHOLS WITH OXONE® AND SODIUM BROMIDE. *Synth. Commun.* **2002,** *32* (14), 2115-2123.

41. Ji, Y.; Dong, C.; Kong, D.; Lu, J., New insights into atrazine degradation by cobalt catalyzed peroxymonosulfate oxidation: Kinetics, reaction products and transformation mechanisms. *J. Hazard. Mater.* **2015,** *285*, 491-500.

42. Huang, Z.; Bao, H.; Yao, Y.; Lu, W.; Chen, W., Novel green activation processes and mechanism of peroxymonosulfate based on supported cobalt phthalocyanine catalyst. *Appl. Catal. B-Environ.* **2014,** *154-155*, 36-43.

43. Buxton, G. V.; Greenstock, C. L.; Helman, W. P.; Ross, A. B., Critical Review of rate constants for reactions of hydrated electrons, hydrogen atoms and hydroxyl radicals (·OH/·O− in Aqueous Solution. *J. Phys. Chem. Ref. Data* **1988,** *17* (2), 513-886.

44. Anipsitakis, G. P.; Dionysiou, D. D., Radical Generation by the Interaction of Transition Metals with Common Oxidants. *Environmental Science & Technology* **2004,** *38* (13), 3705-3712.

45. Jawad, A.; Zhan, K.; Wang, H.; Shahzad, A.; Zeng, Z.; Wang, J.; Zhou, X.; Ullah, H.; Chen, Z.; Chen, Z., Tuning of Persulfate Activation from a Free Radical to a Nonradical Pathway through the Incorporation of Non-Redox Magnesium Oxide. *Environmental Science & Technology* **2020,** *54* (4), 2476-2488.

46. Duan, X.; Sun, H.; Wang, Y.; Kang, J.; Wang, S., N-Doping-Induced Nonradical Reaction on Single-Walled Carbon Nanotubes for Catalytic Phenol Oxidation. *ACS Catal.* **2015,** *5* (2), 553-559.

47. Yun, E.-T.; Lee, J. H.; Kim, J.; Park, H.-D.; Lee, J., Identifying the Nonradical Mechanism in the Peroxymonosulfate Activation Process: Singlet Oxygenation Versus Mediated Electron Transfer. *Environmental Science & Technology* **2018,** *52* (12), 7032-7042.

48. Liang, P.; Zhang, C.; Duan, X.; Sun, H.; Liu, S.; Tade, M. O.; Wang, S., An insight into metal organic framework derived N-doped graphene for the oxidative degradation of persistent contaminants: formation mechanism and generation of singlet oxygen from peroxymonosulfate. *Environmental Science: Nano* **2017,** *4* (2), 315-324.

49. Sankar, M.; Nowicka, E.; Carter, E.; Murphy, D. M.; Knight, D. W.; Bethell, D.; Hutchings, G. J., The benzaldehyde oxidation paradox explained by the interception of peroxy radical by benzyl alcohol. *Nat. Commun.* **2014,** *5* (1), 3332.

50. Chen, C.-M.; Zhang, Q.; Yang, M.-G.; Huang, C.-H.; Yang, Y.-G.; Wang, M.-Z., Structural evolution during annealing of thermally reduced graphene nanosheets for application in supercapacitors. *Carbon* **2012,** *50* (10), 3572-3584.

51. Kesavan, L.; Tiruvalam, R.; Rahim, M. H. A.; bin Saiman, M. I.; Enache, D. I.; Jenkins, R. L.; Dimitratos, N.; Lopez-Sanchez, J. A.; Taylor, S. H.; Knight, D. W.; Kiely, C. J.; Hutchings, G. J., Solvent-Free Oxidation of Primary Carbon-Hydrogen Bonds in Toluene Using Au-Pd Alloy Nanoparticles. *Science* **2011,** *331* (6014), 195.

52. Frei, H., Selective Hydrocarbon Oxidation in Zeolites. *Science* **2006,** *313* (5785), 309.

53. Jin, L.; Feng, P.; Hao, Y.; Hongjuan, W.; Wenxu, Z., Aerobic Liquid-Phase Oxidation of Ethylbenzene to Acetophenone Catalyzed by Carbon Nanotubes. *ChemCatChem* **2013,** *5* (6), 1578-1586.

54. Clark, J. H.; Kybett, A. P.; Landon, P.; Macquarrie, D. J.; Martin, K., Catalytic oxidation of organic substrates using alumina supported chromium and manganese. *J. Chem. Soc., Chem. Commun.* **1989,** (18), 1355-1356.

55. Zhu, C.; Fu, S.; Shi, Q.; Du, D.; Lin, Y., Single-Atom Electrocatalysts. *Angew. Chem. Int. Ed.* **2017,** *56* (45), 13944-13960.

56. Yang, X.-F.; Wang, A.; Qiao, B.; Li, J.; Liu, J.; Zhang, T., Single-Atom Catalysts: A New Frontier in Heterogeneous Catalysis. *Acc. Chem. Res.* **2013,** *46* (8), 1740-1748.

57. Wu, J.; Xiong, L.; Zhao, B.; Liu, M.; Huang, L., Densely Populated Single Atom Catalysts. *Small Methods* **2020,** *4* (2), 1900540.

58. Gong, Y.; Li, M.; Li, H.; Wang, Y., Graphitic carbon nitride polymers: promising catalysts or catalyst supports for heterogeneous oxidation and hydrogenation. *Green Chemistry* **2015,** *17* (2), 715-736.

59. Fu, J.; Yu, J.; Jiang, C.; Cheng, B., g-C3N4-Based Heterostructured Photocatalysts. *Adv. Energy Mater.* **2018,** *8* (3), 1701503.

60. Amsler, J.; Sarma, B. B.; Agostini, G.; Prieto, G.; Plessow, P. N.; Studt, F., Prospects of Heterogeneous Hydroformylation with Supported Single Atom Catalysts. *J. Am. Chem. Soc.* **2020,** *142* (11), 5087-5096.

61. Liu, Y.; Zhang, P.; Liu, J.; Wang, T.; Huo, Q.; Yang, L.; Sun, L.; Qiao, Z.-A.; Dai, S., Gold Cluster–CeO2 Nanostructured Hybrid Architectures as Catalysts for Selective Oxidation of Inert Hydrocarbons. *Chem. Mater.* **2018,** *30* (23), 8579-8586.

62. Rebelo, S. L. H.; Simões, M. M. Q.; Neves, M. G. P. M. S.; Cavaleiro, J. A. S., Oxidation of alkylaromatics with hydrogen peroxide catalysed by manganese(III) porphyrins in the presence of ammonium acetate. *J. Mol. Catal. A: Chem.* **2003,** *201* (1), 9-22.

63. Xie, R.; Fan, G.; Yang, L.; Li, F., Hierarchical flower-like Co–Cu mixed metal oxide microspheres as highly efficient catalysts for selective oxidation of ethylbenzene. *Chem. Eng. J.* **2016,** *288*, 169-178.

64. Wang, Z.; Jiang, Y.; Huo, H.; Hu, Y.; Xu, X.; Wang, P.; Yang, Y.; Lin, K., Synthesis of three-dimensional nitrogen doped meso/macroporous carbon beads for heterogeneous catalytic solvent-free oxidation of ethylbenzene. *Carbon* **2020,** *158*, 226-237.

65. Tong, X.; Xu, J.; Miao, H., Highly Efficient and Metal-Free Aerobic Hydrocarbons Oxidation Process by an o-Phenanthroline-Mediated Organocatalytic System. *Adv. Synth. Catal.* **2005,** *347* (15), 1953-1957.

66. Waser, M.; Jary, W. G.; Pöchlauer, P.; Falk, H., Concerning chemistry, reactivity, and mechanism of transition metal catalysed oxidation of benzylic compounds by means of ozone. *J. Mol. Catal. A: Chem.* **2005,** *236* (1), 187-193.

67. Zhang, P.; Gong, Y.; Li, H.; Chen, Z.; Wang, Y., Solvent-free aerobic oxidation of hydrocarbons and alcohols with Pd@N-doped carbon from glucose. *Nat. Commun.* **2013,** *4* (1), 1593.

68. Lin, X.; Nie, Z.; Zhang, L.; Mei, S.; Chen, Y.; Zhang, B.; Zhu, R.; Liu, Z., Nitrogen-doped carbon nanotubes encapsulate cobalt nanoparticles as efficient catalysts for aerobic and solvent-free selective oxidation of hydrocarbons. *Green Chemistry* **2017,** *19* (9), 2164-2173.

69. Ghanbari, F.; Moradi, M., Application of peroxymonosulfate and its activation methods for degradation of environmental organic pollutants: Review. *Chem. Eng. J.* **2017,** *310*, 41-62.

70. Lim, J.; Yang, Y.; Hoffmann, M. R., Activation of Peroxymonosulfate by Oxygen Vacancies-Enriched Cobalt-Doped Black TiO2 Nanotubes for the Removal of Organic Pollutants. *Environmental Science & Technology* **2019,** *53* (12), 6972-6980.

71. Hu, P.; Long, M., Cobalt-catalyzed sulfate radical-based advanced oxidation: A review on heterogeneous catalysts and applications. *Appl. Catal. B-Environ.* **2016,** *181*, 103-117.

72. Lakhi, K. S.; Park, D.-H.; Singh, G.; Talapaneni, S. N.; Ravon, U.; Al-Bahily, K.; Vinu, A., Energy efficient synthesis of highly ordered mesoporous carbon nitrides with uniform rods and their superior CO2 adsorption capacity. *J. Mater. Chem. A* **2017,** *5* (31), 16220-16230.

73. Zheng, Y.; Jiao, Y.; Zhu, Y.; Li, L. H.; Han, Y.; Chen, Y.; Du, A.; Jaroniec, M.; Qiao, S. Z., Hydrogen evolution by a metal-free electrocatalyst. *Nat. Commun.* **2014,** *5* (1), 3783.

74. Wang, H.; Zhang, X.; Xie, J.; Zhang, J.; Ma, P.; Pan, B.; Xie, Y., Structural distortion in graphitic-C3N4 realizing an efficient photoreactivity. *Nanoscale* **2015,** *7* (12), 5152-5156.

75. Zhao, S.; Wang, T.; Zhou, G.; Zhang, L.; Lin, C.; Veder, J.-P.; Johannessen, B.; Saunders, M.; Yin, L.; Liu, C.; De Marco, R.; Yang, S.-Z.; Zhang, Q.; Jiang, S. P., Controlled One-pot Synthesis of Nickel Single Atoms Embedded in Carbon Nanotube and Graphene Supports with High Loading. *ChemNanoMat* **2020,** *6* (7), 1063-1074.

76. Fan, J.; Qin, H.; Jiang, S., Mn-doped g-C3N4 composite to activate peroxymonosulfate for acetaminophen degradation: The role of superoxide anion and singlet oxygen. *Chem. Eng. J.* **2019,** *359*, 723-732.

77. Yu, J.; Feng, H.; Tang, L.; Pang, Y.; Zeng, G.; Lu, Y.; Dong, H.; Wang, J.; Liu, Y.; Feng, C.; Wang, J.; Peng, B.; Ye, S., Metal-free carbon materials for persulfate-based advanced oxidation process: Microstructure, property and tailoring. *Prog. Mater Sci.* **2020,** *111*, 100654.

78. Duan, X.; Sun, H.; Shao, Z.; Wang, S., Nonradical reactions in environmental remediation processes: Uncertainty and challenges. *Appl. Catal. B-Environ.* **2018,** *224*, 973-982.

79. Verstraeten, S. V.; Lucangioli, S.; Galleano, M., ESR characterization of thallium(III)-mediated nitrones oxidation. *Inorg. Chim. Acta* **2009,** *362* (7), 2305-2310.

80. Han, C.; Duan, X.; Zhang, M.; Fu, W.; Duan, X.; Ma, W.; Liu, S.; Wang, S.; Zhou, X., Role of electronic properties in partition of radical and nonradical processes of carbocatalysis toward peroxymonosulfate activation. *Carbon* **2019,** *153*, 73-80.

81. Tian, W.; Sun, H.; Duan, X.; Zhang, H.; Ren, Y.; Wang, S., Biomass-derived functional porous carbons for adsorption and catalytic degradation of binary micropollutants in water. *J. Hazard. Mater.* **2020,** *389*, 121881.

82. Liang, C.; Su, H.-W., Identification of Sulfate and Hydroxyl Radicals in Thermally Activated Persulfate. *Ind. Eng. Chem. Res.* **2009,** *48* (11), 5558-5562.

83. Yang, Y.; Wang, M.; Shi, P.; Wu, J.; Min, Y.; Xu, Q.; Guo, Y., Recycling of nitrogen-containing waste diapers for catalytic contaminant oxidation: Occurrence of radical and non-radical pathways. *Chem. Eng. J.* **2020,** *384*, 123246.

84. Xu, H.; Jiang, N.; Wang, D.; Wang, L.; Song, Y.; Chen, Z.; Ma, J.; Zhang, T., Improving PMS oxidation of organic pollutants by single cobalt atom catalyst through hybrid radical and non-radical pathways. *Appl. Catal. B-Environ.* **2020,** *263*, 118350.

Chapter 7 Conclusions and Recommendations

7.1 Conclusions

Liquid phase selective oxidations received continuous attention over the past decades and the establishment of green, facile, and highly selective oxidation systems is the key objective of recent research. Carbon-based materials are popular supports to immobilize metal catalysts. Functionalized nanocarbons with tailored surface chemistry and morphology also possess inherent catalytic activity for the activation of different oxidants. Peroxymonosulfate (PMS) is a promising oxidant in advanced oxidation processes to afford high oxidation efficiency towards organic compounds under benign reaction conditions. In this thesis, carbo-catalysts for PMS activation have been successfully applied to liquid phase selective oxidation of alcohols and hydrocarbons to yield their corresponding aldehyde or ketone products. Using modified carbon nanotubes as a benchmark catalyst, the effectiveness of carbon/PMS system at optimized conditions for the selective oxidation of benzyl alcohol (BzOH) into benzaldehyde (BzH) was tested. Nitrogen-doped graphene and graphene-like carbon materials were prepared, which exhibited higher efficiency for the selective oxidation of alcohols. Specially designed experiments were performed to identify the active sites on these catalysts and to gain a comprehensive understanding of the oxidation behaviour during the reaction. The study of graphene and carbon nitride catalysts with single cobalt atomic doping was performed to develop highly efficient and robust catalysts for the selective oxidations of BzOH and ethylbenzene. This thesis opens a new frontier of liquid phase selective oxidations with carbon materials activated PMS oxidant *via* a facile method.

7.1.1 Understanding of oxidation behaviour of benzyl alcohol by peroxymonosulfate *via* carbon nanotubes activation

- The CNTs/PMS system induced free radical generation under the optimised conditions can selectively convert BzOH into BzH with over 80% selectivity.
- The nucleophilic C=O groups on CNTs act as electron donors for the O-O bond cleavage in PMS to generate $^{\bullet}OH$ and $SO_4^{\bullet-}$ radicals.
- The electrophilic oxygen species are consumable active sites to cleave the O-H bond in PMS and generate $SO_5^{\bullet-}$ radicals.

7.1.2 Tailoring collaborative N-O functionalities of graphene oxide for enhanced selective oxidation of benzyl alcohol

- Carbonylated N-doped graphene catalysts are prepared with two methods: N-doping followed with post oxidation treatment; in-situ generation of C=O groups during the N-doping by introducing additive salts.
- BzOH could be selectively oxidized to BzH with NGO activated PMS *via* both non-radical and radical routes, of which the non-radical route delivers higher selectivity towards BzH.
- The electrophilic pyridinic N and nucleophilic carbonyl groups are dual active sites for PMS activation.
- The non-radical oxidation is enabled by mediated electron transfer with pyridinic N and carbonyl forming an electron bridge.
- The unreacted BzOH can quench the over-oxidation of BzH, explaining the absence of deep-oxidation by-products in this reaction system.

7.1.3 Selective oxidation of alcohols by graphene-like carbon with electrophilic oxygen and integrated pyridinic nitrogen active sites

- Graphene-like carbon can be prepared by pyrolysis of starch with low consumption of urea. The synthesis of this catalyst involves no metal catalysts or hazardous wastes.
- Adding nitrate salt into the raw materials during the catalyst preparation contributes to the formation of thin-layered graphene with abundant electrophilic groups.
- The prepared catalyst is active in the selective oxidation of aromatic alcohols into aldehydes or ketones by activated PMS. Both radical and non-radical oxidation processes are observed.
- Electrophilic oxygen species are dominantly responsible for the radical process and the integrated pyridinic N mainly enables the non-radical oxidation. However, single pyridinic N cannot activate PMS.

7.1.4 Cobalt single atom catalysts on carbon supports for highly efficient selective oxidations with activated peroxymonosulfate

- Graphene and carbon nitride are doped with single cobalt atoms to produce single atom catalysts of SACo@NG and SACo@g-C_3N_4.
- The cobalt atoms are chemically coordinated with N atoms on the carbon supports with excellent stability.
- Benzyl alcohol is selectively oxidized to benzaldehyde *via* non-radical and radical routes over SACo@NG/PMS.
- 93.2% acetophenone yield is obtained from ethylbenzene oxidation with SACo@g-C_3N_4/PMS *via* radical pathway.

7.2 Recommendations

This thesis is a pilot study of the catalytic activated PMS in highly selective liquid phase oxidation reactions. The exploration of carbo-catalysis/PMS in organic synthesis is still at the primitive stage. More work could be performed in future study to gain a deeper insight into this research field.

- More substrates and oxidation types could be tested over the carbo-catalyst/PMS system, such as the aliphatic alcohols, cycloalkanes and epoxidation of olefins.
- The origin of the radical/non-radical based oxidation mechanisms should be clarified. The results in chapter 3 suggests that the oxidation of BzOH on CNTs activated PMS is radical-based process, but non-radical dominated oxidative degradation of contaminants has been reported on CNTs activated PMS by previous research. A comparative study could be carried out to unveil the impact of different CNTs on the radical/non-radical oxidation.
- This thesis mainly focused on CNTs and graphene-based materials. Other metal-free catalysts could be explored, such as nanodiamonds, porous carbon, and carbon-doped BN nanosheets.
- Another solid peroxide, peroxydisulfate (PDS) cheaper than PMS could be explored for selective oxidation reactions. Experiments should be conducted to determine the suitable reaction method of PDS activation to attain optimised efficiency in selective oxidation reactions.
- More specific identifications of the oxidizing species could be performed in the future to better understand the mechanism. The oxidation routes are roughly divided into radical and non-radical categories in this thesis. Other oxidizing species, such as peroxide radicals and singlet oxygen, are frequently reported during the activation of PMS. Sufficient experimental proofs should be

provided to determine their roles in selective conversion of organic chemicals in future research.

- The highly efficient single-atom catalysts could be further explored in selective oxidations using oxygen gas as the oxidant.
- Future work could be carried out to avoid the disadvantages of the materials in this thesis. The metal-free carbon materials could be produced in a greener process and exhibit higher activity and stability. The single atom catalysts could employ less toxic metals such as Mn and Fe instead of Co.

APPENDIX Ⅰ: ATTRIBUTION TABLES

Paper **"Understanding of Oxidation Behaviour of Benzyl Alcohol by Peroxymonosulfate via Carbon Nanotubes Activation".** ACS Catalysis. 2020. **Mengting Li, Hongqi Sun, Zhimin Ao*, Shaobin Wang*, Shaomin Liu***

Name	**conception and design**	**Acquisition of data & method**	**Data conditioning & manipulation**	**Analysis & statistical method**	**Interpretation & discussion**	**Final approval**
Mengting Li	☐	☒	☒	☒	☒	☐
I acknowledge that these represent my contribution to the above research output. Sign:						
Hongqi Sun	☒	☐	☐	☐	☒	☐
I acknowledge that these represent my contribution to the above research output. Sign:						
Zhimin Ao	☒	☐	☐	☐	☒	☒
I acknowledge that these represent my contribution to the above research output. Sign:						
Shaobin Wang	☒	☐	☐	☐	☒	☒
I acknowledge that these represent my contribution to the above research output. Sign:						
Shaomin Liu	☒	☐	☐	☐	☒	☒
I acknowledge that these represent my contribution to the above research output. Sign:						

Paper **"Cobalt Single Atoms Embedded in Nitrogen-Doped Graphene for Selective Oxidation of Benzyl Alcohol by Activated Peroxymonosulfate".** Small, 2021. **Shiyong Zhao*, Lianji Zhang, San Ping Jiang*, Shi-Ze Yang, Shaobin Wang, Hongqi Sun, Bernt Johannessen, Shaomin Liu***

Name	**conception and design**	**Acquisition of data & method**	**Data conditioning & manipulation**	**Analysis & statistical method**	**Interpretation & discussion**	**Final approval**
Shiyong Zhao	☒	☒	☒	☐	☒	☒
I acknowledge that these represent my contribution to the above research output. Sign:						
Lianji Zhang	☒	☐	☐	☐	☐	☐
I acknowledge that these represent my contribution to the above research output. Sign:						
San Ping Jiang	☒	☐	☐	☐	☒	☒
I acknowledge that these represent my contribution to the above research output. Sign:						
Shi-Ze Yang	☐	☒	☒	☐	☐	☐
I acknowledge that these represent my contribution to the above research output. Sign:						
Shaobin Wang	☒	☐	☐	☐	☒	☐
I acknowledge that these represent my contribution to the above research output. Sign:						
Hongqi Sun	☒	☐	☐	☐	☒	☐
I acknowledge that these represent my contribution to the above research output. Sign:						
Bernt Johannessen	☐	☒	☒	☐	☐	☐
I acknowledge that these represent my contribution to the above research output. Sign:						
Shaomin Liu	☒	☐	☐	☐	☒	☒
I acknowledge that these represent my contribution to the above research output. Sign:						

Paper **"Atomically dispersed cobalt on graphitic carbon nitride as robust catalyst for selective oxidation of ethylbenzene by peroxymonosulfate".** Journal of Materials Chemistry A, 2021. **Shiyong Zhao*, Shi-Ze Yang, Shaobin Wang, Hongqi Sun, San Ping Jiang*, Bernt Johannessen, Shaomin Liu***

Name	**conception and design**	**Acquisition of data & method**	**Data conditioning & manipulation**	**Analysis & statistical method**	**Interpretation & discussion**	**Final approval**
Shiyong Zhao	☒	☒	☒	☐	☒	☒
I acknowledge that these represent my contribution to the above research output. Sign:						
Shi-Ze Yang	☐	☒	☒	☐	☐	☐
I acknowledge that these represent my contribution to the above research output. Sign:						
Shaobin Wang	☒	☐	☐	☐	☒	☐
I acknowledge that these represent my contribution to the above research output. Sign:						
Hongqi Sun	☒	☐	☐	☐	☒	☐
I acknowledge that these represent my contribution to the above research output. Sign:						
San Ping Jiang	☒	☐	☐	☐	☒	☒
I acknowledge that these represent my contribution to the above research output. Sign:						
Bernt Johannessen	☐	☒	☒	☐	☐	☐
I acknowledge that these represent my contribution to the above research output. Sign:						
Shaomin Liu	☒	☐	☐	☐	☒	☒
I acknowledge that these represent my contribution to the above research output. Sign:						

Paper **"Tailoring collaborative N-O functionalities of graphene oxide for enhanced selective oxidation of benzyl alcohol".** Carbon, 2021. **Fuping Li, Qi Yang, Shaobin Wang,* Hongqi Sun, Qingning Yang, Junwang Tang,* and Shaomin Liu***

Name	**conception and design**	**Acquisition of data & method**	**Data conditioning & manipulation**	**Analysis & statistical method**	**Interpretation & discussion**	**Final approval**
Fuping Li	☐	☒	☐	☐	☒	☐
I acknowledge that these represent my contribution to the above research output. Sign:						
Qi Yang	☐	☐	☐	☐	☒	☐
I acknowledge that these represent my contribution to the above research output. Sign:						
Shaobin Wang	☒	☐	☐	☐	☒	☒
I acknowledge that these represent my contribution to the above research output. Sign:						
Hongqi Sun	☒	☐	☐	☐	☒	☐
I acknowledge that these represent my contribution to the above research output. Sign:						
Qingning Yang	☐	☐	☒	☐	☒	☐
I acknowledge that these represent my contribution to the above research output. Sign:						
Junwang Tang	☒	☐	☐	☐	☒	☒
I acknowledge that these represent my contribution to the above research output. Sign:						
Shaomin Liu	☒	☐	☐	☐	☒	☒
I acknowledge that these represent my contribution to the above research output. Sign:						

Paper **"Selective oxidation of alcohols by graphene-like carbon with electrophilic oxygen and integrated pyridinic nitrogen active sites".** Nanoscale, 2021. **Hongqi Sun, Shaobin Wang,* Yu Dong, and Shaomin Liu**

Name	**conception and design**	**Acquisition of data & method**	**Data conditioning & manipulation**	**Analysis & statistical method**	**Interpretation & discussion**	**Final approval**
Hongqi Sun	☒	☐	☐	☐	☒	☐
I acknowledge that these represent my contribution to the above research output. Sign:						
Shaobin Wang	☒	☐	☐	☐	☒	☒
I acknowledge that these represent my contribution to the above research output. Sign:						
Yu Dong	☐	☐	☐	☐	☒	☐
I acknowledge that these represent my contribution to the above research output. Sign:						
Shaomin Liu	☒	☐	☐	☐	☒	☒
I acknowledge that these represent my contribution to the above research output. Sign:						

APPENDIX II: Copyright Permission Statements

A. Chapter 3, reprinted with permission from "Jiaquan Li, Mengting Li, Hongqi Sun, Zhimin Ao, Shaobin Wang, and Shaomin Liu. Understanding of the Oxidation Behaviour of Benzyl Alcohol by Peroxymonosulfate via Carbon Nanotubes Activation. *ACS Catalysis* 2020, 10 (6), 3516-3525."

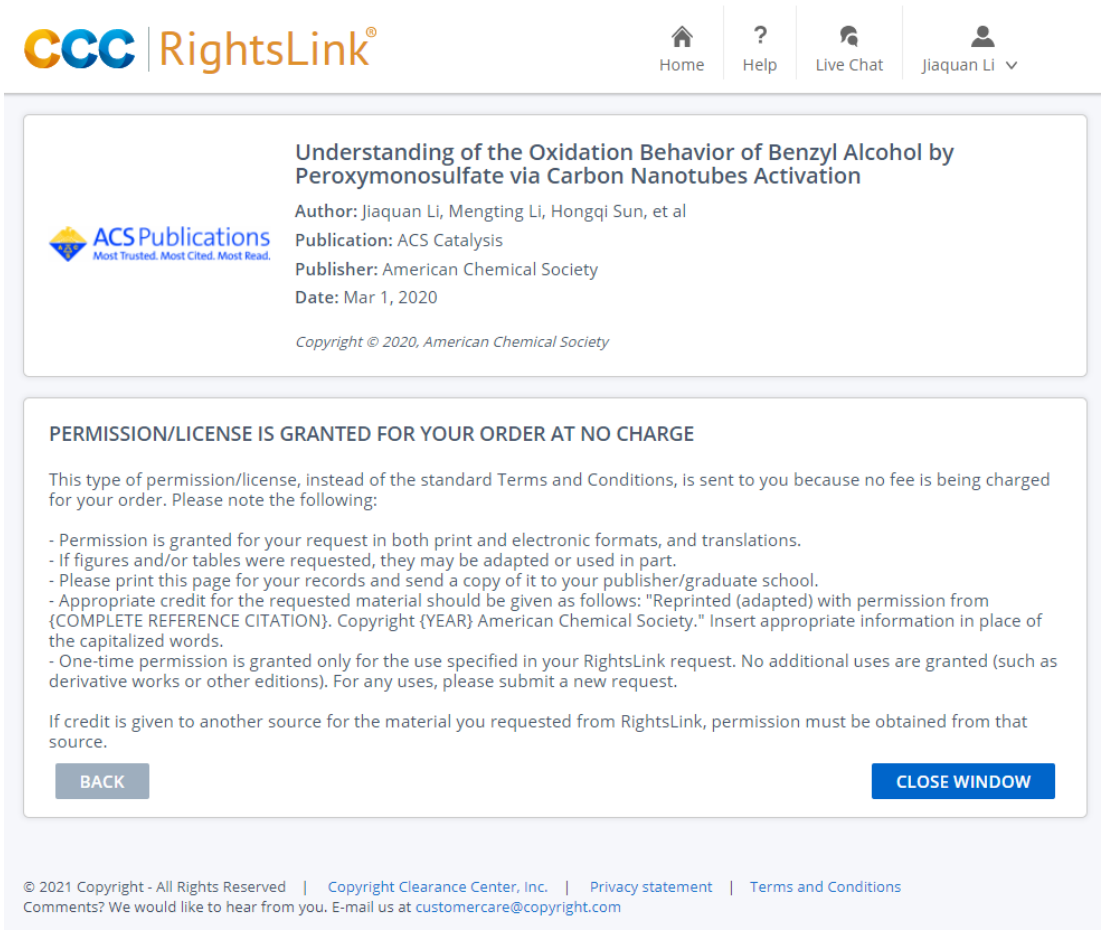

B. Chapter 6, reprinted with permission from "Jiaquan Li, Shiyong Zhao, Lianji Zhang, San Ping Jiang, Shi-Ze Yang, Shaobin Wang, Hongqi Sun, Bernt Johannessen, and Shaomin Liu. Cobalt Single Atoms Embedded in Nitrogen-Doped Graphene for Selective Oxidation of Benzyl Alcohol by Activated Peroxymonosulfate. *Small* 2021, 17 (16), 2004579."

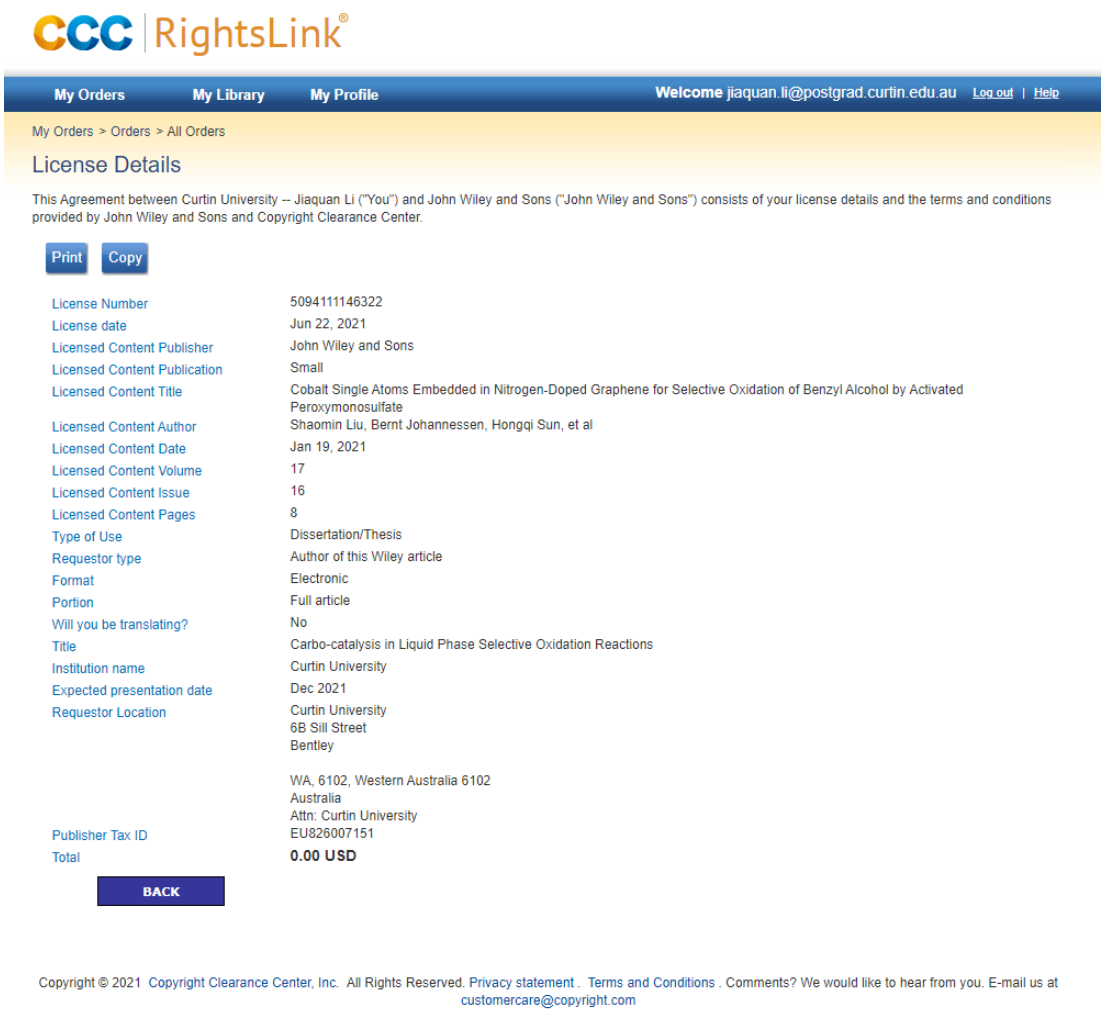

CCC RightsLink®

My Orders | My Library | My Profile | Welcome jiaquan.li@postgrad.curtin.edu.au | Log out | Help

My Orders > Orders > All Orders

License Details

This Agreement between Curtin University -- Jiaquan Li ("You") and John Wiley and Sons ("John Wiley and Sons") consists of your license details and the terms and conditions provided by John Wiley and Sons and Copyright Clearance Center.

Print | Copy

License Number	5094111146322
License date	Jun 22, 2021
Licensed Content Publisher	John Wiley and Sons
Licensed Content Publication	Small
Licensed Content Title	Cobalt Single Atoms Embedded in Nitrogen-Doped Graphene for Selective Oxidation of Benzyl Alcohol by Activated Peroxymonosulfate
Licensed Content Author	Shaomin Liu, Bernt Johannessen, Hongqi Sun, et al
Licensed Content Date	Jan 19, 2021
Licensed Content Volume	17
Licensed Content Issue	16
Licensed Content Pages	8
Type of Use	Dissertation/Thesis
Requestor type	Author of this Wiley article
Format	Electronic
Portion	Full article
Will you be translating?	No
Title	Carbo-catalysis in Liquid Phase Selective Oxidation Reactions
Institution name	Curtin University
Expected presentation date	Dec 2021
Requestor Location	Curtin University 6B Sill Street Bentley WA, 6102, Western Australia 6102 Australia Attn: Curtin University
Publisher Tax ID	EU826007151
Total	**0.00 USD**

BACK

Copyright © 2021 Copyright Clearance Center, Inc. All Rights Reserved. Privacy statement . Terms and Conditions . Comments? We would like to hear from you. E-mail us at customercare@copyright.com

C. Chapter 4, reprinted with permission from "Jiaquan Li, Fuping Li, Qi Yang, Shaobin Wang, Hongqi Sun, Qingning Yang, Junwang Tang, and Shaomin Liu. Tailoring collaborative N-O functionalities of graphene oxide for enhanced selective oxidation of benzyl alcohol. Carbon 2021, 182, 715-724."

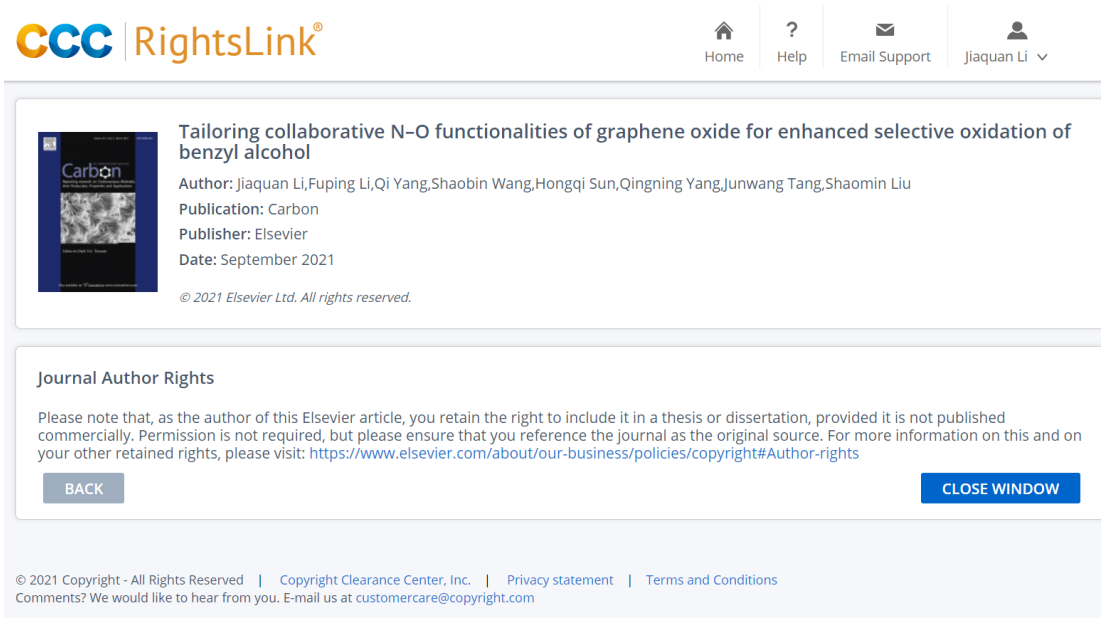

CCC RightsLink®

Home | Help | Email Support | Jiaquan Li

Tailoring collaborative N–O functionalities of graphene oxide for enhanced selective oxidation of benzyl alcohol

Author: Jiaquan Li,Fuping Li,Qi Yang,Shaobin Wang,Hongqi Sun,Qingning Yang,Junwang Tang,Shaomin Liu

Publication: Carbon

Publisher: Elsevier

Date: September 2021

© 2021 Elsevier Ltd. All rights reserved.

Journal Author Rights

Please note that, as the author of this Elsevier article, you retain the right to include it in a thesis or dissertation, provided it is not published commercially. Permission is not required, but please ensure that you reference the journal as the original source. For more information on this and on your other retained rights, please visit: https://www.elsevier.com/about/our-business/policies/copyright#Author-rights

BACK CLOSE WINDOW

© 2021 Copyright - All Rights Reserved | Copyright Clearance Center, Inc. | Privacy statement | Terms and Conditions

Comments? We would like to hear from you. E-mail us at customercare@copyright.com

D. Permission of Reproduction from the Copyright Owner in Chapter 2.

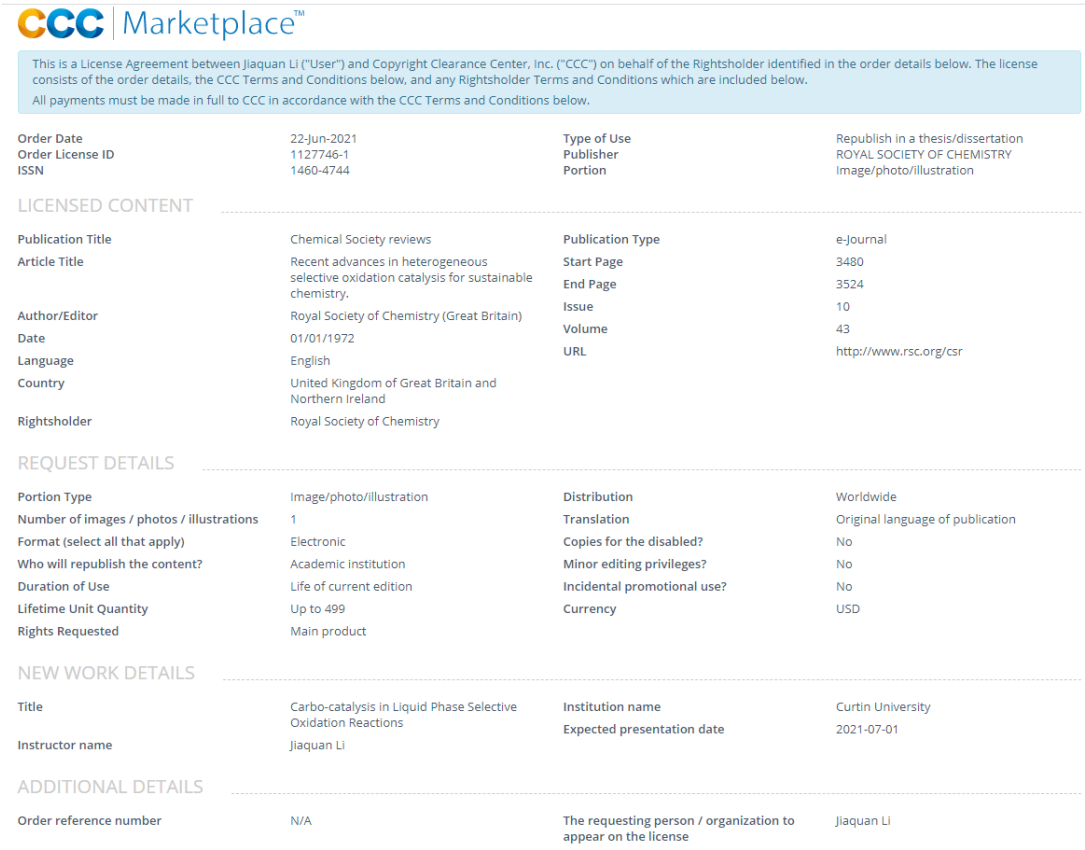

CCC Marketplace™

This is a License Agreement between Jiaquan Li ("User") and Copyright Clearance Center, Inc. ("CCC") on behalf of the Rightsholder identified in the order details below. The license consists of the order details, the CCC Terms and Conditions below, and any Rightsholder Terms and Conditions which are included below.

All payments must be made in full to CCC in accordance with the CCC Terms and Conditions below.

Order Date	22-Jun-2021	Type of Use	Republish in a thesis/dissertation
Order License ID	1127746-1	Publisher	ROYAL SOCIETY OF CHEMISTRY
ISSN	1460-4744	Portion	Image/photo/illustration

LICENSED CONTENT

Publication Title	Chemical Society reviews	Publication Type	e-Journal
Article Title	Recent advances in heterogeneous selective oxidation catalysis for sustainable chemistry.	Start Page	3480
		End Page	3524
Author/Editor	Royal Society of Chemistry (Great Britain)	Issue	10
Date	01/01/1972	Volume	43
Language	English	URL	http://www.rsc.org/csr
Country	United Kingdom of Great Britain and Northern Ireland		
Rightsholder	Royal Society of Chemistry		

REQUEST DETAILS

Portion Type	Image/photo/illustration	Distribution	Worldwide
Number of images / photos / illustrations	1	Translation	Original language of publication
Format (select all that apply)	Electronic	Copies for the disabled?	No
Who will republish the content?	Academic institution	Minor editing privileges?	No
Duration of Use	Life of current edition	Incidental promotional use?	No
Lifetime Unit Quantity	Up to 499	Currency	USD
Rights Requested	Main product		

NEW WORK DETAILS

Title	Carbo-catalysis in Liquid Phase Selective Oxidation Reactions	Institution name	Curtin University
		Expected presentation date	2021-07-01
Instructor name	Jiaquan Li		

ADDITIONAL DETAILS

Order reference number	N/A	The requesting person / organization to appear on the license	Jiaquan Li

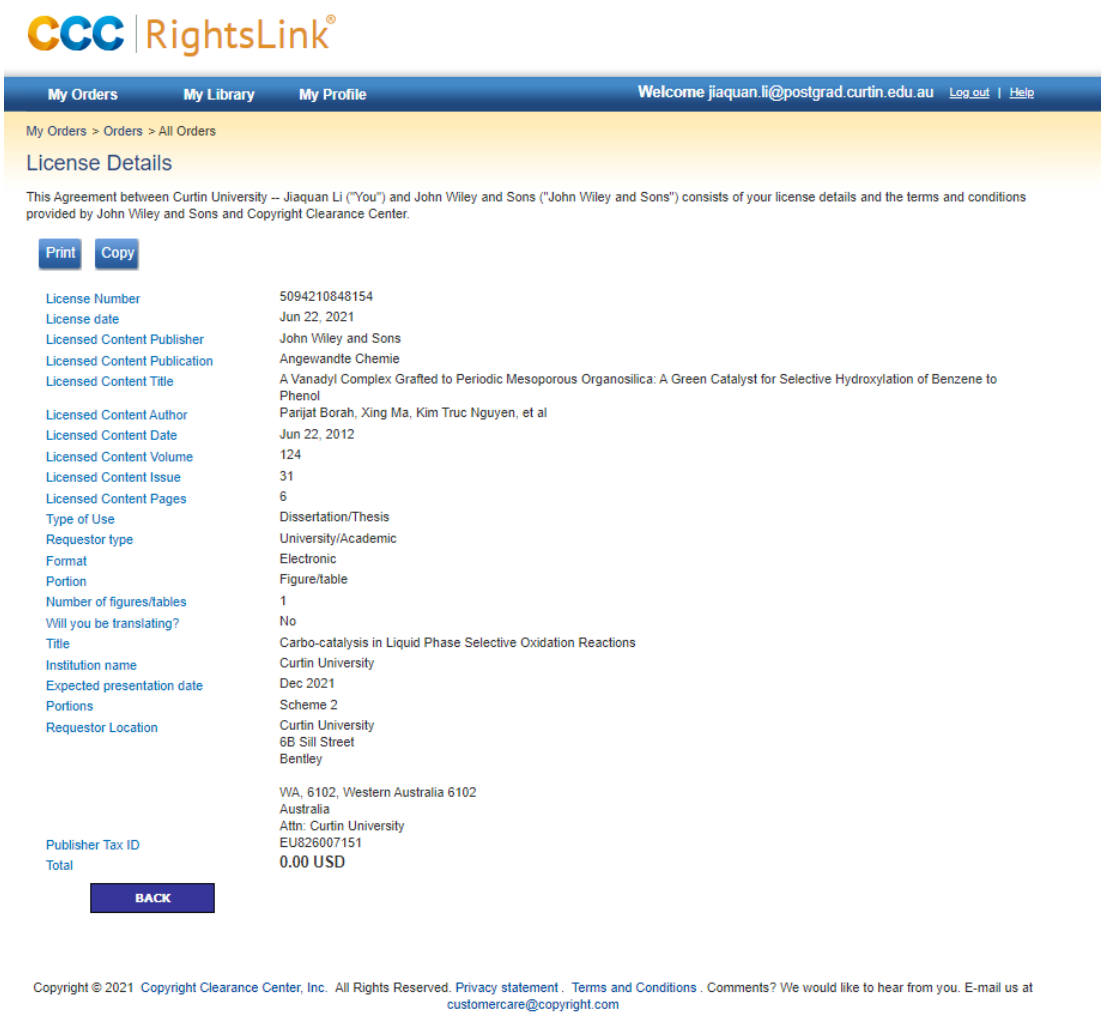

CCC RightsLink®

My Orders | My Library | My Profile | Welcome jiaquan.li@postgrad.curtin.edu.au Log out | Help

My Orders > Orders > All Orders

License Details

This Agreement between Curtin University -- Jiaquan Li ("You") and John Wiley and Sons ("John Wiley and Sons") consists of your license details and the terms and conditions provided by John Wiley and Sons and Copyright Clearance Center.

Print Copy

License Number	5094210848154
License date	Jun 22, 2021
Licensed Content Publisher	John Wiley and Sons
Licensed Content Publication	Angewandte Chemie
Licensed Content Title	A Vanadyl Complex Grafted to Periodic Mesoporous Organosilica: A Green Catalyst for Selective Hydroxylation of Benzene to Phenol
Licensed Content Author	Parijat Borah, Xing Ma, Kim Truc Nguyen, et al
Licensed Content Date	Jun 22, 2012
Licensed Content Volume	124
Licensed Content Issue	31
Licensed Content Pages	6
Type of Use	Dissertation/Thesis
Requestor type	University/Academic
Format	Electronic
Portion	Figure/table
Number of figures/tables	1
Will you be translating?	No
Title	Carbo-catalysis in Liquid Phase Selective Oxidation Reactions
Institution name	Curtin University
Expected presentation date	Dec 2021
Portions	Scheme 2
Requestor Location	Curtin University 6B Sill Street Bentley WA, 6102, Western Australia 6102 Australia Attn: Curtin University
Publisher Tax ID	EU826007151
Total	0.00 USD

BACK

CCC | RightsLink®

My Orders | My Library | My Profile | Welcome jiaquan.li@postgrad.curtin.edu.au | Log out | Help

My Orders > Orders > All Orders

License Details

This Agreement between Curtin University -- Jiaquan Li ("You") and John Wiley and Sons ("John Wiley and Sons") consists of your license details and the terms and conditions provided by John Wiley and Sons and Copyright Clearance Center.

Print | Copy

License Number	5094211045769
License date	Jun 22, 2021
Licensed Content Publisher	John Wiley and Sons
Licensed Content Publication	Angewandte Chemie
Licensed Content Title	Selective Aerobic Oxidation of Benzylic Alcohols Catalyzed by Carbon-Based Catalysts: A Nonmetallic Oxidation System
Licensed Content Author	Masa-aki Kakimoto, Teruaki Hayakawa, Yuta Nabae, et al
Licensed Content Date	Dec 28, 2009
Licensed Content Volume	122
Licensed Content Issue	2
Licensed Content Pages	5
Type of Use	Dissertation/Thesis
Requestor type	University/Academic
Format	Electronic
Portion	Figure/table
Number of figures/tables	1
Will you be translating?	No
Title	Carbo-catalysis in Liquid Phase Selective Oxidation Reactions
Institution name	Curtin University
Expected presentation date	Dec 2021
Portions	Scheme 1
Requestor Location	Curtin University 6B Sill Street Bentley WA, 6102, Western Australia 6102 Australia Attn: Curtin University
Publisher Tax ID	EU826007151
Total	0.00 USD

BACK

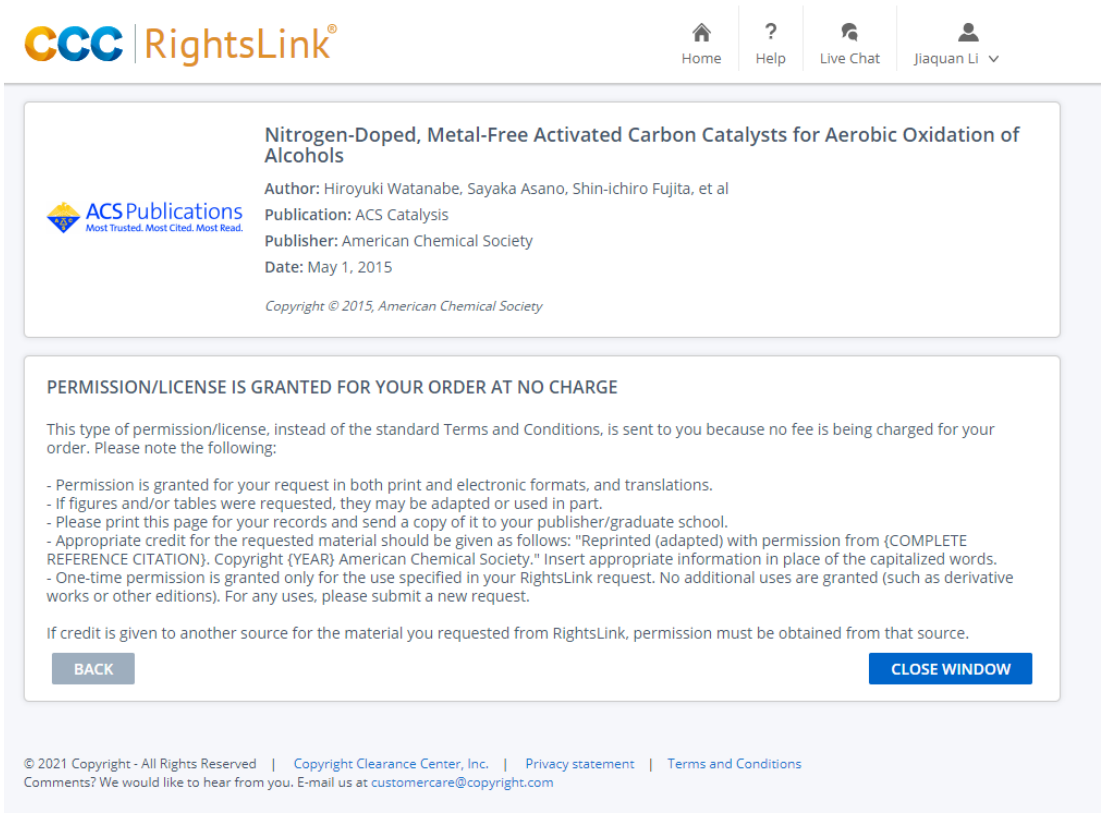

CCC RightsLink®

Home | Help | Live Chat | Jiaquan Li

ACS Publications
Most Trusted. Most Cited. Most Read.

Nitrogen-Doped, Metal-Free Activated Carbon Catalysts for Aerobic Oxidation of Alcohols

Author: Hiroyuki Watanabe, Sayaka Asano, Shin-ichiro Fujita, et al
Publication: ACS Catalysis
Publisher: American Chemical Society
Date: May 1, 2015

Copyright © 2015, American Chemical Society

PERMISSION/LICENSE IS GRANTED FOR YOUR ORDER AT NO CHARGE

This type of permission/license, instead of the standard Terms and Conditions, is sent to you because no fee is being charged for your order. Please note the following:

- Permission is granted for your request in both print and electronic formats, and translations.
- If figures and/or tables were requested, they may be adapted or used in part.
- Please print this page for your records and send a copy of it to your publisher/graduate school.
- Appropriate credit for the requested material should be given as follows: "Reprinted (adapted) with permission from {COMPLETE REFERENCE CITATION}. Copyright {YEAR} American Chemical Society." Insert appropriate information in place of the capitalized words.
- One-time permission is granted only for the use specified in your RightsLink request. No additional uses are granted (such as derivative works or other editions). For any uses, please submit a new request.

If credit is given to another source for the material you requested from RightsLink, permission must be obtained from that source.

BACK | CLOSE WINDOW

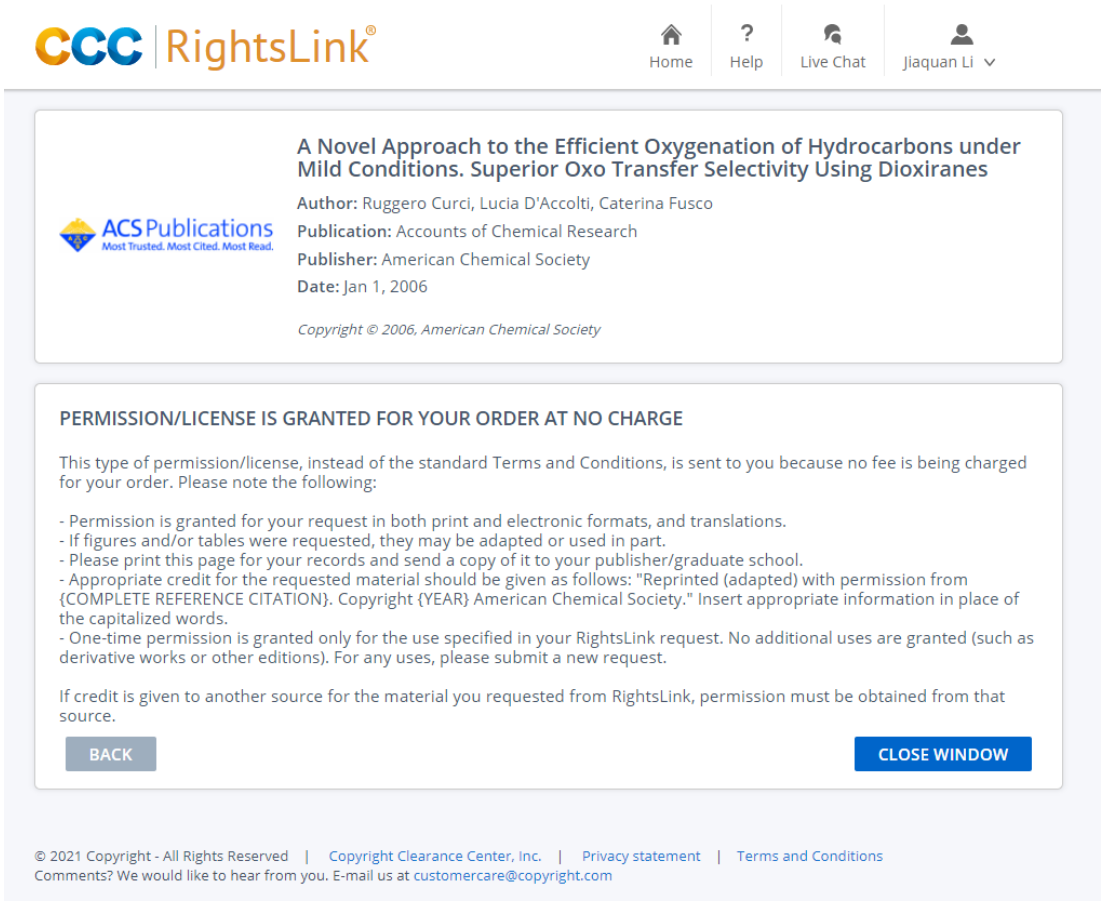

CCC RightsLink®

Home | Help | Live Chat | Jiaquan Li

ACS Publications
Most Trusted. Most Cited. Most Read.

A Novel Approach to the Efficient Oxygenation of Hydrocarbons under Mild Conditions. Superior Oxo Transfer Selectivity Using Dioxiranes

Author: Ruggero Curci, Lucia D'Accolti, Caterina Fusco
Publication: Accounts of Chemical Research
Publisher: American Chemical Society
Date: Jan 1, 2006

Copyright © 2006, American Chemical Society

PERMISSION/LICENSE IS GRANTED FOR YOUR ORDER AT NO CHARGE

This type of permission/license, instead of the standard Terms and Conditions, is sent to you because no fee is being charged for your order. Please note the following:

- Permission is granted for your request in both print and electronic formats, and translations.
- If figures and/or tables were requested, they may be adapted or used in part.
- Please print this page for your records and send a copy of it to your publisher/graduate school.
- Appropriate credit for the requested material should be given as follows: "Reprinted (adapted) with permission from {COMPLETE REFERENCE CITATION}. Copyright {YEAR} American Chemical Society." Insert appropriate information in place of the capitalized words.
- One-time permission is granted only for the use specified in your RightsLink request. No additional uses are granted (such as derivative works or other editions). For any uses, please submit a new request.

If credit is given to another source for the material you requested from RightsLink, permission must be obtained from that source.

BACK | CLOSE WINDOW

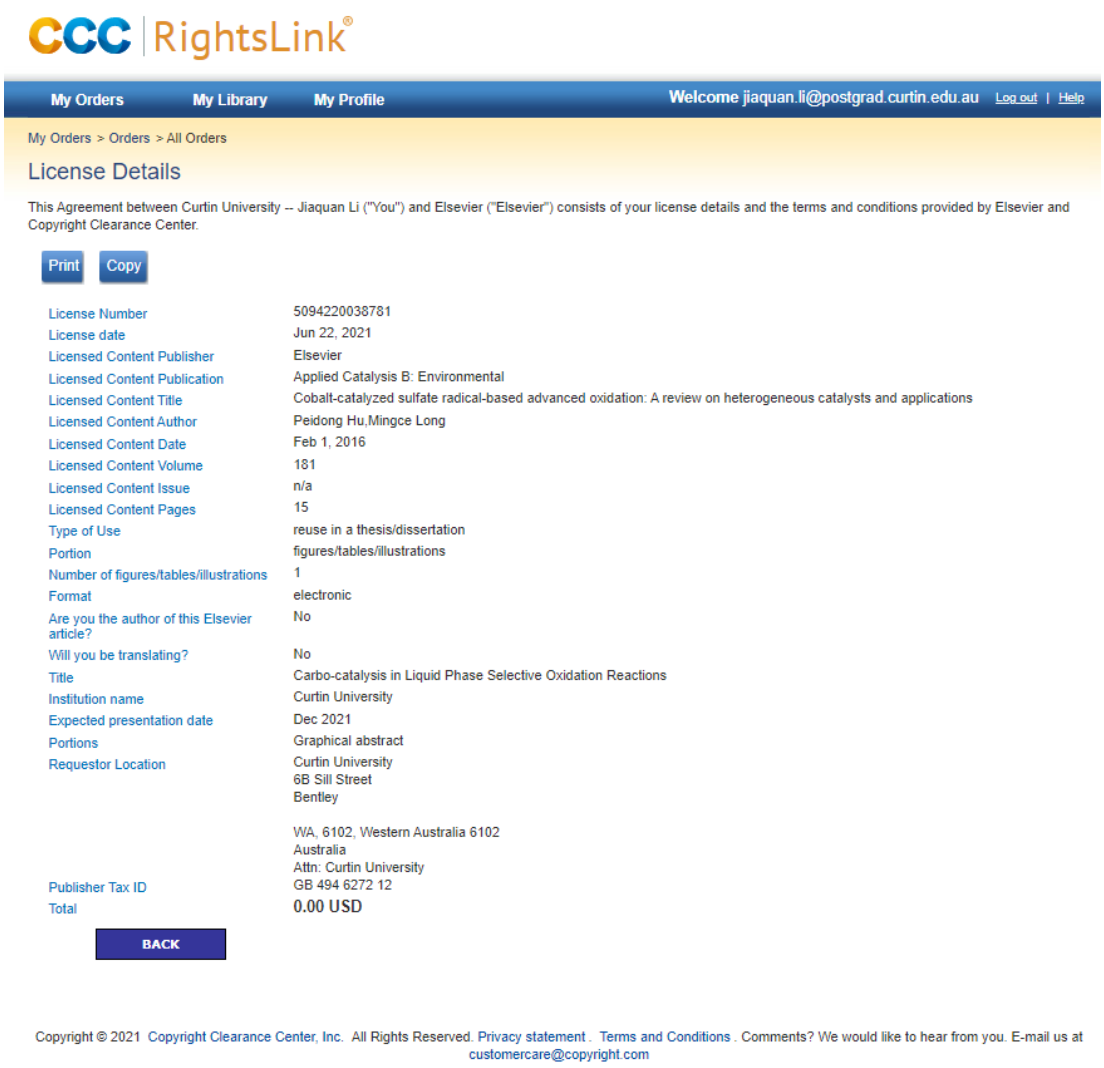

CCC RightsLink®

My Orders | My Library | My Profile | Welcome jiaquan.li@postgrad.curtin.edu.au | Log out | Help

My Orders > Orders > All Orders

License Details

This Agreement between Curtin University -- Jiaquan Li ("You") and Elsevier ("Elsevier") consists of your license details and the terms and conditions provided by Elsevier and Copyright Clearance Center.

Print | Copy

License Number	5094220038781
License date	Jun 22, 2021
Licensed Content Publisher	Elsevier
Licensed Content Publication	Applied Catalysis B: Environmental
Licensed Content Title	Cobalt-catalyzed sulfate radical-based advanced oxidation: A review on heterogeneous catalysts and applications
Licensed Content Author	Peidong Hu,Mingce Long
Licensed Content Date	Feb 1, 2016
Licensed Content Volume	181
Licensed Content Issue	n/a
Licensed Content Pages	15
Type of Use	reuse in a thesis/dissertation
Portion	figures/tables/illustrations
Number of figures/tables/illustrations	1
Format	electronic
Are you the author of this Elsevier article?	No
Will you be translating?	No
Title	Carbo-catalysis in Liquid Phase Selective Oxidation Reactions
Institution name	Curtin University
Expected presentation date	Dec 2021
Portions	Graphical abstract
Requestor Location	Curtin University 6B Sill Street Bentley WA, 6102, Western Australia 6102 Australia Attn: Curtin University
Publisher Tax ID	GB 494 6272 12
Total	0.00 USD

BACK

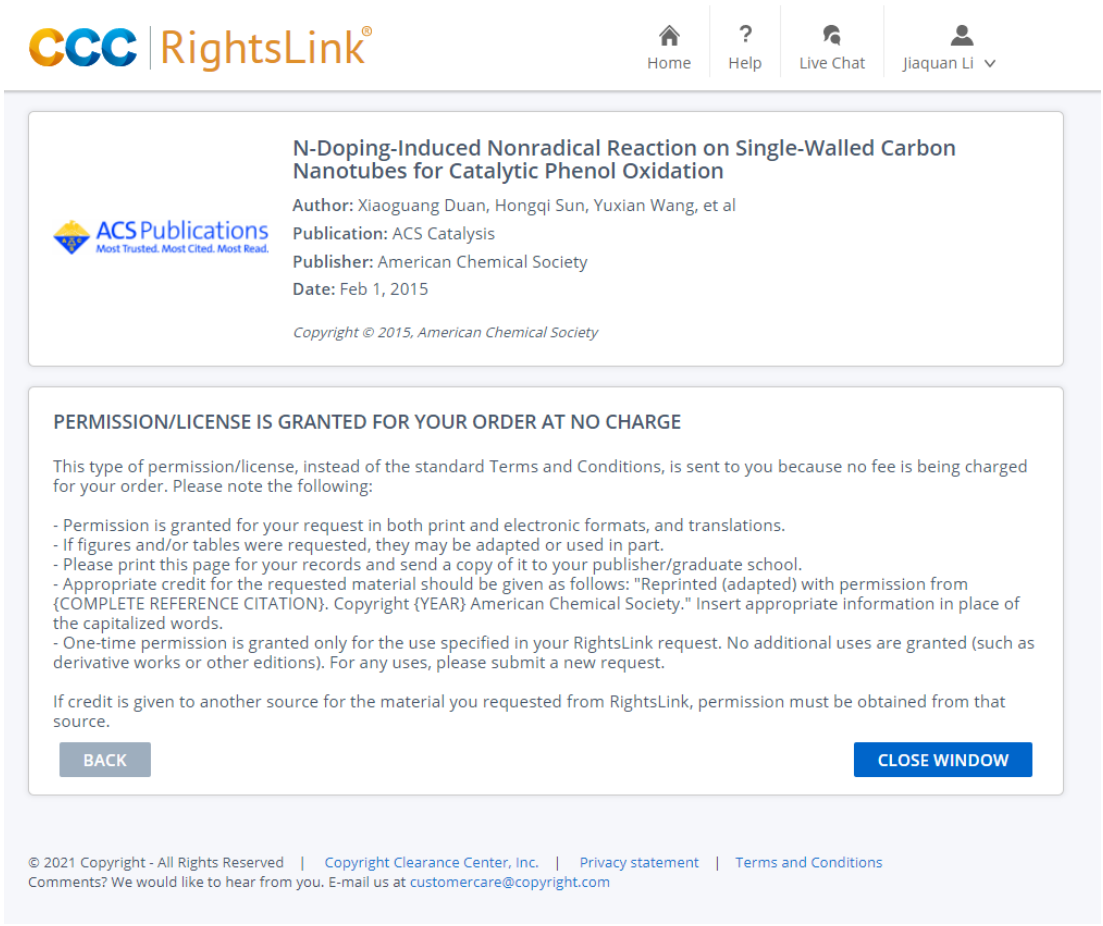

CCC RightsLink

Home | Help | Live Chat | Jiaquan Li

ACS Publications
Most Trusted. Most Cited. Most Read.

N-Doping-Induced Nonradical Reaction on Single-Walled Carbon Nanotubes for Catalytic Phenol Oxidation

Author: Xiaoguang Duan, Hongqi Sun, Yuxian Wang, et al
Publication: ACS Catalysis
Publisher: American Chemical Society
Date: Feb 1, 2015

Copyright © 2015, American Chemical Society

PERMISSION/LICENSE IS GRANTED FOR YOUR ORDER AT NO CHARGE

This type of permission/license, instead of the standard Terms and Conditions, is sent to you because no fee is being charged for your order. Please note the following:

- Permission is granted for your request in both print and electronic formats, and translations.
- If figures and/or tables were requested, they may be adapted or used in part.
- Please print this page for your records and send a copy of it to your publisher/graduate school.
- Appropriate credit for the requested material should be given as follows: "Reprinted (adapted) with permission from {COMPLETE REFERENCE CITATION}. Copyright {YEAR} American Chemical Society." Insert appropriate information in place of the capitalized words.
- One-time permission is granted only for the use specified in your RightsLink request. No additional uses are granted (such as derivative works or other editions). For any uses, please submit a new request.

If credit is given to another source for the material you requested from RightsLink, permission must be obtained from that source.

BACK | CLOSE WINDOW